Stony Brook University

Form and Function of the Anthropoid Forefoot

A Dissertation Presented

by

Pedro Jesús Fernández III

to

The Graduate School

In Partial Fulfillment of the

Requirements

for the Degree of

Doctor of Philosophy

in

Anthropology

(Concentration – Physical Anthropology)

Stony Brook University

May 2016

Stony Brook University

The Graduate School

Pedro Jesús Fernández III

We, the dissertation committee for the above candidate for the

Doctor of Philosophy degree, hereby recommend

acceptance of this dissertation.

William L. Jungers – Dissertation Advisor
Distinguished Teaching Professor Emeritus, Department of Anatomical Sciences

Brigitte Demes – Chairperson of Defense
Professor, Department of Anatomical Sciences

Randall L. Susman
Professor and Chair, Department of Anatomical Sciences

Sergio Almécija
Assistant Professor, Department of Anthropology, The George Washington University

Biren A. Patel
Assistant Professor, Deparment of Cell and Neurobiology, University of Southern California School of Medicine

This dissertation is accepted by the Graduate School

Charles Taber

Dean of the Graduate School
Abstract of the Dissertation

Form and Function of the Anthropoid Forefoot

by

Peter J. Fernández III

Doctor of Philosophy

in

Anthropology

(Concentration – Physical Anthropology)

Stony Brook University

2016

The transition to our uniquely human gait—terrestrial bipedalism—is the hallmark of our lineage. Abundant fossil evidence confirms that it was the adoption of a terrestrial bipedal gait that first set hominins apart from other apes. Therefore, a thorough understanding of postcranial functional morphology is necessary in order to gain as much insight as possible from the current known fossil material. When compared to our closest relatives, the living apes, it is clear that a suite of morphological changes have occurred in the human postcranial skeleton broadly, including modifications at the vertebral column, shoulder, wrist, hand, pelvis, ankle and foot. The human foot in particular is strikingly different from that of any other primate, and a better understanding of its functional morphology would allow researchers to better reconstruct the locomotor behavior of extinct hominin groups.

Despite their theorized importance in bipedal locomotion, the morphological details of the anthropoid forefoot (i.e., metatarsophalangeal) joints have not been thoroughly quantified. To that end, I present here a detailed morphometric analysis of anthropoid forefoot shape and form using modern 3-dimensional geometric morphometric (3DGM) techniques in a broad phylogenetic context in order to capture functionally meaningful aspects of forefoot shape. The appositional articular surfaces of the metatarsus and proximal pedal phalanges were quantified, and then hypotheses about forefoot functional morphology were tested by exploring shape space, constant and variable-rate models of shape evolution, patterns of forefoot joint covariance, and the correlation between forefoot morphology and kinematic performance.

Results revealed several broad patterns in anthropoid forefoot evolution. First, it seems the lateral forefoot began to evolve first, with the hallux retaining a primitive form until relatively late in evolution; a similar pattern was found in the pedal phalanges, which looked more primitive than the metatarsals overall. This staggered timing of forefoot evolution perhaps reflects the importance of arboreal locomotion persisting well into the hominin lineage. Evidence of convergent evolution between highly terrestrial cercopithecoids and hominins was found. Correlations with kinematic data in human and chimpanzee forefoot joints suggest that dorsal robusticity is strongly correlated with forefoot dorsiflexion range of motion.

Dedication

To my family—PJ, Mercedes, Thomas, Andy.

Table of Contents

List of Tables

List of Figures

List of Institutional Abbreviations

AMNH – American Museum of Natural History, New York

ANSP – Academy of Natural Sciences of Philadelphia, Philadelphia

CMNH – Cleveland Museum of Natural History, Cleveland

CPRC – Caribbean Primate Research Center, San Juan

LACM – Los Angeles County Museum, Los Angeles

MCZ – Museum of Comparative Zoology, Cambridge

RMCA – Royal Museum for Central Africa, Tervuren

SAM-I – South African Museum—Iziko, Cape Town

SBU – Stony Brook University (collections held within the Department of Anatomical Sciences)

UCT – University of Cape Town (collections held within the Department of Human Biology)

USNM – National Museum of Natural History, Washington, DC

Acknowledgements

This dissertation was supported by the Wenner-Gren Foundation (Dissertation Fieldwork Grant), the W. Burghardt Turner Fellowship Research Grant, and the NSF-Alliance for Graduate Education and the Professoriate Transformation (AGEP-T) Frontiers of Research and Academic Models of Excellence (FRAME) summer research grant. Research presented in Chapter 6 was additionally supported by the National Science Foundation (NSF) and the Leakey Foundation. Grant numbers: NSF-BCS 1316947, NSF-BCS-1317047, NSF-BCS 1317029. I thank Terry Kensler and the Laboratory for Primate Morphology and Genetics of the CPRC for providing access to specimens in their care. The CPRC is funded by the National Institutes of Heath (NIH 8 P40 OD012217-25). I thank Tautis Skorka, Bino Varghese and Grant Dagliyan for facilitating micro CT scanning at the USC Molecular Imaging Center. A tremendous thanks to Tim White and Gen Suwa for access to the *Ar. ramidus* micro CT scans, which were delivered by Caley Orr. Special thanks go out to all the curatorial and collection managers staff at the visited institutions (see above), especially J. Chupasko, S. Canington, E. Gilissen, and E. Bartnick.

This work would not have been possible without the help of my incredible dissertation committee, which internally included my dissertation advisor Bill Jungers, defense chair Brigitte Demes, and Randy Susman. Bill, I thank you tremendously for taking me in as a clueless second year grad student working on a class project, and eventually helping me grow that little project into this dissertation. I was afraid this dissertation would be impossible to finish up once you retired from Stony Brook, but your continued involvement and encouragement was crucial to me in the later stages of this work. You are an insane repository of knowledge and I'm excited to get these papers out with you going forward. Brigitte, your ability to question every axiom of my writing both awes and terrifies me. Your approach, to build everything up from sound, functional fundamentals, has allowed me to go beyond being just a comparative morphologist, and really allowed me to become a functional morphologist, which at times was a challenging undertaking but also a very rewarding experience. I guess that after five years at Stony Brook, you have finally convinced me that experimental research is where it's at! Now I have to re-learn everything…Finally, Randy, both your banter and sharp attention to detail in my functional hypotheses was invaluable. As the resident master of all things hand and foot, I was extremely lucky to learn about these structures from the best. Our discussions on joint congruence and function continue to marinate in my mind, and in fact is one of the main reasons why I hope to devote my next project entirely to that topic.

In addition to my internal members, I especially have to thank both of my external committee members, Biren Patel and Sergio Almécija, who were both postdoctoral researchers at Stony Brook in my early grad school years. Biren was there in my first year and helped guide me through both gross anatomy and my first research project in Fred Grine's Human Evolution course. I can safely say that without his guidance, I would've had no idea how to navigate graduate school. Biren left for California the following year but we have continued to collaborate, which included a summer in 2014 where I worked out of his lab. Many tacos were consumed. Biren contributed very substantially to this work in a variety of ways; he provided the grand majority of the monkey scan data, established the CT scanning protocols, taught me how to use Amira's segmentation editor, and provided a lot of formative input on how to frame the hypotheses for this research. I met Sergio after Biren left Stony Brook, this time as a still mostly clueless second year student. Sergio was the first person to put me on to foot bones, a topic that would eventually swell into this dissertation. At the time (~Oct, 2012), we were just looking at

forefoot characters for a class project. This eventually became a publication and after sufficient expansion, my dissertation. Like Biren, Sergio also contributed substantially to this work. Together we scanned many African ape postcrania, and Sergio also scanned and graciously allowed me to use some of the fossils included in this dissertation. Sergio vastly expanded my knowledge of 3DGM and phylogenetic comparative methods, and taught me the majority of the analytical techniques I've employed here. He has always read through anything I send him thoroughly, and was definitely my go-to person while he was here. So again, thank you guys—Biren and Sergio—so much for your continued input on my work.

Some other current and former IDPAS faculty I'd like to thank include Fred Grine, for helping me connect with the South African curators and collections staff and being a great course director to work for in undergraduate human anatomy, Erik Seiffert for being a generally awesome dude and a hilarious anatomy lecturer, Gabrielle Russo for advice on professional development and for giving me the opportunity to lecture in her class, Ian Wallace, for his very detailed feedback on the 'big picture' aspects of this project, and finally Jeroen Smaers, for constructive feedback on phylogenetic comparative methods.

Beyond Stony Brook faculty, I must also acknowledge three other incredible collaborators that helped shape this dissertation work. The first, Caley Orr, was actually also a postdoc at SBU when I started graduate school, but I did not interact with him very much. Once I had some concrete research ideas, I started reaching out to Caley. His feedback has always been very positive and supportive, and he is definitely one of the nicest people I have ever encountered. Caley also sent me an incredible number of fossil scans for this project, many of which were quite hard to come by. Likewise, Matt Tocheri has also helped shape this work from afar. Although I've never met Matt, he's always been enthusiastic about my work, and has contributed all of the *H. floresiensis* scans presented here. Lastly, Dan Proctor, who undertook a similar dissertation back in 2010 on the proximal half of the metatarsals, deserves my utmost praise for sharing his entire database with me, including scans taken on original material of all the South African specimens that appear in this dissertation. He did all this despite not knowing who I was, and before I had any publications out—I was essentially a random graduate student. I hope his open-access policy to his data is adopted by other researchers—Dan, you are an amazingly generous person.

To round out the Stony Brook experience, I'd like to extend my sincerest, warmest thanks and gratitude to all of those current and former SBU graduate students who helped me at one point or another along the torturous and often isolating road that is graduate school, including: Erin Achilles, Stephanie Blatch, Stevie Carnation, Fanny Cornejo, Sharon Doyle, Simone Hoffman, Nick Holowka, Rachel Jacobs, Abby Koppa, Stephanie Maiolino, Carrie Mongle, Allison Nesbitt, Abi Nishimura, Evelyn Pain, Rachel Perlman, Clara Scarry, Bonnie Sumner, Nathan Thompson, Jesse Wolfhagen, and Andrew Zamora. In particular I have to single out Nick Holowka and Nathan Thompson who both provided me with a lot of advice on various aspects of my dissertation, and generally served as incredible mentors while I attempted to stagger through every new hurdle in graduate school. I guess you could also say we had some rowdy times back in those early years, too. You guys definitely bring up those around you, and I have certainly benefitted from this. I also want to thank a few of my former students at Stony Brook, both undergrads and grads, for their friendship and contributions to this dissertation. First and foremost I must thank Billy Wiedemann, for being an incredible undergrad student in my ANP 300 class (the best), and for the considerable amount of work he put in towards the data processing for this dissertation. Billy started working with me in 2015, and has produced nothing

but excellent work for me ever since. Best of luck to you in medical school! Additionally, two other former undergraduates of mine, Lindsay Roblyer and Maritza Sierra, also contributed to data collection/processing. Much love goes out to my former PA/PT/medical/dental anatomy students, including Ross Edmunds, who skipped class in order to make it out for my defense, thanks man!

I have to back up the timeline a bit to my second crack at undergrad and give thanks to the Illinois anthro crew circa 2007-2010. These were some formative years for me in phys anth, and it's when I met a few individuals that would prove to be very influential in my life. Although I originally was not an anthropology major, I was attracted to classes like anatomy, osteology, and human evolution. In these classes I met John Polk, Charles Roseman, Scott Williams, and Mark Grabowski. I was lucky to learn from all of these mentors, and am happy to still be in contact with some of them. I'll also give a shout out to Madeline Keleher and Aimee Carbaugh, my old osteology lab partners, who are now killing it in grad school. To reach way back into the (prehistoric) Wisconsin years, I want to also recognize my good friend Michael Yaari—thank you sir for your acerbic wit, your enduring friendship, and your face. The mere fact that we're still friends despite the seemingly endless barrage of complaints I hurled at you regarding writing, figures, p values, revisions, and whatever other miscellaneous neuroticisms I may have voiced to you during our frequent fireside gchats testifies to your stalwart character. I owe you a beer.

To end, I extend my final and deepest, most sincere thanks to my family—my parents (PJ and Mercedes), and two brothers (Thomas and Andy). I love you all and this has been a crazy ride, especially in the last half decade or so. Your unwavering and at times overwhelming (mom) support really helped keep me sane over these intense and often unpredictable years. Regardless, I made it through in no small part thanks to all of you, and I only hope I can return the favor to any and all of you going forward. Plus, I am a doctor now after all (just one of dubious helpfulness). This is an exciting time for the Fernández tribe, and I'm eager to see where we all end up in a couple of years. As for me, I'm not entirely sure what lies ahead, but I can say that it (probably) won't involve monkey toe bones.

Chapter 1

Introduction

1.1 Introduction

The narrative of how humans evolved is a continually changing one, punctuated by the discovery of new fossils that can better inform our understanding of hominin evolution. These often fragmentary remains preserve evolutionary changes to the structural form of the hominin skeleton that occurred in the late Miocene (White et al., 1994; Senut et al., 2001), the Pliocene (Johanson et al., 1982; Latimer et al., 1982; Clarke and Tobias, 1995), and has even given physical anthropologists insight into hominin evolution occurring into the very late Pleistocene (Jungers et al., 2009). New finds in east Africa (Haile-Selassie et al., 2012; Jungers et al., 2015) and South Africa (Berger et al., 2010; Berger et al., 2015) continue to be described, new species of *Australopithecus* and *Homo* are defined, and the story of human evolution becomes increasingly complex. One fixed factor in this narrative however is that all early hominin material described so far demonstrates anatomical changes to the postcranial skeleton thought to better facilitate orthograde, bipedal walking on terrestrial substrates. Indeed, abundant fossil evidence confirms that it was the adoption of a terrestrial bipedal gait that first set hominins apart from other apes. Therefore, a thorough understanding of postcranial functional morphology is necessary in order to gain as much insight as possible from the current known fossil material. When compared to our closest living relatives, the common chimpanzee and bonobo (*Pan* sp.), it is clear that a suite of morphological changes have occurred in the human postcranial skeleton broadly, including modifications at the vertebral column (Lovejoy, 2005; Ward and Latimer, 2005; Williams et al., 2013), shoulder (Larson, 2007, 2009; Green and Alemseged, 2012), wrist (Marzke, 1983; Lewis, 1989; Tocheri et al., 2007), hand (Marzke, 1983; Susman, 1998; Almécija et al., 2010), pelvis (McHenry, 1975; Grabowski et al., 2011), ankle (Morton, 1922, 1924; Midlo, 1934; Elftman and Manter, 1935b, a; Wood-Jones, 1944) and foot (Elftman and Manter, 1935b;

Susman, 1983). Within the lower limb, many of these morphological changes are thought to improve stability and mechanical advantage for terrestrial bipedalism by significantly increasing effective limb length, altering muscle attachment sites and lever arms, and modifying joints for the greater stability required for bearing weight entirely upon the hind limbs.

Because it is the part of the hind limb that is in direct contact with the substrate, the foot must adapt to changing locomotor repertoires over time. Thus, the functional morphology of the primate foot is of utmost relevance to reconstructing locomotor behavior from the fossil record. Most primates are characterized by a grasping foot that facilitates both arboreal and terrestrial locomotion to varying degrees depending on the species and its habitat use. This is accomplished by a widely abducted hallux that has been present at least since the ancestor of Euprimates (Bloch and Boyer, 2002), and opposes the highly internally rotated lesser toes in apes (Morton, 1922; Drapeau and Harmon, 2013). Amongst extant primates, humans are the sole exception to this pattern and instead possess a permanently adducted hallux. The human foot is further distinguished from that of other apes by its reduced toe length (Ray 2 – 5; Susman, 1983), primarily accomplished by reduced phalangeal length (Indjeian et al., 2016), a relatively elongate tarsus (Susman, 1983), stable midfoot joints (DeSilva, 2010; Proctor, 2010b), and the presence of a longitudinal arch supported by bony and soft tissue structures (Morton, 1922; Elftman and Manter, 1935b; Lewis, 1980; Susman, 1983). The robust, adducted human hallux and the rest of the forefoot (i.e., metatarsophalangeal—MTP) joints act in concert with soft tissue structures in the midfoot (Hicks, 1954), to render the human foot into a stiff, propulsive lever that does not deform much during terrestrial bipedality (Morton, 1922, 1924; Elftman and Manter, 1935b, a; Lewis, 1980; Gomberg, 1985; Sarrafian, 1987; Harcourt-Smith and Aiello, 2004; but see Bates et al., 2013; DeSilva and Gill, 2013). The principal soft tissue structure in the midfoot interacting with the MTPJs is the plantar aponeurosis—a strong layer of fibrous tissue that originates at the calcaneal tuberosity and terminates distally unto the proximal phalangeal (PP) base at each of the MTPJs. The plantar aponeurosis is tightened when the MTPJs are in dorsiflexion (i.e., extension); this action both stiffens the midfoot and raises the height of the longitudinal arch just prior to lift-off at the end of stance phase. Chimpanzees lack or demonstrate a very weakly developed plantar aponeurosis in comparison to humans (Susman, 1983; pers. obs.) and this is likely because they lack this interaction between the midfoot and forefoot (i.e., the windlass mechanism; Hicks, 1954). Given this fundamental difference between apes and humans at the

forefoot, hypotheses about forefoot functional morphology have been proposed by several researchers since Hicks (Bojsen-Møller, 1979; Stern and Susman, 1983; Latimer and Lovejoy, 1990a), and essentially posit that a more dorsally oriented MTPJ morphology (metatarsal and phalangeal) should facilitate increased dorsiflexion range of motion (ROM) at the MTPJs, allowing the foot to undergo the human-like midfoot stiffening needed for increased propulsion and stability during walking. A more plantarly oriented MTPJ morphology is hypothesized to increase plantarflexion ROM for arboreal pedal grasping because the joint curvature is maximally oriented plantarly (Stern and Susman, 1983; Hamrick, 1996; Ward et al., 2011).

Despite their hypothesized importance in hominin gait reconstruction, many aspects MTPJ morphology have not been rigorously investigated using quantitative measures. Some researchers have qualitatively described dorsally oriented MT heads as those whose articular surface projects superiorly above the MT shaft (diaphysis) as "dorsally domed" (Latimer et al., 1982; Lovejoy et al., 2009; Ward et al., 2011; DeSilva et al., 2012; Haile-Selassie et al., 2012). In addition to dorsal orientation, other researchers have emphasized mediolateral expansion of the dorsal aspect of the MT head as necessary for joint stability under increased loads such as during a modern human-like push off mechanism. Distal dorsal expansion of the MT head allows for "close-packing" of the synovial MTPJs via tightening of the collateral MTP ligaments in the dorsiflexed configuration; in the close-packed position, the contact surface of the MT head and PP base articular surfaces is maximized and tightening of collateral ligaments limits joint motion in other anatomical planes of motion when the MTPJs are dorsiflexed, thus increasing joint stability when maximum joint congruency is achieved (MacConaill and Basmajian, 1969; Stern and Susman, 1983; Susman et al., 1984; Susman and Brain, 1988; Susman and de Ruiter, 2004). Researchers have argued that "dorsal canting" of the pedal phalangeal base is functionally related to increased MTPJ dorsiflexion excursions as well (Latimer and Lovejoy, 1990a; Duncan et al., 1994; Haile-Selassie, 2001; Kimbel and Delezene, 2009; Griffin and Richmond, 2010). Dorsal canting has been described as a dorsally oriented slant to the phalangeal base seen in humans, some hominoids (Griffin and Richmond, 2010), but not in other anthropoids. Other researchers have noted a dorsally extended rim of bone corresponding with a deeply excavated phalangeal base (Latimer et al., 1982) in addition to dorsal canting as important for human-like bipedalism. One main component to this dissertation is to provide a detailed morphometric quantification the subtle shape differences that exist between extant and fossil primate MTPJs in

a broad phylogenetic context to verify (or refute) the currently existing hypotheses about forefoot functional morphology (described above).

1.2 Background

1.2.1: Functional morphology of the metatarsals

Metatarsal form and function differs greatly throughout the primate order. In strepsirrhines, the hallux is widely abducted and articulates at a saddle joint with the medial cuneiform (Gebo, 1993, 2014) whereas in anthropoids this joint is relatively flatter. Humans have the flattest hallucal tarsometatarsal joint which is thought to be predictive of an adducted hallux (Latimer and Lovejoy, 1990b; Harcourt-Smith, 2002). Within anthropoids, the degree of hallucal abduction seems to bear some relationship to terrestriality (Morton, 1924; Tocheri et al., 2011) and although some highly terrestrial primate species (e.g., *Papio*) exhibit shape changes related to terrestriality in MT head morphology (Fernández et al., 2015; see Chapters 2 – 3), it is modern humans and hominins that display the very derived hallucal form—short, robust, and with marked dorsal reorganization of the distal articular surface. The human hallucal head is very mediolaterally expanded and dorsally oriented with articular surface overlapping unto the dorsal diaphysis of the bone. Plantarly, the human hallux is marked by two shallow grooves (contra the oblique, acute facets in apes) for articulation with hallucal sesamoid bones that are thought to protect the tendon of mm. flexor hallucis longus (Richardson, 1999; Stern, pers. comm.) and increase the moment arm of mm. flexor hallucis brevis (Aper et al., 1996), a muscle which is comparatively large in humans and thought to generate additional power at the first MTPJ during push off (Aiello and Dean, 1990). Because the longitudinal arch is most pronounced medially and collapsed laterally during the support phase (Palastanga et al., 2002), the human distal tarsal bones are raised from the ground on the medial side, and the bases of the more medial metatarsals along with them (e.g., MT 1 – MT 3). When moving across the transverse tarsal joint laterally however, the longitudinal arch of the foot is less pronounced, and the tarsal and metatarsal bases more plantarly situated. This results in internally rotated MT bases which necessitates external rotation of the MT head about the diaphysis to allow the plantar surface of the MT head to rest on the substrate (Morton, 1922; Elftman and Manter, 1935b; Drapeau and Harmon, 2013). Consequently, the hallux and MT 2 in humans do not show much MT head torsion, whereas MT 3 – 5 demonstrate pronounced torsion (i.e., external rotation). This is in

contrast to apes, whose feet lack a longitudinal arch but possess a transverse arch (Weidenreich, 1923; Elftman and Manter, 1935a; Sarmiento, 1994). In apes, the hallux is strongly externally rotated so as to oppose the lesser toes. Within the lesser toes, MT 2 demonstrates pronounced internal rotation to allow opposition with the ape hallux. The remainder of the lesser toes demonstrate little torsion relative to the MT base, but are oriented such that the plantar surface faces the hallux for grasping (Drapeau and Harmon, 2013). Cercopithecoid monkeys, who also lack a fully developed plantar aponeurosis (but see Sarmiento, 1983) and have a very flexible midfoot (DeSilva, 2010), demonstrate a different pattern. The cercopithecoid hallux is less externally rotated like in humans, the MT 2 is internally rotated in colobines but is more human-like in terrestrial cercopithecines, and the remaining cercopithecoid lesser toes all demonstrate external rotation, like that of humans (Drapeau and Harmon, 2013).

The hallucal form of hominins is well preserved in the fossil record, and currently fossil hominins represented by hallucal remains include (in chronological order): *Ardipithecus ramidus* (Lovejoy et al., 2009), the 'Burtele hominin' (Haile-Selassie et al., 2012), *Australopithecus afarensis* (Stern and Susman, 1983; Latimer and Lovejoy, 1990b), various unattributed South African specimens likely belonging either to *Australopithecus*, *Paranthropus*, or early *Homo* (Susman and Brain, 1988; Susman, 1989; Susman and de Ruiter, 2004; Zipfel et al., 2009; DeSilva et al., 2012), early *Homo* from east Africa (Day and Napier, 1964; Kidd et al., 1996; Jungers et al., 2015), the Dmanisi hominins (Lordkipanidze et al., 2007; Pontzer et al., 2010), *Homo neanderthalensis* (Trinkaus, 1983), *Homo floresiensis* (Jungers et al., 2009), and the recently described *Homo naledi* from Gauteng, South Africa (Berger et al., 2015; Harcourt-Smith et al., 2015). Of these hallucal metatarsals, the grand majority do not look entirely human-like, although they have generally been described as such. However, many of these hominins demonstrate at least some of the derived traits associated with humans. The earlier hominins (i.e., *Ardipithecus*) possess a very ape-like hallux, whereas *Australopithecus* is more intermediate in its morphology. *Au. afarensis* demonstrates a more adducted hallux with a more dorsally oriented hallucal head compared to *Ardipithecus*, but lacks the robust widening observed in humans and later hominins. The same is true for much of the South African material, the Dmanisi hominins, the Burtele foot, and early *Homo*. While the *H. floresiensis* MT 1 certainly is robust, it is not entirely human-like either (Jungers et al., 2009). Peculiarly, the *H. naledi* foot looks essentially modern (Harcourt-Smith et al., 2015) although it looks more primitive (i.e., like

early *Homo*) elsewhere postcranially and cranially. Firm geochronological dates for this taxon are still unavailable but the material from the Dinaledi chamber is purported to be quite young (Williams, pers. comm.). In modern humans, the non-hallucal metatarsals are generally similar to one another in form, likely because of their serial homology in development (Young et al., 2010). The morphology in the lesser toes is similar to what is seen in the hallux—dorsally oriented and robust MT heads. Non-hallucal specimens are known from the same hominins listed earlier, but additionally there are some notable, isolated lesser toes that have caused debate amongst physical anthropologists. Occasionally, non-hallucal MTs have been considered diagnostic of bipedalism and the presence of a longitudinal arch (Ward et al., 2011; an MT 4) based on the qualitative assessment of its MT head shape and orientation. Another controversial fossil is the isolated MT 2 from South Africa, StW 89 (Deloison, 2003; DeSilva et al., 2012), which has proven to be quite vexing because it lacks any associated craniodental remains, and presents with a strange mosaicism that looks neither entirely ape nor human-like. The *Ardipithecus* assemblage includes a nearly intact MT 3, which has been argued to look quite human-like (Lovejoy et al., 2009). There has been considerable variation in the *Au. afarensis* metatarsals, with some looking more derived than others (Latimer et al., 1982). Other material from early *Homo* has been described as looking essentially human-like. Although the functional morphology of the hominin forefoot joints has been discussed thoroughly, it has principally only been discussed in qualitative terms. However, subjective measures of functional morphology often fail or are subject to biases. First, qualitative descriptions of the pedal morphology in question tend to vary somewhat between studies (Latimer et al., 1982; Susman, 1983; Susman and Brain, 1988; Latimer and Lovejoy, 1990a; Lovejoy et al., 2009; Ward et al., 2011; Drapeau and Harmon, 2013), which makes it difficult to pin down what is being analyzed. Second, although many fossil hominins appear human-like in one aspect of MT head morphology, most are mosaic, and display mosaicism in different ways. The *Ardipithecus* MT 1 and StW 89 may have some dorsal orientation present in the MT head, but the majority of the articular surface is still oriented plantarly. When viewed distally, many of these fossils, particularly the South African material and the Dmanisi bones of similar age, lack the derived dorsal widening and flattening of the dorsal metatarsal head, and instead more closely resemble the chimpanzee condition. This has recently been observed in similarly aged east African hominins as well (Jungers et al., 2015). Additionally, a known but undescribed right MT 1 from the Baringo

district in Kenya, KNM-BK 63 (~500 Ka) attributed to *Homo* cf. *erectus* (Leakey et al., 1970; Solan and Day, 1992; Deino and McBrearty, 2002; Fisher and MBrearty, 2002) has also been qualitatively described as lacking robusticity (Meldrum, 2007). KNM-BK 63 shows a little more robusticity than the earlier *Homo* material, but the plantar surface has deep, obliquely slanted facets for the hallucal sesamoids that look chimpanzee-like and unlike the shallow grooves seen in modern humans. If these MTPJ morphologies reflect function in that they are adaptations to terrestrial bipedalism, then we should expect to see some of these characters in other primates who are also very terrestrial, as these groups are putting biomechanical demands upon their MTPJs similar to those forth put in the MTPJs of humans.

1.2.2: Functional morphology of the proximal pedal phalanges

Morphological properties of the proximal phalanges (both pedal and manual) have long been thought to be reflective of substrate use in primates. The bones of the hand of foot that are in frequent and repetitive contact with arboreal substrates must be able to resist bending strains incurred during both manual and pedal grasping, and this is thought to be the mechanism which drives increased phalangeal curvature (Preuschoft, 1970) seen in many extant and fossil hominoids. In addition to phalangeal curvature, different metrics capturing a variety of phalangeal morphological properties, including relative lengths, robusticities, and proportions have been used to infer the locomotor behavior of extinct hominins, hominoids, and primates more generally (Susman, 1979; Bush et al., 1982; Latimer et al., 1982; Stern and Susman, 1983; Latimer and Lovejoy, 1990a; Stern et al., 1995; Jungers et al., 1997; Alba et al., 2003; Almécija et al., 2007; Deane and Begun, 2008; Almécija et al., 2009; Patel, 2009; Alba et al., 2010; Almécija et al., 2015). In particular, the discovery of a largely intact *Australopithecus afarensis* forefoot in Hadar (A.L. 333-115; Latimer et al., 1982) has offered researchers much insight into forefoot functional morphology of this Pliocene hominin. Some work has shown that the hominins represented at the 333 locality likely practiced both arboreal and terrestrial locomotion (Stern and Susman, 1983; ; Susman et al., 1984), but other workers have disagreed with this interpretation (Latimer and Lovejoy, 1990a; Ward, 2002). As part of their counterargument, Latimer and Lovejoy (1990a) remarked on the proximal phalangeal base orientation of the Hadar fossils, and how they, like human phalanges, possessed a pronounced dorsal slant (i.e., "dorsal canting"). This property was a qualitative assessment of the proximal pedal base orientation

when a given pedal phalanx was laid flat on a substrate. Those specimens with dorsal canting exhibited a dorso-distal slant to the phalangeal base, which in humans is terminated by a pronounced dorsal rim of bone that some believe acts as a bony "stop" during high dorsiflexion excursions (Latimer et al., 1982), similar to the stabilizing morphologies seen in the weight bearing rays of knuckle-walking primates that prevent hyperextension of the metacarpophalangeal joints (Tuttle, 1967; Tuttle, 1970). Since then, new hominin pedal phalangeal fossils have been described as dorsally canted, and sometimes this feature alone becomes diagnostic of bipedalism in a hominin (Haile-Selassie et al., 2001). There are serious pitfalls to the dorsal canting quantification techniques used so far (see Section 1.2.4), and therefore a more robust quantification of this morphology is needed. In addition to quantifying this morphology for many of the known hominin pedal phalanges, three new PPs will also be included in this dissertation, including two unpublished hallucal phalanges from Liang Bua (Tocheri, pers. comm.), and an unpublished hallucal phalanx from the newly discovered foot from East Turkana, KNM-ER 64062 (Jungers et al., 2015).

1.2.3 The role of foot posture and substrate use on forefoot morphology and mechanics

Modern humans begin stance phase of the gait cycle with a heel-strike followed by full-contact plantigrady (FCP), where the entire plantar surface of the foot is in contact with the substrate at mid-stance before pushing off from dorsiflexed toes at the end of stance. During push off, the plantar aponeurosis is taut and the longitudinal arch of the foot is raised. Most monkeys have a plantar aponeurosis that originates from the plantaris tendon that serves to plantarflex the foot (Sarmiento, 1983; Nowak et al., 2010); in apes, the plantar aponeurosis is less developed than in humans (Susman, 1983; pers. obs.), which contributes to more midfoot flexibility—a likely adaptation to locomotion on arboreal substrates (Schmitt and Larson, 1995; Vereecke et al., 2003; DeSilva, 2010; Nowak et al., 2010). In addition to these soft tissue differences, apes and monkeys demonstrate different foot postures during locomotion. Unlike the well characterized pedal posture of modern humans, the foot posture of other primates has been the subject of much debate (Morton, 1922, 1924; Tuttle, 1970; Gebo, 1992, 1993; Schmitt and Larson, 1995; Vereecke et al., 2003; Nowak et al., 2010). Although great apes were once grouped under a common category of "heel-strike plantigrady" with humans (Schmitt and Larson, 1995), later work (Vereecke et al., 2003; Nowak et al., 2010) has further divided the

category of "plantigrady" (complete heel contact with the substrate at some point during support phase) into inverted heel-strike plantigrady (IHSP) versus full-contact plantigrady in order to account for the different configuration of the ape foot at initial ground contact in comparison to humans. In great apes, it is mostly the lateral side of the foot which is frequently in contact with the substrate (Vereecke et al., 2003). In lesser apes, the heel makes contact with the substrate at the same time as the midfoot and they are thus distinct from the heel-striking great apes("mid-foot plantigrade" ,MFP); Atelines also adopt this foot posture, and this may be an example of convergent evolution (Gebo, 1992). Although no anthropoid is purely digitigrade (Patel, pers. comm.), other anthropoids can be grouped into the well-defined categories laid out in Schmitt and Larson (1995) as exhibiting varying degrees of "digitigrady" (DG; where the heads of the metatarsals bear weight during support phase but the remainder of the foot does not contact the substrate) and "semiplantigrady" (SP; when some portion of the plantar surface, but not the entire heel, contacts the substrate at any point during support phase). Differences in foot posture (Schmitt and Larson, 1995; Vereecke et al., 2003; Nowak et al., 2010) are relevant to forefoot functional morphology because in a digitigrade/semi-digitigrade (DG/SP) posture, the ankle (talocrural) joint is plantarflexed, thus leaving the MTPJs in a habitually dorsiflexed configuration; in the full plantigrade foot posture, the MTP joints are not habitually dorsiflexed.

In addition to foot posture, substrate use is thought to play a dramatic role in the form of the forefoot. Terrestrial species such as baboons and patas monkeys have been observed to regularly dorsiflex their forefoot joints to human-like excursions (Meldrum, 1991) and thus these joints would presumably be subjected to similar loading conditions to humans, although markedly reduced because of body size differences and the spreading of load across a quadrupedal gait. There is some experimental evidence that supports the notion that terrestrial taxa are better equipped to utilize their forefoot joints in dorsiflexion, with the more terrestrial African apes (Doran, 1992, 1993; Doran, 1996; Doran and McNeilage, 1998; Fleagle, 2013) demonstrating much more MTPJ dorsiflexion capability than the more arboreal orangutan (55° vs 20°; Tuttle, 1970). That said, although African apes have the physical capability to dorsiflex their forefoot joints to the level seen in humans, they rarely do so. *In vivo* kinematic comparisons between humans and African apes demonstrate that humans stereotypically dorsiflex all of their MTPJs to high excursions (Caravaggi et al., 2009; Griffin et al., 2010a; Holowka and Fernández, 2016; see Chapter 6) during bipedal walking, whereas African apes dorsiflex their MTPJs

significantly less. Within genera, some species and individuals within species are more terrestrial due to food acquisition or large body size (Doran, 1997; Tocheri et al., 2011), and so it is possible for closely related species that employ divergent positional behaviors to have these differences reflected in their forefoot morphology, and this has already been observed more proximally in the lower limb in groups of closely related monkeys (Strasser, 1992; Gebo and Sargis, 1994; Polk, 2004) and apes (Tocheri et al., 2011; Dunn et al., 2014; Knigge et al., 2015; Tocheri et al., 2016). Clinical studies have revealed that pathological reduction of MTPJ dorsiflexion ROM is significantly correlated with reduced stride length and walking velocity (Laroche et al., 2006), and it is reasonable to suspect that primitive retentions in hominin MTPJ morphology that may reduce MTPJ dorsiflexion ROM or stability such as the plantarly oriented MT head in StW 89 or the ML narrow dorsal MT 1 heads seen many early hominin fossils would at minimum reduce walking velocity and perhaps increase cost of transport when adopting a modern human-like striding bipedal gait. Thus, it is critical to quantify the morphological differences between fossil hominins, modern humans, and other extant primates with a diverse repertoire of locomotor behaviors in order to tease apart subtleties in the MTPJ characters associated with function

1.2.4 Previous investigations of MTPJ functional morphology

Qualitative descriptions of MT head "dorsal doming" are often reported in the hominin pedal fossil literature (Stern and Susman, 1983; Susman and Brain, 1988; Susman and de Ruiter, 2004; Jungers et al., 2009; Lovejoy et al., 2009; Ward et al., 2011; DeSilva et al., 2012; Haile-Selassie et al., 2012; Harcourt-Smith et al., 2015), but quantitative data on distal MT surface morphology is lacking (but see Congdon et al., (2011) for an abstract using a non-landmark 3D based approach), making it difficult to ascertain more precisely the functional importance of dorsal MT head orientation and dorsal MT head expansion to modern human-like bipedalism. While modern human MTs have both of these morphologies, fossil hominin MTs sometimes lack one of these features (Pontzer et al., 2010; DeSilva et al., 2012). Griffin et al. (2010b) approached MTPJ functional morphology using high resolution μCT scans of internal bone structure to quantify differences between humans and apes. However, results from this study were inconsistent in that only one standard metric of internal bone anatomy, anisotropy, reliably separated humans from other taxa. Additionally, recent protocols developed on the analyses of

trabecular bone architecture caution that these studies are critically sensitive to volume of interest (VOI) size and location, especially in smaller bones with complex arthroses such as those of the hands and feet (Kivell et al., 2011). Because Griffin et al. (2010b) used ROIs instead of capturing all of the trabecular architecture globally in their study, results from this work may be driven by aspects of the ROI as well as functional differences reflected in the trabecular structure.

Dorsal canting of the phalangeal base was quantified using linear metrics not long after its introduction into the literature (Latimer et al., 1982; Stern and Susman, 1983; Latimer and Lovejoy, 1990a) by Duncan and colleagues (1994). Their results demonstrated considerable overlap between hominoids (e.g., *Gorilla*) and humans in terms of canting angle. Since researchers have hypothesized that dorsal canting of the phalangeal base is predictive of human-like joint mechanics in the forefoot (i.e., high MTPJ dorsiflexion angles at the end of stance phase), these results were difficult to interpret. The quantification of dorsal phalangeal canting has since been revisited several times (Rein and Harrison, 2007; Griffin and Richmond, 2010; Rein, 2011; Rein and McCarty, 2012) but has only been quantified using the same or similar indirect measure of canting angle that does not completely characterize a complex joint surface like the phalangeal base (MacLatchy and Bossert, 1996), and the functional morphology of pedal phalangeal base morphology is still unclear. One limitation of dorsal phalangeal canting as measured in prior work (Duncan et al., 1994; Griffin and Richmond, 2010) is that it can only be assessed on complete specimens. Since many pedal phalangeal fossils are fragmentgary (see Chapter 4), another method robust to fragmentary specimens is needed to test hypotheses about forefoot functional morphology in hominins. With the expanding array of pedal material described in recent years since the fossil discoveries at Hadar (Jungers et al., 2009; Lovejoy et al., 2009; Haile-Selassie et al., 2012; Harcourt-Smith et al., 2015; Jungers et al., 2015), now is an ideal time to apply new methods that can potentially capture functional differences in phalangeal base morphology without relying on complete specimens.

1.3. Goals of Dissertation

The goal of this dissertation is to 1) gain a better understanding of the functional morphology of the MTPJs 2) discern whether the hypothesized functional characters of the forefoot are strictly bipedal adaptations, or more generalizable adaptations to increased

terrestriality in a given lineage 3) attempt to better understand the evolutionary MTPJ shape changes that occurred in the hominin lineage, in order to reconstruct the timeline for foot evolution 4) gain a better understanding of how the MTPJs function together as a covarying unit, and 5) to explore whether these hypothesized functional properties of the MTPJs effect function as measured by experimental data. Because of the disproportionate role hallucal metatarsal head in forefoot biomechanics, Chapter 2 solely investigates its functional morphology of the in a diverse sample of extant anthropoids and extinct hominins by using 3-dimensional geometric morphometric (3DGM) techniques so that the form of the MT head can be captured in an *a priori* manner without any assumptions of what the derived morphologies "should" look like. Afterwards, modern phylogenetic analyses are conducted in order to speak to the evolution of shape in the hallucal head throughout anthropoids and hominins. Chapter 3 investigates the functional morphology of the lesser metatarsals (MT 2 – MT 5) using the same 3DGM and phylogenetic techniques employed in Chapter 2. Chapter 4 examines the functional morphology of the proximal pedal phalangeal base (PP 1, 3, 5) using the same multivariate 3DGM and phylogenetic techniques employed in Chapter 2 and 3. Chapter 5 brings together data sets from Chapter 2, 3 and 4 in an analysis of covariance in order to determine how the shape changes in one aspect of the MTPJs track shape changes in another. The MTPJ covariance was explored in MTPJs 1, 3 and 5. This allows us to view broad patterns in forefoot joint evolution in anthropoids, and also gives information as to which pedal rays are covarying more than others. Chapter 6 provides an experimental test of the hypothesized forefoot functional morphologies by examining the relationship between form and function using 3D kinematic and morphometric data. Chapter 7 summarizes the findings of this dissertation and provides avenues of future research to explore based on the conclusions drawn here. Taken together, the chapters provide novel morphological signals that can be used to more accurately assess the locomotor behavior of extinct hominins, and serves as a robust dataset for the interpretation of future fossil pedal material.

1.4 References

Aiello, L., Dean, C., 1990. An introduction to human evolutionary anatomy. Academic Press, London.

Alba, D.M., Almécija, S., Moyà-Solà, S., 2010. Locomotor inferences *in Pierolapithecus* and *Hispanopithecus:* Reply to. J. Hum. Evol. 59, 143-149.

Alba, D.M., Moyà-Solà, S., Köhler, M., 2003. Morphological affinities of the *Australopithecus afarensis* hand on the basis of manual proportions and relative thumb length. J. Hum. Evol. 44, 225-254.

Almécija, S., Alba, D.M., Moyà-Solà, S., 2009. Pierolapithecus and the functional morphology of Miocene ape hand phalanges: paleobiological and evolutionary implications. J. Hum. Evol. 57, 284-297.

Almécija, S., Alba, D.M., Moyà-Solà, S., Köhler, M., 2007. Orang-like manual adaptations in the fossil hominoid *Hispanopithecus laietanus*: first steps towards great ape suspensory behaviours. Proc. Royal Soc. B. 274, 2375-2384.

Almécija, S., Moyà-Solà, S., Alba, D.M., 2010. Early origin for human-like precision grasping: a comparative study of pollical distal phalanges in fossil hominins. PLoS ONE 5, e11727.

Almécija, S., Smaers, J.B., Jungers, W.L., 2015. The evolution of human and ape hand proportions. Nat. Commun. 6.

Aper, R.L., Saltzman, C.L., Brown, T.D., 1996. The effect of hallux sesamoid excision on the flexor hallucis longus moment arm. Clinical Orthopaedics and Related Research 325, 209-217.

Bates, K.T., Collins, D., Savage, R., McClymont, J., Webster, E., Pataky, T.C., D'Aout, K., Sellers, W.I., Bennett, M.R., Crompton, R.H., 2013. The evolution of compliance in the human lateral mid-foot. Proc. Royal Soc. B. 280, 20131818.

Berger, L.R., de Ruiter, D.J., Churchill, S.E., Schmid, P., Carlson, K.J., Dirks, P.H.G.M., Kibii, J.M., 2010. *Australopithecus sediba*: a new species of *Homo*-like australopith from South Africa. Science 328, 195-204.

Berger, L.R., Hawks, J., de Ruiter, D.J., Churchill, S.E., Schmid, P., Delezene, L.K., Kivell, T.L., Garvin, H.M., Williams, S.A., DeSilva, J.M., Skinner, M.M., Musiba, C.M., Cameron, N., Holliday, T.W., Harcourt-Smith, W., Ackermann, R.R., Bastir, M., Bogin, B., Bolter, D., Brophy, J., Cofran, Z.D., Congdon, K.A., Deane, A.S., Dembo, M., Drapeau, M., Elliott, M.C., Feuerriegel, E.M., Garcia-Martinez, D., Green, D.J., Gurtov, A., Irish, J.D., Kruger, A., Laird, M.F., Marchi, D., Meyer, M.R., Nalla, S., Negash, E.W., Orr, C.M., Radovcic, D., Schroeder, L., Scott, J.E., Throckmorton, Z., Tocheri, M.W., VanSickle, C., Walker, C.S., Wei, P., Zipfel, B., 2015. *Homo naledi*, a new species of the genus *Homo* from the Dinaledi Chamber, South Africa. eLife 4.

Bloch, J.I., Boyer, D.M., 2002. Grasping primate origins. Science 298, 1606-1610.

Bojsen-Møller, F., 1979. Calcaneocuboid joint and stability of the longitudinal arch of the foot at high and low gear push off. J. Anat. 129, 165-176.

Bush, M.E., Lovejoy, C.O., Johanson, D.C., Coppens, Y., 1982. Hominid carpal, metacarpal, and phalangeal bones recovered from the Hadar formation: 1974–1977 collections. Am. J. Phys. Anthropol. 57, 651-677.

Caravaggi, P., Pataky, T., Goulermas, J.Y., Savage, R., Crompton, R., 2009. A dynamic model of the windlass mechanism of the foot: evidence for early stance phase preloading of the plantar aponeurosis. J. Exp. Biol. 212, 2491-2499.

Clarke, R., Tobias, P., 1995. Sterkfontein member 2 foot bones of the oldest South African hominid. Science 269, 521-524.

Congdon, K.A., Ward, C.V., Kimbel, W.H., 2011. The first complete fourth metatarsal of *Australopithecus afarensis* from Hadar. Ethiopia. Am. J. Phys. Anthropol. 144, 111.

Day, M., Napier, J., 1964. Hominid fossils from Bed I, Olduvai Gorge, Tanganyika: fossil foot bones. Nature 201, 969-970.

Deane, A.S., Begun, D.R., 2008. Broken fingers: retesting locomotor hypotheses for fossil hominoids using fragmentary proximal phalanges and high-resolution polynomial curve fitting (HR-PCF). J. Hum. Evol. 55, 691-701.

Deino, A.L., McBrearty, S., 2002. $^{40}Ar/^{39}Ar$ dating of the Kapthurin Formation, Baringo, Kenya. J. Hum. Evol. 42, 185-210.

Deloison, Y., 2003. Anatomie des os fossils de pieds des hominids d'Afrique du suddates entre 2,4 et 3,5 millions d'annés. Interprétation quant à leur mode de locomotion. Biométrie Hum. Anthropol. 21, 189-230.

DeSilva, J.M., 2010. Revisiting the "midtarsal break". Am. J. Phys. Anthropol. 141, 245-258.

DeSilva, J.M., Gill, S.V., 2013. Brief communication: a midtarsal (midfoot) break in the human foot. Am. J. Phys. Anthropol. 151, 495-499.

DeSilva, J.M., Proctor, D.J., Zipfel, B., 2012. A complete second metatarsal (StW 89) from Sterkfontein Member 4, South Africa. J. Hum. Evol. 63, 487-496.

Doran, D.M., 1992. The ontogeny of chimpanzee and pygmy chimpanzee locomotor behavior: a case study of paedomorphism and its behavioral correlates. J. Hum. Evol. 23, 139-157.

Doran, D.M., 1993. Sex differences in adult chimpanzee positional behavior: the influence of body size on locomotion and posture. Am. J. Phys. Anthropol. 91, 99-115.

Doran, D.M., 1996. Comparative positional behavior of the African apes, in: McGrew, W.C., Marchant, L.F., Nishida, T. (Eds.), Great ape societies University Press, Cambridge, pp. 213-224-.

Doran, D.M., 1997. Ontogeny of locomotion in mountain gorillas and chimpanzees. J. Hum. Evol. 32, 323-344.

Doran, D.M., McNeilage, A., 1998. Gorilla ecology and behavior. Evol. Anthropol. 6, 120-131.

Drapeau, M.S.M., Harmon, E.H., 2013. Metatarsal torsion in monkeys, apes, humans and australopiths. J. Hum. Evol. 64, 93-108.

Duncan, A.S., Kappelman, J., Shapiro, L.J., 1994. Metatarsophalangeal joint function and positional behavior in *Australopithecus afarensis*. Am. J. Phys. Anthropol. 93, 67-81.

Dunn, R.H., Tocheri, M.W., Orr, C.M., Jungers, W.L., 2014. Ecological divergence and talar morphology in gorillas. Am. J. Phys. Anthropol. 153, 526-541.

Elftman, H., Manter, J., 1935a. Chimpanzee and human feet in bipedal walking. Am. J. Phys. Anthropol. 20, 69-79.

Elftman, H., Manter, J., 1935b. The evolution of the human foot, with especial reference to the joints. J. Anat. 70, 56-67.

Fernández, P.J., Almécija, S., Patel, B.A., Orr, C.M., Tocheri, M.W., Jungers, W.L., 2015. Functional aspects of metatarsal head shape in humans, apes, and Old World monkeys. J. Hum. Evol. 86, 136-146.

Fisher, R., MBrearty, S., 2002. The comparative morphology of hominin postcranial remains from the Kaputhrian formation, Baringo district, Kenya. Am. J. Phys. Anthropol. 34, 70.

Fleagle, J.G., 2013. Primate adaptation and evolution. Academic Press, San Diego.

Gebo, D.L., 1992. Locomotor and postural behavior in *Alouatta palliata* and *Cebus capucinus*. Am. J. Primatol. 26, 277-290.

Gebo, D.L., 1993. Postcranial adaptation in nonhuman primates. Northern Illinois University Press, DeKalb.

Gebo, D.L., 2014. Primate comparative anatomy. Johns Hopkins University Press, Baltimore

Gebo, D.L., Sargis, E.J., 1994. Terrestrial adaptations in the postcranial skeletons of guenons. Am. J. Phys. Anthropol. 93, 341-371.

Gomberg, D.N., 1985. Functional differences of three ligaments of the transverse tarsal joint in hominoids. J. Hum. Evol. 14, 553-562.

Grabowski, M.W., Polk, J.D., Roseman, C.C., 2011. Divergent patterns of integration and reduced constraint in the human hip and the origins of bipedalism. Evolution 65, 1336-1356.

Green, D.J., Alemseged, Z., 2012. *Australopithecus afarensis* scapular ontogeny, function, and the role of climbing in human evolution. Science 338, 514-517.

Griffin, N.L., D'Août, K., Richmond, B., Gordon, A., Aerts, P., 2010a. Comparative in vivo forefoot kinematics of *Homo sapiens* and *Pan paniscus*. J. Hum. Evol. 59, 608-619.

Griffin, N.L., D'Août, K., Ryan, T.M., Richmond, B.G., Ketcham, R.A., Postnov, A., 2010b. Comparative forefoot trabecular bone architecture in extant hominids. J. Hum. Evol. 59, 202-213.

Griffin, N.L., Richmond, B.G., 2010. Joint orientation and function in great ape and human proximal pedal phalanges. Am. J. Phys. Anthropol. 141, 116-123.

Haile-Selassie, Y., 2001. Late Miocene hominids from the Middle Awash, Ethiopia. Nature 412, 178-181.

Haile-Selassie, Y., Saylor, B.Z., Deino, A., Levin, N.E., Alene, M., Latimer, B.M., 2012. A new hominin foot from Ethiopia shows multiple Pliocene bipedal adaptations. Nature 483, 565-569.

Hamrick, M.W., 1996. Articular size and curvature as determinants of carpal joint mobility and stability in strepsirhine primates. J. Morphol. 230, 113-127.

Harcourt-Smith, W.E.H., 2002. Form and function in the hominoid tarsal skeleton. University College London.

Harcourt-Smith, W.E.H., Aiello, L.C., 2004. Fossils, feet and the evolution of human bipedal locomotion. J. Anat. 204, 403-416.

Harcourt-Smith, W.E.H., Throckmorton, Z., Congdon, K.A., Zipfel, B., Deane, A.S., Drapeau, M.S.M., Churchill, S.E., Berger, L.R., DeSilva, J.M., 2015. The foot of *Homo naledi*. Nat. Commun. 6.

Hicks, J.H., 1954. The mechanics of the foot: II. the plantar aponeurosis and the arch. J. Anat. 88, 25-30.21.

Holowka, N.B., Fernández, P.J., 2016. Functional morphology of the metatarsophalangeal joints in chimpanzees and humans: a kinematic and morphometric approach. Am. J. Phys. Anthropol. 159, 176.

Indjeian, Vahan B., Kingman, Garrett A., Jones, Felicity C., Guenther, Catherine A., Grimwood, J., Schmutz, J., Myers, Richard M., Kingsley, David M., 2016. Evolving new skeletal traits by cis-regulatory changes in bone morphogenetic proteins. Cell 164, 45-56.

Johanson, D.C., Lovejoy, C.O., Kimbel, W.H., White, T.D., Ward, S.C., Bush, M.E., Latimer, B.M., Coppens, Y., 1982. Morphology of the Pliocene partial hominid skeleton (A.L. 288-1) from the Hadar formation, Ethiopia. Am. J. Phys. Anthropol. 57, 403-451.

Jungers, W.L., Godfrey, L.R., Simons, E.L., Chatrath, P.S., 1997. Phalangeal curvature and positional behavior in extinct sloth lemurs (Primates, Palaeopropithecidae). Proc. Nat. Acad. Sci. 94, 11998-12001.

Jungers, W.L., Grine, F.E., Leakey, M.G., Leakey, L., Brown, F., Yang, D., Tocheri, M.W., 2015. New hominin fossils from Ileret (Kolom Odiet), Kenya. Am. J. Phys. Anthropol. 156, 181.

Jungers, W.L., Harcourt-Smith, W.E.H., Wunderlich, R.E., Tocheri, M.W., Larson, S.G., Sutikna, T., Due, R.A., Morwood, M.J., 2009. The foot of *Homo floresiensis*. Nature 459, 81-84.

Kidd, R.S., O'Higgins, P., Oxnard, C.E., 1996. The OH8 foot: a reappraisal of the functional morphology of the hindfoot utilizing a multivariate analysis. J. Hum. Evol. 31, 269-291.

Kimbel, W.H., Delezene, L.K., 2009. "Lucy" redux: A review of research on *Australopithecus afarensis*. Am. J. Phys. Anthropol. 140, 2-48.

Kivell, T.L., Skinner, M.M., Lazenby, R., Hublin, J.-J., 2011. Methodological considerations for analyzing trabecular architecture: an example from the primate hand. J. Anat. 218, 209-225.

Knigge, R.P., Tocheri, M.W., Orr, C.M., McNulty, K.P., 2015. Three-dimensional geometric morphometric analysis of talar morphology in extant gorilla taxa from highland and lowland habitats. Anat. Rec. 298, 277-290.

Laroche, D., Pozzo, T., Ornetti, P., Tavernier, C., Maillefert, J.F., 2006. Effects of loss of metatarsophalangeal joint mobility on gait in rheumatoid arthritis patients. Rheumatology 45, 435-440.

Larson, S.G., 2007. Evolutionary transformation of the hominin shoulder. Evol. Anthropol. 16, 172-187.

Larson, S.G., 2009. Evolution of the hominin shoulder: early *Homo*, in: Grine, F.E., Fleagle, J.G., Leakey, R.E. (Eds.), The first humans – origin and early evolution of the genus

Homo: contributions from the third Stony Brook Human Evolution Symposium and Workshop October 3 – October 7, 2006. Springer Netherlands, Dordrecht, pp. 65-75.

Latimer, B., Lovejoy, C.O., 1990a. Metatarsophalangeal joints of *Australopithecus afarensis*. Am. J. Phys. Anthropol. 83, 13-23.

Latimer, B.M., Lovejoy, C.O., 1990b. Hallucal tarsometatarsal joint in *Australopithecus afarensis*. Am. J. Phys. Anthropol. 82, 125-133.

Latimer, B.M., Lovejoy, C.O., Johanson, D.C., Coppens, Y., 1982. Hominid tarsal, metatarsal, and phalangeal bones recovered from the Hadar formation: 1974–1977 collections. Am. J. Phys. Anthropol. 57, 701-719.

Leakey, M., Tobias, P.V., Martyn, J.E., Leakey, R.E.F., 1970. An Acheulean industry with prepared core technique and the discovery of a contemporary hominid mandible at Lake Baringo, Kenya. Prec. Prehist. Soc. 35, 48-76.

Lewis, O.J., 1980. The joints of the evolving foot. Part III. The fossil evidence. J. Anat. 131, 275-298.

Lewis, O.J., 1989. Functional morphology of the evolving hand and foot. Oxford University Press, Oxford.

Lordkipanidze, D., Jashashvili, T., Vekua, A., de Leon, M.S.P., Zollikofer, C.P.E., Rightmire, G.P., Pontzer, H., Ferring, R., Oms, O., Tappen, M., Bukhsianidze, M., Agusti, J., Kahlke, R., Kiladze, G., Martinez-Navarro, B., Mouskhelishvili, A., Nioradze, M., Rook, L., 2007. Postcranial evidence from early *Homo* from Dmanisi, Georgia. Nature 449, 305-310.

Lovejoy, C.O., 2005. The natural history of human gait and posture: part 1. spine and pelvis. Gait & Posture 21, 95-112.

Lovejoy, C.O., Latimer, B., Suwa, G., Asfaw, B., White, T.D., 2009. Combining prehension and propulsion: the foot of *Ardipithecus ramidus*. Science 326, 72, 72e71-72e78.

MacConaill, M.A., Basmajian, J.V., 1969. Muscles and movements. Williams & Williams Baltimore.

MacLatchy, L.M., Bossert, W.H., 1996. An analysis of the articular surface distribution of the femoral head and acetabulum in anthropoids, with implications for hip function in Miocene hominoids. J. Hum. Evol. 31, 425-453.

Marzke, M.W., 1983. Joint functions and grips of the *Australopithecus afarensis* hand, with special reference to the region of the capitate. J. Hum. Evol. 12, 197-211.

McHenry, H., 1975. Biomechanical interpretation of the early hominid hip. J. Hum. Evol. 4, 343-355.

Meldrum, D.J., 1991. Kinematics of the cercopithecine foot on arboreal and terrestrial substrates with implications for the interpretation of hominid terrestrial adaptations. Am. J. Phys. Anthropol. 84, 273-289.

Meldrum, D.J., 2007. Letter to the editor:hyperbipeds—or—from biped to strider. Am. J. Phys. Anthropol. 134, 292-294.

Midlo, C., 1934. Form of hand and foot in primates. Am. J. Phys. Anthropol. 19, 337-389.

Morton, D.J., 1922. Evolution of the human foot. Am. J. Phys. Anthropol. 5, 305-336.

Morton, D.J., 1924. Evolution of the human foot II. Am. J. Phys. Anthropol. 7, 1-52.

Nowak, M.G., Carlson, K.J., Patel, B.A., 2010. Apparent density of the primate calcaneo-cuboid joint and its association with locomotor mode, foot posture, and the "midtarsal break". Am. J. Phys. Anthropol. 142, 180-193.

Palastanga, N., Field, D., Soames, R., 2002. Anatomy and human movement. Butterworth-Heinemann, Oxford.

Patel, B.A., 2009. Not so fast: speed effects on forelimb kinematics in cercopithecine monkeys and implications for digitigrade postures in primates. Am. J. Phys. Anthropol. 140, 92-112.

Polk, J.D., 2004. Influences of limb proportions and body size on locomotor kinematics in terrestrial primates and fossil hominins. J. Hum. Evol. 47, 237-252.

Pontzer, H., Rolian, C., Rightmire, G.P., Jashashvili, T., Ponce de León, M.S., Lordkipanidze, D., Zollikofer, C.P.E., 2010. Locomotor anatomy and biomechanics of the Dmanisi hominins. J. Hum. Evol. 58, 492-504.

Preuschoft, H., 1970. Functional anatomy of the lower extremity, in: Bourne, G.H. (Ed.), The chimpanzee, vol. 3. Karger, Basel, pp. 221-294.

Proctor, D.J., 2010. Three-dimensional morphometrics of the proximal metatarsal articular surfaces of *Gorilla*, *Pan*, *Hylobates*, and shod and unshod humans. University of Iowa.

Rein, T., Harrison, T., 2007. Quantifying the angle of orientation of the metatarsophalangeal joint surface of proximal phalanges in extant primates. Am. J. Phys. Anthropol. 132, 197-197.

Rein, T.R., 2011. The correspondence between proximal phalanx morphology and locomotion: implications for inferring the locomotor behavior of fossil catarrhines. Am. J. Phys. Anthropol. 146, 435-445.

Rein, T.R., McCarty, L.A., 2012. Metacarpophalangeal joint orientation in anthropoid manual phalanges. The Anatomical Record: Advances in Integrative Anatomy and Evolutionary Biology 295, 2057-2068.

Richardson, G.E., 1999. Hallucal sesamoid pain: causes and surgical treatment. Journal of the American Academy of Orthopaedic Surgeons 7, 270-278.

Sarmiento, E.E., 1983. The significance of the heel process in anthropoids. International Journal of Primatology 4, 127-152.

Sarmiento, E.E., 1994. Terrestrial traits in the hands and feet of gorillas. Am. Mus. Novit. 3091, 1-56.

Sarrafian, S.K., 1987. Functional characteristics of the foot and plantar aponeurosis under tibiotalar loading. Foot Ankle 8, 4-18.

Schmitt, D., Larson, S.G., 1995. Heel contact as a function of substrate type and speed in primates. Am. J. Phys. Anthropol. 96, 39-50.

Senut, B., Pickford, M., Gommery, D., Mein, P., Cheboi, K., Coppens, Y., 2001. First hominid from the Miocene (Lukeino Formation, Kenya). C. R. Acad. Sci. Paris Séria IIa 332, 137-144.

Solan, M., Day, M.H., 1992. The Baringo (Kapthurin) ulna. J. Hum. Evol. 22, 307-313.

Stern, J.T., Jungers, W.L., Susman, R.L., 1995. Quantifying phalangeal curvature: An empirical comparison of alternative methods. Am. J. Phys. Anthropol. 97, 1-10.

Stern, J.T., Susman, R.L., 1983. The locomotor anatomy of *Australopithecus afarensis*. Am. J. Phys. Anthropol. 60, 279-317.

Strasser, E., 1992. Hindlimb proportions, allometry, and biomechanics in old world monkeys (Primates, Cercopithecidae). Am. J. Phys. Anthropol. 87, 187-213.

Susman, R.L., 1979. Comparative and functional morphology of hominoid fingers. Am. J. Phys. Anthropol. 50, 215-236.

Susman, R.L., 1983. Evolution of the human foot: evidence from Plio-Pleistocene hominids. Foot Ankle 3, 365-376.

Susman, R.L., 1989. New hominid fossils from the Swartkrans formation (1979–1986 excavations): postcranial specimens. Am. J. Phys. Anthropol. 79, 451-474.

Susman, R.L., 1998. Hand function and tool behavior in early hominids. J. Hum. Evol. 35, 23-46.

Susman, R.L., Brain, T.M., 1988. New first metatarsal (SKX 5017) from Swartkrans and the gait of *Paranthropus robustus*. Am. J. Phys. Anthropol. 77, 7-15.

Susman, R.L., de Ruiter, D.J., 2004. New hominin first metatarsal (SK 1813) from Swartkrans. J. Hum. Evol. 47, 171-181.

Susman, R.L., Stern, J.J.T., Jungers, W.L., 1984. Arboreality and bipedality in the Hadar hominids. Folia Primatol. 43, 113-156.

Tocheri, M.W., Dommain, R., McFarlin, S.C., Burnett, S.E., Troy Case, D., Orr, C.M., Roach, N.T., Villmoare, B., Eriksen, A.B., Kalthoff, D.C., Senck, S., Assefa, Z., Groves, C.P.,

Jungers, W.L., 2016. The evolutionary origin and population history of the grauer gorilla. Am. J. Phys. Anthropol. 159, 4-18.

Tocheri, M.W., Orr, C.M., Larson, S.G., Sutikna, T., Jatmiko, Saptomo, E.W., Due, R.A., Djubiantono, T., Morwood, M.J., Jungers, W.L., 2007. The primitive wrist of *Homo floresiensis* and its implications for hominin evolution. Science 317, 1743-1745.

Tocheri, M.W., Solhan, C.R., Orr, C.M., Femiani, J., Frohlich, B., Groves, C.P., Harcourt-Smith, W.E., Richmond, B.G., Shoelson, B., Jungers, W.L., 2011. Ecological divergence and medial cuneiform morphology in gorillas. J. Hum. Evol. 60, 171-184.

Trinkaus, E., 1983. Functional aspects of Neandertal pedal remains. Foot Ankle 3, 377-390.

Tuttle, R.H., 1967. Knuckle-walking and the evolution of hominoid hands. Am. J. Phys. Anthropol. 26, 171-206.

Tuttle, R.H., 1970. Postural, propulsive, and prehensile capabilites in the cheiridia of chimpanzees, and other great apes, in: Bourne, G.H. (Ed.), The chimpanzee. Karger, Basel, pp. 167-263.

Vereecke, E., D'Août, K., De Clercq, D., Van Elsacker, L., Aerts, P., 2003. Dynamic plantar pressure distribution during terrestrial locomotion of bonobos (*Pan paniscus*). Am. J. Phys. Anthropol. 120, 373-383.

Ward, C.V., 2002. Interpreting the posture and locomotion of *Australopithecus afarensis*: where do we stand? Am. J. Phys. Anthropol. 119, 185-215.

Ward, C.V., Kimbel, W.H., Johanson, D.C., 2011. Complete fourth metatarsal and arches in the foot of *Australopithecus afarensis*. Science 331, 750-753.

Ward, C.V., Latimer, B., 2005. Human evolution and the development of spondylolysis. Spine 30, 1808-1814.

Weidenreich, F., 1923. Evolution of the human foot. Am. J. Phys. Anthropol. 6, 1-10.

White, T.D., Suwa, G., Asfaw, B., 1994. *Australopithecus ramidus*, a new species of early hominid from Aramis, Ethiopia Nature 371, 306-312.

Williams, S.A., Ostrofsky, K.R., Frater, N., Churchill, S.E., Schmid, P., Berger, L.R., 2013. The vertebral column of *Australopithecus sediba*. Science 340.

Wood-Jones, F., 1944. Structure and function as seen in the foot. Bailliere and Co. , London.

Young, N.M., Wagner, G.P., Hallgrímsson, B., 2010. Development and the evolvability of human limbs. Proc. Nat. Acad. Sci. 107, 3400-3405.

Zipfel, B., DeSilva, J.M., Kidd, R.S., 2009. Earliest complete hominin fifth metatarsal—Implications for the evolution of the lateral column of the foot. Am. J. Phys. Anthropol. 140, 532-545.

Chapter 2

Shape Analysis of the Anthropoid Hallux (MT 1)

2.1 Introduction

Obligate terrestrial bipedalism practiced by modern humans is a unique locomotor behavior amongst extant primates, and its adoption was likely very influential towards the development of advanced social systems and material culture that typify modern human culture. Once hominins transitioned to obligate terrestrial bipedalism, broad morphological changes in their pedal anatomy evolved that allowed the foot to better drive a striding bipedal gait. The hominin forefoot is a particularly informative region of postcranial functional anatomy because aspects of forefoot morphology seem strongly tied to locomotor behavior generally (Susman, 1983; Latimer and Lovejoy, 1990; Griffin et al., 2010a; Fernández et al., 2015) and thus hominin forefoot remains offer paleoanthropologists key insight into when and how bipedalism first evolved in the human lineage.

Hallucal form and function differs greatly throughout the primate order. In prosimians, the hallux is widely abducted and articulates at a saddle joint with the medial cuneiform (Gebo, 1993; Gebo, 2014) whereas anthropoids lack a saddle-shaped configuration at this joint. Within anthropoids, the degree of hallucal abduction seems to bear some relationship to terrestriality (e.g., Morton, 1924; Schultz, 1934; Tocheri et al., 2011) and although some highly terrestrial primate species (e.g., *Papio*) exhibit shape changes related to terrestriality in MT head morphology (Fernández et al., 2015), it is modern humans and fossil hominins that display the very derived hallucal form—short, robust, and with marked dorsal reorganization of the distal MT articular surface. These morphological changes likely relate to the biomechanical role played by the hominin forefoot in terrestrial bipedalism whereby the metatarsophalangeal joints (MTPJs) act as the fulcrum point to a second class lever system that provides mechanical advantage when propelling the body weight forward at the end of stance phase (Carrier et al., 1994), at least in those hominins who possess an adducted hallux. The fulcrumating MTPJs have

been described as the drum to a windlass pulley mechanism (Hicks, 1954) that raises the height of the longitudinal arch while also stiffening the midfoot via tensing of the plantar aponeurosis. With these conformational changes, the foot acts as a relatively rigid lever that does not deform much during terrestrial bipedalism, allowing for improved propulsive forces at lift-off. In the windlass mechanism, the hallucal (MT 1) head has been theorized to be the most important "drum" driving the mechanism in humans because of the relative diameter of its head and the weight it bears late in stance. The larger diameter of the hallucal head flanked plantarly by two large hallucal sesamoids is thought to cause the majority of the midfoot tightening during dorsiflexion of the MTPJs (Bojsen-Møller, 1979). Similarly, the dorsal orientation of the MT 1 head is thought to facilitate increased dorsiflexion range of motion (ROM) by allowing the proximal phalanx to slide further dorsally onto the MT head, upon the expanded articular surface. Kinematic studies have shown that humans dorsiflex their MTPJs to higher excursions than *Pan* in the medial (Griffin et al., 2010a) and lateral (Holowka and Fernández, 2016) forefoot. Detailed kinematic and morphometric investigations of the MTPJs demonstrate that certain morphologies of the MT heads including dorsal robusticity (i.e., mediolateral wideness of the dorsal MT head) and dorsal orientation are likely related to function (e.g., dorsiflexion ROM) and dorsal orientation of the MT head are likely related to function (e.g., dorsiflexion ROM) (Fernández and Holowka, In Revision), and thus can be used to infer the locomotor behavior of extinct hominins.

Surprisingly, despite its theorized implications in bipedal propulsion and stability, MT head surface morphology has not been described quantitatively (but see Griffin et al., 2010b for assessment of its internal skeletal structure). Qualitative descriptions of MT head "dorsal doming" are often reported in the hominin pedal fossil literature (Stern and Susman, 1983; Susman and Brain, 1988; Susman and deRuiter, 2004; Jungers et al., 2009; Lovejoy et al., 2009; Ward et al., 2011; DeSilva et al., 2012; Haile-Selassie et al., 2012; Harcourt-Smith et al., 2015), but quantitative data of the distal MT surface morphology is somewhat lacking (Susman and Brain, 1988; Susman and deRuiter, 2004; Congdon et al., 2011), making it difficult to ascertain more precisely the functional importance of dorsal MT head orientation and dorsal MT head expansion to modern human-like bipedalism. While most early hominin fossils qualitatively demonstrate some modern human-like characters in their MTPJ morphology, often these simultaneously manifest with ape-like plesiomorphic traits. Although there is general consensus

on the morphologies present in most early hominin MT 1s in the fossil record, debate persists on the usefulness of inferring locomotion from primitive retentions in fossil pedal morphology (Stern, 2000; Ward, 2002). Some researchers argue that primitive retentions (symplesiomorphies) are uninformative for reconstruction of locomotor behavior (e.g., Latimer and Lovejoy, 1990; Latimer, 1991) and thus reconstruct early hominin (e.g., *Au. afarensis*) locomotor behavior as essentially identical to that of modern humans—obligate terrestrial bipeds. This approach leads to selected (Latimer and Lovejoy, 1989; 1990a; 1990b) or sometimes single (Haile-Selassie, 2001; Ward et al., 2011) derived traits becoming diagnostic of modern human-like bipedalism based on qualitative assessment of one character in one forefoot element alone. In modern humans, pathological reduction of MTPJ dorsiflexion excursions is significantly correlated with reduced stride length and walking velocity (Laroche et al., 2006), and it is possible that ape-like MTPJ morphologies sometimes present in hominins may reduce MTPJ dorsiflexion ROM or stability such as the plantarly oriented MT 1 head in StW 595 (DeSilva et al., 2012) or the ML narrow dorsal MT 1 heads seen in some early *Homo* fossils (Dmanisi MT 1s, KNM-ER 64062, several South African specimens) (Susman and Brain, 1988; Susman and deRuiter, 2004; Pontzer et al., 2010; Jungers et al., 2015). This would at minimum reduce locomotor efficiency when adopting a modern human-like striding bipedal gait in these fossil taxa. With a growing body of relatively complete hominin foot specimens available to researchers (Clarke and Tobias, 1995; Lordkipanidze et al., 2007; Jungers et al., 2009, 2015; Lovejoy et al., 2009; Zipfel et al., 2011; Haile-Selassie et al., 2012; Berger et al., 2015), MTPJ functional morphology is becoming increasingly relevant to our understanding of early hominin locomotor behavior and must be rigorously quantified to diagnose the functional affinity of these pedal features in human evolution. To that end, I analyze here a diverse sample of anthropoids and fossil hominins in order to resolve the evolutionary shape changes that underlined the evolution of modern human-like bipedalism.

I previously quantified the distal MT surface in a sample of catarrhines, which demonstrated humans to be unique in the MTPJ anatomy across all rays (Fernández et al., 2015). Here, I expand on this earlier investigation by greatly increasing species sampling across anthropoids, increasing the number of individuals sampled per species, and including fossil hominins which allow the data to be analyzed in an informative phylogenetic framework. Based on my previous investigations, I hypothesize that shape variables will closely track functional

aspects of MT head morphology. Although some cercopithecoid monkeys and mountain gorillas (*Gorilla beringei*) are also very terrestrial, I do not predict that this will be reflected in their hallucal head morphologies due to the abducted position of their halluces, which do not contribute much to forefoot dorsiflexion in the sagittal plane, and in cercopithecoid the hallux is highly abbreviated and has left the substrate prior to the lesser toes, which remain pushing-off later into stance. I predict that early fossil hominins (e.g., *Ar. ramidus*, *Au. afarensis*) will fall within the range of extant apes because of their hypothesized reliance on arboreal and terrestrial substrates, whereas later hominins (various early and later *Homo* species) will fall within modern-human ranges of variation, reflecting their increasingly obligate bipedal locomotor behavior.

2.2 Materials and Methods

2.2.1 Extant Sample

I quantified shape differences in the distal hallux within a comparative sample of 382 first metatarsals (a subset of ~2,600 sampled forefoot elements) drawn from 34 anthropoid species, and included for shape analyses those species represented with an average sample size of ~10 metatarsals (Table 2.1). Male-to-female sex ratios were roughly even, although sex data unknown for the *Homo* sample. In highly dimorphic species (e.g., *Gorilla*, *Pongo*), statistical tests for sex differences were performed, no significant differences were found, and thus the data were pooled. Non-human wild-shot specimens were sampled from the American Museum of Natural History (AMNH), the Smithsonian's National Museum of Natural History (USNM), the Academy of Natural Sciences of Philadelphia (ANSP), the Museum of Comparative Zoology at Harvard University (MCZ), the Cleveland Museum of Natural History (CMNH), the Natural History Museum of Los Angeles County (LACM), the Royal Museum for Central Africa (RMCA), and collections in the department of Anatomical Sciences at Stony Brook University (SBU) and the Laboratory for Primate Morphology and Genetics housed within the Caribbean Primate Research Center (CPRC). Habitually shod and unshod modern humans were sampled from the Iziko Museum at Cape Town (ICT), collections housed in the Department of Human Biology at the University of Cape Town (UCT), and from SBU (modern humans from south Asia). The presumably unshod (Roberts, 1989; Sealy and Pfeiffer, 2000; Stock and Pfeiffer, 2001; Proctor, 2013) populations collected at ICT and UCT come from pre-pastoral, Late Stone

Age populations in South Africa and the dated material ranged from 9000 – 2000 years bp. Only adult, non-pathological specimens were sampled, from the right side if available. If right-sided elements were unavailable, left-sided elements were mirror imaged during data processing and analysis using Geomagic Studio 2012 (see subsection 2.2.3). All monkey (except *Presbytis*) and hylobatid data were very generously provided to me by Dr. Biren A. Patel (Department of Cell & Neurobiology, University of Southern California). These data were contributed mostly in the form of raw medical imaging data that was later segmented into polygonal models by me (see subsection 2.2.3 for more detail regarding scanning protocols). Additionally, Dr. Sergio Almécija (Department of Anthropology, The George Washington University) also generously provided 3D laser scanned polygonal models of *Gorilla* and *Pan* sp. from the AMNH (see subsection 2.2.3 for more detail regarding scanning protocols). The extant data contributed by Drs. Patel and Almécija were not limited to the hallux, but also included all MTs and PPs analyzed in most subsequent chapters (see Chapters 3 – 5).

2.2.2 Fossil Sample

This dissertation samples most of the available fossil forefoot material, 10 of which are fossil MT 1s (n = 37; Fig. 2.1). The fossils included in the MT 1 analyses are listed in Table 2.2 and include some specimens not yet analyzed quantitatively in the literature (e.g., KNM-ER 64062, KNM-BK 63) and others not assigned to a specific taxon (e.g., StW 562, StW 595). For the purposes of the phylogenetic analyses however, they were provisionally assigned to *Australopithecus africanus* (see below). The rest of the fossil sample includes material from the following taxa:

Ardipithecus ramidus

ARA-VP-6/500-089 is a nearly complete right MT 1 recovered from Aramis located near the Daam Aatu Basaltic Tuff; the immediately underlying Gaala Vitric Tuff Complex is dated to 4.4 Ma (White et al., 1994). The specimen has a damaged proximal base but the distal articular surface is nearly intact. The joint anatomy at the first tarsometatarsal joint in *Ar. ramidus* suggests that the hallux was abducted (Lovejoy et al., 2009) like that of African apes. The dorsal surface is not expanded (i.e., "dorsally domed") as it is in humans, although some dorsal expansion is apparent in the *Ar. ramidus* MT 3 (ARA-VP-6/505). The *Ardipithecus* fossils were micro CT scanned by Dr. Gen Suwa and Dr. Tim White (Lovejoy et al., 2009), who allowed

partial scans of these bones including only the distal articular surfaces to be included in this dissertation.

Australopithecus afarensis

A.L.-333-115A is the distal half of an MT 1 found in the Denan Dora member of the Hadar Formation and is slightly younger than the AL-288-1 ("Lucy") material and the Laetoli footprints, at around 3.0 Ma (Aronson et al., 1977). It showcases marked dorsal expansion of the MT head, but the overall robusticity of the bone is reduced compared to that of modern humans. Thirteen bones were extracted from a single lump of matrix, strongly suggesting that the MTs and proximal phalanges (PP) correspond to one individual. A scan of the hallux (A.L. 333-115A) taken from high quality research casts housed at the Institute of Human Origins at the Arizona State University was provided by Dr. Caley Orr (Department of Cell and Developmental Biology, School of Medicine, University of Colorado – Denver) and Dr. William Kimbel (Institute of Human Origins, Arizona State University).

Australopithecus africanus

Both StW 562 and StW 595 are from Sterkfontein member 4, which puts their age between 2.6 – 2.0 Ma. It has been noted that StW 562 is qualitatively much more human-like than StW 595 (Clarke, 2008), and this readily observed by differences in their MT head morphology. StW 595 lacks the dorsal MT head expansion typically seen in humans and often seen in hominins, resembling instead the Burtele MT 1 (BRT-VP-2/73; 3.4 Ma), which may belong to *Au. afarensis*, the newly proposed species, *Australopithecus deyiremeda* (Haile-Selassie et al., 2015), or a yet unnamed taxon. Although StW 562 and StW 595 cannot be attributed to one particular taxon (Deloison, 2003), there are several evolutionary hypotheses debated by researchers concerning their taxonomic placement. First, these pedal bones may represent both *P. robustus* (StW 595) and *Au. africanus* (StW 562) based on the large morphological differences observed in their proximal articular surfaces (Proctor, 2010b). Second, they may both belong to a large temporal span within *Au. africanus* (DeSilva et al., 2012); lower limb material attributed to *Au. africanus* including the pelvis (Häusler and Berger, 2001; Häusler, 2002), knee (Heiple and Lovejoy, 1970), ankle (DeSilva, 2009), and foot (Harcourt-Smith, 2002; Zipfel et al., 2009) are quite human-like (DeSilva et al., 2012) and StW 562 fits well with this lower limb pattern. However, it is possible that these fossils belong to a separate, yet unnamed taxon ancestral to both *Au. africanus* and *P. robustus* (Clarke, 2008) with

highly variable forefoot morphology. For the purposes of my phylogenetically-informed analyses, I have included the material within the same taxon, *Au. africanus*, but shifting them to other taxa based on different evolutionary hypotheses did not greatly change the results. Laser scans of the original StW 562 and StW 595 specimens were provided by Dr. Daniel Proctor scanned using protocols detailed in his dissertation (Proctor, 2010b).

Paranthropus robustus

SKX 5017 is a left MT 1 from member 1 lower bank, Swartkrans. This member has nearly exclusively (> 95%) produced *Paranthropus robustus* specimens (Susman, 1988), and SKX 5017 has been assigned to this genus (Susman and Brain, 1988; Susman, 1989; Susman et al., 2001, Zipfel and Kidd, 2006). SKX 5017 was laser scanned using a NextEngine HD Pro 3D laser scanner at a resolution of 10,000 points/in^2 at the Ditsong Museum of South Africa (formerly the Transvaal Museum) in Pretoria, South Africa by Dr. Daniel Proctor, who very generously provided the scan and most of the other original fossil scans from the South African localities included in this work.

SK 1813 is a right MT 1 identified from a box containing faunal collections labeled "channel fill" at the Ditsong Museum of South Africa by Darryl J. de Ruiter (Susman and de Ruiter, 2004). It is unclear whether SK1813 was originally recovered from Swartkrans hanging Member 1 or Member 2, bracketing its geological age anywhere between 1.8 to 1.1 Ma. Qualitative description has aligned it with *P. robustus* (Susman and de Ruiter, 2004; Zipfel and Kidd, 2006; Proctor, 2010b), but its head morphology is similar to *Homo erectus*, both the African and Dmanisi specimens (see below). Dr. Daniel Proctor provided the SK 1813 scan (laser scanned, 10,000 points/in^2).

Homo erectus

In 2013, new fossil hominins were discovered from Kolom Odiet, near Ileret, West Turkana, Kenya (Jungers et al., 2015). Two partial skeletons were found, and one of these, KNM-ER 64062, preserves most of the MT heads and the proximal hallucal phalanx. These elements were recovered just above the KBS Tuff, dated to 1.89 Ma (Jungers et al., 2015). The MT 1 has both primitive and derived features; the fossil has marked dorsal expansion of the articular surface, but retains a plantarly pinched form to the MT head reminiscent of *Pan*, resulting in highly angular grooves for the hallucal sesamoids as opposed to the rounded grooves present in modern humans. Although KNM-ER 64062 has not been attributed to a specific

species, it has preliminarily been attributed to genus *Homo*. Based on its age, locality, and qualitative similarity to KNM-BK 63 and the Dmanisi MT 1s (D2671, D3442), I have tentatively assigned KNM-ER 64062 to *Homo* cf. *erectus (*or *ergaster* to some) in order to include it in the phylogenetic comparative analyses, although it could possibly belong in *Homo rudolfensis* (but probably not *H. habilis* based on comparisons to OH 8).

KNM-BK 63 is a known but essentially undescribed right MT 1 attributed to *Homo* cf. *erectus* (Leakey et al., 1969; Solan and Day, 1992; Deino and McBrearty, 2002; Fisher and McBrearty, 2002) described as lacking robusticity (Meldrum, 2007). It was found at the Baringo Kapthurin formation, part of the Tugen hills, Kenya, above the gray Tuff (> 780 Ka) and was subsequently dated to around 500 Ka (Deino and McBrearty, 2002). Like KNM-ER 64062, KNM-BK 63 has both primitive and derived morphologies. The MT head qualitatively appears extremely dorsally domed, but also retains the same ape-like plantar "wedging" found in the KNM-ER 64062. KNM-BK 63 is housed at the Kenya National Museum in Nairobi; Dr. Ashley Hammond kindly provided me with a laser scan of the original specimen.

Homo floresiensis

Pedal fossils from the diminutive hominin *Homo floresiensis* were first excavated from Liang Bua in 2003, a limestone cave on the island of Flores, eastern Indonesia (Brown et al., 2004). The left MT 1 found from LB 1 is notably shorter than that of modern humans (Jungers et al., 2009), but its morphology at the base is qualitatively very similar to that of modern human with a dorsally wide, flat articular surface. Published dates for this material have recently been pushed back considerably, although originally thought to be only ~36-18ka (Brown et al., 2004), recent geochronological analyses have argued that the date is closer to ~100-60ka (Sutikna et al., 2016), and I have used these updated dates in all analyses. Medical CT scans of high quality research casts of the LB 1 material were graciously provided by Dr. Matthew Tocheri. These were scanned on a Siemens medical CT scanner in Jakarta.

Homo naledi

The recently described hominin fossils from Rising Star, Gauteng, South Africa (Berger et al., 2015) offers researchers access to an unprecedented amount of hominin postcranial material, including many new pedal fossils. Among these new fossils is a largely intact right MT 1, U.W.101-1443. The fossil presents some damage to the medial aspect of the plantar surface of the MT head, which was reconstructed in Geomagic Studio 2012 (Fig. 2.2). Additionally, the

proximomedial part of the proximal articular surface is missing. The MT 1 is derived, closely resembling the modern human condition in many respects. The geological complexity of the Rising Star cave system has thus far precluded any geological dating of the *H. naledi* material. Because of this, I have chosen to include *H. naledi* in an unresolved polytomy with *H. erectus* and *H. floresiensis*, which offers the most conservative phylogenetic view of those taxa. Laser surface scans of the *Homo naledi* pedal fossils were obtained from MorphoSource (http://morphosource.org/).

2.2.3 Shape analyses

MT 1 head morphology was explored using 3-D digital polygon models reconstructed n from medical computed tomography (CT), micro computed tomography (μCT) and 3-dimensional (3D) laser surface scans. All imaging data was pooled because measurement error due to imaging modality is insignificant (Tocheri et al., 2011). Scans were conducted using a NextEngine 3D laser scanner (10,000 pts/inch^2 resolution per scan, 12 scans per bone), a General Electric Lightspeed VCT Scanner at Health Sciences Center, Stony Brook University (120 kV, 250 mA, 1mm slice thickness, 0.187 mm reconstruction increment, bone plus reconstruction), or with micro CT, depending on the size of the specimen. The micro CT scans were obtained using either a SCANCO Medical μCT 50 specimen scanner or a SCANCO Medical vivaCT 75 preclinical scanner housed in the Molecular Imaging Center at the University of Southern California and the Department of Biomedical Engineering at Stony Brook University, respectively. Specimens were scanned with a voxel resolution of 40-80 microns. 3D models from laser scans were merged using ScanStudio HD PRO (NextEngine, Inc) and Geomagic Studio 2012 SR1 (3D Systems, Inc) software packages. 3-D models from CT and μCT scans were constructed from DICOM data using Amira 5.3.3 software (Visage Imaging, Inc.). Any scanning artifacts or anomalies in polygonal meshes was corrected in Geomagic and MeshLab 1.3.2 (Visual Computing Lab—ISTI—CNR).

The 3-D shape of the hallucal metatarsal head was evaluated using a landmark-based approach. A 7x7 3-D surface patch of nine user-defined landmarks and 40 semi-landmarks was applied using *Landmark Editor* (Wiley et al., 2005) following the methods detailed in Fernández et al. (2015). The effect of semilandmark patch density (e.g., 5x5 and 9x9 3-D surface patches) was explored but did not significantly impact the results. This landmark set has been shown to be repeatable while also capturing the full articular surface morphology of the metatarsal head. The

surface patch was bounded mediolaterally by the proximal termination of the distal epicondyles, dorsally at the proximal termination of the distal articular surface, and plantarly at the proximal termination of the plantar condyles. The anatomical location of each landmark is described in Table 6.2 (see Chapter 6).

Semi-landmarks were slid using the minimized Procrustes distance criterion (Rohlf, 2010) but similar results were obtained using minimized bending energy algorithms (Bookstein, 1997). The slid coordinates were then subjected to a Generalized Procrustes Analysis (GPA) (Gower, 1975), and then principal component analysis (PCA) was used to summarize and explore the observed variation in metatarsal head shape. Articular surface polygonal mesh warps were constructed to visualize shape changes. Significant differences in PC scores between taxonomic groups were analyzed using multivariate analysis of variance (MANOVA); Tukey's HSD was used for pairwise *post hoc* between-species and between-ray comparisons. All PCs explaining at least 5% of the total shape variance were included in such analyses, but PC 1 and PC 2 are known to capture the relevant morphology (Fernández et al., 2015). Box-and-whisker plots depicting interquartile range, median, and total range (Tukey, 1977) are shown for PC 1 and PC 2 in order to visualize the variation between species in specific MT head morphologies. Semi-landmark sliding, GPA, PCA, regressions, and all phylogenetic analyses (see below) were performed in the R packages *Geomorph* (ver. 2.17, Adams and Otárola-Castillo 2013; Adams et al., 2015) and *SURFACE* (Ingram and Mahler, 2013). Boxplots, MANOVAs, and *post hoc* tests were performed in R 3.1.3 base package. Mesh warps were made in *Landmark editor* using thin-plate splines (TPS) deformations described in Bookstein (1989).

2.2.4 Phylogenetic analyses

Phylogenetic trees

A consensus ultrametric phylogenetic tree of extant anthropoid taxa was obtained from 10kTrees (ver. 3; Arnold et al., 2010). This tree was constructed using Bayesian phylogenetic analyses on eleven mitochondrial and six autosomal genes from 301 primate species (34 sampled in this dissertation; Fig. 2.3) available at GenBank (http://www.ncbi.nlm.nih.gov/genbank. The proposed hominin phylogeny was added *post hoc* to the anthropoid tree and is based on Strait and Grine (2004), with some nomenclatural differences and the addition of new hominin taxa (but see Dembo et al., 2015). For the fossil species, as a criterion of standardization, ghost

lineages of one million years were added to the published age of the fossil following Almécija et al. (2015). To provide a taxonomically conservative framework for these analyses, I included *H. naledi* in an unresolved polytomy with *H. erectus* and *H. floresiensis* (Fig. 2.2.1).

Phylogenetic signal

To assess the level of phylogenetic patterning in the shape data (i.e., to see how related species resemble one another), the degree of phylogenetic signal in the shape data was calculated relative to what is expected under a Brownian motion model of evolution. This is done using a permutation test where shape data at the tips of the phylogeny are randomized relative to the tree. For geometric morphometric data, the approach taken was a mathematical generalization of the Blomberg's K statistic (Blomberg et al. 2003), K_{mult}, most appropriate for highly multivariate data (Adams, 2014). The use of Blomberg's K is a ratio between mean-squared error of the tip data and mean-squared error of the phylogenetic tree's variance-covariance matrix. $K < 1$ suggest more within-clade than between-clade variance, $K \sim 1$ reflects Brownian motion such that the variance at the tips accurately reflects phylogenetic relatedness, and $K > 1$ suggests more between-clade variance than within-clade variance (Almécija et al., 2015).

Allometric regressions

In order to explore the effects of body size on MT head shape, multivariate allometric regressions were conducted in a phylogenetic context (i.e., phylogenetic least-squares regression, PGLS). Hallucal head size was estimated from the sample by logged MT 1 centroid size. Log MT 1 centroid size was then regressed on shape variables (i.e., PCs). A Procrustes ANOVA was performed under a Brownian motion model of evolution, in a manner designed to accommodate high-dimensional (3D shape) datasets (Adams, 2014). A permutation test (n = 10,000 iterations) was run across the tips of the phylogeny, and estimates of statistical values were obtained from the permuted data which then are compared to the observed value to assess significance.

Phylomorphospace

To visualize directionality and extent of evolutionary shape changes (Rohlf 2002; Klingenberg and Gidaszewski 2010) in the anthropoid MT 1, the consensus anthropoid phylogenetic tree was plotted against a morphospace constructed on the basis of a species-means PCA using the R package "phytools" (Revell, 2012). Prior to this step, the ancestral states at

each node are inferred using a maximum likelihood approach. In order to better calibrate the ancestral state reconstructions, a large number of fossils are included in the phylomorphospace analyses because they have greater weight than extant groups in this reconstructions. In the phylomorphospace, relative branch lengths are used to visualize the amount of shape change that occurred through evolutionary time such that long branch lengths indicate more evolutionary shape change and short branch lengths indicate less evolutionary shape change for any given taxon. Results of the phylomorphospace plots were explored both with and without calibrating the tree with fossils, and the results were very similar between the two, suggesting that the evolutionary signals found here in the MT 1 head are robust.

Multi-regime OU modeling

Ornstein–Uhlenbeck (OU) modeling was performed in the R package *SURFACE* (Ingram and Mahler, 2013). OU modeling differs from Brownian motion in that it incorporates stabilizing selection by introducing a parameter (α) that determines the rate of adaptive evolution towards an optimum trait values (θ—adaptive peak). This standard OU model has been modified into multiple-optima OU models allowing optima to vary across the phylogeny. In these implementations the parameters are typically defined *a priori*, which allows testing the relative likelihood of different evolutionary scenarios. Importantly, this approach allows fitting multivariate data (e.g., shape data), circumventing issues that stem from iteratively fitting univariate data. Although this OU model fitting approach comprises a powerful way of comparing the likelihood of alternative evolutionary scenarios, it leaves open the possibility that the 'best-fit' evolutionary scenario is not included in the research design. To solve this, Ingram and Mahler (2013) expanded the OU model fitting approach by developing a way to estimate the number of shifts and their locations on the phylogeny, rather than assuming them *a priori*. This method was developed specifically to identify instances of convergent evolution and can be used to extract the evolutionary scenario that indicates the best statistical fit (as determined by lowest AICc score) between the phylogeny and the observed measurements. Instances of convergent evolution (i.e., same evolutionary "regimes") are then painted onto the phylogeny, whereas non-convergent evolutionary regimes are painted onto the phylogeny in greyscale. Regimes are understood to be a group of taxanomic units that are inferred to be evolving under similar evolutionary regimes (Almécija et al., 2015) and the adaptive peak is the optimal phenotypic value that characterize the different regimes. To verify instances of convergence, *SURFACE*

evaluates whether the AICc score can be further improved by allowing different species to shift towards shared adaptive regimes. If the AICc score is improved, this would provide evidence of convergence towards that particular regime.

2. 3 Results

2.3.1 PCA/MANOVA

PCAs separated major clades as well as genera in some cases into distinct clusters on the morphospace scatterplots (Fig. 2.5) on PC 1 and PC 2. MANOVAs confirmed significant differences in MT 1 shape variables (PCs) among species and *post hoc* tests further revealed significant differences among all of the groups in the sample (Table 2.3). Because PC 1 and PC 2 captured the relevant distal articular surface morphology (see below), results for these two axes are reported in further detail. For MT 1, PC 1 separated humans from all taxa except *Gorilla beringei* ($p < 0.0001$; Table 2.3); great apes generally overlapped with each other but *Pan* was significantly different from all except *Pongo abelii* ($p < 0.0001$). Gibbons were significantly different from the great apes on PC 1 ($p < 0.0001$) and resembled the monkey condition on this axis, similar to their proximal phalangeal base morphology (see Chapter 4). Within monkeys, the New World sample (NWMs) generally separated from all other taxa ($p < 0.0001$), but *Ateles* overlapped with some cercopithecoid groups (e.g., *Presbytis, Macaca, Chlorocebus*). Additionally, *Cebus* was found to be significantly different from all groups on PC 1 except for *Alouatta*. The cercopithecoids largely overlapped each other; however, when comparing within species and subspecies (Table 2.3), *Macaca mulatta* was significantly different from *Macaca nemestrina* ($p < 0.0001$), but different species of *Pan, Gorilla*, and *Pongo* were not found to be significantly different from each other on PC 1. On PC 2, humans were significantly different from all groups except *Papio, Macaca*, and *Nasalis* ($p < 0.0001$; Table 2.4). Great apes largely overlapped but within species and subspecies *post hoc* tests revealed significant differences between Grauer's g*orilla* (*G. b. graueri*) ($p < 0.0001$) and both mountain (*G. b. beringei*) and western (*G. g. gorilla*) gorillas (Table 2.4). Additionally, *Pan troglodytes* was significantly different from *Pan paniscus* ($p < 0.0001$). Other taxa (e.g., gibbons and all monkeys) largely overlapped on this axis.

2.3.2 Comparative aspects of shape

Extant anthropoids

Shape variables PC 1 (23% variance explained) and PC 2 (16% variance explained) mapped onto MT head orientation and robusticity in a similar pattern to previous analyses (Fernández et al., 2015), but with minor differences. The amount of variance explained by PC 1 and PC 2 decreased somewhat in this analysis, but this is expected given the larger and more diverse extant sample. PC 1 tracked a variety of shape changes in the MT head (Fig. 2.6), particularly simultaneous shape changes to the dorsal and plantar parts of the MT 1 head. High PC 1 scores are typified by a robust, wide, flat head and a broad plantar surface with shallow grooves for the hallucal sesamoids, a very human-like pattern. PC 1 also captures MT head orientation, with higher PC 1 scores having more dorsal articular surface area, but this was better captured in PC 2. 3D shape morphs constructed using low PC 1 scores revealed marked plantar wedging of the MT head, with strongly angled facets/grooves for the hallucal sesamoids—a typical ape-like condition. PC 2 seems to closely track the overall dorsal versus plantar orientation of the MT head, but also carries information about the robusticity of the dorsal MT head. In the 3D morphs with high PC 2 scores (but PC 1 set at 0), the resulting morphs had a dorsally oriented MT head but the dorsal part of the head was rounded and narrow, a mosaic pattern seen in some fossil hominins (see below). Low PC 2 scores describe a very plantarly oriented MT head, often seen in *Pongo, Gorilla,* and *Pan* specimens. Box-and-whisker plots (Figs. 2.6a-b) show that the modern human MT 1 shape range overlaps with fossil hominins and apes on PC 1, and fossil hominins and monkeys on PC 2.

Fossil hominins

Fossil hominin hallucal head morphology was found to be quite variable, spanning much of the anthropoid morphospace. *Homo naledi* (U.W. 101-1443) was the only fossil MT 1 to fall directly within the modern human cloud (Fig. 2.6), but most of the other fossil hominin MT 1s overlapped the modern human range on either PC 1 or PC 2 (Figs. 2.7a-b). StW 595 had the lowest PC 2 score out of all the sampled fossils and this reflects its very plantar, ape-like head orientation. It did overlap humans on PC 1 but overall was found to be most similar to *Gorilla*. Similarly, ARA-VP-6/500-089, KNM-ER 64062, and StW 562 also overlapped the modern human PC 1 range, but with ape-like PC 2 scores. LB1 and KNM-ER 64062 are closer to the human cloud, and fall within the human morphospace when the sample is restricted to only include extant hominoids and fossils. However, their position in the general anthropoid

morphospace is informative. KNM-ER 64062 has very human-like dorsal head orientation, but its relatively narrow, rounded head and plantar condylar morphology push it outside the range of modern humans. The same is true for ARA-VP-6/500-089. Interestingly, although KNM-BK 63 does not fall within the human minimum convex polygon, it does fall within the human range of variation on PC 1 and is well within the human range of variation on PC 2. This reflects its strongly dorsally oriented but narrow and rounded MT head, which resembles the PC 2 morph shown on the top left of Figure 2.6. SK 1813 displays a similar pattern, but falls just outside the human range on PC 1. The other MT 1 from Swartkrans, SKX 5017, is more primitive in its MT head morphology, falling only within the human range on PC 2, but well outside the range of humans on PC 1. A.L.-333-115A fell close to the human range in PC 2, but fell far outside the human range on PC 1.

2.3.3 Phylogenetic comparative analyses

Multivariate allometric phylogenetic regressions (PGLS) of centroid size on shape variables (PCs) revealed that metatarsal head size is not a significant determinant of MT 1 head shape ($r^2 = 0.11$; p = NS). These results suggest that shape differences observed in the MT 1 data are being driven by phylogenetic and/or functional differences in the sample. Permutation tests for phylogenetic signal did reveal significant phylogenetic patterning in the anthropoid MT 1 shape data ($p = 0.017$), but not when fossil taxa were included (p = ns), suggesting that perhaps function is driving differences observed in MT head shape more so than phylogeny. Results from the multi-regime OU modeling (Fig. 2.4) in *SURFACE* showed no evidence for convergence between primate clades studied, but did reveal three regime shifts towards different adaptive optima. The first regime includes NWMs, the second cercopithecoids, and the third hominoids. This result included data from PC 1 and PC 2 together, and the method did not converge when using only 1 shape variable, because the *SURFACE* algorithm does not function well with only one variable. Although the inclusion of additional PCs may have improved convergence in some cases, I chose to restrict the analyses to those PCs that were functionally interpretable.

Phylomorphospace plots illustrated several broad patterns in the evolutionary shape change of the anthropoid MT 1 head (Fig. 2.7). Generally, great apes were quite variable in the phylomorphospace compared to gibbons and monkeys. NWMs demonstrate relatively little evolutionary shape change after diverging from catarrhines and head towards their own adaptive

optima characterized by low PC 1 and PC 2 scores. Cercopithecoids also show relatively little evolutionary shape change (except *Presbytis* and *M. mulatta*), and are situated intermediately between the New World monkeys and great apes. Gibbon MT head shape trends towards the cercopithecine optima, a pattern also present in their lateral MTs and proximal phalanges (see Chapters 3, 4). In great apes, *Pan*, *Pongo*, and *Gorilla* all clustered near the bottom right of the morphospace with similar amounts of shape change, but *Pan* is more derived on PC 1. Within hominins, mosaic evolution is well captured in the phylomorphospace plot by showing major evolutionary shape changes occurring multiple times within the hominin clade. The stem hominin is reconstructed as having MT 1 head morphology more similar to *Ar. ramidus*, which has an overall plesiomorphic hallucal shape. *Au. africanus* and *Au. afarensis* have both undergone much MT 1 head shape change, although in different directions. *P. robustus* shows great evolutionary change at MT 1, towards a unique corner of the morphospace, similar to the derived nature of *Paranthropus* generally. The MT 1 of *H. floresiensis*, although undoubtedly derived, still differs from what is seen in modern humans and other extinct *Homo*. *H. naledi* and *H. erectus* more closely approximate the modern condition, but the phylomorphospace plot suggests that the majority of the derived morphology present in modern humans took place after *H. sapiens* split with early *Homo*, i.e., in a relatively short amount evolutionary time.

2.4 Discussion

Shape analyses on the extant anthropoid and fossil hominin hallux provided mixed support for my hypotheses and predictions. While shape analyses did capture the hallucal characters of functional interest, my hypothesis of human convergence with other terrestrial anthropoids was rejected based on the multi OU modeling analyses. I suspect this may change when more data from across the MTPJs are analyzed simultaneously, but that analysis will test for convergence in anthropoid forefoot joint shape generally, and will only be applicable to fossils where most of the MTPJs are intact (e.g., KNM-ER 64062, A.L.-333-115, La Ferrassie 1). For now, the hallucal head shape analyzed in isolation does not seem to be a target of convergent evolution within anthropoids. OU modeling did however reveal three distinct adaptive optima, which does correspond to the general layout of the MT 1 tangent space. Great apes began to evolve different hallucal head shapes, perhaps due to increasing body size and terrestriality. Although explicit evidence for terrestrial shape convergence was not found in the hallucal head,

instances of extensive overlap between modern *Homo* and *G. beringei* on PC 1 to the exclusion of all other groups suggested that some shape change perhaps in response to increased terrestriality is occurring in this taxon. Grauer's gorillas were found to be distinct from mountain or eastern gorillas, but this may be due to genetic drift and in-breeding present in their very small population (Yamagiwa et al., 1993; Tocheri et al., 2016), leading to unusual phenotypes in this subspecies. The overlap of some *Nasalis* specimens within the human distribution was observed in previous forefoot shape analyses (Fernández et al., 2015) and while unclear, it seems largely driven by plantar condylar morphology because *Nasalis* has shallow plantar grooves, like humans. Moreover, despite its arboreal nature, the *Nasalis* hallux is not oriented plantarly to the same degree seen in apes or other colobines (e.g., Presbytis). The hallucal data for *Nasalis* does not typify the rest of the *Nasalis* forefoot (Fernández et al., 2015), and other shape analyses (Fernández, unpublished elliptical Fourier analysis data) also confirm this. Future work will incorporate more colobine species to see if *Nasalis* is an unusual outlier, or if other colobine monkeys share this pattern. The shape analysis results on the Swartkrans and Hadar material provides further evidence that these hominins still lacked all of the lower limb synapomorphies present in modern humans, suggesting that they practiced bipedalism in a different manner than modern humans, perhaps adopting the facultative bent-knee, bent-hip gait that others have suggested (Stern and Susman, 1983; Susman et al., 1984). The pattern found in Swartkrans and Hadar also has been qualitatively observed in the Dmanisi and Burtele material, and I strongly suspect that these fossils would plot near SK 1813, SKX 5017, and A.L.-333-115A in the MT 1 morphospace, at least on PC 1, but further analyses including these specimens are needed to confirm these suspicions. My findings lend support to arguments laid out recently by Harcourt-Smith et al. (2015) that the foot of *H. naledi* is essentially modern and its MT head shape certainly supports a modern human-like windlass push off mechanism. Although the Rising Star material has yet to be dated, it is suspected to be relatively young (Williams, pers. comm.). Thus, it is unclear as to how the foot of *H. naledi* impacts the evolution of the modern human forefoot. Regardless, it does provide a clear example of a hominin in South Africa with pedal bones essentially indistinguishable from modern humans.

When phylogenetic relationships are plotted onto the morphospace after reconstructing ancestral morphologies, the fossil hominin data suggests that much evolutionary hallucal shape change has occurred within hominins, and that it occurred in a different ways amongst the extinct

hominin taxa. The last common ancestor (LCA) of chimpanzees and humans was reconstructed as having a MT 1 similar in shape to *Ar. ramidus*, the most basal hominin currently known from forefoot material. This result suggests that stem hominins likely possessed a primitive, abducted hallux like that seen in *Ar. ramidus*, a hominin which probably required a push off axis more similar to that seen in extant chimpanzees (between MTPJ 2 and MTPJ 3; Holowka and Fernández, 2016) than in modern humans (between MTPJ 1 and MTPJ 2) because the abducted hallux is not heavily recruited during MTPJ dorsiflexion at lift-off. Further within the hominin clade, *Au. afarensis* and *Au. africanus* both have undergone much MT 1 head shape change, although in different directions. The high amount of shape change observed in these taxa presumably occurred in response to the biomechanical demands imposed by increased terrestrial bipedalism. I caution the *Au. africanus* position in the morphospace as contentious, however, because of the dubious taxonomic affiliations of the StW 562 and StW 595 MT 1s (Clarke, 2008; DeSilva et al., 2012). If these two fossils are placed into two different groups, then *Au. afarensis* and *Au. africanus* would fall much more closely together in the morphospace and another, yet unnamed taxon would occupy a space near *Ar. ramidus*. Because of the poor pedal fossil record available for *Au. africanus*, and the lack of MT heads preserved in *Au. sediba* (Berger et al., 2010), the picture of early hominin hallucal head shape evolution in South Africa ultimately remains unclear. However, the difference between these two fossils in shape space is greater than the range of variation seen in a single species of *Pan* or *Gorilla*, which lends support for these two fossils representing different species. Despite this, StW 562 and StW 595 still both fall within the range of variation seen in extant *Pan* and *Gorilla*, and so they could at least belong to the same genus (i.e., *Australopithecus*), assuming these ancestral lineages possessed ranges of morphological variation comparable to those of extant hominoids. *P. robustus* occupies a unique region of the morphospace; it is most similar to *H. erectus* and *H. sapiens* on PC 2, but is far more monkey-like on PC 1. This results in a dorsally oriented but dorsally narrow, rounded MT head. Such a configuration presumably facilitated increased dorsiflexion ROM at the MTPJs, but perhaps not to the extent seen in modern humans, due to impacts on hallucal MTPJ stability. Taken together, the overall pattern seen in the *P. robustus* MT 1 is not unlike what has been observed in other derived *P. robustus* postcranial elements (Susman, 1988), providing further evidence that *Paranthropus* was more human-like in its postcranial morphology than previously thought, in contrast to other aspects of its forefoot morphology (Proctor, 2008; Proctor, 2010a;

Proctor, 2010b). The MT 1 of *H. floresiensis*, although undoubtedly derived, still differs from what is seen in modern humans and other extinct *Homo*. It is remarkably short, even when compared to pygmy humans and the foot to lower limb proportions are more similar to chimpanzees than to modern humans (Jungers et al., 2009). In the phylomorphospace analyses, *H. floresiensis* deviates significantly on PC 1 from other early *Homo*, supporting the notion that *H. floresiensis* did not adopt a modern human-like gait (Jungers et al., 2009). *H. erectus* more closely approximates the modern condition; the older fossil I provisionally attributed to *H.* cf. *erectus*, KNM-ER 64062, possesses essentially modern human-like dorsal and chimpanzee-like plantar aspects of its MT 1 head. The geologically younger *H. erectus* specimen, KNM-BK 63, displays the same pattern, but is more extreme, especially in its plantar morphology. Neither the KNM-ER 65062 nor the KNM-BK 63 configuration is entirely modern, and it is possible that the gait of *H. erectus* resembled that of *H. floresiensis*, its nearest neighbor in the phylomorphospace, more closely than modern humans.

Collectively, hallucal head evolution within hominins diversifies into a multitude of configurations. No consensus pattern towards a modern human-like hallucal head emerges in the fossil record until *H. naledi*, an undated specimen. Regardless, these findings suggest that the emergence of a human-like MT 1 occurs relatively late in hominin evolution. Indeed, the overall pattern of anthropoid MTPJ evolution seems to be that the lateral, non-hallucal MTs are the first digits to undergo evolutionary shape changes related to bipedalism, whereas the hallux retains a more primitive morphology until relatively late in human evolution. I suspect that because early hominins (e.g., *Ar. ramidus*, *Au. afarensis)* still spent a significant amount of their time in the trees, the hallux retained some primitive characters that facilitated facultative pedal grasping in these groups, thereby resulting in the mosaic nature of the hallux observed in many fossil hominins. The comparative MTPJ shape data for fossils that preserve medial and lateral MT heads supports this hypothesis (see Chapter 3; Chapter 6) and corroborates prior work that suggests initial evolutionary change first acted upon the lateral column of the foot (Zipfel et al., 2009; DeSilva et al., 2012; Proctor, 2013). Only once hominins fully committed to obligate terrestrial bipedalism with a fully adducted hallux did the MT 1 head begin to reshape into a modern-like form.

2. 5 References

Adams, D.C., 2014. A generalized K statistic for estimating phylogenetic signal from shape and other high-dimensional multivariate data. Sys. Biol. 63, 685-697.

Adams, D.C., Collyer, M.L., Otárola-Castillo, E., Sherratt, E., 2015. Geomorph: software for geometric morphometric analyses. R package version 2.1.2.

Adams, D.C., Otárola-Castillo, E., 2013. Geomorph: an R package for the collection and analysis of geometric morphometric shape data. Meth. Ecol. Evol. 4, 393-399.

Almécija, S., Orr, C.M., Tocheri, M.W., Patel, B.A., Jungers, W.L., 2015. Exploring phylogenetic and functional signals in complex morphologies: yhe hamate of extant anthropoids as a test-case study. Anat. Rec. 298, 212-229.

Arnold, C., Matthews, L.J., Nunn, C.L., 2010. The 10kTrees website: a new online resource for primate phylogeny. Evol. Anthropol. 19, 114-118.

Aronson, J.L., Schmitt, T.J., Walter, R.C., 1977. New geochronologic and palaeomagnetic data for the hominid-bearing Hadar Formation of Ethiopia. Nature 267, 323-327.

Berger, L.R., de Ruiter, D.J., Churchill, S.E., Schmid, P., Carlson, K.J., Dirks, P.H.G.M., Kibii, J.M., 2010. *Australopithecus sediba:* a new species of *Homo*-like australopith from South Africa. Science 328, 195-204.

Berger, L.R., Hawks, J., de Ruiter, D.J., Churchill, S.E., Schmid, P., Delezene, L.K., Kivell, T.L., Garvin, H.M., Williams, S.A., DeSilva, J.M., Skinner, M.M., Musiba, C.M., Cameron, N., Holliday, T.W., Harcourt-Smith, W., Ackermann, R.R., Bastir, M., Bogin, B., Bolter, D., Brophy, J., Cofran, Z.D., Congdon, K.A., Deane, A.S., Dembo, M., Drapeau, M., Elliott, M.C., Feuerriegel, E.M., Garcia-Martinez, D., Green, D.J., Gurtov, A., Irish, J.D., Kruger, A., Laird, M.F., Marchi, D., Meyer, M.R., Nalla, S., Negash, E.W., Orr, C.M., Radovcic, D., Schroeder, L., Scott, J.E., Throckmorton, Z., Tocheri, M.W., VanSickle, C., Walker, C.S., Wei, P., Zipfel, B., 2015. *Homo naledi*, a new species of the genus *Homo* from the Dinaledi Chamber, South Africa. eLife 4.

Bergeson, D., 1998. Patterns of suspensory feeding in *Alouatta palliata*, *Ateles geoffroyi*, and *Cebus capucinus*, in: Strasser, E., Fleagle, J.G., Rosenberger, A.L., McHenry, H. (Eds.), Primate locomotion. Plenum Press, New York, pp. 45-60.

Blomberg, S.P., Garland, T., Ives, A.R., Crespi, B., 2003. Testing for phylogenetic singnal in comparative data: behavioral traits are more labile. Evolution 57, 717-745.

Bojsen-Møller, F., 1979. Calcaneocuboid joint and stability of the longitudinal arch of the foot at high and low gear push off. J. Anat. 129, 165-176.

Bookstein, F.L., 1997. Morphometric tools for landmark data: geometry and biology. Cambridge University Press, Cambridge.

Bookstein, F.L., 1989. Principal warps: thin-plate splines and the decomposition of deformations. IEEE Computer Society 11, 567-585.

Boonratana, R., 2000. Ranging behavior of proboscis monkeys (*Nasalis larvatus*) in the Lower Kinabatangan, Northern Borneo. International Journal of Primatology 21, 497-518.

Brown, P., Sutikna, T., Morwood, M.J., Soejono, R.P., Jatmiko, Wayhu Saptomo, E., Awe Due, R., 2004. A new small-bodied hominin from the Late Pleistocene of Flores, Indonesia. Nature 431, 1055-1061.

Cant, J.G.H., 1987. Positional behavior of female bornean orangutans (*Pongo pygmaeus*). Am. J. Primatol. 12, 71-90.

Cant, J.G.H., 1988. Positional behavior of long-tailed Macaques (*Macaca fascicularis*) in Northern Sumatra. Am. J. Phys. Anthropol. 76, 29-37.

Cant, J.G.H., Youlatos, D., Rose, M.D., 2001. Locomotor behavior of *Lagothrix lagothricha* and *Ateles belzebuth* in Yasuni National Park, Ecuador: general patterns and nonsuspensory modes. J. Hum. Evol. 41, 141-166.

Carrier, D.R., Heglund, N.C., Earls, K.D., 1994. Variable gearing during locomotion in the human musculoskeletal system. Science 265, 651-653.

Clarke, R., Tobias, P., 1995. Sterkfontein member 2 foot bones of the oldest South African hominid. Science 269, 521-524.

Clarke, R.J., 2008. Latest information on Sterkfontein's *Australopithecus* skeleton and a new look at *Australopithecus*. South African Journal of Science 104, 443-449.

Congdon, K.A., Ward, C.V., Kimbel, W.H., 2011. The first complete fourth metatarsal of *Australopithecus afarensis* from Hadar. Ethiopia. Am. J. Phys. Anthropol. 144, 111.

Deino, A.L., McBrearty, S., 2002. $^{40}Ar/^{39}Ar$ dating of the Kapthurin Formation, Baringo, Kenya. J. Hum. Evol. 42, 185-210.

Deloison, Y., 2003. Anatomie des os fossils de pieds des hominids d'Afrique du suddates entre 2,4 et 3,5 millions d'annés. Interprétation quant à leur mode de locomotion. Biométrie Hum. Anthropol. 21, 189-230.

DeSilva, J.M., 2009. Functional morphology of the ankle and the likelihood of climbing in early hominins. Proc. Nat. Acad. Sci. 106, 6567-6572.

DeSilva, J.M., Proctor, D.J., Zipfel, B., 2012. A complete second metatarsal (StW 89) from Sterkfontein Member 4, South Africa. J. Hum. Evol. 63, 487-496.

Doran, D.M., 1992. The ontogeny of chimpanzee and pygmy chimpanzee locomotor behavior: a case study of paedomorphism and its behavioral correlates. J. Hum. Evol. 23, 139-157.

Doran, D.M., 1993. Sex differences in adult chimpanzee positional behavior: the influence of body size on locomotion and posture. Am. J. Phys. Anthropol. 91, 99-115.

Dunbar, R.I.M., Dunbar, E.P., 1974. Ecological relations and niche separation between sympatric terrestrial primates in Ethiopia. Folia Primatol. 21, 36-60.

Dunn, R.H., Tocheri, M.W., Orr, C.M., Jungers, W.L., 2014. Ecological divergence and talar morphology in gorillas. Am. J. Phys. Anthropol. 153, 526-541.

Fernández, P.J., Almécija, S., Patel, B.A., Orr, C.M., Tocheri, M.W., Jungers, W.L., 2015. Functional aspects of metatarsal head shape in humans, apes, and Old World monkeys. J. Hum. Evol. 86, 136-146.

Fisher, R., MBrearty, S., 2002. The comparative morphology of hominin postcranial remains from the Kaputhrian formation, Baringo district, Kenya. Am. J. Phys. Anthropol. 34, 70.

Fleagle, J.G., 2013. Primate adaptation and evolution. Academic Press, San Diego.

Gebo, D.L., 1993. Postcranial adaptation in nonhuman primates. Northern Illinois University Press, DeKalb.

Gebo, D.L., 2014. Primate comparative anatomy. Johns Hopkins University Press, Baltimore.

Gosselin-Ildari, A.D., 2013. The evolution of the human foot, with special reference to the joints. Stony Brook University.

Gower, J.C., 1975. Generalized Procrustes analysis. Psychometrika 40, 33-51.

Griffin, N.L., D'Août, K., Richmond, B., Gordon, A., Aerts, P., 2010a. Comparative in vivo forefoot kinematics of *Homo sapiens* and *Pan paniscus*. J. Hum. Evol. 59, 608-619.

Griffin, N.L., D'Août, K., Ryan, T.M., Richmond, B.G., Ketcham, R.A., Postnov, A., 2010b. Comparative forefoot trabecular bone architecture in extant hominids. J. Hum. Evol. 59, 202-213.

Haile-Selassie, Y., 2001. Late Miocene hominids from the Middle Awash, Ethiopia. Nature 412, 178-181.

Haile-Selassie, Y., Gibert, L., Melillo, S.M., Ryan, T.M., Alene, M., Deino, A., Levin, N.E., Scott, G., Saylor, B.Z., 2015. New species from Ethiopia further expands Middle Pliocene hominin diversity. Nature 521, 483-488.

Haile-Selassie, Y., Saylor, B.Z., Deino, A., Levin, N.E., Alene, M., Latimer, B.M., 2012. A new hominin foot from Ethiopia shows multiple Pliocene bipedal adaptations. Nature 483, 565-569.

Harcourt-Smith, W.E.H., 2002. Form and function in the hominoid tarsal skeleton. University College London.

Harcourt-Smith, W.E.H., Throckmorton, Z., Congdon, K.A., Zipfel, B., Deane, A.S., Drapeau, M.S.M., Churchill, S.E., Berger, L.R., DeSilva, J.M., 2015. The foot of *Homo naledi*. Nat. Commun. 6.

Häusler, M., 2002. New insights into the locomotion of *Australopithecus africanus* based on the pelvis. Evol. Anthropol. 11, 53-57.

Häusler, M., Berger, L., 2001. Stw 441/465: a new fragmentary ilium of a small-bodied *Australopithecus africanus* from Sterkfontein, South Africa. J. Hum. Evol. 40, 411-417.

Heiple, K.G., Lovejoy, C.O., 1971. The distal femoral anatomy of *Australopithecus*. Am. J. Phys. Anthropol. 35, 75-84.

Hicks, J.H., 1954. The mechanics of the foot: II. the plantar aponeurosis and the arch. J. Anat. 88, 25-30.21.

Ingram, T., Mahler, D.L., 2013. SURFACE: detecting convergent evolution from comparative data by fitting Ornstein-Uhlenbeck models with stepwise Akaike Information Criterion. Meth. Ecol. Evol. 4, 416-425.

Iwata, H., Ukai, Y., 2002. SHAPE: a computer program package for quantitative evaluation of biological shapes based on elliptic Fourier descriptors. J. Hered. 93, 384-385.

Jungers, W.L., Grine, F.E., Leakey, M.G., Leakey, L., Brown, F., Yang, D., Tocheri, M.W., 2015. New hominin fossils from Ileret (Kolom Odiet), Kenya. Am. J. Phys. Anthropol. 156, 181.

Jungers, W.L., Harcourt-Smith, W.E.H., Wunderlich, R.E., Tocheri, M.W., Larson, S.G., Sutikna, T., Due, R.A., Morwood, M.J., 2009. The foot of *Homo floresiensis*. Nature 459, 81-84.

Jungers, W.L., Burr, D.B., Cole, M.S., 1998. Body size and scaling of long bone geometry, bone strength, and positional behavior in cercopithecoid primates, in: Strasser, E., Fleagle, J.G., Rosenberger, A.L. (Eds.), Primate locomotion: recent advances. Springer, New York.

Klingenberg, C.P., 2011. MorphoJ: an integrated software package for geometric morphometrics. Mol. Ecol. Resour. 11, 353-357.

Klingenberg, C.P., Gidaszewski, N.A., 2010. Testing and quantifying phylogenetic signals and homoplasy in morphometric data. Sys. Biol. 59, 245-261.

Knigge, R.P., Tocheri, M.W., Orr, C.M., McNulty, K.P., 2015. Three-dimensional geometric morphometric analysis of talar morphology in extant gorilla taxa from highland and lowland habitats. Anat. Rec. 298, 277-290.

Laroche, D., Pozzo, T., Ornetti, P., Tavernier, C., Maillefert, J.F., 2006. Effects of loss of metatarsophalangeal joint mobility on gait in rheumatoid arthritis patients. Rheumatology 45, 435-440.

Latimer, B., Lovejoy, C.O., 1989. The calcaneus of *Australopithecus afarensis* and its implications for the evolution of bipedality. Am. J. Phys. Anthropol. 78, 369-386.

Latimer, B., Lovejoy, C.O., 1990a. Metatarsophalangeal joints of *Australopithecus afarensis*. Am. J. Phys. Anthropol. 83, 13-23.

Latimer, B.M., 1991. Locomotor adaptations in *Australopithecus afarensis:* the issue of arboreality, in: Coppens, Y., Senut, B. (Eds.), Origine(s) de la bipédie chez les hominidés. SNRS, Paris.

Latimer, B.M., Lovejoy, C.O., 1990b. Hallucal tarsometatarsal joint in *Australopithecus afarensis*. Am. J. Phys. Anthropol. 82, 125-133.

Lordkipanidze, D., Jashashvili, T., Vekua, A., de Leon, M.S.P., Zollikofer, C.P.E., Rightmire, G.P., Pontzer, H., Ferring, R., Oms, O., Tappen, M., Bukhsianidze, M., Agusti, J., Kahlke, R., Kiladze, G., Martinez-Navarro, B., Mouskhelishvili, A., Nioradze, M., Rook,

L., 2007. Postcranial evidence from early *Homo* from Dmanisi, Georgia. Nature 449, 305-310.

Lovejoy, C.O., Latimer, B., Suwa, G., Asfaw, B., White, T.D., 2009. Combining prehension and propulsion: the foot of *Ardipithecus ramidus*. Science 326, 72, 72e71-72e78.

Meldrum, D.J., 1991. Kinematics of the cercopithecine foot on arboreal and terrestrial substrates with implications for the interpretation of hominid terrestrial adaptations. Am. J. Phys. Anthropol. 84, 273-289.

Meldrum, D.J., 2007. Letter to the editor:hyperbipeds—or—from biped to strider. Am. J. Phys. Anthropol. 134, 292-294.

Morton, D.J., 1924. Evolution of the human foot II. Am. J. Phys. Anthropol. 7, 1-52.

Nakagawa, N., 1989. Activity budget and diet of patas monkeys in Kala Maloue National Park, Cameroon: a preliminary report. Primates 30, 27-34.

Nowak, M.G., Carlson, K.J., Patel, B.A., 2010. Apparent density of the primate calcaneo-cuboid joint and its association with locomotor mode, foot posture, and the "midtarsal break". Am. J. Phys. Anthropol. 142, 180-193.

Pontzer, H., Rolian, C., Rightmire, G.P., Jashashvili, T., Ponce de León, M.S., Lordkipanidze, D., Zollikofer, C.P.E., 2010. Locomotor anatomy and biomechanics of the Dmanisi hominins. J. Hum. Evol. 58, 492-504.

Proctor, D.J., 2010a. Brief communication: shape analysis of the MT 1 proximal articular surface in fossil hominins and shod and unshod *Homo*. Am. J. Phys. Anthropol. 143, 631-637.

Proctor, D.J., 2010b. Three-dimensional morphometrics of the proximal metatarsal articular surfaces of *Gorilla*, *Pan*, *Hylobates*, and shod and unshod humans. University of Iowa.

Proctor, D.J., 2013. Proximal metatarsal articular surface shape and the evolution of a rigid lateral foot in hominins. J. Hum. Evol. 65, 761-769.

Revell, L.J., 2012. phytools: an R package for phylogenetic comparative biology (and other things). Methods Ecol. Evol. 3, 217-223.

Roberts, N., 1989. The Holocene--an environment history Basil Blackwell Inc. , Oxford.

Rohlf, F.J., 2002. Geometric morphometrics and phylogeny, in: MacLeod, N., Forey, P.L. (Eds.), Morphology, shape, and phylogeny. Taylor & Francis, London, pp. 175-193.

Rohlf, F.J., 2010. tspRelw: relative warps analysis. Version 1.49. Department of Ecology and Evolution, University of New York at Stony Brook, Stony Brook.

Rose, M., 1979. Positional behavior of natural populations: some quantitative results of a field study of *Colobus guereza* and *Cercopithecus atheiops*, in: Morbeck, M.E., Preuschoft, H., Gomberg, N. (Eds.), Environment, behavior, and morphology: dynamic interactions in primates. Gustav Fischer, New York.

Schmitt, D., Larson, S.G., 1995. Heel contact as a function of substrate type and speed in primates. Am. J. Phys. Anthropol. 96, 39-50.

Schultz, A.H., 1934. Some distinguishing characters of the mountain gorilla. J. Mammal. 15, 51-61

Sealy, J., Pfeiffer, S., 2000. Diet, body size, and landscape use among Holocene people in the Southern Cape, South Africa. Curr. Anthropol. 41, 642-655.

Solan, M., Day, M.H., 1992. The Baringo (Kapthurin) ulna. J. Hum. Evol. 22, 307-313.

Stern Jr, J.T., Susman, R.L., 1983. The locomotor anatomy of *Australopithecus afarensis*. Am. J. Phys. Anthropol. 60, 279-317.

Stern, J.T., 2000. Climbing to the top: a personal memoir of *Australopithecus afarensis*. Evol. Anthropol. 9, 111-148.

Stock, J., Pfeiffer, S., 2001. Linking structural variability in long bone diaphyses to habitual behaviors: Foragers from the southern African Later Stone Age and the Andaman Islands. Am. J. Phys. Anthropol. 115, 337-348.

Strait, D.S., Grine, F.E., 2004. Inferring hominoid and early hominid phylogeny using craniodental characters: the role of fossil taxa. J. Hum. Evol. 47, 399-452.

Susman, R., 1988. Hand of *Paranthropus robustus* from Member 1, Swartkrans: fossil evidence for tool behavior. Science 240, 781-784.

Susman, R.L., 1983. Evolution of the human foot: evidence from Plio-Pleistocene hominids. Foot Ankle 3, 365-376.

Susman, R.L., 1989. New hominid fossils from the Swartkrans formation (1979–1986 excavations): postcranial specimens. Am. J. Phys. Anthropol. 79, 451-474.

Susman, R.L., Brain, T.M., 1988. New first metatarsal (SKX 5017) from Swartkrans and the gait of *Paranthropus robustus*. Am. J. Phys. Anthropol. 77, 7-15.

Susman, R.L., de Ruiter, D., Brain, C.K., 2001. Recently identified postcranial remains of *Paranthropus* and early *Homo* from Swartkrans Cave, South Africa. J. Hum. Evol. 41, 607-629.

Susman, R.L., de Ruiter, D.J., 2004. New hominin first metatarsal (SK 1813) from Swartkrans. J. Hum. Evol. 47, 171-181.

Susman, R.L., Stern, J.J.T., Jungers, W.L., 1984. Arboreality and bipedality in the Hadar hominids. Folia Primatol. 43, 113-156.

Sutikna, T., Tocheri, M.W., Morwood, M.J., Saptomo, E.W., Jatmiko, Awe, R.D., Wasisto, S., Westaway, K.E., Aubert, M., Li, B., Zhao, J.-x., Storey, M., Alloway, B.V., Morley, M.W., Meijer, H.J.M., van den Bergh, G.D., Grün, R., Dosseto, A., Brumm, A., Jungers, W.L., Roberts, R.G., 2016. Revised stratigraphy and chronology for Homo floresiensis at Liang Bua in Indonesia. Nature 532, 366-369.

Thorpe, S.K.S., Crompton, R.H., 2005. Locomotor ecology of wild orangutans (*Pongo pygmaeus abelii*) in the Gunung Leuser Ecosystem, Sumatra, Indonesia: a multivariate analysis using log-linear modelling. Am. J. Phys. Anthropol. 127, 58-78.

Tocheri, M.W., Solhan, C.R., Orr, C.M., Femiani, J., Frohlich, B., Groves, C.P., Harcourt-Smith, W.E., Richmond, B.G., Shoelson, B., Jungers, W.L., 2011. Ecological divergence and medial cuneiform morphology in gorillas. J. Hum. Evol. 60, 171-184.

Tukey, J.W., 1977. Exploratory data analysis. Pearson.

Tuttle, R.H., 1981. Evolution of hominid bipedalism and prehensile capabilities. Philos. T. Roy. Soc. B. 292, 89-94.

Vereecke, E., D'Août, K., De Clercq, D., Van Elsacker, L., Aerts, P., 2003. Dynamic plantar pressure distribution during terrestrial locomotion of bonobos (*Pan paniscus*). Am. J. Phys. Anthropol. 120, 373-383.

Ward, C.V., 2002. Interpreting the posture and locomotion of *Australopithecus afarensis*: where do we stand? Am. J. Phys. Anthropol. 119, 185-215.

Ward, C.V., Kimbel, W.H., Johanson, D.C., 2011. Complete fourth metatarsal and arches in the foot of *Australopithecus afarensis*. Science 331, 750-753.

White, T.D., Suwa, G., Asfaw, B., 1994. *Australopithecus ramidus*, a new species of early hominid from Aramis, Ethiopia Nature 371, 306-312.

Wiley, D.F., Amenta, N., Alcantara, D.A., Ghosh, D., Kil, Y.J., Delson, E., Harcourt-Smith, W.E.H., Rohlf, F.J., John, K.S., Hamann, B., 2005. Evolutionary morphing IEEE Visualization Conference, Minneapolis, MN, 431-438.

Yamagiwa, J., Mwanza, N., Spangenberg, A., Maruhashi, T., Yumoto, T., Fischer, A., Steinhauer-Burkart, B., 1993. A census of the eastern lowland gorillas *Gorilla gorilla graueri* in Kahuzi-Biega national park with reference to mountain gorillas *G. g. beringei* in the Virunga region, Zaire. Biol Conserv 64, 83-89.

Zipfel, B., DeSilva, J.M., Kidd, R.S., 2009. Earliest complete hominin fifth metatarsal—Implications for the evolution of the lateral column of the foot. Am. J. Phys. Anthropol. 140, 532-545.

Zipfel, B., DeSilva, J.M., Kidd, R.S., Carlson, K.J., Churchill, S.E., Berger, L.R., 2011. The foot and ankle of *Australopithecus sediba*. Science 333, 1417-1420.

Zipfel, B., Kidd, R., 2006. Hominin first metatarsals (SKX 5017 and SK 1813) from Swartkrans: a morphometric analysis. Homo 57, 117-131.

Taxon	Locomotor Mode[1]	Foot Posture[2]	µCT	CT	Laser Scan
Hominoids					
Homo sapiens	B	FCP	-	22	18
Gorilla beringei beringei	KW/C	IHSP	-	3	13
Gorilla beringei graueri	KW/C	IHSP	-	3	11
Gorilla gorilla gorilla	KW/C	IHSP	-	4	29
Pan paniscus	KW/C	IHSP	-	1	18
Pan troglodytes	KW/C	IHSP	-	7	32
Pongo abelii	S	IHSP	-	-	10
Pongo pygmaeus	S	IHSP	-	-	13
Hylobates lar	R	MFP	17	-	-
Cercopithecoids					
Chlorocebus aethiops	TQ	DG/SP	9	-	-
Erythrocebus patas	TQ	DG	10	-	-
Macaca fascicularis	TQ	DG/SP	10	-	-
Macaca mulatta	TQ	DG/SP	16	-	-
Macaca nemestrina	TQ	DG/SP	8	-	-
Papio ursinus	TQ	DG/SP	14	-	-
Nasalis larvatus	AQ	DG/SP	15	-	-
Presbytis rubicunda	AQ	DG/SP	-	-	18
Ceboids (NWMs)					
Alouatta seniculus	AQ	DG/SP	21	-	-
Ateles fusciceps	AQ/S	DG/SP	18	-	-
Cebus apella	AQ	DG/SP	21	-	-

Table 2.1. **Extant anthropoids included in MT 1 shape analyses**. [1] B = biped; KW/C = knuckle-walking/climber; S = suspensory/quadrumanous climber = R ricochetal brachiator; TQ = terrestrial quadruped; AQ = arboreal quadruped. *Ateles* has been shown to be more suspensory than other NWMs (Bergeson, 1998, Cant et al., 2001).
[2]FCP = full contact plantigrade; IHSP = inverted heel-strike plantigrade; MFP = midfoot plantigrade; DG/SP = digitigrade/semiplantigrade. Foot postures and general locomotor categories were determined based on descriptions in the literature (Dunbar and Dunbar, 1974; Rose, 1979; Nakagawa, 1989; Doran, 1992; Doran, 1993; Schmitt and Larson, 1995; Cant, 1987; Cant, 1988; Jungers et al., 1998; Boonratana, 2000; Cant et al., 2001; Vereecke et al., 2003; Nowak et al., 2010; Fleagle, 2013; Gosselin-Ildari, 2013).

Accession Number	Geological Age (Ma)	Taxon	Locality	Observation
ARA-VP-6/500-089	4.4	*Ardipithecus ramidus*	Aramis, Ethiopia	Original (μCT)
A.L. 333-115A	3.0	*Australopithecus afarensis*	Hadar, Ethiopia	Cast (LS)
StW 562	2.6 – 2.0	*Australopithecus africanus*	Sterkfontein Member 4	Original (LS)
StW 595	2.6 – 2.0	*Australopithecus africanus*	Sterkfontein Member 4	Original (LS)
KNM-ER 64062	1.88	*Homo* sp. (cf. *erectus*)	Above KBS tuff, Ileret	Original (μCT)
SKX 5017	1.8	*Paranthropus robustus*	Swartkrans Member 1	Original (LS)
SK 1813	1.8 – 1.1	*Paranthropus robustus*	Swartkrans Member 1 or 2	Original (LS)
KNM-BK 63	0.5	*Homo* cf. *erectus*	Baringo Kapthurin, Kenya	Original (LS)
LB 1	~0.1 – 0.06	*Homo floresiensis*	Liang Bua, Indonesia	Original (CT)
U.W. 101-1443	Undated	*Homo naledi*	Gauteng, South Africa	Original (LS)

Table 2.2. **Fossil hominins included in the MT 1 shape analyses**. See text (Materials and Methods) for geological age estimates and taxonomic determinations. CT = computed tomography; μCT = micro-computed tomography; LS = 3D Laser surface Scan.

Species	*A. seniculus*	*A. fusciceps*	*C. apella*	*C. aethiops*	*E. patas*	*M. mulatta*	*M. nemestrina*	*M. fascicularis*	*P. ursinus*	*N. larvatus*	*P. rubicunda*
A. seniculus	1.0000	-	-	-	-	-	-	-	-	-	-
A. fusciceps	ns	1.0000	-	-	-	-	-	-	-	-	-
C. apella	ns	**<0.0001**	1.0000	-	-	-	-	-	-	-	-
C. aethiops	**<0.0001**	ns	**<0.0001**	1.0000	-	-	-	-	-	-	-
E. patas	**<0.0001**	**<0.0001**	**<0.0001**	**<0.001**	1.0000	-	-	-	-	-	-
M. mulatta	ns	ns	**<0.0001**	ns	**<0.0001**	1.0000	-	-	-	-	-
M. nemestrina	**<0.0001**	**<0.0001**	**<0.0001**	**<0.001**	ns	ns	1.0000	-	-	-	-
M. fascicularis	**<0.0001**	ns	**<0.0001**	ns	ns	ns	ns	1.0000	-	-	-
P. ursinus	**<0.0001**	**<0.0001**	**<0.0001**	**<0.05**	ns	ns	ns	ns	1.0000	-	-
N. larvatus	**<0.0001**	**<0.0001**	**<0.0001**	**<0.0001**	**<0.0001**	**<0.0001**	ns	ns	ns	1.0000	-
P. rubicunda	**<0.0001**	ns	**<0.0001**	ns	**<0.0001**	ns	ns	ns	**<0.05**	**<0.0001**	1.0000
H. lar	**<0.0001**	**<0.05**	**<0.0001**	**<0.05**	ns	**<0.0001**	**<0.0001**	ns	ns	ns	**<0.05**
P. abelii	**<0.0001**	**<0.0001**	**<0.0001**	**<0.004**	ns	**<0.0001**	**<0.0001**	ns	ns	ns	**<0.01**
P. pygmaeus	**<0.0001**	**<0.0001**	**<0.0001**	**<0.0001**	ns	**<0.0001**	**<0.0001**	**<0.0001**	**<0.05**	ns	**<0.0001**
G. beringei	**<0.0001**	**<0.0001**	**<0.0001**	**<0.0001**	**<0.0001**	**<0.0001**	**<0.0001**	**<0.0001**	**<0.0001**	ns	**<0.0001**
G.g. gorilla	**<0.0001**	**<0.0001**	**<0.0001**	**<0.0001**	**<0.001**	**<0.0001**	**<0.0001**	**<0.0001**	**<0.0001**	ns	**<0.0001**
G.b. graueri	**<0.0001**	**<0.0001**	**<0.0001**	**<0.0001**	ns	**<0.0001**	**<0.0001**	**<0.0001**	**<0.001**	ns	**<0.0001**
P. paniscus	**<0.0001**	**<0.001**	**<0.0001**	ns	ns	**<0.001**	**<0.0001**	ns	ns	ns	**<0.0001**
P. troglodytes	**<0.0001**	**<0.0001**	**<0.0001**	ns	ns	**<0.0001**	**<0.0001**	ns	ns	ns	**<0.0001**
H. sapiens	**<0.0001**	**<0.0001**	**<0.0001**	**<0.0001**	**<0.0001**	**<0.0001**	**<0.0001**	**<0.0001**	**<0.0001**	**<0.0001**	**<0.0001**

(Continued on next page)

Table 2.3: *Post-hoc* Tukey's HSD results on PC 1 comparing anthropoid genera following a MANOVA on MT 1 shape variables (PC 1 – PC 5). PC 1 primarily tracked MT head robusticity. Humans and mountain gorillas overlap to the exclusion of all other groups. Bold = significance at $\alpha = 0.05$.

Species	*H. lar*	*P. abelii*	*P. pygmaeus*	*G. beringei*	*G.g. gorilla*	*G.g. graueri*	*P. paniscus*	*P. troglodytes*	*H. sapiens*
A. seniculus	-	-	-	-	-	-	-	-	-
A. fusciceps	-	-	-	-	-	-	-	-	-
C. 56aella	-	-	-	-	-	-	-	-	-
C. aethiops	-	-	-	-	-	-	-	-	-
E. patas	-	-	-	-	-	-	-	-	-
M. mulatta	-	-	-	-	-	-	-	-	-
M. nemestrina	-	-	-	-	-	-	-	-	-
M. fascicularis	-	-	-	-	-	-	-	-	-
P. ursinus	-	-	-	-	-	-	-	-	-
N. larvatus	-	-	-	-	-	-	-	-	-
P. rubicunda	-	-	-	-	-	-	-	-	-
H. lar	1.0000	-	-	-	-	-	-	-	-
P. abelii	ns	1.0000	-	-	-	-	-	-	-
P. pygmaeus	**<0.01**	ns	1.0000	-	-	-	-	-	-
G. beringei	ns	**<0.001**	ns	1.0000	-	-	-	-	-
G.g. gorilla	ns	**<0.05**	ns	ns	1.0000	-	-	-	-
G.b. graueri	**<0.001**	ns	ns	ns	ns	1.0000	-	-	-
P. paniscus	ns	ns	**<0.0001**	**<0.0001**	**<0.0001**	**<0.0001**	1.0000	-	-
P. troglodytes	ns	ns	**<0.001**	**<0.0001**	**<0.001**	**<0.001**	ns	1.0000	-
H. sapiens	**<0.0001**	**<0.0001**	**<0.01**	ns	**<0.0001**	**<0.001**	**<0.0001**	**<0.0001**	1.0000

Table 2.3: *Post-hoc* Tukey's HSD results on PC 1 comparing anthropoid species following a MANOVA on MT 1 shape variables (PC 1 – PC 5). PC 1 principally tracked MT head robusticity. Humans overlap with *Gorilla* and *Pongo*. Bold = significance at $\alpha = 0.05$.

Species	*A. seniculus*	*A. fusciceps*	*C. apella*	*C. aethiops*	*E. patas*	*M. mulatta*	*M. nemestrina*	*M. fascicularis*	*P. ursinus*	*N. larvatus*	*P. rubicunda*
A. seniculus	1.0000	-	-	-	-	-	-	-	-	-	-
A. fusciceps	ns	1.0000	-	-	-	-	-	-	-	-	-
C. apella	ns	ns	1.0000	-	-	-	-	-	-	-	-
C. aethiops	ns	ns	ns	1.0000	-	-	-	-	-	-	-
E. patas	ns	ns	ns	ns	1.0000	-	-	-	-	-	-
M. mulatta	ns	ns	ns	ns	ns	1.0000	-	-	-	-	-
M. nemestrina	ns	ns	ns	ns	ns	ns	1.0000	-	-	-	-
M. fascicularis	ns	ns	ns	ns	ns	ns	ns	1.0000	-	-	-
P. ursinus	ns	ns	**<0.001**	ns	ns	ns	ns	ns	1.0000	-	-
N. larvatus	ns	ns	**<0.0001**	ns	ns	**<0.001**	ns	ns	ns	1.0000	-
P. rubicunda	ns	ns	ns	ns	ns	ns	ns	ns	**<0.001**	**<0.005**	1.0000
H. lar	**<0.001**	**<0.05**	ns	ns	**<0.01**	ns	**<0.005**	ns	**<0.0001**	**<0.0001**	ns
P. abelii	**<0.0001**	**<0.0001**	**<0.01**	**<0.0001**	**<0.0001**	**<0.005**	**<0.0001**	**<0.0001**	**<0.0001**	**<0.0001**	**<0.01**
P. pygmaeus	**<0.0001**	**<0.0001**	**<0.0001**	**<0.0001**	**<0.0001**	**<0.0001**	**<0.0001**	**<0.0001**	**<0.0001**	**<0.0001**	**<0.0001**
G. beringei	**<0.0001**	**<0.0001**	**<0.0001**	**<0.0001**	**<0.0001**	**<0.0001**	**<0.0001**	**<0.0001**	**<0.0001**	**<0.0001**	**<0.0001**
G.g. gorilla	**<0.0001**	**<0.0001**	**<0.0001**	**<0.0001**	**<0.0001**	**<0.0001**	**<0.0001**	**<0.0001**	**<0.0001**	**<0.0001**	**<0.0001**
G.g. graueri	ns	ns	ns	ns	**<0.0001**	ns	**<0.05**	ns	**<0.001**	**<0.0001**	ns
P. paniscus	**<0.0001**	**<0.001**	**<0.0001**	**<0.0001**	**<0.0001**	**<0.001**	**<0.0001**	**<0.0001**	**<0.0001**	**<0.0001**	**<0.0001**
P. troglodytes	**<0.0001**	**<0.001**	ns	ns	**<0.0001**	ns	**<0.0001**	**<0.05**	**<0.0001**	**<0.0001**	ns
H. sapiens	**<0.0001**	**<0.0001**	**<0.0001**	**<0.001**	**<0.001**	ns	ns	**<0.05**	ns	**<0.0001**	**<0.0001**

(Continued on next page)

Table 2.4 *Post-hoc* Tukey's HSD results on PC 2 comparing anthropoid species following a MANOVA on MT 1 shape variables (PC 1 – PC 5). PC 2 primarily tracked MT head orientation. Humans are unique amongst apes but overlap with cercopithecoids.

Species	*H. lar*	*P. abelii*	*P. pygmaeus*	*G. beringei*	*G.g. gorilla*	*G.g. graueri*	*P. paniscus*	*P. troglodytes*	*H. sapiens*
A. seniculus	-	-	-	-	-	-	-	-	-
A. fusciceps	-	-	-	-	-	-	-	-	-
C. apella	-	-	-	-	-	-	-	-	-
C. aethiops	-	-	-	-	-	-	-	-	-
E. patas	-	-	-	-	-	-	-	-	-
M. mulatta	-	-	-	-	-	-	-	-	-
M. nemestrina	-	-	-	-	-	-	-	-	-
M. fascicularis	-	-	-	-	-	-	-	-	-
P. ursinus	-	-	-	-	-	-	-	-	-
N. larvatus	-	-	-	-	-	-	-	-	-
P. rubicunda	-	-	-	-	-	-	-	-	-
H. lar	1.0000	-	-	-	-	-	-	-	-
P. abelii	ns	1.0000	-	-	-	-	-	-	-
P. pygmaeus	**<0.0001**	ns	1.0000	-	-	-	-	-	-
G. beringei	**<0.0001**	ns	ns	1.0000	-	-	-	-	-
G.g. gorilla	**<0.0001**	ns	ns	ns	1.0000	-	-	-	-
G.g. graueri	ns	ns	**<0.0001**	**<0.0001**	**<0.0001**	1.0000	-	-	-
P. paniscus	**<0.001**	ns	ns	**<0.0001**	ns	**<0.001**	1.0000	-	-
P. troglodytes	ns	ns	**<0.0001**	**<0.0001**	**<0.0001**	ns	**<0.0001**	1.0000	-
H. sapiens	**<0.0001**	**<0.0001**	**<0.0001**	**<0.0001**	**<0.0001**	**<0.0001**	**<0.0001**	**<0.0001**	1.0000

Table 2.4: *Post-hoc* Tukey's HSD results on PC 2 comparing anthropoid species following a MANOVA on MT 1 shape variables (PC 1 – PC 5). PC 2 principally tracked MT head orientation. Humans are unique amongst apes but overlap with cercopithecoids. Bold = significance at $\alpha = 0.05$.

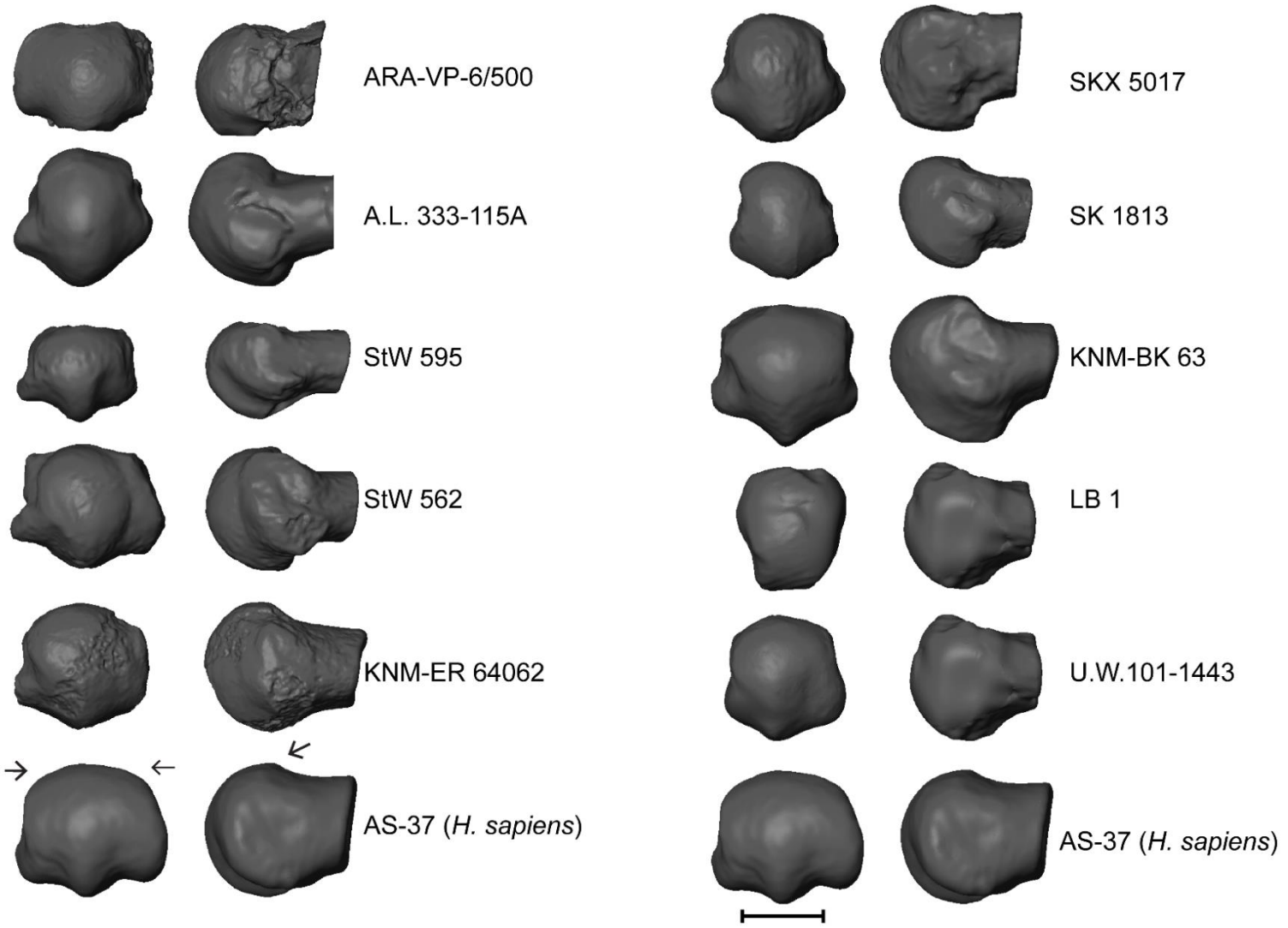

Figure 2.1: Comparative morphology of fossil first metatarsals (MT 1). Note that Homo is characterized by dorsal overlap of the distal articular surface onto the MT shaft and by wide flattening of the dorsal articular surface (arrows). Left column: distal views. Right column: lateral views. Bar: 1 cm.

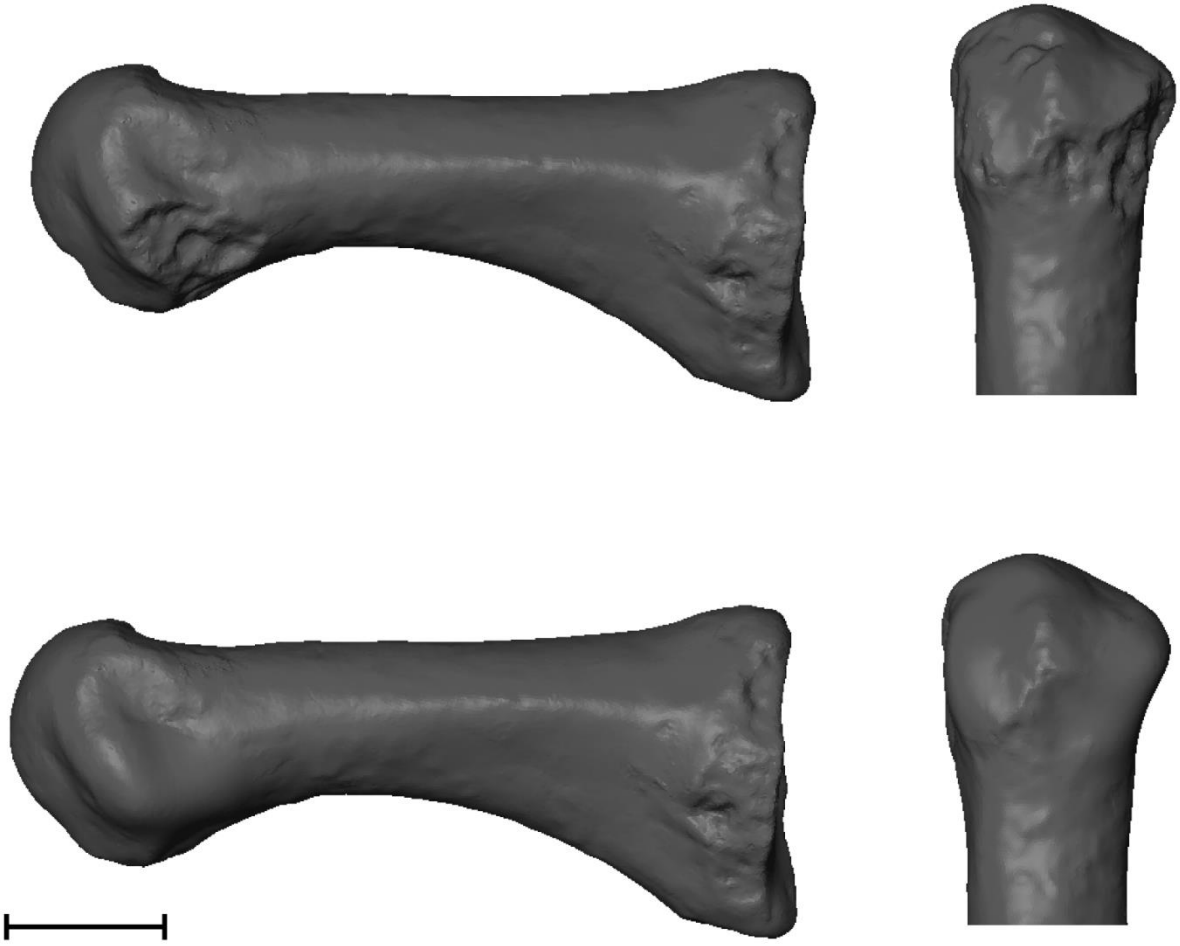

Figure 2.2: *Homo naledi* MT 1 (U.W.101-1443) pre (top) and post (bottom) reconstruction in Geomagic Studio 2012. Only the plantolateral part of the distal articular surface, which had broken off of the fossil MT 1, was reconstructed. No other reconstruction was needed for the rest of the fossil sample. Left: Lateral view. Right: Plantar view. Bar: 1 cm.

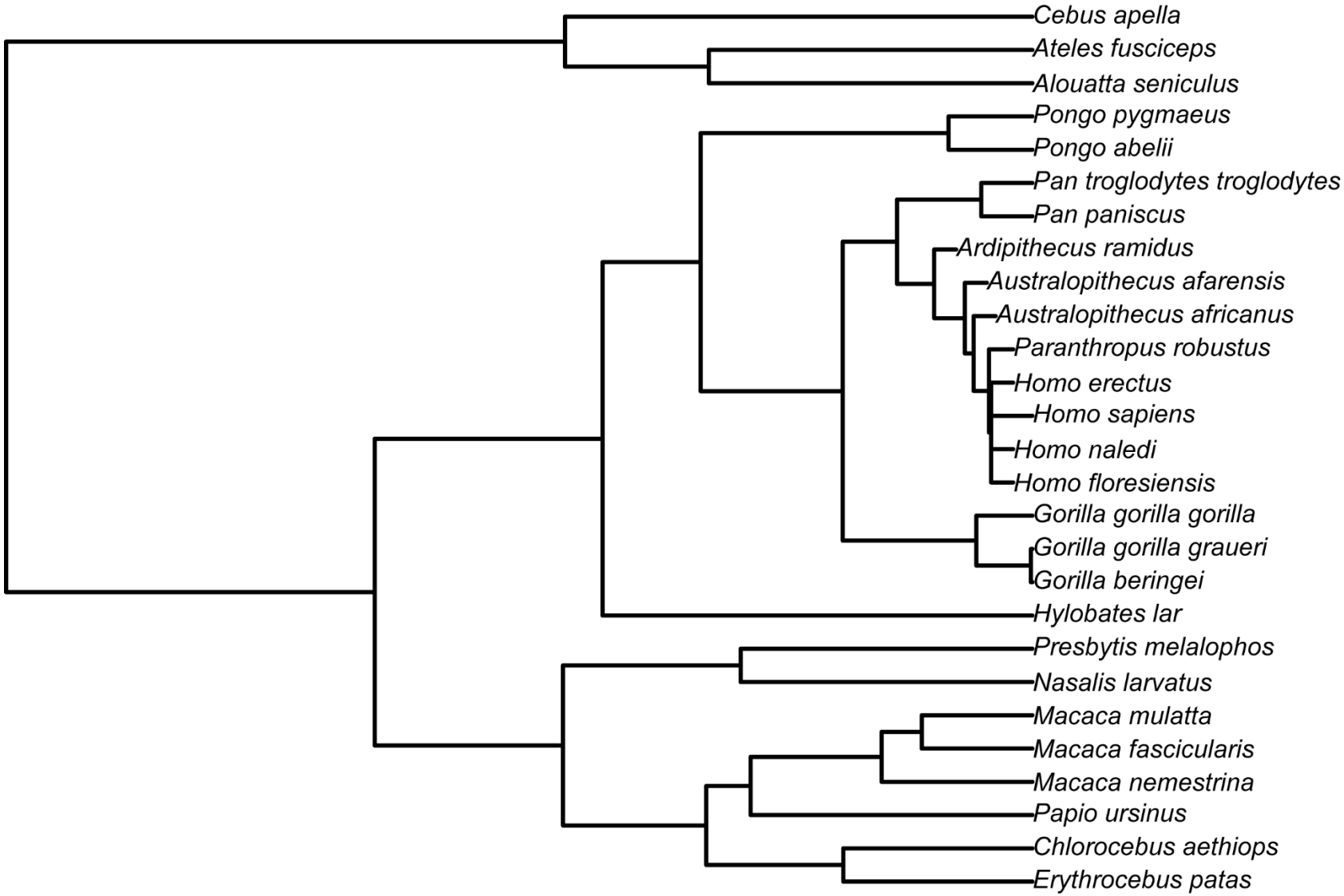

Figure 2.3: Ultrametric phylogenetic tree used for all *SURFACE* analyses. Branches proportional to time. See Figure 2.3.1 for hominin tree.

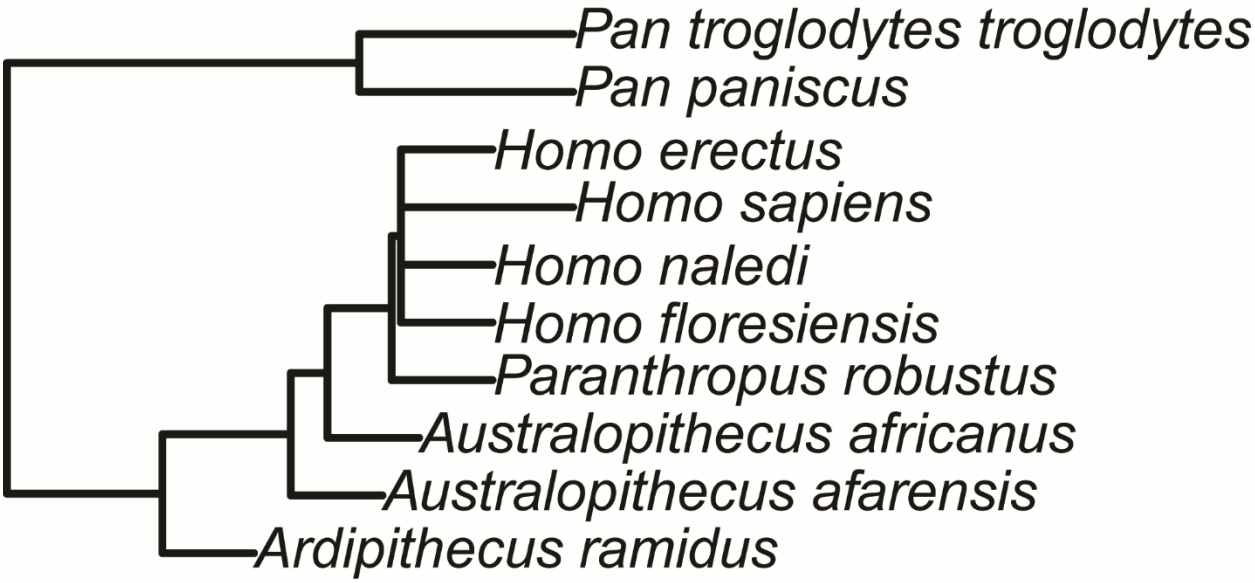

Figure 2.3.1: The hominin clade, based on craniodental characters from Strait and Grine (2004). Branch lengths proportional to time. *Homo erectus*, *Homo floresiensis*, and *Homo naledi* were inputted as an unresolved polytomy in the *SURFACE* analyses, in order to take the most conservative interpretation of this material, whose chronological dating is either not present or debated.

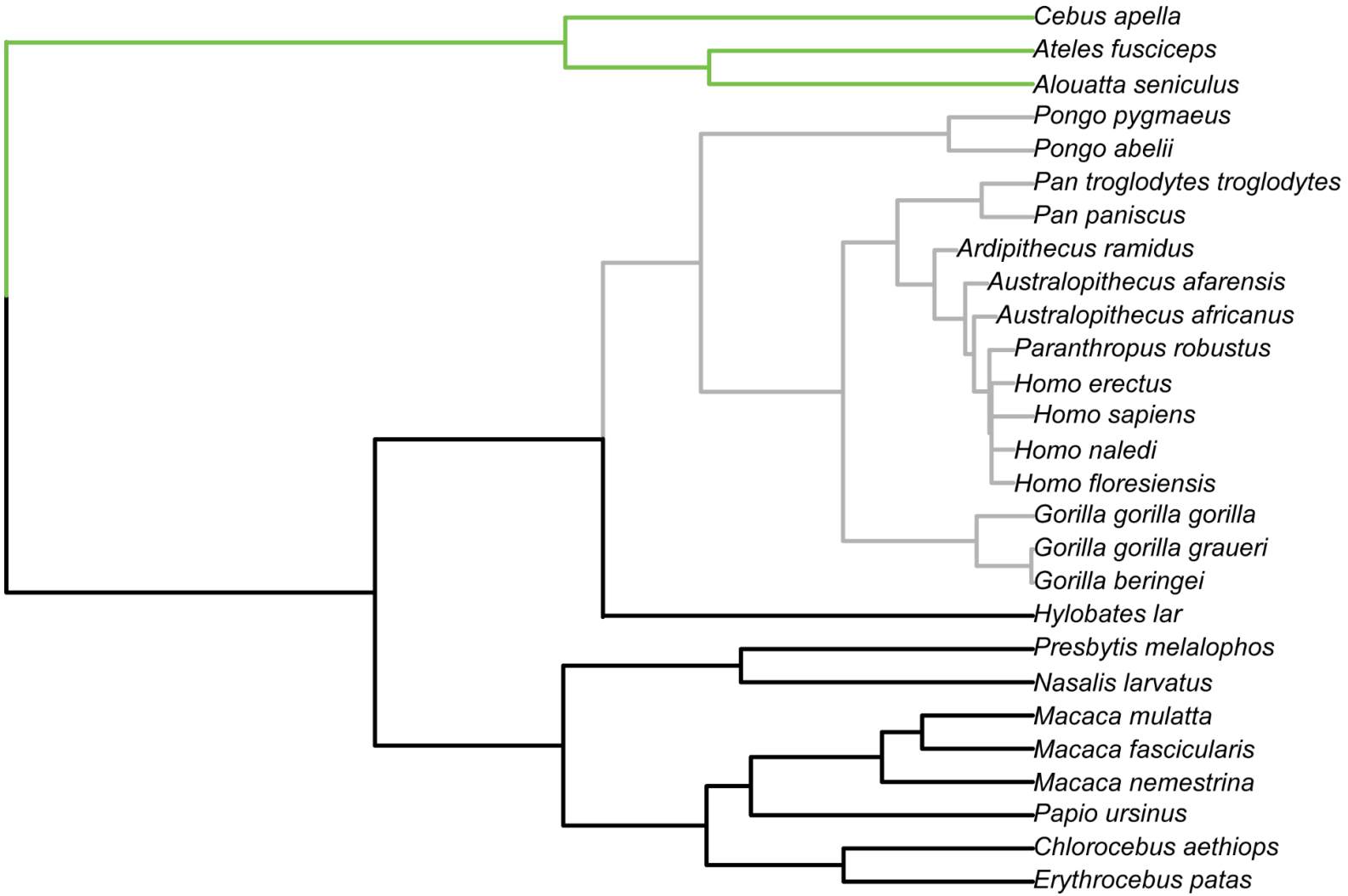

Figure 2.4: Time-calibrated phylogenetic tree with estimated adaptive regimes painted onto the tree branches. Adaptive regimes are based on PC 1 (MT 1 head robusticity, plantar morphology) and PC 2 (MT 1 head orientation) scores. No evidence for convergence between anthropoid clades was found. The three regime shifts towards different adaptive optima includes NWMs (green), cercopithecoids and gibbons (black), and great apes (gray).

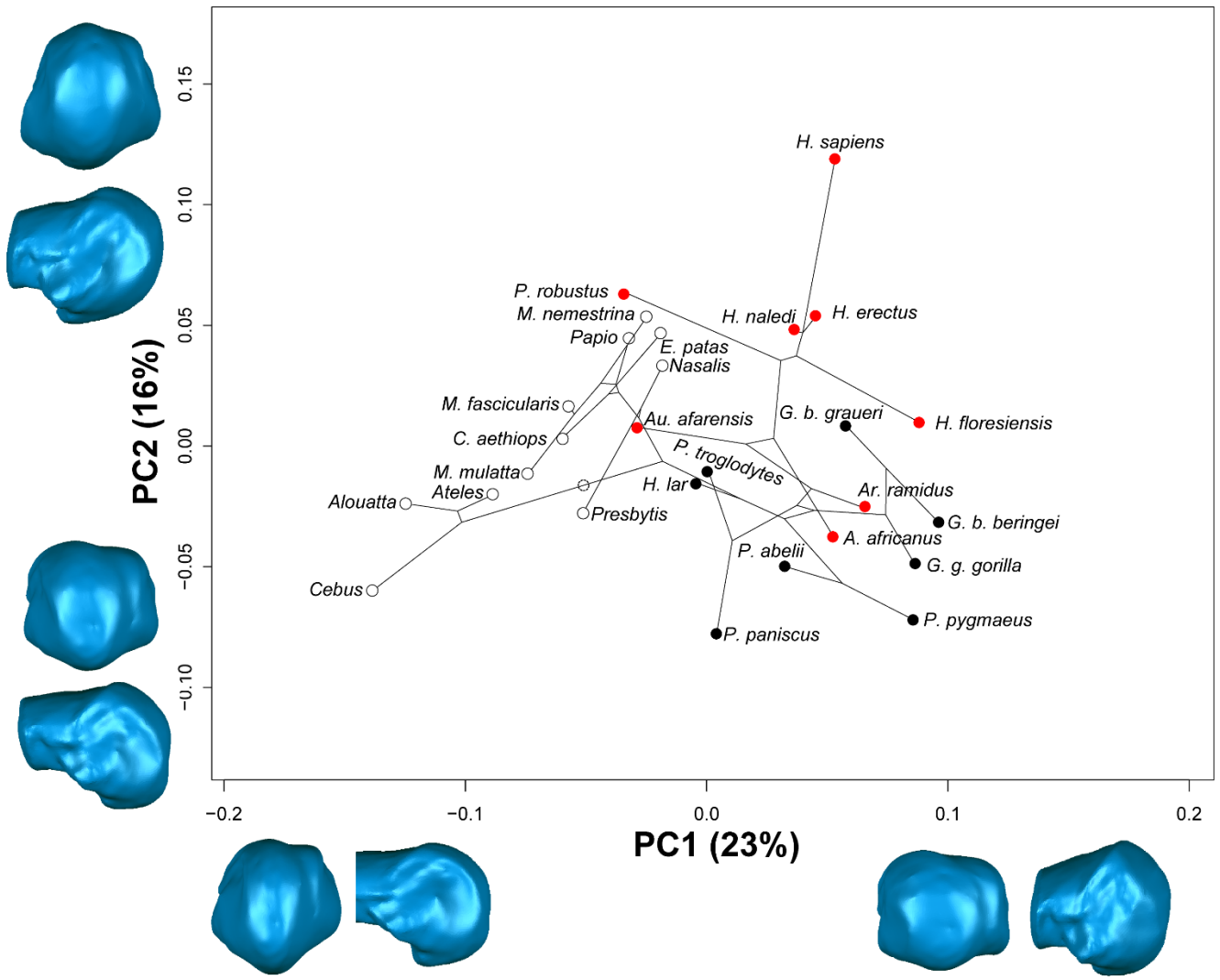

Figure 2.5: Phylomorphospace plot of the anthropoid molecular phylogeny superimposed upon a species-means bivariate PCA scatterplot. Upon diverging towards their respective adaptive optima, NWMs, cercopithecoids and gibbons undergo relatively little evolutionary shape change in the MT 1 head compared to great apes. Within hominins, major evolutionary shape changes occurred in *Ardipithecus*, *Australopithecus*, *Paranthropus*, and *Homo*.

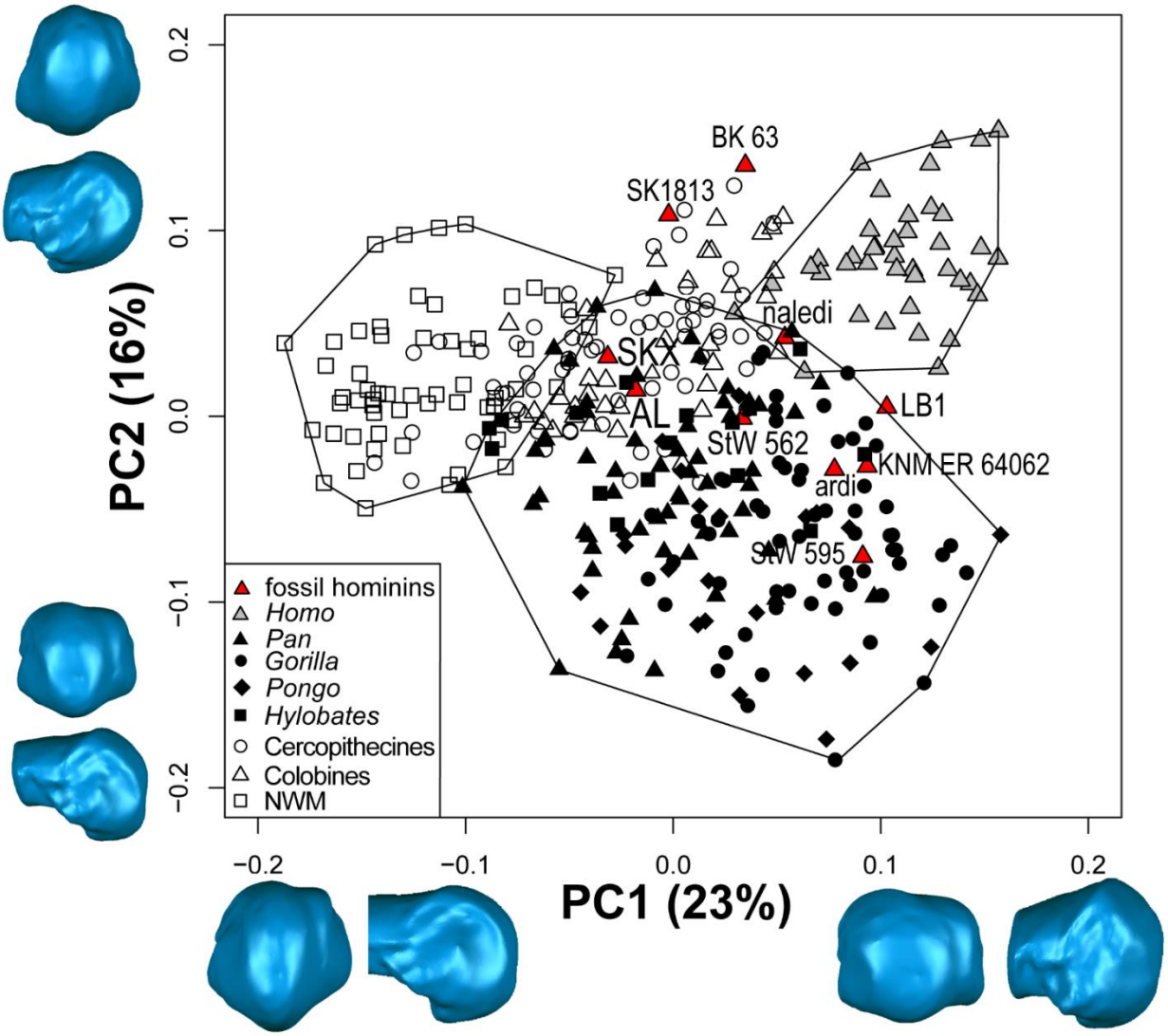

Figure 2.6: PCA scatterplot of PC 1 vs. PC 2 for MT 1. Note the general separation of NWMs (open rectangles), apes (filled shapes), and humans (gray triangles). Minimum convex polygons are constructed for these groups to illustrate their ranges in the morphospace. Cercopithecoids (open shapes) overlap somewhat with all of these taxa and its polygon is removed to improve clarity. Fossil hominins (red triangles) primarily fall within the ape polygon or somewhere intermediate between the great ape and human polygon. PC 1 strongly tracked dorso-plantar orientation of the MT head and plantar condylar morphology whereas PC 2 tracked dorsal MT 1 head robusticity. 3D surface morphs in lateral and distal views represent articular shape differences of observed extremes (PC 1: -0.15 - 0.15; PC 2: -0.08 - 0.12).

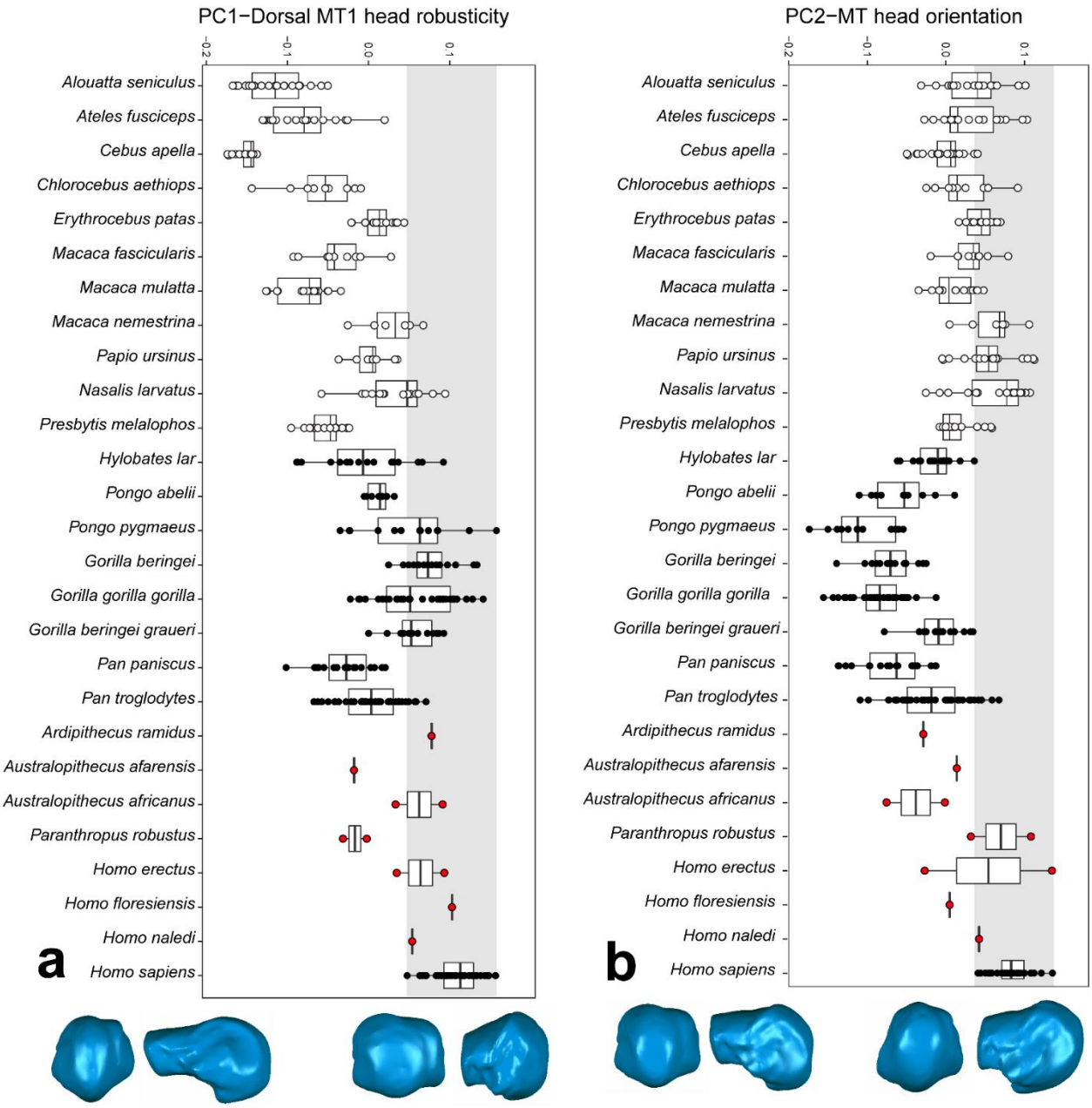

Figure 2.7: Cleveland box-and-whisker plots of PC 1 (a) and PC 2 (b) scores for the anthropoid MT 1. 3D surface morphs represent articular shape differences of observed extremes (PC 1/2: -0.18-0.15). Polygons are shown in distal and lateral views. Generally, humans overlap with monkeys and hominins in PC 1 (dorso-plantar head orientation), and apes/hominins in PC 2 (dorsal head robusticity). Shaded bar: modern human range. Vertical bars: median. Rectangles: interquartile range. Horizontal bars: range.

Chapter 3

Shape Analysis of the Anthropoid Lesser Toes (MT 2 – MT 5)

3.1 Introduction

Physical anthropologists tend to focus on the hallux because in many hominins it is at least partially or completely adducted (Day and Napier, 1964; Clarke and Tobias, 1995; Jungers et al., 2009; Pontzer et al., 2010; Jungers et al., 2015; Harcourt-Smith et al., 2015) and in this configuration the hallux contributes disproportionally to forefoot function (Bojsen-Møller, 1979). However, the lesser toes (i.e., MT 2 – MT 5) are of keen interest in their own right, and provide most of the propulsive force in the sagittal plane at the end of stance in those primate species that possess a divergent or diminutive hallux (Meldrum, 1991; Holowka and Fernández, 2016). Additionally, the lesser toes contribute significantly to forefoot function in bipedalism as well (Holowka and Fernández, 2016), and in cases where the pedal fossil material available is scarce and/or missing the hallux, information gleaned from the lesser toes can be very important in determining the locomotor behavior of a given fossil hominin. In modern humans, the non-hallucal metatarsals are generally similar to one another in form, perhaps in part because of their serial homology in development (Young et al., 2010). The human morphology at the lesser toes is similar to what is seen in the hallux in functionally important ways, with dorsally oriented and robust MT heads. Non-hallucal specimens are known from the same fossil hominins discussed in Chapter 2 (see Materials and Methods), but additionally there are some notable, isolated non-hallucal metatarsals that have caused great debate amongst physical anthropologists. Of these, the most well-known is A.L. 333-160, an intact MT 4 attributed to *Australopithecus afarensis.* It has been argued that A.L. 333-160 is diagnostic of bipedalism and the presence of a longitudinal arch in the absence of any other pedal material considered (Ward et al., 2011) based in part on the qualitative assessment of its MT head shape and orientation. Another controversial fossil is the isolated MT 2 from South Africa, StW 89 (Deloison, 2003; DeSilva et al., 2012), which has proven to be quite vexing because it lacks any associated craniodental remains, and presents with

a strange mosaicism that looks neither entirely ape- nor entirely human-like. The *Ardipithecus* assemblage includes a nearly intact MT 3, ARA-VP-6/500-505, which has been argued to look quite human-like (Lovejoy et al., 2009), especially compared to its comparatively primitive hallux (see Chapter 2). There is considerable variation in the *Au. afarensis* metatarsals, with some looking more derived than others (Latimer et al., 1982), even within the single individual represented by the A.L. 333-115 material. Other material from early *Homo* like the lesser MTs of KNM-ER 64062 (Jungers et al., 2015) have been described as looking essentially human-like, which again is in contrast to its hallux, which does not look entirely modern.

Although the functional morphology of the hominin forefoot joints has been discussed thoroughly (Latimer et al., 1982; Susman, 1983; Latimer and Lovejoy, 1990; Susman and Brain, 1988; Susman and deRuiter, 2004), relatively little quantitative work exists for the MT heads of the lesser toes. The qualitative descriptions of the pedal morphology in the literature tend to vary somewhat between studies and focus on different aspects (Latimer et al., 1982; Susman, 1983; Susman and Brain, 1988; Latimer and Lovejoy, 1990a; Lovejoy et al., 2009; Ward et al., 2011; Drapeau and Harmon, 2013), which makes it difficult to make meaningful comparisons. Often, fossil hominin specimens appear human-like in one aspect of MT head morphology, but are also often mosaic in total morphological pattern (Stern and Susman, 1991). For example, the *Ardipithecus* MT 1 and StW 89 may have some dorsal orientation present in the MT head, but the majority of the articular surface is still oriented plantarly. To better address questions about forefoot functional morphology, the lesser metatarsals (II – V) in a broad sample of anthropoids and fossil hominins are subjected in this chapter to multivariate 3-dimensional (3D) analyses in order to quantify their hypothesized correlates of function. If dorsal orientation of the MT head facilitates greater potential for dorsiflexion at the MTPJs (Susman, 1983; Stern and Susman, 1983; Susman and de Ruiter, 2004; Ward et al., 2011, 2012; DeSilva et al., 2012), one might also expect to see at least some evidence of dorsal MT head orientation in digitigrade, more habitually terrestrial genera such as *Papio* and *Erythrocebus* (Meldrum, 1991; Schmitt and Larson, 1995; but see Patel, 2010). Therefore, I predict that humans will still be unique in consistently demonstrating all of these derived morphologies simultaneously, but I also suspect that more terrestrial and more digitigrade taxa will show some degree of convergence with humans. In contrast, I predict that habitually arboreal quadrupeds and suspensory species should have more plantarly oriented metatarsal heads than their more terrestrial counterparts. Although

African apes are more terrestrial than Asian apes (Doran, 1992, 1993, 1996; Fleagle, 2013), they also exhibit pedal grasping adaptations for vertical climbing of large supports and *Pan* sp. frequently engage in suspension (Tuttle, 1970; Bojsen-Møller, 1979; Lewis, 1980; DeSilva, 2008, 2009). Moreover, African apes do not greatly dorsiflex their toes during the push off phase of knuckle-walking quadrupedalism (Griffin et al., 2010b; Holowka et al., 2014; Holowka and Fernández, 2016); accordingly, despite their typical use of terrestrial locomotion during travel, I predict that African apes will demonstrate little to no dorsal reorganization of the MT head.

3.2 Materials and Methods

The methods are identical to those described in Chapter 2, with differences in the sample detailed below.

3.2.1 Extant Sample

I quantified shape differences in the distal MT 2 – 5 within a comparative sample of 1,385 non-hallucal anthropoid metatarsals (Table 3.1 – 3.4), collected and processed from the same institutions and protocols listed in Chapter 2. Male-to-female sex ratios were roughly even, although sex data unknown for the *Homo* sample. In highly dimorphic species (e.g., *Gorilla*, *Pongo*), statistical tests for sex differences were performed, no significant differences were found, and thus the data were pooled.

3.2.2 Fossil Sample

I analyzed 19 fossil MT 2 – 5 heads (Table 3.5; Figs. 3.1 – 3.4), all from fossil hominins described in Chapter 2; more specific information about the specimens analyzed follows below:

Ardipithecus ramidus

ARA-VP-6/500-505 is a nearly intact left MT 3 recovered from Aramis, located near the Daam Aatu Basaltic Tuff (~4.4 Ma; White et al., 1994). The MT head is oriented dorsally with slight external rotation present, more similar to the condition seen in modern humans than in apes (Lovejoy et al., 2009). The *Ardipithecus* MT 3 was micro CT scanned by Dr. Gen Suwa and Dr. Tim White (Lovejoy et al., 2009), who allowed partial scans of these bones including only the distal articular surfaces to be included in this dissertation. Note that for analysis with ARA-

VP-6/505, landmarks 1 and 9 (see Fernández et al., 2015; Table 2) were removed in order to include the scan of this fossil, which only included the distal articular surface.

Australopithecus afarensis

A.L. 333-115B-E are all distal fragments of MT 2 – 5 found along with the A.L. 333-72 in the Denan Dora member of the Hadar Formation (~3.0 Ma; Aronson et al., 1977). A.L. 333-72 is either a distal MT 2 or MT 3 (Latimer et al., 1982), but resembles A.L. 333-115B much more than it does A.L. 333-115C. For this reason, along with supporting data from eigenanalyses, (see MT 2 results section), I attribute A.L. 333-72 to MT 2. A.L.-333-160 is a complete left MT 4 thought to be essentially very human-like by some researchers (Ward et al., 2011), but not others (Mitchell et al., 2012). The complete MT 4 was found in 2000 during sieving of the Denen Dora 2 submember of the Hadar Formation, within the 333 locality (Ward et al., 2011). All A.L. 333 scans were provided by Dr. Caley Orr and Dr. William Kimbel, laser scanned from high quality research casts housed at the Institute for Human Origins (Arizona State University).

Australopithecus africanus

StW 89, a complete left MT 2 found by Alan Hughes in 1980 was first referenced by Clarke (1995), who thought it may have been recovered from Sterkfontein Member 5 (Proctor, 2010). However, subsequent studies (Kuman and Clarke, 2000; Deloison, 2003; DeSilva et al., 2012) have determined that StW 89 is from Member 4. Some researchers think that member 4 contains only by *Au. africanus* (Pickering and Kramers, 2010), while others (Clarke, 1988; Schwartz and Tattersall, 2005; Clarke, 2008) suggest that Member 4 represents a mixed assemblage of fossil hominins. No craniodental remains are associated with StW 89, but morphometric studies have attributed it to *Au. africanus* (DeSilva et al., 2012). Thus, for the purposes of the phylogenetic analyses conducted in this dissertation, I have included StW 89 under this taxon.

StW 114 is a complete and well preserved right MT 5 found by Alan Hughes in 1982, originally thought to belong to Sterkfontein Member 5, but subsequent analyses (Kuman and Clarke, 2000) have placed the fossil as recovered from either Member 4 or Member 5 (2.6-1.5 Ma; Zipfel et al., 2009). Pickering et al. (2004) assessed StW 114 as coming from *Au. africanus*, a finding later researchers have agreed with (Zipfel et al., 2009; DeSilva et al., 2012). However,

given the complex stratigraphy present at Sterkfontein, StW 114 could also belong to *Paranthropus robustus*, or early *Homo*. I tentatively assign it to *Au. africanus* based on prior assessments. A laser scan of both StW 89 and StW 114 were provided by Dr. Proctor, taken from the original specimens housed at the University of Witswatersrand WIT following the scanning protocol detailed in his dissertation (Proctor, 2010).

Paranthropus robustus

SKX 33380 is the distal three-fourths of a left MT 5. It is derived from Swartkrans Member 3, whose craniodental remains have consisted entirely of *Paranthropus* (Grine, 1988). It has been qualitatively described as human-like (Susman, 1988); Dr. Daniel Proctor provided a laser scan, taken from the original specimen housed at the Ditsong Museum of South Africa (SAM-D; formerly the Transvaal Museum) in Pretoria, South Africa.

Homo sp.

In 2013, new fossil hominins were discovered from Kolom Odiet, near Ileret, West Turkana, Kenya (Jungers et al., 2015). Two partial skeletons were found, and one of these, KNM-ER 64062, preserves MT heads 1, 2, 3, 5, as well as the proximal hallucal phalanx. These elements were recovered just above the KBS Tuff, dated to 1.89 Ma. See Chapter 2 (Materials and Methods) for a more complete description.

Homo floresiensis

Pedal fossils from the diminutive hominin *Homo floresiensis* were first excavated from Liang Bua (LB1) in 2003, a limestone cave on the island of Flores, eastern Indonesia (Brown et al., 2004). Included in this analysis are the MT 2 – 5 heads scanned from high quality research casts, provided by Dr. Tocheri. See Chapter 2 (Materials and Methods) for additional details.

Homo naledi

Undated pedal fossils from a new hominin uncovered in the Rising Star cave system, Gauteng, South Africa (Berger et al., 2015) has yielded a largely complete right foot (Harcourt-Smith et al., 2015), of which the MT 2 (U.W. 101-1458), and MT 4 (U.W. 101-269) are included in this analysis. An MT 3 and MT 5 were recovered, but the distal portion of the bone was too poorly preserved for 3D shape analyses. See Chapter 2 (Materials and Methods) for additional details.

3.3 Results

3.3.1 Allometric regressions

Multivariate, phylogenetically corrected least-squares (PGLS) allometric regressions of size (logged centroid size) on shape variables (PCs and Procrustes coordinates) revealed that size was not a significant factor influencing MT head shape, except for in MT 5 ($p < 0.05$; but only 8.2% shape predicted by centroid size). These results suggest that shape differences observed in the MT 2 – MT 4 data are being driven by phylogenetic and/or functional differences in the sample (see below). Although size was a significant correlate of shape in MT 5, the variance explained is quite low, and thus it is likely that function and phylogenetics still play a primary role in MT head shape in the fifth metatarsal as well.

3.3.2 PCA/MANOVA

For MT 2 – MT 5, PCAs broadly ordinated the data into Ape, Old World monkey (OWM), and human clusters within the tangent space. New World monkeys (NWMs), particularly *Ateles*, overlapped with apes in most PCA plots, whereas *Cebus* and *Alouatta* often formed a separate platyrrhine cluster. In the more medial digits (e.g., MT 2, MT 3), *Erythrocebus patas* also formed its own distinct cluster in the morphospace. Unlike what was seen in the hallucal data (see Chapter 2), hominin species generally fell within the modern human minimum convex polygon, and these results are discussed in more detail below. MANOVAs confirmed differences in MT 2 – 5 shape variables among species and post-hoc tests further revealed specific significant differences among all of the groups in the sample.

3.3.3 Comparative aspects of shape

Similar to previous work on MT head shape analysis (Fernández et al., 2015), PC 1 and PC 2 captured the morphologies hypothesized to play important functional roles in terrestrial bipedalism. PC 1 tracked overall MT head robusticity, epicondylar breadth, and dorsal MT head shape. High PC 1 scores typify mediolaterally wide MT heads with a wide epicondylar breadth, and an expanded, flat dorsal MT head. Low PC 1 scores typify a mediolaterally narrow MT head with a narrow epicondylar breadth, and a reduced, rounded and narrow dorsal MT head. The exception is in MT 5, which follows the same pattern but the PC 1 scores are reversed (i.e., negative values correspond to flat, wide MT heads in MT 5). PC 2 tracked the overall orientation

of the MT head in the sagittal plane such that high PC 2 values describe very dorsally oriented MT heads, and negative PC 2 values describe very plantarly oriented MT heads. More detailed results regarding all eigenanalyses, MANOVA, and phylogenetic analyses are presented below for each metatarsal.

3.3.4 MT 2

Extant anthropoids

Significant differences between species in MT 2 head shape variables are presented in Table 3.6 for PC 1 and Table 3.7 for PC 2. On PC 1 (21% variance explained), there is much overlap in the total range of variation between all apes and some platyrrhines (*Alouatta*, *Ateles*), which occupy low PC 1 values, and the rest of the Old World monkey (OWMs) sample and *Cebus* in the higher range of PC 1 values (Fig. 3.5; 3.6a). Humans occupy a space of midrange PC 1 values, intermediate between apes and OWMs. *Post-hoc* tests with species as a fixed factor on PC 1 revealed that within Apes, all subspecies overlapped each other as well as the NWM *A. seniculus*, to the exclusion of all other monkeys ($p < 0.05$). Within NWMs, *Ateles* was distinct from all other groups on PC 1 ($p < 0.05$) except *Alouatta*, and *Cebus* separated from all groups except the colobine monkeys (*N. larvatus*, *P. rubicunda*) and guenons (*C. aethiops*). In OWMs, guenons overlapped with all other OWM taxa but separated from very digitigrade *E. patas*, which were unique in PC 1 scores ($p < 0.05$). The most terrestrial macaque sampled, *M. mulatta*, overlapped with other cercopithecines but were significantly different from colobines ($p < 0.0001$) and NWMs ($p < 0.0001$). This pattern was similar to what was seen in other *Macaca* groups, except for *M. fascicularis*, which was significantly different from *Papio* ($p < 0.05$) as well. Colobine species overlapped with each other as well as *Cebus*, guenons, and some macaques (*M. nemestrina*), to the exclusion of all other groups ($p < 0.05$). Human PC 1 scores were significantly different from all monkey taxa ($p < 0.05$) and most Ape taxa ($p < 0.01$) except for *P. abelii*, *G. beringei*, and *G. b. graueri*. Within subspecies, no significant differences were found on PC 1 score between subspecies of *Macaca*, *Gorilla*, or *Pan*.

In PC 2 (14% variance explained), *post-hoc* tests revealed significant differences among and between the general ape, human, and monkey clusters (Fig 3.5; Fig 3.6b). Among apes, bonobos (*P. paniscus*) were significantly different from all other apes ($p < 0.0001$) including common chimpanzees (*P. troglodytes*), overlapping with much of the OWM sample. Other apes

completely overlapped with each other and most monkeys except for *Papio* ($p < 0.05$) and *M. fascicularis* ($p < 0.05$). NWMs generally overlapped each other but *Alouatta* separated from *Cebus* ($p < 0.05$). *Alouatta* and *Ateles* both also overlapped with colobines and apes, but *Alouatta* separated from all OWM groups ($p < 0.05$) whereas *Ateles* overlapped with everything except for the distinct morphologies found in humans, Patas monkeys, and bonobos. Indeed, humans and patas monkeys formed distinct clusters in the morphospace due to very high PC 2 scores. However, these clusters did not overlap each other due to PC 1 differences in the two species. No significant differences were found on PC 2 score between species of *Macaca*, *Pongo*, and species/subspecies of *Gorilla*.

Fossil hominins

Unlike what was seen in MT 1, hominin MT 2 morphology looks very modern human-like indeed (Fig 3.5; Fig 3.6a,b). *Au. afarensis* (A.L. 333-115B, A.L. 333-72), *Homo* (KNM-ER 64062), *H. floresiensis* (LB 1), and *H. naledi* (U.W. 101-1458) all fall within the *Homo* minimum convex polygon. A.L. 333-72 and KNM-ER 64062 fall towards the extreme perimeter of the human cloud due to high PC 1 scores, whereas the other hominin fossils fall close to the mean value for modern humans. One MT 2, StW 89, does not fall within the human cloud, and based on minimized Procrustes distances, more closely resembles *E. patas*. Although StW 89 is well within the human range on PC 2, its PC 1 score is far outside the range of human variation, and instead is more similar to what is seen in extant OWMs.

3.3.5 Phylogenetic comparative analyses

Permutation tests for phylogenetic signal did reveal significant phylogenetic patterning in the anthropoid MT 2 shape data ($p = 0.0001$), but closely related species were less phenotypically similar to one another than expected under Brownian motion ($K_{mult} \sim 0.56$), as is generally the case when $K_{mult} < 1$. When $K_{mult} > 1$, then more phenotypic similarity exists in the shape data than expected under Brownian motion (Adams, 2014). Results from the multi-regime OU modeling in *SURFACE* showed three regime shifts towards different adaptive optima, including evidence for one convergent regime (Fig. 3.7, red bars). Evidence for convergence towards the same adaptive optimum occurred between hominins and *Erythrocebus*, and this was largely driven by PC 2, but PC 1 and 2 were both included in the *SURFACE* analysis. I limited

the analyses to PCs 1 and 2, because I only included those shape variables that were functionally interpretable. Non-convergent regimes included a separate regime for cercopithecines (Fig. 3.7, gray bars), and a regime shared by NWMs, apes, and colobines (Fig 3.7, black bars).

Phylomorphospace plots illustrated several broad patterns in the evolutionary shape change of the anthropoid MT 2 head (Fig. 3.8). Generally, apes, cercopithecines, colobines, and hominins separated into distinct clusters in the phylomorphospace. Exceptions include the very derived patas monkey morphology, the stem hominin branch, and the overlap of *Alouatta* and *Ateles* with apes to the exclusion of *Cebus*, which falls near the colobines. Branch lengths indicate that apes demonstrate relatively little evolutionary shape change except for bonobos, whereas hominins diverged greatly towards their own adaptive optima characterized by high PC 2 and intermediate PC 1 scores. Cercopithecoids also show relatively little evolutionary shape change, except for patas monkeys which shows great evolutionary shape change in the MT 2 head as it converges with the hominin form in the morphospace. Within NWMs, *Cebus* shows great evolutionary shape change, resembling colobines more so than other platyrrhines, which have an ape-like morphology. Within hominins, there is considerable evolutionary change between genus *Australopithecus* and *Homo*, mostly on PC 2. Additionally, *Au. africanus* deviates more than the other hominins on PC 1. Within *Homo*, there is little evolutionary change, but *H. floresiensis, H. naledi*, and modern humans converge towards the same region of the morphospace, away from the *H. erectus* PC 1 shape. Unlike what was seen in MT 1 (see chapter 2), the modern human-like form of the MT 2 appears relatively early in human evolution.

3.3.6 MT 3

Extant anthropoids

In MT 3, PC 1 (29% variance explained) significantly distinguishes most species in the sample from each other (Fig 3.9; Fig 3.10a). *Post-hoc* tests confirm that generally, cercopithecines overlap each other to the exclusion of other groups ($p < 0.0001$; Table 3.8), but guenons and patas monkeys separate from all groups except *Papio* ($p < 0.05$). *Pongo* sp. is significantly different from all apes but overlapped with *Ateles* and *Homo*. Grauer's gorillas separated from western lowland gorillas (*G. g. gorilla*; $p < 0.01$) and *Pan* sp. Gibbons were significantly different from *Pongo* sp. ($p < 0.0001$), *Ateles*, and *Alouatta* ($p < 0.0001$). In

platyrrhines, *Alouatta* and *Ateles* displayed a similar pattern of significant separation from all OWM groups ($p < 0.0001$), but had overlap with most ape species. *Cebus*, which was different from the other NWMs ($p < 0.0001$), showed a completely different pattern. Cebus monkeys separated from all apes ($p < 0.01$), and most monkey groups as well ($p < 0.0001$), but not from the colobines. Lastly, modern humans are significantly different from all groups ($p < 0.01$) except *Pongo* sp., and no significant differences between species within a genus were found outside *Gorilla*.

In PC 2 (12% variance explained), *post-hoc* tests on species revealed significance separation patterns similar to what was observed in MT 2 PC 2 (Fig 3.9; Fig 3.10b). Again, *H. sapiens* and *E. patas* were found to be statistically significant from all other groups ($p < 0.0001$; Table 3.9), but not from each other due to high PC 2 scores. Likewise, bonobos separated from all other apes ($p < 0.0001$) on PC 2 but largely overlapped with monkeys, whereas other apes all overlapped with each other as well as with most monkeys. Chimpanzees, however, were significantly different from *Ateles* and *Cebus* ($p < 0.05$), and most OWM groups ($p < 0.001$) except for *Macaca* and *Nasalis*. NWM groups all overlapped each other, and overlapped with most other groups as well. The same pattern was seen in OWMs, but with *E. patas* separating from all non-human groups ($p < 0.0001$) and *C. aethiops* separating from most apes ($p < 0.05$), and humans ($p < 0.0001$). No significant differences were found on PC 2 score between species/subspecies of *Macaca*, *Pongo*, and *Gorilla*.

Fossil hominins

While most fossil hominins represented by an MT 3 plotted close to the human morphospace in the eigenanalyses, overall the results were not as conclusively human-like as for the MT 2 fossil data. The only hominin fossil that fell within the human minimum convex polygon was early *Homo* (KNM-ER 64062); *H. floresiensis* (LB 1), and *Ar. ramidus* (ARA-VP-6/500-505) plotted very closely to the human polygon, but fell just outside due to low PC 1 scores, probably due to some taphonomic damage (*H. floresiensis*) and missing data (*Ar. ramidus*). *Au. afarensis* (A.L 333-115C) however unequivocally falls deep within the ape distribution, fitting within the convex polygon of any and all apes included in this analysis.

3.3.7 Phylogenetic comparative analyses

Permutation tests for phylogenetic signal did reveal significant phylogenetic patterning in the anthropoid MT 3 shape data ($p = 0.0001$; $K_{mult} \sim 0.30$). Results from the multi-regime OU modeling in *SURFACE* were similar to the MT 2 *SURFACE* results, showing three regime shifts towards different adaptive optima, including evidence for one convergent regime. Importantly, however, the MT 3 dataset includes fossil data for *Ar. ramidus.* Evidence for convergence towards the same adaptive optimum occurred between hominins and *Erythrocebus* (Fig. 3.11, red bars), and was again largely driven by PC 2. Non-convergent regimes included a separate regime for cercopithecines (Fig. 3.11, gray bars), and a regime shared by NWMs, apes, and colobines (Fig 3.11, black bars).

The MT 3 phylomorphospace produced a similar ordination to what was observed in MT 2 (Fig. 3.12). Some notable differences however include a somewhat less derived *E. patas* MT 3 head compared to its MT 2, and an overall greater amount of evolutionary shape occurred within the hominin clade, as well as between apes and *Ar. ramidus*, which looks much more human-like than ape-like in MT 3 morphology, unlike the very ape-like *Ardipithecus* MT 1. Much forefoot evolution continued between *Ardipithecus* and *Australopithecus*, and this is illustrated on PC 1. The *Homo* clade likewise is quite variable, with large evolutionary shape changes still occurring relatively late in MT 3 compared to MT 2.

3.3.8 MT 4

Extant anthropoids

Like MT 3, MT 4 also demonstrated much species-level separation on the PC 1 axis (29% variance explained; Fig 3.13; Fig 3.14a). *Post-hoc* tests demonstrated that *Pongo* sp. was different from other apes ($p < 0.0001$; Table 3.10) and OWMs ($p < 0.05$), but overlapped with NWMs. Gibbons overlapped with *Pongo* but not with other apes ($p < 0.0001$) or monkeys ($p < 0.01$). Humans separated from all groups ($p < 0.05$) except *Pongo* and *Cebus*. Patas monkeys separated from all groups ($p < 0.0001$) due to very high PC 1 values. Guenons and macaques overlap to the exclusion of other monkeys ($p < 0.05$) and apes ($p < 0.0001$). In NWMs, *Cebus* separated from most groups but not colobines ($p < 0.05$); *Alouatta* and *Ateles* were again very similar to each other but not *Cebus* ($p < 0.0001$), separating from all other monkey groups ($p <$

0.0001) and most apes ($p < 0.05$). No significant differences were found on PC 1 score between species/subspecies of *Macaca*, *Pongo*, *Gorilla*, or *Pan*.

Significant differences found in PC 2 (12% variance explained) for MT 4 are reduced somewhat from what is found in MT 2 and MT 3 (Fig 3.13; Fig 3.14b). Modern humans still separate from all other groups ($p < 0.0001$), but there is much overlap elsewhere in the sample on this shape variable (Table 3.11). While bonobos are still different from other most apes ($p < 0.0001$), in MT 4 they overlap with *P. abelii*, *G. b. graueri*, and most monkeys. NWMs largely overlap with everything but humans, although *Cebus* also separates from all ape genera as well ($p < 0.01$). Likewise, while patas monkeys separated from all non-human groups in MT 2 and MT 3, in MT 4 they overlap with other most other monkeys and some apes, and no longer have PC 2 values in the interquartile range of modern humans. Within subspecies, no significant differences were found on PC 2 score between subspecies of *Macaca*, *Pongo*, and *Gorilla*.

Fossil hominins

In MT 4, early hominins (*Au. afarensis)* MT head shape plotted most closely to apes, whereas later hominins (*H. floresiensis*, *H. naledi*) fell closer to the modern human shape distribution. Although *H. naledi* remains undated, its inclusion within genus *Homo* presumes it emerged after *Australopithecus*. The very complete *H. naledi* MT 4 (U.W. 101-269) was the only fossil to fall directly within the modern human polygon. LB 1 was well within the human PC 2 range, but retained an ape-like PC 1 score, and so occupies an intermediate portion of the morphospace between apes and humans. Two *Au. afarensis* specimens (A.L. 333-115D, A.L. 333-160) fell in the middle of the ape distribution, plotting right next to each other. A.L. 333-160 is a very well preserved, intact MT 4 previously thought to be essentially human-like (Ward et al., 2011), however, results from this shape analysis provide support for an ape-like MT 4 MT head morphology in *Au. afarensis*.

3.3.9 Phylogenetic comparative analyses

Permutation tests for phylogenetic signal did reveal significant phylogenetic patterning in the anthropoid MT 4 shape data ($p = 0.0001$; $K_{mult} \sim 0.26$). Results from the multi-regime OU modeling of the MT 4 shape data were unlike what was seen in the MT 2 and MT 3 *SURFACE* results, showing three regime shifts towards different adaptive optima, but providing no evidence

for any convergence. Evidence towards three non-convergent regimes included one regime for cercopithecoids (Fig. 3.15, green bars), one regime for genus *Homo* (Fig. 3.15, light grey bars), and one regime for apes, NWMs, and *Australopithecus* (Fig 3.15, black bars).

The MT 4 phylomorphospace generally produced a similar ordination to what was observed in MT 3 (Fig. 3.16), with some important differences. The most immediate difference is the position of *Au. afarensis* in MT 4 compared to MT 3 and MT 2. In MT 4, *Au. afarensis* seems to have retained an entirely ape-like form in both fossils from the 333 locality. In early *Homo*, this changes greatly, and the MT 4 looks similar to that of modern humans. *Au. afarensis* exhibits a mosaic gradient in its MT head morphology, with MT 2 > MT 3 > MT 4 in terms of human-like morphology observed. The *Au. afarensis* MT 5 however does not follow this pattern (see below).

3.3.10 MT 5

Extant anthropoids

Results of the MT 5 PC 1 (24% variance explained) shape data look similar to those of MT 4 (Fig. 3.17, Fig 3.18a), but with less significant separation of species overall (Table 3.12). First, all apes overlap with each other and most apes likewise overlap with *Alouatta* and *Ateles* except for lowland ($p < 0.001$) and Grauer's ($p < 0.0001$) gorillas, and bonobos ($p < 0.01$). Humans separate from all groups except *Cebus* and *Presbytis*. Patas monkeys are again distinguished by very high PC 1 scores from all groups ($p < 0.001$). Guenons and macaques overlap to the exclusion of other monkeys ($p < 0.05$) and apes ($p < 0.0001$). In NWMs, *Cebus* separates from all groups ($p < 0.001$) except *Presbytis* and *Homo*. *Ateles* overlaps with all apes except Grauer's gorillas ($p < 0.05$), and separates from all other monkeys ($p < 0.0001$). *Alouatta* is similar ($p < 0.0001$), but has more overlap with the ape clade (e.g., gorillas and bonobos). No significant differences were found on PC 1 score between subspecies of *Macaca*, *Pongo*, *Gorilla*, or *Pan*.

Results of the MT 5 PC 2 (15 % variance explained) shape data look very similar to those of MT 4 (Fig. 3.17, Fig 3.18b). Like MT 2 – MT 4, humans separate as a distinct cluster in the morphospace due to high PC 2 scores ($p < 0.0001$; Table 3.13). Other species with outlying PC 2 scores include patas monkeys, which separate from the more arboreal colobines, NWMs, and

some apes ($p < 0.05$). Additionally, *M. mulatta* separates from most groups ($p < 0.05$), but not NWMs, and *Presbytis* separates from apes ($p < 0.0001$). Within platyrrhines, there is much overlap with all groups, but *Alouatta* separates from most apes ($p < 0.05$) and baboons ($p < 0.05$). All other monkeys largely overlap with each other. *M. mulatta* was significantly different from both other macaque species ($p < 0.05$), and *G. g. gorilla* was different from Grauer's gorilla ($p < 0.05$).

Fossil hominins

MT 5 included fossil MTs from five hominins, most of which looked essentially human-like. *Au. afarensis* (A.L. 333-115E), *Au. africanus* (StW 114), *Homo* (KNM-ER 64062), and *H. floresiensis* (LB 1) all fell within the human minimum convex polygon. One fossil hominin, *P. robustus* (SKX 33380), was within the human PC 2 score range but fell far outside the human PC 1 range, and fell within the edge of the ape morphospace. Like many fossil hominins, this specimen displays a mosaic morphology that when put through eigenanalyses, results in PC scores more similar to extant apes than humans overall. Although MT 5 shape is effected by size (see *Allometric Regressions*), centroid size explains less than 10% of the variance and a functional signal still emerges. It also still provides important phylogenetic information for researchers, in that MT 5 shape data still seems to separate bipedal hominins from all other groups, with PC 2 as the main discriminating axis.

3.3.11 Phylogenetic analyses

Permutation tests for phylogenetic signal did reveal significant phylogenetic patterning in the anthropoid MT 5 shape data ($p = 0.0001$; $K_{mult} \sim 0.22$). Results from the multi-regime OU modeling of the MT 5 shape data are very similar to the MT 4 *SURFACE* results, differing only in that the entire hominin clade is included in one non-convergent regime, instead of just genus *Homo*. The other regimes are identical to those found for MT 4, and there is no evidence for any convergent regime. Evidence towards three non-convergent regimes included one regime for cercopithecoids (Fig. 3.19, green bars), one regime for hominins (Fig. 3.19, light grey bars), and one regime for apes and NWMs (Fig 3.19, black bars).

The tree-like structure seen at first glance of the MT 5 phylomorphospace reflects the strong phylogenetic effects that underlie the shape data in this element (Fig 3.20). Generally, branch lengths suggest that greater evolutionary change has occurred within monkeys and

hominins than within apes. The hominin MT 5 shape evolved rapidly from the ape condition on PC 2, looking essentially modern by ~ 3.2 Ma. *Paranthropus* however evolved a unique, mosaic morphology in the MT 5 head, which was intermediate between hominins and apes. This interpretation relies on the hominin phylogeny reconstructed by Strait and Grine (2004). Within genus *Homo,* there is little evolutionary change.

3.4 Discussion

Extant anthropoids

Shape analyses of the anthropoid non-hallucal forefoot provided strong support for my hypotheses and predictions. Eigenanalyses captured the functional characters of the metatarsal head (e.g., head orientation and robusticity), and yielded many intriguing results throughout the metatarsals. Unlike what was observed in the hallucal data alone (see Chapter 2), analyses of all the metatarsals allowed for a more complete picture of forefoot evolution. OU modeling supported my hypothesis that humans would show convergence in the forefoot with highly terrestrial taxa. The OU modeling analysis found evidence for a convergent regime between hominins and *Erythrocebus patas* in the MT 2 and MT 3 shape data. Patas are the most digitigrade (Meldrum, 1991; Gebo and Sargis, 1994; Nowak et al., 2010) and cursorial (*sensu* Patel, 2009) of the primates, with many morphological differences separating them from closely related cercopithecines (e.g., vervet monkeys) including relatively longer hind limbs (Strasser, 1992; Polk, 2004), forelimbs (Polk, 2004), and an elongated tarsus (Strasser, 1992). These morphological differences likely contribute to the higher locomotor speeds observed in patas monkeys compared to other cercopithecines (Polk, 2004; Arsuaga and Martinez, 2006; Patel, 2009), as well as their lower cost of locomotion compared to baboons (Polk, 2004). My shape analyses provide additional morphological support for the cursorial nature of patas monkey—they displayed unique MT head morphology, especially in MT 2 and MT 3. This finding lends support to the kinematic observation that the central axis of the foot appears to pass through digit III in cercopithecines, with the hallux contributing little to forefoot dorsiflexion on terrestrial substrates (Meldrum, 1991). Patas monkeys consistently had extreme PC 1 values, owing to markedly wide, robust MT heads, as well as high PC 2 values, which denote a dorsally oriented MT head. Additionally, the wide patas MT heads are often terminated proximodorsally by a wide, transverse ridge of bone similar to what is seen in the weight-bearing metacarpals (MC 3,

4) of knuckle-walkers (Susman, 1979). It is likely that the overall morphology of the patas distal metatarsus allows for improved forefoot joint stability during the habitually dorsiflexed foot postures of this highly cursorial primate. Convergent regimes were not found between hominins and other terrestrial primates in MT 4 or MT 5, and this is probably due to the reduced functional importance of these forefoot joints in generating propulsive forces at the end of stance phase in primates generally; kinematic data in humans and chimpanzees support this notion (see Chapter 5). Convergent phenotypes were not found between hominins and other highly terrestrial anthropoids such as baboons (*Papio* sp.) or mountain gorillas (*G. b. beringei*), and these findings suggest that substrate use itself does not determine MT head shape. However, aspects of MT head shape in these more terrestrial taxa did show some similarities to humans. For instance, *Papio* likewise demonstrated the extremely high PC 1 scores observed in *E. patas*, suggesting a similar mechanism of forefoot joint stability is present in this terrestrial species as well. Still, baboons did not demonstrate the human-like PC 2 scores that clearly separated them and *E. patas* from the rest of the sample.

Although substrate use and foot posture are only two of many variables (e.g., phylogeny, developmental constraint, allometry) affecting forefoot joint shape, when the anthropoid phylogeny is mapped onto the tangent shape space, one can immediately visualize the drastic evolutionary shape changes that have taken place in some of the anthropoid lineages studied here. Beyond the strikingly derived forefoot of the patas monkey, the phylomorphospace plots also illustrated major differences in branch lengths within the hominin clade as well as in bonobos. Bonobos are known to be more arboreal than chimpanzees (Doran, 1993; Doran, 1996), and this difference appears to be reflected in the forefoot anatomy. Bonobos score especially low on PC 2, more so than any other ape; this position in the morphospace demonstrates a very plantarly oriented MT head, which may reflect their more arboreal lifetysle compared to chimpanzees. Still, they score lower on PC 2 than orangutans, suggesting that other factors besides substrate use are at play here. Within NWMs, *Alouatta* and *Ateles* are much more ape-like in the shape analyses, whereas *Cebus* tends to fall most closely to the colobines. This may reflect an increase in suspension and less reliance on quadrupedalism and leaping in *Ateles* (Gebo, 1992) and *Alouatta* (Fleagle and Mittermeier, 1980; Cant et al., 2001) when compared to *Cebus*. Like *Cebus*, colobine monkeys tend to be predominately reliant on arboreal quadrupedalism and leaping (Fleagle, 1978, 1980; Boonratana, 2000). Amongst the subspecies

of *Gorilla*, Grauer's gorillas (*G. b. graueri*) consistently demonstrated a significantly different MT head shape when compared to western lowland gorillas (*G. g. gorilla*). Typically, the PC scores of Grauer's gorilla MTs were more robust and appeared adapted to increased terrestriality. One possibility for the shape differences observed amongst *Gorilla* species is that most of the Grauer's gorillas sampled from the RMCA derive from highland habitats, and have shown ecological adaptations to increased terrestriality elsewhere in the lower limb (Knigge et al., 2015). However, as another population of highland gorillas, the mountain gorillas (*G. b. beringei*) were not found to be significantly different from the lowland species, these morphological differences may not reflect any functional difference, but rather may reflect the population history of the severely bottlenecked Grauer's gorilla, a population that likely emerged from a mountain gorilla founder group before experiencing this severe bottleneck (Tocheri et al., 2016). Other subspecies comparisons (*Pongo*, *Macaca*) did not reveal any significant shape differences. When male specimens of the somewhat more terrestrial Bornean orangutan (*P. pygmaeus*) were analyzed separately, no significant evidence for a more terrestrial like MT head shape was found between them and male specimens of the more exclusively arboreal Sumatran species (*P. abelii*). Sumatran orangutans rarely descend to the ground because of predation threat by large felids. However, these felids are not present in the Bornean orangutan's habitats, and thus they come to the ground more often (Rijksen, 1978; Galdikas, 1988). Within *Macaca*, the most terrestrial species sampled was the Rhesus macaque (*M. mulatta*), and this species showed similarities to *Papio* and patas monkeys on PC 1, especially in MT 2, which is probably the most functionally relevant forefoot element in the terrestrial quadrupedal gait cycle (Meldrum, 1991), whereas the other macaques sampled did not show this similarity. It is probably that generally, the macaques are too semi-terrestrial, with many species displaying significant amounts of both arboreal and terrestrial positional behavior (Rodman, 1979; Cant, 1988), such that their forefoot morphology has remained largely similar to one another throughout evolutionary time.

Fossil hominins

In the MT 2 – MT 5 data, fossil hominins generally fall within the human range of shape variation on both PC 1 and PC 2. This is mostly the case in MT 2, with fossil members of genus *Homo* all falling within the interquartile range of human shape variation on PC 2. *H. naledi* also falls within this range on PC 1, and is the most modern-like of all the analyzed hominin MT 2s in

terms of overall shape. LB 1 and KNM-ER 64062 fall outside of the interquartile range on PC 1 but are still within the total range of human variation. A.L. 333 and StW 89 both fall within the modern human interquartile range of variation on PC 2, but StW 89 does not overlap with humans on PC 1, and instead is more similar to terrestrial and semi-terrestrial cercopithecoids on this axis. The taxonomic affiliation of StW 89 is typically said to be *Au. africanus* but is not definitive due to a lack of craniodental remains associated with the specimen, and unfortunately my eigenanalyses preclude me from definitely placing it into any one particular hominin taxon. On PC 1, the fossil overlaps with cercopithecoid monkeys to the exclusion of hominoids, and on PC 2 it is most similar to the *Au. afarensis* specimens from the 333 locality. Interestingly, studies on MT torsion found StW 89 to be intermediate between cercopithecoids and humans as well (Drapeau and Harmon, 2013). In fact, the torsion value they report for StW 89 is closer to the mean of cercopithecoids than it is to humans, a finding observed by others as well (DeSilva et al., 2012). Overall, StW 89 does not particularly resemble a cercopithecoid metatarsal (e.g., curved diaphysis, mediolaterally broad proximal articular surface), and I do not suggest that it is a fossil cercopithecoid. If it belongs to *Au. africanus*, then this hominin is similar to *Au. afarensis* (and modern humans) on PC 2 and is thus certainly dorsally 'domed', but its morphology on PC 1 remains unique amongst hominins. Future MT head fossil discoveries from South Africa, particularly those of *Au. sediba*, would help clarify this debate.

In the MT 3 fossils, *Australopithecus* and *Homo* specimens fell within the human range of variation on PC 1, but *Ardipithecus* was outside the modern human range, and more closely resembled a chimpanzee or gorilla on this axis. On PC 2, all hominins were human-like except *Au. afarensis*, which fell very close to the mean chimpanzee value on this axis. In the MT 3 shape analyses, landmarks taken on the epicondyles were excluded from the Procrustes superimposition because these areas were missing from our *Ar. ramidus* scan. However, based on an image of the full ARA-VP-6/505 scan in the literature (Lovejoy et al., 2009), I strongly suspect that its PC 1 score, which is largely influenced by epicondylar breadth, would look similar to modern humans. Although its hallux is clearly divergent and ape-like in its MT head morphology (Lovejoy et al., 2009; Chapter 2), the *Ar. ramidus* MT 3 is very human-like, and this is resolved on PC 2 even with the epicondylar points missing. Concerning *Au. afarensis*, the Procrustes distances show that it was most similar to *Pan* in the MT 3 morphospace because of its very low PC 2 scores. The *Au. afarensis* forefoot is peculiar in that it has some very human-

looking MT heads (MT 2, MT 5), and some very chimpanzee-looking heads as well (MT 3, MT 4). While such a morphology may be indicative of mixed substrate use in this species, a finding supported by other researchers of metatarsal morphology (Proctor, 2013), it is important to note that substrate use is only one factor out of several (e.g., phylogenetic constraint, developmental constraint) that likely determines MT head shape.

The MT 4 morphospace includes fossils from LB 1, *H. naledi*, and A.L. 333. *H. naledi* by far resembles the human MT 4 shape most closely, on both PC 1 and PC 2. This finding shows that all *H. naledi* specimens complete enough for shape analysis (MT 1, MT 2, MT 4), have essentially looked entirely human-like. This agrees with findings about the Naledi foot overall (Berger et al., 2015; Harcourt-Smith et al., 2015), and shows that amongst the diversity of South African hominins, one species already had an essentially modern human-like foot. Accurate dating of these specimens could be critical to the evolutionary timeline of the evolution of bipedalism, but these particular fossils are suspected to be quite young (Williams, pers. comm); if this is true, then the *H. naledi* fossil dates would not be particularly helpful. Another surprising finding in the MT 4 data is the shape analysis of A.L. 333-160, a complete MT 4 with some human-like aspects to its morphology (e.g., proximal articular surface, MT head torsion; Ward et al., 2011). Quantitative shape analysis however disagrees with this finding, and shows the *Au. afarensis* MT 4 to look very much like its MT 3—i.e., chimpanzee-like. This is true for both the nearly complete 333-160 specimen, as well as the fragmentary 333-115 specimen. Both fall in the middle of the *Pan* and *Gorilla* range on PC 2, far outside the human range of variation. The MT 4 actually looks somewhat less human-like than the MT 3, which also falls just outside the human range on PC 1, but is again within the chimpanzee range. *H. floresiensis* is more intermediate on MT 4, with a chimpanzee-like PC 1 score and human-like PC 2 score. This is the only *H. floresiensis* metatarsal which looks somewhat ape-like.

MT 5 analyses included several hominins, and was the only metatarsal outside the hallux where *Paranthropus* was represented. The *Paranthropus* specimen (SKX 33380) has been qualitatively observed as human-like (Susman, 1989) and while that is true for PC 2 (although it is borderline chimpanzee-like on this axis as well), this specimen looked definitively more ape-like on PC 1. In this way, SKX 33380 is very similar to the hallucal specimens SK 1813 and SKX 5017, both of which are typified by ape-like PC 1 scores and human-like PC 2 scores, and

are also attributed to *Paranthropus*. This pattern is unique and not similar to either what is seen in *Australopithecus, Ardipithecus*, or early *Homo*, suggesting different and probably less efficacious forefoot bipedal mechanics in *Paranthropus* compared to later *Homo* and modern humans. Other MT 5 specimens included *Au. afarensis*, *Au. africanus*, *H.* sp, and *H. floresiensis*. All of these specimens fell within the total range of human shape variation, but specimens from genus *Homo* were most similar to modern humans, falling within the human interquartile range on PC 2 (along with *Au. afarensis*).

Overall, the results show broad separations into ape, Old World monkey (OWM), and human clusters, with some key separations and convergences, mostly due to PC 2 (MT head orientation). Throughout the MT data however, it appears that the strength of the functional signal is concentrated more in the medial forefoot with the hallux (see Chapter 2) and metatarsals 2 and 3, with a diminished signal present in MT 4 and 5. This is supported by the convergent regimes found in MT 2 and 3 but not 4 and 5, the significant allometric signal and phylogenetic structure to the morphospace in MT 5, and by quantitative 3D kinematic data in humans and chimpanzees (see chapter 5). These 3D shape data is consistent with a greatly diminished dorsiflexion excursion across the forefoot, with higher dorsiflexion angles observed medially and lower dorsiflexion angles observed laterally, with especially insignificant amounts of dorsiflexion occurring at MT 5, even in humans (see Chapter 5). Despite its dubious functional importance, MT 5, like all of the non-hallucal metatarsals, still conveys important phylogenetic information, which is important for fossil hominin taxonomic assessment. Moreover, it is likely that even though MT 4 and MT 5 do not contribute much functionally to bipedal push off, their shape is probably at least partially due to developmental effects related to the serial development of the metapodials (Strasser, 1994; Indjeian et al., 2016), and thus its shape reflects that of the more functionally relevant medial digits. Critically, unlike what was generally seen in the hallucal data, hominin MT 2 – 5 head shape looked very similar to that of extant modern humans, which corroborates prior work that suggests initial evolutionary change first acted upon the lateral column of the foot (Proctor, 2013). In all cases, hominins were discriminated from all other non-human groups due to PC 2 score, which was related to dorsal head orientation (i.e., "dorsal doming"). Even in those fossil specimens that appeared mosaic in MT head shape like *Paranthropus* (SK 1813, SKX 5017) and StW 89, the fossils demonstrated human-like PC 2 scores and thus were likely to have come from a biped based on their MT head orientation and

dorsal expansion of the MT head articular surface unto the metatarsal diaphysis. Based on my findings across the anthropoid and hominin forefoot, it seems probable that the lateral forefoot began evolving a human-like joint shape that would accommodate the increased terrestriality practiced by early hominins while maintaining an abducted, grasping hallux in order to maintain climbing prowess, which would have been helpful to avoid predation and for foraging. Later in human evolution, when hominins fully committed to obligate terrestrial bipedalism, the hallux then began to take its distinct, modern form.

3.5 References

Arsuaga, J., Martinez, M., 2006. The chosen species: the long march of human evolution. Blackwell Publishing, Ltd. , Malden

Berger, L.R., Hawks, J., de Ruiter, D.J., Churchill, S.E., Schmid, P., Delezene, L.K., Kivell, T.L., Garvin, H.M., Williams, S.A., DeSilva, J.M., Skinner, M.M., Musiba, C.M., Cameron, N., Holliday, T.W., Harcourt-Smith, W., Ackermann, R.R., Bastir, M., Bogin, B., Bolter, D., Brophy, J., Cofran, Z.D., Congdon, K.A., Deane, A.S., Dembo, M., Drapeau, M., Elliott, M.C., Feuerriegel, E.M., Garcia-Martinez, D., Green, D.J., Gurtov, A., Irish, J.D., Kruger, A., Laird, M.F., Marchi, D., Meyer, M.R., Nalla, S., Negash, E.W., Orr, C.M., Radovcic, D., Schroeder, L., Scott, J.E., Throckmorton, Z., Tocheri, M.W., VanSickle, C., Walker, C.S., Wei, P., Zipfel, B., 2015. *Homo naledi*, a new species of the genus *Homo* from the Dinaledi Chamber, South Africa. eLife 4.

Bojsen-Møller, F., 1979. Calcaneocuboid joint and stability of the longitudinal arch of the foot at high and low gear push off. J. Anat. 129, 165-176.

Boonratana, R., 2000. Ranging behavior of proboscis monkeys (*Nasalis larvatus*) in the Lower Kinabatangan, Northern Borneo. International Journal of Primatology 21, 497-518.

Brown, P., Sutikna, T., Morwood, M.J., Soejono, R.P., Jatmiko, Wayhu Saptomo, E., Awe Due, R., 2004. A new small-bodied hominin from the Late Pleistocene of Flores, Indonesia. Nature 431, 1055-1061.

Cant, J.G.H., 1988. Positional behavior of long-tailed Macaques (*Macaca fascicularis*) in Northern Sumatra. Am. J. Phys. Anthropol. 76, 29-37.

Cant, J.G.H., Youlatos, D., Rose, M.D., 2001. Locomotor behavior of *Lagothrix lagothricha* and *Ateles belzebuth* in Yasuni National Park, Ecuador: general patterns and nonsuspensory modes. J. Hum. Evol. 41, 141-166.

Clarke, R., 1988. A new *Australopithecus* cranium from Sterkfontain and its bearing on the ancestry of *Paranthropus* in: Grine, F.E. (Ed.), Evolutionary history of the "robust" australopithecines Transaction Publishers, New Brunswick pp. 285-292.

Clarke, R., Tobias, P., 1995. Sterkfontein member 2 foot bones of the oldest South African hominid. Science 269, 521-524.

Clarke, R.J., 2008. Latest information on Sterkfontein's *Australopithecus* skeleton and a new look at *Australopithecus*. South African Journal of Science 104, 443-449.

Deloison, Y., 2003. Anatomie des os fossils de pieds des hominids d'Afrique du suddates entre 2,4 et 3,5 millions d'annés. Interprétation quant à leur mode de locomotion. Biométrie Hum. Anthropol. 21, 189-230.

DeSilva, J.M., 2008. Vertical climbing adaptations in the anthropoid ankle and midfoot: implications for locomotion in Miocene catarrhines and Plio-Pleistocene hominins. University of Michigan.

DeSilva, J.M., 2009. Functional morphology of the ankle and the likelihood of climbing in early hominins. Proc. Nat. Acad. Sci. 106, 6567-6572.

DeSilva, J.M., Proctor, D.J., Zipfel, B., 2012. A complete second metatarsal (StW 89) from Sterkfontein Member 4, South Africa. J. Hum. Evol. 63, 487-496.

Doran, D.M., 1992. The ontogeny of chimpanzee and pygmy chimpanzee locomotor behavior: a case study of paedomorphism and its behavioral correlates. J. Hum. Evol. 23, 139-157.

Doran, D.M., 1993a. Comparative locomotor behavior of chimpanzees and bonobos: the influence of morphology on locomotion. Am. J. Phys. Anthropol. 91, 83-98.

Doran, D.M., 1993b. Sex differences in adult chimpanzee positional behavior: the influence of body size on locomotion and posture. Am. J. Phys. Anthropol. 91, 99-115.

Doran, D.M., 1996. Comparative positional behavior of the African apes, in: McGrew, W.C., Marchant, L.F., Nishida, T. (Eds.), Great ape societies University Press, Cambridge, pp. 213-224-.

Drapeau, M.S.M., Harmon, E.H., 2013. Metatarsal torsion in monkeys, apes, humans and australopiths. J. Hum. Evol. 64, 93-108.

Fernández, P.J., Almécija, S., Patel, B.A., Orr, C.M., Tocheri, M.W., Jungers, W.L., 2015. Functional aspects of metatarsal head shape in humans, apes, and Old World monkeys. J. Hum. Evol. 86, 136-146.

Fleagle, J.G., 1978. Locomotion, posture and habitat utilization of two sympatric Malaysian leaf-monkeys (*Presbytis obscura* and *Presbytis melalophos)*, in: Montgomery, G. (Ed.), Ecology of arboreal folivores. Smithsonian Press, Washington, D.C., pp. 243-251.

Fleagle, J.G., 1980. Locomotion and posture, in: Chivers, D. (Ed.), Malayan forest primates: ten years' study in tropical rain forest. Plenum Press, pp. 191-207.

Fleagle, J.G., 2013. Primate adaptation and evolution. Academic Press, San Diego.

Fleagle, J.G., Mittermeier, R.A., 1980. Locomotor behavior, body size, and comparative ecology of seven Surinam monkeys. Am. J. Phys. Anthropol. 52, 301-314.

Galdikas, B.M.F., 1988. Orangutan diet, range, and activity at Tanjung Puting, Central Borneo. International Journal of Primatology 9, 1-35.

Gebo, D.L., 1992. Locomotor and postural behavior in *Alouatta palliata* and *Cebus capucinus*. Am. J. Primatol. 26, 277-290.

Gebo, D.L., Sargis, E.J., 1994. Terrestrial adaptations in the postcranial skeletons of guenons. Am. J. Phys. Anthropol. 93, 341-371.

Griffin, N.L., D'Août, K., Richmond, B., Gordon, A., Aerts, P., 2010. Comparative in vivo forefoot kinematics of *Homo sapiens* and *Pan paniscus*. J. Hum. Evol. 59, 608-619.

Grine, F.E., 1988. New craniodental fossils of *Paranthropus* from the Swartkrans Formation and their significance in "robust" australopithecine evolution, in: Grine, F.E. (Ed.), Evolutionary history of the "robust" australopithecines Transaction Publishers, New Brunswick, pp. 223-243.

Harcourt-Smith, W.E.H., Throckmorton, Z., Congdon, K.A., Zipfel, B., Deane, A.S., Drapeau, M.S.M., Churchill, S.E., Berger, L.R., DeSilva, J.M., 2015. The foot of *Homo naledi*. Nat. Commun. 6.

Holowka, N.B., O'Neill, M.C., Demes, B., 2014. Three-dimensional foot kinematics of chimpanzees and humans during bipedal location. Am. J. Phys. Anthropol. 153, 144.

Indjeian, Vahan B., Kingman, Garrett A., Jones, Felicity C., Guenther, Catherine A., Grimwood, J., Schmutz, J., Myers, Richard M., Kingsley, David M., 2016. Evolving new skeletal traits by cis-regulatory changes in bone morphogenetic proteins. Cell 164, 45-56.

Jungers, W.L., Grine, F.E., Leakey, M.G., Leakey, L., Brown, F., Yang, D., Tocheri, M.W., 2015. New hominin fossils from Ileret (Kolom Odiet), Kenya. Am. J. Phys. Anthropol. 156, 181.

Knigge, R.P., Tocheri, M.W., Orr, C.M., McNulty, K.P., 2015. Three-dimensional geometric morphometric analysis of talar morphology in extant gorilla taxa from highland and lowland habitats. Anat. Rec. 298, 277-290.

Kuman, K., Clarke, R.J., 2000. Stratigraphy, artefact industries and hominid associations for Sterkfontein, Member 5. J. Hum. Evol. 38, 827-847.

Latimer, B., Lovejoy, C.O., 1990. Metatarsophalangeal joints of *Australopithecus afarensis*. Am. J. Phys. Anthropol. 83, 13-23.

Latimer, B.M., Lovejoy, C.O., Johanson, D.C., Coppens, Y., 1982. Hominid tarsal, metatarsal, and phalangeal bones recovered from the Hadar formation: 1974–1977 collections. Am. J. Phys. Anthropol. 57, 701-719.

Lewis, O.J., 1980. The joints of the evolving foot. Part III. The fossil evidence. J. Anat. 131, 275-298.

Lovejoy, C.O., Latimer, B., Suwa, G., Asfaw, B., White, T.D., 2009. Combining prehension and propulsion: the foot of *Ardipithecus ramidus*. Science 326, 72, 72e71-72e78.

Meldrum, D.J., 1991. Kinematics of the cercopithecine foot on arboreal and terrestrial substrates with implications for the interpretation of hominid terrestrial adaptations. Am. J. Phys. Anthropol. 84, 273-289.

Mitchell, P.J., Sarmiento, E.E., Meldrum, D.J., 2012. The AL 333-160 fourth metatarsal from Hadar compared to that of humans, great apes, baboons and proboscis monkeys: non-conclusive evidence for pedal arches or obligate bipedality in Hadar hominins. Homo 63, 336-367.

Nowak, M.G., Carlson, K.J., Patel, B.A., 2010. Apparent density of the primate calcaneo-cuboid joint and its association with locomotor mode, foot posture, and the "midtarsal break". Am. J. Phys. Anthropol. 142, 180-193.

Patel, B.A., 2009. Not so fast: speed effects on forelimb kinematics in cercopithecine monkeys and implications for digitigrade postures in primates. Am. J. Phys. Anthropol. 140, 92-112.

Patel, B.A., 2010. Functional morphology of cercopithecoid primate metacarpals. J. Hum. Evol. 58, 320-337.

Pickering, R., Kramers, J.D., 2010. Re-appraisal of the stratigraphy and determination of new U-Pb dates for the Sterkfontein hominin site, South Africa. J. Hum. Evol. 59, 70-86.

Pickering, T.R., Clarke, R.J., Moggi-Cecchi, J., 2004. Role of carnivores in the accumulation of the Sterkfontein Member 4 hominid assemblage: a taphonomic reassessment of the complete hominid fossil sample (1936–1999). Am. J. Phys. Anthropol. 125, 1-15.

Polk, J.D., 2004. Influences of limb proportions and body size on locomotor kinematics in terrestrial primates and fossil hominins. J. Hum. Evol. 47, 237-252.

Proctor, D.J., 2010. Three-dimensional morphometrics of the proximal metatarsal articular surfaces of *Gorilla, Pan, Hylobates*, and shod and unshod humans. University of Iowa.

Proctor, D.J., 2013. Proximal metatarsal articular surface shape and the evolution of a rigid lateral foot in hominins. J. Hum. Evol. 65, 761-769.

Rijksen, H.D., 1978. A field study on Sumatran orang utans (*Pongo pygmaeus abelii* Lesson 1827) : ecology, behaviour and conservation. Veenman, Wageningen.

Rodman, P.S., 1979. Skeletal differentiation of *Macaca fascicularis* and *Macaca nemestrina* in relation to arboreal and terrestrial quadrupedalism. Am. J. Phys. Anthropol. 51, 51-62.

Schmitt, D., Larson, S.G., 1995. Heel contact as a function of substrate type and speed in primates. Am. J. Phys. Anthropol. 96, 39-50.

Schwartz, J., Tattersall, I., 2005. The human fossil record craniodental morphology of genus *Homo* (Africa and Asia). Wiley-Liss.

Stern, J.T., Susman, R.L., 1983. The locomotor anatomy of *Australopithecus afarensis*. Am. J. Phys. Anthropol. 60, 279-317.

Stern, J. T., Susman, R.L., 1991. "Total morphological pattern" versus the "magic trait": conflicting approaches to the study of early hominid bipedalism." In: Coppens, Y., Senut, B., (Eds.), Origine (s) de la bipédie chez les Hominidés. Cahiers de Paleoanthropologie, CNRS, Paris 99-112.

Strait, D.S., Grine, F.E., 2004. Inferring hominoid and early hominid phylogeny using craniodental characters: the role of fossil taxa. J. Hum. Evol. 47, 399-452.

Strasser, E., 1992. Hindlimb proportions, allometry, and biomechanics in old world monkeys (Primates, Cercopithecidae). Am. J. Phys. Anthropol. 87, 187-213.

Strasser, E., 1994. Relative development of the hallux and pedal digit formulae in Cercopithecidae. J. Hum. Evol. 26, 413-440.

Susman, R., 1988. Hand of *Paranthropus robustus* from Member 1, Swartkrans: fossil evidence for tool behavior. Science 240, 781-784.

Susman, R.L., 1979. Comparative and functional morphology of hominoid fingers. Am. J. Phys. Anthropol. 50, 215-236.

Susman, R.L., 1983. Evolution of the human foot: evidence from Plio-Pleistocene hominids. Foot Ankle 3, 365-376.

Susman, R.L., 1989. New hominid fossils from the Swartkrans formation (1979–1986 excavations): postcranial specimens. Am. J. Phys. Anthropol. 79, 451-474.

Susman, R.L., Brain, T.M., 1988. New first metatarsal (SKX 5017) from Swartkrans and the gait of *Paranthropus robustus*. Am. J. Phys. Anthropol. 77, 7-15.

Susman, R.L., de Ruiter, D.J., 2004. New hominin first metatarsal (SK 1813) from Swartkrans. J. Hum. Evol. 47, 171-181.

Tocheri, M.W., Dommain, R., McFarlin, S.C., Burnett, S.E., Troy Case, D., Orr, C.M., Roach, N.T., Villmoare, B., Eriksen, A.B., Kalthoff, D.C., Senck, S., Assefa, Z., Groves, C.P.,

Jungers, W.L., 2016. The evolutionary origin and population history of the grauer gorilla. Am. J. Phys. Anthropol. 159, 4-18.

Tuttle, R.H., 1970. Postural, propulsive, and prehensile capabilites in the cheiridia of chimpanzees, and other great apes, in: Bourne, G.H. (Ed.), The chimpanzee. Karger, Basel, pp. 167-263.

Tuttle, R.H., 1981. Evolution of hominid bipedalism and prehensile capabilities. Philos. T. Roy. Soc. B. 292, 89-94.

Ward, C.V., Kimbel, W.H., Harmon, E.H., Johanson, D.C., 2012. New postcranial fossils of *Australopithecus afarensis* from Hadar, Ethiopia (1990–2007). J. Hum. Evol. 63, 1-51.

Ward, C.V., Kimbel, W.H., Johanson, D.C., 2011. Complete fourth metatarsal and arches in the foot of *Australopithecus afarensis*. Science 331, 750-753.

White, T.D., Suwa, G., Asfaw, B., 1994. *Australopithecus ramidus*, a new species of early hominid from Aramis, Ethiopia Nature 371, 306-312.

Young, N.M., Wagner, G.P., Hallgrímsson, B., 2010. Development and the evolvability of human limbs. Proc. Nat. Acad. Sci. 107, 3400-3405.

Zipfel, B., DeSilva, J.M., Kidd, R.S., 2009. Earliest complete hominin fifth metatarsal—Implications for the evolution of the lateral column of the foot. Am. J. Phys. Anthropol. 140, 532-545.

Taxon	**Locomotor Mode[1]**	**Foot Posture[2]**	**µCT**	**CT**	**Laser Scan**
Hominoids					
Homo sapiens	B	FCP	-	22	14
Gorilla beringei beringei	KW/C	IHSP	-	3	14
Gorilla beringei graueri	KW/C	IHSP	-	3	10
Gorilla gorilla gorilla	KW/C	IHSP	-	4	29
Pan paniscus	KW/C	IHSP	-	1	16
Pan troglodytes	KW/C	IHSP	-	7	30
Pongo abelii	S	IHSP	-	-	10
Pongo pygmaeus	S	IHSP	-	-	13
Hylobates lar	R	MFP	18	-	-
Cercopithecoids					
Chlorocebus aethiops	TQ	DG/SP	7	-	-
Erythrocebus patas	TQ	DG	18	-	-
Macaca fascicularis	TQ	DG/SP	9	-	-
Macaca mulatta	TQ	DG/SP	15	-	-
Macaca nemestrina	TQ	DG/SP	7	-	-
Papio ursinus	TQ	DG/SP	13	-	-
Nasalis larvatus	AQ	DG/SP	15	-	-
Presbytis rubicunda	AQ	DG/SP	-	-	20
Ceboids (NWMs)					
Alouatta seniculus	AQ	DG/SP	18	-	-
Ateles fusciceps	AQ/S	DG/SP	12	-	-
Cebus apella	AQ	DG/SP	18	-	-

Table 3.1. **Extant anthropoids included in MT 2 shape analyses**. See Table 2.1 for abbreviation key.

Taxon	**Locomotor Mode[1]**	**Foot Posture[2]**	**µCT**	**CT**	**Laser Scan**
Hominoids					
Homo sapiens	B	FCP	-	20	10
Gorilla beringei beringei	KW/C	IHSP	-	3	15
Gorilla beringei graueri	KW/C	IHSP	-	3	8
Gorilla gorilla gorilla	KW/C	IHSP	-	4	30
Pan paniscus	KW/C	IHSP	-	1	15
Pan troglodytes	KW/C	IHSP	-	7	29
Pongo abelii	S	IHSP	-	-	9
Pongo pygmaeus	S	IHSP	-	-	14
Hylobates lar	R	MFP	18	-	-
Cercopithecoids					
Chlorocebus aethiops	TQ	DG/SP	8	-	-
Erythrocebus patas	TQ	DG	18	-	-
Macaca fascicularis	TQ	DG/SP	11	-	-
Macaca mulatta	TQ	DG/SP	16	-	-
Macaca nemestrina	TQ	DG/SP	8	-	-
Papio ursinus	TQ	DG/SP	13	-	-
Nasalis larvatus	AQ	DG/SP	16	-	-
Presbytis rubicunda	AQ	DG/SP	-	-	21
Ceboids (NWMs)					
Alouatta seniculus	AQ	DG/SP	17	-	-
Ateles fusciceps	AQ/S	DG/SP	11	-	-
Cebus apella	AQ	DG/SP	16	-	-

Table 3.2. **Extant anthropoids included in MT 3 shape analyses**. See Table 2.1 for abbreviation key.

Taxon	**Locomotor Mode[1]**	**Foot Posture[2]**	**µCT**	**CT**	**Laser Scan**
Hominoids					
Homo sapiens	B	FCP	-	18	7
Gorilla beringei beringei	KW/C	IHSP	-	3	7
Gorilla beringei graueri	KW/C	IHSP	-	3	11
Gorilla gorilla gorilla	KW/C	IHSP	-	4	32
Pan paniscus	KW/C	IHSP	-	1	16
Pan troglodytes	KW/C	IHSP	-	7	23
Pongo abelii	S	IHSP	-	-	7
Pongo pygmaeus	S	IHSP	-	-	12
Hylobates lar	R	MFP	15	-	-
Cercopithecoids					
Chlorocebus aethiops	TQ	DG/SP	7	-	-
Erythrocebus patas	TQ	DG	17	-	-
Macaca fascicularis	TQ	DG/SP	8	-	-
Macaca mulatta	TQ	DG/SP	16	-	-
Macaca nemestrina	TQ	DG/SP	7	-	-
Papio ursinus	TQ	DG/SP	12	-	-
Nasalis larvatus	AQ	DG/SP	14	-	-
Presbytis rubicunda	AQ	DG/SP	-	-	15
Ceboids (NWMs)					
Alouatta seniculus	AQ	DG/SP	16	-	-
Ateles fusciceps	AQ/S	DG/SP	13	-	-
Cebus apella	AQ	DG/SP	19	-	-

Table 3.3. **Extant anthropoids included in MT 4 shape analyses**. See Table 2.1 for abbreviation key.

Taxon	**Locomotor Mode[1]**	**Foot Posture[2]**	**µCT**	**CT**	**Laser Scan**
Hominoids					
Homo sapiens	B	FCP	-	21	10
Gorilla beringei beringei	KW/C	IHSP	-	3	15
Gorilla beringei graueri	KW/C	IHSP	-	1	10
Gorilla gorilla gorilla	KW/C	IHSP	-	4	33
Pan paniscus	KW/C	IHSP	-	1	16
Pan troglodytes	KW/C	IHSP	-	7	29
Pongo abelii	S	IHSP	-	-	9
Pongo pygmaeus	S	IHSP	-	-	14
Hylobates lar	R	MFP	17	-	-
Cercopithecoids					
Chlorocebus aethiops	TQ	DG/SP	8	-	-
Erythrocebus patas	TQ	DG	17	-	-
Macaca fascicularis	TQ	DG/SP	9	-	-
Macaca mulatta	TQ	DG/SP	16	-	-
Macaca nemestrina	TQ	DG/SP	8	-	-
Papio ursinus	TQ	DG/SP	12	-	-
Nasalis larvatus	AQ	DG/SP	16	-	-
Presbytis rubicunda	AQ	DG/SP	-	-	20
Ceboids (NWMs)					
Alouatta seniculus	AQ	DG/SP	16	-	-
Ateles fusciceps	AQ/S	DG/SP	11	-	-
Cebus apella	AQ	DG/SP	18	-	-

Table 3.4. **Extant anthropoids included in MT 5 shape analyses**. See Table 2.1 for abbreviation key.

Accession Number	Geological Age (Ma)	Element	Taxon	Locality	Observation
ARA-VP-6/500-505	4.4	MT 3	*Ardipithecus ramidus*	Aramis, Ethiopia	Original (μCT)
A.L. 333-115B-E	3.0	MT 2 - 5	*Australopithecus afarensis*	Hadar, Ethiopia	Cast (LS)
A.L. 333-72, 160	3.2 – 3.0	MT 2*, 4	*Australopithecus afarensis*	Hadar, Ethiopia	Cast (LS)
StW 89	2.6 – 2.0	MT 2	*Australopithecus africanus*	Sterkfontein Member 4	Original (LS)
KNM-ER 64062	1.88	MT 2, 3, 5	*Homo* sp. (cf. *erectus*)	Above KBS tuff, Ileret	Original (μCT)
StW 114	2.6 – 1.5	MT 5	*Australopithecus africanus*	Sterkfontein Member 4 or 5	Original (LS)
SKX 33380	1.2 – 1.0	MT 5	*Paranthropus robustus*	Swartkrans Member 3	Original (LS)
LB 1	~0.1 – 0.06	MT 2 - 5	*Homo floresiensis*	Liang Bua, Indonesia	Original (CT)
U.W. 101-1458, 269	Undated	MT 2, 4	*Homo naledi*	Gauteng, South Africa	Original (LS)

Table 3.5. **Fossil hominins included in the MT 2 - 5 shape analyses**. Please see text (Materials and Methods) for geological age estimates and taxonomic determinations. *Distal MT fragment described as coming from either MT 2 or MT 3 (Latimer and Lovejoy, 1990), see Materials and Methods.

Species	*A. seniculus*	*A. fusciceps*	*C. apella*	*C. aethiops*	*E. patas*	*M. mulatta*	*M. nemestrina*	*M. fascicularis*	*P. ursinus*	*N. larvatus*	*P. rubicunda*
A. seniculus	1.0000	-	-	-	-	-	-	-	-	-	-
A. fusciceps	ns	1.0000	-	-	-	-	-	-	-	-	-
C. apella	**<0.0001**	**<0.0001**	1.0000	-	-	-	-	-	-	-	-
C. aethiops	**<0.0001**	**<0.0001**	ns	1.0000	-	-	-	-	-	-	-
E. patas	**<0.0001**	**<0.0001**	**<0.0001**	**<0.0001**	1.0000	-	-	-	-	-	-
M. mulatta	**<0.0001**	**<0.0001**	**<0.0001**	ns	**<0.05**	1.0000	-	-	-	-	-
M. nemestrina	**<0.0001**	**<0.0001**	ns	ns	**<0.0001**	ns	1.0000	-	-	-	-
M. fascicularis	**<0.0001**	**<0.0001**	**<0.0001**	ns	**<0.0001**	ns	ns	1.0000	-	-	-
P. ursinus	**<0.0001**	**<0.0001**	**<0.0001**	ns	ns	ns	ns	**<0.05**	1.0000	-	-
N. larvatus	**<0.0001**	**<0.0001**	ns	ns	**<0.0001**	**<0.0001**	ns	ns	**<0.0001**	1.0000	-
P. rubicunda	**<0.0001**	**<0.0001**	ns	ns	**<0.0001**	**<0.0001**	ns	**<0.05**	**<0.0001**	ns	1.0000
H. lar	ns	**<0.05**	**<0.0001**	**<0.0001**	**<0.0001**	**<0.0001**	**<0.0001**	**<0.0001**	**<0.0001**	**<0.0001**	**<0.0001**
P. abelii	ns	**<0.0001**	**<0.01**	**<0.0001**	**<0.0001**	**<0.0001**	**<0.0001**	**<0.0001**	**<0.0001**	**<0.05**	**<0.05**
P. pygmaeus	ns	**<0.05**	**<0.0001**	**<0.0001**	**<0.0001**	**<0.0001**	**<0.0001**	**<0.0001**	**<0.0001**	**<0.0001**	**<0.0001**
G. beringei	ns	**<0.0001**	**<0.0001**	**<0.0001**	**<0.0001**	**<0.0001**	**<0.0001**	**<0.0001**	**<0.0001**	**<0.0001**	**<0.0001**
G.g. gorilla	ns	**<0.0001**	**<0.0001**	**<0.0001**	**<0.0001**	**<0.0001**	**<0.0001**	**<0.0001**	**<0.0001**	**<0.0001**	**<0.0001**
G.b. graueri	ns	**<0.01**	**<0.0001**	**<0.0001**	**<0.0001**	**<0.0001**	**<0.0001**	**<0.0001**	**<0.0001**	**<0.0001**	**<0.0001**
P. paniscus	ns	**<0.05**	**<0.0001**	**<0.0001**	**<0.0001**	**<0.0001**	**<0.0001**	**<0.0001**	**<0.0001**	**<0.0001**	**<0.0001**
P. troglodytes	ns	**<0.0001**	**<0.0001**	**<0.0001**	**<0.0001**	**<0.0001**	**<0.0001**	**<0.0001**	**<0.0001**	**<0.0001**	**<0.0001**
H. sapiens	**<0.0001**	**<0.0001**	**<0.01**	**<0.0001**	**<0.0001**	**<0.0001**	**<0.0001**	**<0.0001**	**<0.0001**	**<0.0001**	**<0.05**

(Continued on next page)

Table 3.6: *Post-hoc* Tukey's HSD results on PC 1 comparing anthropoid genera following a MANOVA on MT 2 shape variables (PC 1 – PC 5). PC 1 principally tracked MT head robusticity. Humans overlap with *Gorilla* and *Pongo*. Bold = significance at $\alpha = 0.05$.

Species	*H. lar*	*P. abelii*	*P. pygmaeus*	*G. beringei*	*G.g. gorilla*	*G.g. graueri*	*P. paniscus*	*P. troglodytes*	*H. sapiens*
A. seniculus	-	-	-	-	-	-	-	-	-
A. fusciceps	-	-	-	-	-	-	-	-	-
C. apella	-	-	-	-	-	-	-	-	-
C. aethiops	-	-	-	-	-	-	-	-	-
E. patas	-	-	-	-	-	-	-	-	-
M. mulatta	-	-	-	-	-	-	-	-	-
M. nemestrina	-	-	-	-	-	-	-	-	-
M. fascicularis	-	-	-	-	-	-	-	-	-
P. ursinus	-	-	-	-	-	-	-	-	-
N. larvatus	-	-	-	-	-	-	-	-	-
P. rubicunda	-	-	-	-	-	-	-	-	-
H. lar	1.0000	-	-	-	-	-	-	-	-
P. abelii	ns	1.0000	-	-	-	-	-	-	-
P. pygmaeus	ns	ns	1.0000	-	-	-	-	-	-
G. beringei	ns	ns	ns	1.0000	-	-	-	-	-
G.g. gorilla	ns	ns	ns	ns	1.0000	-	-	-	-
G.b. graueri	ns	ns	ns	ns	ns	1.0000	-	-	-
P. paniscus	ns	ns	ns	ns	ns	ns	1.0000	-	-
P. troglodytes	ns	ns	ns	ns	ns	ns	ns	1.0000	-
H. sapiens	**<0.0001**	ns	**<0.01**	ns	**<0.0001**	ns	**<0.0001**	**<0.0001**	1.0000

Table 3.6: *Post-hoc* Tukey's HSD results on PC 1 comparing anthropoid genera following a MANOVA on MT 2 shape variables (PC 1 – PC 5). PC 1 principally tracked MT head robusticity. Humans overlap with *Gorilla* and *Pongo*. Bold = significance at $\alpha = 0.05$.

Species	*A. seniculus*	*A. fusciceps*	*C. apella*	*C. aethiops*	*E. patas*	*M. mulatta*	*M. nemestrina*	*M. fascicularis*	*P. ursinus*	*N. larvatus*	*P. rubicunda*
A. seniculus	1.0000	-	-	-	-	-	-	-	-	-	-
A. fusciceps	ns	1.0000	-	-	-	-	-	-	-	-	-
C. apella	**<0.05**	ns	1.0000	-	-	-	-	-	-	-	-
C. aethiops	**<0.05**	ns	ns	1.0000	-	-	-	-	-	-	-
E. patas	**<0.0001**	**<0.0001**	**<0.0001**	**<0.0001**	1.0000	-	-	-	-	-	-
M. mulatta	**<0.05**	ns	ns	ns	**<0.0001**	1.0000	-	-	-	-	-
M. nemestrina	**<0.05**	ns	ns	ns	**<0.0001**	ns	1.0000	-	-	-	-
M. fascicularis	**<0.001**	ns	ns	ns	**<0.0001**	ns	ns	1.0000	-	-	-
P. ursinus	**<0.0001**	ns	ns	ns	**<0.0001**	ns	ns	ns	1.0000	-	-
N. larvatus	ns	ns	**<0.05**	ns	**<0.0001**	ns	ns	**<0.05**	**<0.01**	1.0000	-
P. rubicunda	ns	ns	ns	ns	**<0.0001**	ns	ns	ns	ns	ns	1.0000
H. lar	ns	ns	**<0.01**	**<0.05**	**<0.0001**	**<0.05**	**<0.05**	**<0.01**	**<0.01**	ns	ns
P. abelii	ns	ns	**<0.05**	ns	**<0.0001**	ns	ns	**<0.05**	**<0.01**	ns	ns
P. pygmaeus	ns	ns	**<0.0001**	**<0.01**	**<0.0001**	**<0.01**	**<0.01**	**<0.01**	**<0.0001**	ns	**<0.05**
G. beringei	ns	ns	**<0.05**	ns	**<0.0001**	ns	ns	**<0.05**	**<0.05**	ns	ns
G.g. gorilla	ns	ns	**<0.05**	ns	**<0.0001**	ns	ns	**<0.05**	**<0.01**	ns	ns
G.b. graueri	ns	ns	**<0.01**	**<0.05**	**<0.0001**	ns	ns	**<0.05**	**<0.01**	ns	ns
P. paniscus	**<0.0001**	**<0.05**	ns	ns	**<0.0001**	ns	ns	ns	ns	**<0.0001**	ns
P. troglodytes	ns	ns	**<0.01**	**<0.05**	**<0.0001**	**<0.05**	**<0.05**	**<0.01**	**<0.0001**	ns	ns
H. sapiens	**<0.0001**	**<0.0001**	**<0.0001**	**<0.0001**	ns	**<0.0001**	**<0.0001**	**<0.0001**	**<0.0001**	**<0.0001**	**<0.0001**

(Continued on next page)

Table 3.7: *Post-hoc* Tukey's HSD results on PC 2 comparing anthropoid genera following a MANOVA on MT 2 shape variables (PC 1 – PC 5). PC 2 principally tracked dorso-plantar MT head orientation. Humans and patas monkeys are convergent on PC 2, to the exclusion of all other groups. Bold = significance at $\alpha = 0.05$.

Species	*H. lar*	*P. abelii*	*P. pygmaeus*	*G. beringei*	*G.g. gorilla*	*G.g. graueri*	*P. paniscus*	*P. troglodytes*	*H. sapiens*
A. seniculus	-	-	-	-	-	-	-	-	-
A. fusciceps	-	-	-	-	-	-	-	-	-
C. apella	-	-	-	-	-	-	-	-	-
C. aethiops	-	-	-	-	-	-	-	-	-
E. patas	-	-	-	-	-	-	-	-	-
M. mulatta	-	-	-	-	-	-	-	-	-
M. nemestrina	-	-	-	-	-	-	-	-	-
M. fascicularis	-	-	-	-	-	-	-	-	-
P. ursinus	-	-	-	-	-	-	-	-	-
N. larvatus	-	-	-	-	-	-	-	-	-
P. rubicunda	-	-	-	-	-	-	-	-	-
H. lar	1.0000	-	-	-	-	-	-	-	-
P. abelii	ns	1.0000	-	-	-	-	-	-	-
P. pygmaeus	ns	ns	1.0000	-	-	-	-	-	-
G. beringei	ns	ns	ns	1.0000	-	-	-	-	-
G.g. gorilla	ns	ns	ns	ns	1.0000	-	-	-	-
G.b. graueri	ns	ns	ns	ns	ns	1.0000	-	-	-
P. paniscus	**<0.0001**	**<0.0001**	**<0.0001**	**<0.0001**	**<0.0001**	**<0.0001**	1.0000	-	-
P. troglodytes	ns	ns	ns	ns	ns	ns	**<0.0001**	1.0000	-
H. sapiens	**<0.0001**	**<0.0001**	**<0.0001**	**<0.0001**	**<0.0001**	**<0.0001**	**<0.0001**	**<0.0001**	1.0000

Table 3.7: *Post-hoc* Tukey's HSD results on PC 2 comparing anthropoid genera following a MANOVA on MT 2 shape variables (PC 1 – PC 5). PC 2 principally tracked dorso-plantar MT head orientation. Humans and patas monkeys are convergent on PC 2, to the exclusion of all other groups. Bold = significance at $\alpha = 0.05$.

Species	*A. seniculus*	*A. fusciceps*	*C. apella*	*C. aethiops*	*E. patas*	*M. mulatta*	*M. nemestrina*	*M. fascicularis*	*P. ursinus*	*N. larvatus*	*P. rubicunda*
A. seniculus	1.0000	-	-	-	-	-	-	-	-	-	-
A. fusciceps	ns	1.0000	-	-	-	-	-	-	-	-	-
C. apella	**<0.0001**	**<0.0001**	1.0000	-	-	-	-	-	-	-	-
C. aethiops	**<0.0001**	**<0.0001**	ns	1.0000	-	-	-	-	-	-	-
E. patas	**<0.0001**	**<0.0001**	**<0.0001**	ns	1.0000	-	-	-	-	-	-
M. mulatta	**<0.0001**	**<0.0001**	**<0.0001**	**<0.05**	**<0.0001**	1.0000	-	-	-	-	-
M. nemestrina	**<0.0001**	**<0.0001**	ns	**<0.01**	**<0.0001**	ns	1.0000	-	-	-	-
M. fascicularis	**<0.0001**	**<0.0001**	**<0.0001**	**<0.01**	**<0.0001**	ns	ns	1.0000	-	-	-
P. ursinus	**<0.0001**	**<0.0001**	**<0.0001**	ns	ns	**<0.0001**	**<0.0001**	**<0.0001**	1.0000	-	-
N. larvatus	**<0.0001**	**<0.0001**	ns	**<0.0001**	**<0.0001**	ns	ns	ns	**<0.0001**	1.0000	-
P. rubicunda	**<0.0001**	**<0.0001**	ns	**<0.0001**	**<0.0001**	ns	ns	ns	**<0.0001**	ns	1.0000
H. lar	ns	ns	**<0.0001**	**<0.0001**	**<0.0001**	**<0.0001**	**<0.0001**	**<0.0001**	**<0.0001**	**<0.0001**	**<0.0001**
P. abelii	ns	**<0.0001**	**<0.01**	**<0.0001**	**<0.0001**	**<0.0001**	**<0.0001**	**<0.0001**	**<0.0001**	**<0.0001**	**<0.0001**
P. pygmaeus	ns	**<0.001**	**<0.0001**	**<0.0001**	**<0.0001**	**<0.0001**	**<0.0001**	**<0.0001**	**<0.0001**	**<0.0001**	**<0.0001**
G. beringei	**<0.001**	ns	**<0.0001**	**<0.0001**	**<0.0001**	**<0.0001**	**<0.0001**	**<0.0001**	**<0.0001**	**<0.0001**	**<0.0001**
G.g. gorilla	ns	ns	**<0.0001**	**<0.0001**	**<0.0001**	**<0.0001**	**<0.0001**	**<0.0001**	**<0.0001**	**<0.0001**	**<0.0001**
G.b. graueri	**<0.0001**	**<0.05**	**<0.0001**	**<0.0001**	**<0.0001**	**<0.0001**	**<0.0001**	**<0.0001**	**<0.0001**	**<0.0001**	**<0.0001**
P. paniscus	ns	ns	**<0.0001**	**<0.0001**	**<0.0001**	**<0.0001**	**<0.0001**	**<0.0001**	**<0.0001**	**<0.0001**	**<0.0001**
P. troglodytes	ns	ns	**<0.0001**	**<0.0001**	**<0.0001**	**<0.0001**	**<0.0001**	**<0.0001**	**<0.0001**	**<0.0001**	**<0.0001**
H. sapiens	**<0.0001**	**<0.0001**	**<0.01**	**<0.0001**	**<0.0001**	**<0.0001**	**<0.0001**	**<0.0001**	**<0.0001**	**<0.0001**	**<0.0001**

(Continued on next age)

Table 3.8: *Post-hoc* Tukey's HSD results on PC 1 comparing anthropoid genera following a MANOVA on MT 3 shape variables (PC 1 – PC 5). PC 1 principally tracked MT head robusticity. Humans overlap with *Pongo*. Bold = significance at $\alpha = 0.05$.

Species	*H. lar*	*P. abelii*	*P. pygmaeus*	*G. beringei*	*G.g. gorilla*	*G.g. graueri*	*P. paniscus*	*P. troglodytes*	*H. sapiens*
A. seniculus	-	-	-	-	-	-	-	-	-
A. fusciceps	-	-	-	-	-	-	-	-	-
C. apella	-	-	-	-	-	-	-	-	-
C. aethiops	-	-	-	-	-	-	-	-	-
E. patas	-	-	-	-	-	-	-	-	-
M. mulatta	-	-	-	-	-	-	-	-	-
M. nemestrina	-	-	-	-	-	-	-	-	-
M. fascicularis	-	-	-	-	-	-	-	-	-
P. ursinus	-	-	-	-	-	-	-	-	-
N. larvatus	-	-	-	-	-	-	-	-	-
P. rubicunda	-	-	-	-	-	-	-	-	-
H. lar	1.0000	-	-	-	-	-	-	-	-
P. abelii	**<0.0001**	1.0000	-	-	-	-	-	-	-
P. pygmaeus	**<0.0001**	ns	1.0000	-	-	-	-	-	-
G. beringei	ns	**<0.0001**	**<0.0001**	1.0000	-	-	-	-	-
G.g. gorilla	ns	**<0.0001**	**<0.0001**	ns	1.0000	-	-	-	-
G.b. graueri	ns	**<0.0001**	**<0.0001**	ns	**<0.01**	1.0000	-	-	-
P. paniscus	ns	**<0.001**	**<0.05**	ns	ns	**<0.01**	1.0000	-	-
P. troglodytes	ns	**<0.0001**	**<0.0001**	ns	ns	**<0.01**	ns	1.0000	-
H. sapiens	**<0.0001**	ns	ns	**<0.0001**	**<0.0001**	**<0.0001**	**<0.0001**	**<0.0001**	1.0000

Table 3.8: *Post-hoc* Tukey's HSD results on PC 1 comparing anthropoid genera following a MANOVA on MT 3 shape variables (PC 1 – PC 5). PC 1 principally tracked MT head robusticity. Humans overlap with *Pongo*. Bold = significance at $\alpha = 0.05$.

Species	*A. seniculus*	*A. fusciceps*	*C. apella*	*C. aethiops*	*E. patas*	*M. mulatta*	*M. nemestrina*	*M. fascicularis*	*P. ursinus*	*N. larvatus*	*P. rubicunda*
A. seniculus	1.0000	-	-	-	-	-	-	-	-	-	-
A. fusciceps	ns	1.0000	-	-	-	-	-	-	-	-	-
C. apella	ns	ns	1.0000	-	-	-	-	-	-	-	-
C. aethiops	**<0.05**	ns	ns	1.0000	-	-	-	-	-	-	-
E. patas	**<0.0001**	**<0.0001**	**<0.0001**	**<0.0001**	1.0000	-	-	-	-	-	-
M. mulatta	ns	ns	ns	ns	**<0.0001**	1.0000	-	-	-	-	-
M. nemestrina	ns	ns	ns	ns	**<0.0001**	ns	1.0000	-	-	-	-
M. fascicularis	ns	ns	ns	ns	**<0.0001**	ns	ns	1.0000	-	-	-
P. ursinus	ns	ns	ns	ns	**<0.0001**	ns	ns	ns	1.0000	-	-
N. larvatus	ns	ns	**<0.05**	**<0.0001**	**<0.0001**	ns	ns	**<0.01**	**<0.05**	1.0000	-
P. rubicunda	ns	ns	ns	ns	**<0.0001**	ns	ns	ns	ns	**<0.005**	1.0000
H. lar	ns	ns	ns	**<0.005**	**<0.0001**	ns	ns	ns	ns	ns	ns
P. abelii	ns	ns	ns	ns	**<0.0001**	ns	ns	ns	ns	ns	ns
P. pygmaeus	ns	ns	ns	ns	**<0.0001**	ns	ns	ns	ns	ns	ns
G. beringei	ns	ns	ns	**<0.05**	**<0.0001**	ns	ns	ns	ns	ns	ns
G.g. gorilla	ns	ns	**<0.05**	**<0.01**	**<0.0001**	ns	ns	**<0.05**	ns	ns	**<0.05**
G.b. graueri	ns	ns	ns	**<0.05**	**<0.0001**	ns	ns	ns	ns	ns	ns
P. paniscus	**<0.0001**	ns	ns	ns	**<0.0001**	ns	ns	ns	ns	**<0.0001**	ns
P. troglodytes	ns	**<0.05**	**<0.0001**	**<0.0001**	**<0.0001**	ns	ns	**<0.005**	**<0.0001**	ns	**<0.001**
H. sapiens	**<0.0001**	**<0.0001**	**<0.0001**	**<0.0001**	ns	**<0.0001**	**<0.0001**	**<0.0001**	**<0.0001**	**<0.0001**	**<0.0001**

(Continued on next page)

Table 3.9: *Post-hoc* Tukey's HSD results on PC 2 comparing anthropoid genera following a MANOVA on MT 3 shape variables (PC 1 – PC 5). PC 2 principally tracked dorso-plantar MT head orientation. Humans and patas monkeys are convergent on PC 2, to the exclusion of all other groups. Bold = significance at $\alpha = 0.05$.

Species	*H. lar*	*P. abelii*	*P. pygmaeus*	*G. beringei*	*G.g. gorilla*	*G.g. graueri*	*P. paniscus*	*P. troglodytes*	*H. sapiens*
A. seniculus	-	-	-	-	-	-	-	-	-
A. fusciceps	-	-	-	-	-	-	-	-	-
C. apella	-	-	-	-	-	-	-	-	-
C. aethiops	-	-	-	-	-	-	-	-	-
E. patas	-	-	-	-	-	-	-	-	-
M. mulatta	-	-	-	-	-	-	-	-	-
M. nemestrina	-	-	-	-	-	-	-	-	-
M. fascicularis	-	-	-	-	-	-	-	-	-
P. ursinus	-	-	-	-	-	-	-	-	-
N. larvatus	-	-	-	-	-	-	-	-	-
P. rubicunda	-	-	-	-	-	-	-	-	-
H. lar	1.0000	-	-	-	-	-	-	-	-
P. abelii	ns	1.0000	-	-	-	-	-	-	-
P. pygmaeus	ns	ns	1.0000	-	-	-	-	-	-
G. beringei	ns	ns	ns	1.0000	-	-	-	-	-
G.g. gorilla	ns	ns	ns	ns	1.0000	-	-	-	-
G.b. graueri	ns	ns	ns	ns	ns	1.0000	-	-	-
P. paniscus	**<0.0001**	**<0.001**	**<0.0001**	**<0.0001**	**<0.0001**	**<0.0001**	1.0000	-	-
P. troglodytes	ns	ns	ns	ns	ns	ns	**<0.0001**	1.0000	-
H. sapiens	**<0.0001**	**<0.0001**	**<0.0001**	**<0.0001**	**<0.0001**	**<0.0001**	**<0.0001**	**<0.0001**	1.0000

Table 3.9: *Post-hoc* Tukey's HSD results on PC 2 comparing anthropoid genera following a MANOVA on MT 3 shape variables (PC 1 – PC 5). PC 2 principally tracked dorso-plantar MT head orientation. Humans and patas monkeys are convergent on PC 2, to the exclusion of all other groups. Bold = significance at $\alpha = 0.05$.

Species	*A. seniculus*	*A. fusciceps*	*C. apella*	*C. aethiops*	*E. patas*	*M. mulatta*	*M. nemestrina*	*M. fascicularis*	*P. ursinus*	*N. larvatus*	*P. rubicunda*
A. seniculus	1.0000	-	-	-	-	-	-	-	-	-	-
A. fusciceps	ns	1.0000	-	-	-	-	-	-	-	-	-
C. apella	**<0.0001**	ns	1.0000	-	-	-	-	-	-	-	-
C. aethiops	**<0.0001**	**<0.0001**	**<0.0001**	1.0000	-	-	-	-	-	-	-
E. patas	**<0.0001**	**<0.0001**	**<0.0001**	**<0.05**	1.0000	-	-	-	-	-	-
M. mulatta	**<0.0001**	**<0.0001**	**<0.0001**	ns	**<0.0001**	1.0000	-	-	-	-	-
M. nemestrina	**<0.0001**	**<0.0001**	**<0.05**	ns	**<0.0001**	ns	1.0000	-	-	-	-
M. fascicularis	**<0.0001**	**<0.0001**	**<0.01**	ns	**<0.0001**	ns	ns	1.0000	-	-	-
P. ursinus	**<0.0001**	**<0.0001**	**<0.0001**	ns	**<0.0001**	ns	ns	ns	1.0000	-	-
N. larvatus	**<0.0001**	**<0.0001**	ns	**<0.0001**	**<0.0001**	ns	ns	ns	**<0.001**	1.0000	-
P. rubicunda	**<0.0001**	**<0.0001**	ns	**<0.0001**	**<0.0001**	**<0.05**	ns	ns	**<0.0001**	ns	1.0000
H. lar	**<0.0001**	**<0.01**	**<0.0001**	**<0.0001**	**<0.0001**	**<0.0001**	**<0.0001**	**<0.0001**	**<0.0001**	**<0.0001**	**<0.0001**
P. abelii	ns	ns	**<0.05**	**<0.0001**	**<0.0001**	**<0.0001**	**<0.0001**	**<0.0001**	**<0.0001**	**<0.0001**	**<0.0001**
P. pygmaeus	ns	**<0.05**	ns	**<0.0001**	**<0.0001**	**<0.0001**	**<0.0001**	**<0.0001**	**<0.0001**	**<0.005**	**<0.05**
G. beringei	ns	ns	**<0.0001**	**<0.0001**	**<0.0001**	**<0.0001**	**<0.0001**	**<0.0001**	**<0.0001**	**<0.0001**	**<0.0001**
G.g. gorilla	**<0.001**	ns	**<0.0001**	**<0.0001**	**<0.0001**	**<0.0001**	**<0.0001**	**<0.0001**	**<0.0001**	**<0.0001**	**<0.0001**
G.b. graueri	**<0.0001**	**<0.01**	**<0.0001**	**<0.0001**	**<0.0001**	**<0.0001**	**<0.0001**	**<0.0001**	**<0.0001**	**<0.0001**	**<0.0001**
P. paniscus	**<0.001**	ns	**<0.0001**	**<0.0001**	**<0.0001**	**<0.0001**	**<0.0001**	**<0.0001**	**<0.0001**	**<0.0001**	**<0.0001**
P. troglodytes	**<0.001**	ns	**<0.0001**	**<0.0001**	**<0.0001**	**<0.0001**	**<0.0001**	**<0.0001**	**<0.0001**	**<0.0001**	**<0.0001**
H. sapiens	**<0.05**	**<0.0001**	ns	**<0.0001**	**<0.0001**	**<0.0001**	**<0.0001**	**<0.0001**	**<0.0001**	**<0.0001**	**<0.05**

(Continued on next page)

Table 3.10: ***Post-hoc*** **Tukey's HSD results on PC 1 comparing anthropoid genera following a MANOVA on MT 4 shape variables (PC 1 – PC 5)**. PC 1 principally tracked MT head robusticity. Humans overlap with *Cebus* and *Pongo*. Bold = significance at $\alpha = 0.05$.

Species	*H. lar*	*P. abelii*	*P. pygmaeus*	*G. beringei*	*G.g. gorilla*	*G.g. graueri*	*P. paniscus*	*P. troglodytes*	*H. sapiens*
A. seniculus	-	-	-	-	-	-	-	-	-
A. fusciceps	-	-	-	-	-	-	-	-	-
C. apella	-	-	-	-	-	-	-	-	-
C. aethiops	-	-	-	-	-	-	-	-	-
E. patas	-	-	-	-	-	-	-	-	-
M. mulatta	-	-	-	-	-	-	-	-	-
M. nemestrina	-	-	-	-	-	-	-	-	-
M. fascicularis	-	-	-	-	-	-	-	-	-
P. ursinus	-	-	-	-	-	-	-	-	-
N. larvatus	-	-	-	-	-	-	-	-	-
P. rubicunda	-	-	-	-	-	-	-	-	-
H. lar	1.0000	-	-	-	-	-	-	-	-
P. abelii	**<0.001**	1.0000	-	-	-	-	-	-	-
P. pygmaeus	**<0.0001**	ns	1.0000	-	-	-	-	-	-
G. beringei	ns	ns	**<0.0001**	1.0000	-	-	-	-	-
G.g. gorilla	ns	ns	**<0.0001**	ns	1.0000	-	-	-	-
G.b. graueri	ns	**<0.001**	**<0.0001**	ns	ns	1.0000	-	-	-
P. paniscus	ns	**<0.05**	**<0.0001**	ns	ns	ns	1.0000	-	-
P. troglodytes	ns	**<0.05**	**<0.0001**	ns	ns	ns	ns	1.0000	-
H. sapiens	**<0.0001**	ns	ns	**<0.0001**	**<0.0001**	**<0.0001**	**<0.0001**	**<0.0001**	1.0000

Table 3.10: ***Post-hoc*** **Tukey's HSD results on PC 1 comparing anthropoid genera following a MANOVA on MT 4 shape variables (PC 1 – PC 5)**. PC 1 principally tracked MT head robusticity. Humans overlap with *Cebus* and *Pongo*. Bold = significance at $\alpha = 0.05$.

Species	*A. seniculus*	*A. fusciceps*	*C. apella*	*C. aethiops*	*E. patas*	*M. mulatta*	*M. nemestrina*	*M. fascicularis*	*P. ursinus*	*N. larvatus*	*P. rubicunda*
A. seniculus	1.0000	-	-	-	-	-	-	-	-	-	-
A. fusciceps	ns	1.0000	-	-	-	-	-	-	-	-	-
C. apella	**<0.01**	ns	1.0000	-	-	-	-	-	-	-	-
C. aethiops	ns	ns	ns	1.0000	-	-	-	-	-	-	-
E. patas	ns	ns	**<0.0001**	**<0.0001**	1.0000	-	-	-	-	-	-
M. mulatta	**<0.001**	ns	ns	ns	**<0.0001**	1.0000	-	-	-	-	-
M. nemestrina	ns	ns	**<0.01**	**<0.05**	ns	ns	1.0000	-	-	-	-
M. fascicularis	ns	ns	**<0.01**	ns	ns	ns	ns	1.0000	-	-	-
P. ursinus	ns	ns	ns	ns	**<0.001**	ns	ns	ns	1.0000	-	-
N. larvatus	ns	ns	ns	ns	**<0.05**	ns	ns	ns	ns	1.0000	-
P. rubicunda	**<0.0001**	ns	ns	ns	**<0.0001**	**<0.0001**	ns	**<0.0001**	ns	**<0.001**	1.0000
H. lar	ns	ns	**<0.001**	ns	ns	ns	**<0.0001**	ns	ns	ns	**<0.0001**
P. abelii	ns	ns	ns	ns	**<0.005**	ns	**<0.0001**	ns	ns	ns	ns
P. pygmaeus	ns	ns	**<0.01**	**<0.05**	ns	ns	**<0.0001**	ns	ns	ns	**<0.05**
G. beringei	ns	ns	**<0.0001**	**<0.05**	ns	ns	**<0.0001**	ns	ns	ns	**<0.0001**
G.g. gorilla	ns	ns	**<0.001**	ns	**<0.05**	ns	**<0.0001**	ns	ns	ns	**<0.0001**
G.b. graueri	ns	ns	ns	ns	**<0.05**	ns	**<0.0001**	ns	ns	ns	**<0.001**
P. paniscus	**<0.001**	ns	ns	ns	**<0.0001**	**<0.0001**	**<0.0001**	**<0.001**	ns	**<0.05**	ns
P. troglodytes	ns	ns	**<0.0001**	**<0.005**	ns	ns	**<0.0001**	ns	ns	ns	**<0.0001**
H. sapiens	**<0.0001**	**<0.0001**	**<0.0001**	**<0.0001**	**<0.0001**	**<0.0001**	**<0.0001**	**<0.0001**	**<0.0001**	**<0.0001**	**<0.0001**

(Continued on next page)

Table 3.11: *Post-hoc* Tukey's HSD results on PC 2 comparing anthropoid genera following a MANOVA on MT 4 shape variables (PC 1 – PC 5). PC 2 principally tracked dorso-plantar MT head orientation. Humans are unique on PC 2, with very high PC 2 scores. Bold = significance at $\alpha = 0.05$.

Species	*H. lar*	*P. abelii*	*P. pygmaeus*	*G. beringei*	*G.g. gorilla*	*G.g. graueri*	*P. paniscus*	*P. troglodytes*	*H. sapiens*
A. seniculus	-	-	-	-	-	-	-	-	-
A. fusciceps	-	-	-	-	-	-	-	-	-
C. apella	-	-	-	-	-	-	-	-	-
C. aethiops	-	-	-	-	-	-	-	-	-
E. patas	-	-	-	-	-	-	-	-	-
M. mulatta	-	-	-	-	-	-	-	-	-
M. nemestrina	-	-	-	-	-	-	-	-	-
M. fascicularis	-	-	-	-	-	-	-	-	-
P. ursinus	-	-	-	-	-	-	-	-	-
N. larvatus	-	-	-	-	-	-	-	-	-
P. rubicunda	-	-	-	-	-	-	-	-	-
H. lar	1.0000	-	-	-	-	-	-	-	-
P. abelii	ns	1.0000	-	-	-	-	-	-	-
P. pygmaeus	ns	ns	1.0000	-	-	-	-	-	-
G. beringei	ns	ns	ns	1.0000	-	-	-	-	-
G.g. gorilla	ns	ns	ns	ns	1.0000	-	-	-	-
G.b. graueri	ns	ns	ns	ns	ns	1.0000	-	-	-
P. paniscus	**<0.0001**	ns	**<0.0001**	**<0.0001**	**<0.0001**	ns	1.0000	-	-
P. troglodytes	ns	ns	ns	ns	ns	ns	**<0.0001**	1.0000	-
H. sapiens	**<0.0001**	**<0.0001**	**<0.0001**	**<0.0001**	**<0.0001**	**<0.0001**	**<0.0001**	**<0.0001**	1.0000

Table 3.11: *Post-hoc* Tukey's HSD results on PC 2 comparing anthropoid genera following a MANOVA on MT 4 shape variables (PC 1 – PC 5). PC 2 principally tracked dorso-plantar MT head orientation. Humans are unique on PC 2, with very high PC 2 scores. Bold = significance at $\alpha = 0.05$.

Species	*A. seniculus*	*A. fusciceps*	*C. apella*	*C. aethiops*	*E. patas*	*M. mulatta*	*M. nemestrina*	*M. fascicularis*	*P. ursinus*	*N. larvatus*	*P. rubicunda*
A. seniculus	1.0000	-	-	-	-	-	-	-	-	-	-
A. fusciceps	ns	1.0000	-	-	-	-	-	-	-	-	-
C. apella	**<0.0001**	**<0.001**	1.0000	-	-	-	-	-	-	-	-
C. aethiops	**<0.0001**	**<0.0001**	**<0.0001**	1.0000	-	-	-	-	-	-	-
E. patas	**<0.0001**	**<0.0001**	**<0.0001**	**<0.0001**	1.0000	-	-	-	-	-	-
M. mulatta	**<0.0001**	**<0.0001**	**<0.0001**	ns	**<0.0001**	1.0000	-	-	-	-	-
M. nemestrina	**<0.0001**	**<0.0001**	**<0.0001**	ns	**<0.0001**	ns	1.0000	-	-	-	-
M. fascicularis	**<0.0001**	**<0.0001**	**<0.0001**	ns	**<0.0001**	ns	ns	1.0000	-	-	-
P. ursinus	**<0.0001**	**<0.0001**	**<0.0001**	ns	**<0.001**	ns	ns	ns	1.0000	-	-
N. larvatus	**<0.0001**	**<0.0001**	**<0.001**	ns	**<0.0001**	ns	ns	ns	**<0.05**	1.0000	-
P. rubicunda	**<0.0001**	**<0.0001**	ns	**<0.05**	**<0.0001**	**<0.001**	**<0.001**	**<0.001**	**<0.0001**	ns	1.0000
H. lar	**<0.0001**	ns	**<0.0001**	**<0.0001**	**<0.0001**	**<0.0001**	**<0.0001**	**<0.0001**	**<0.0001**	**<0.0001**	**<0.0001**
P. abelii	ns	ns	**<0.001**	**<0.0001**	**<0.0001**	**<0.0001**	**<0.0001**	**<0.0001**	**<0.0001**	**<0.0001**	**<0.0001**
P. pygmaeus	ns	ns	**<0.0001**	**<0.0001**	**<0.0001**	**<0.0001**	**<0.0001**	**<0.0001**	**<0.0001**	**<0.0001**	**<0.0001**
G. beringei	ns	ns	**<0.0001**	**<0.0001**	**<0.0001**	**<0.0001**	**<0.0001**	**<0.0001**	**<0.0001**	**<0.0001**	**<0.0001**
G.g. gorilla	**<0.001**	ns	**<0.0001**	**<0.0001**	**<0.0001**	**<0.0001**	**<0.0001**	**<0.0001**	**<0.0001**	**<0.0001**	**<0.0001**
G.b. graueri	**<0.0001**	**<0.05**	**<0.0001**	**<0.0001**	**<0.0001**	**<0.0001**	**<0.0001**	**<0.0001**	**<0.0001**	**<0.0001**	**<0.0001**
P. paniscus	**<0.01**	ns	**<0.0001**	**<0.0001**	**<0.0001**	**<0.0001**	**<0.0001**	**<0.0001**	**<0.0001**	**<0.0001**	**<0.0001**
P. troglodytes	ns	ns	**<0.0001**	**<0.0001**	**<0.0001**	**<0.0001**	**<0.0001**	**<0.0001**	**<0.0001**	**<0.0001**	**<0.0001**
H. sapiens	**<0.05**	**<0.0001**	ns	**<0.0001**	**<0.0001**	**<0.0001**	**<0.0001**	**<0.0001**	**<0.0001**	**<0.0001**	ns

(Continued on next page)

Table 3.12: *Post-hoc* Tukey's HSD results on PC 1 comparing anthropoid genera following a MANOVA on MT 5 shape variables (PC 1 – PC 5). PC 2 principally tracked dorso-plantar MT head orientation. Bold = significance at $\alpha = 0.05$.

Species	*H. lar*	*P. abelii*	*P. pygmaeus*	*G. beringei*	*G.g. gorilla*	*G.g. graueri*	*P. paniscus*	*P. troglodytes*	*H. sapiens*
A. seniculus	-	-	-	-	-	-	-	-	-
A. fusciceps	-	-	-	-	-	-	-	-	-
C. apella	-	-	-	-	-	-	-	-	-
C. aethiops	-	-	-	-	-	-	-	-	-
E. patas	-	-	-	-	-	-	-	-	-
M. mulatta	-	-	-	-	-	-	-	-	-
M. nemestrina	-	-	-	-	-	-	-	-	-
M. fascicularis	-	-	-	-	-	-	-	-	-
P. ursinus	-	-	-	-	-	-	-	-	-
N. larvatus	-	-	-	-	-	-	-	-	-
P. rubicunda	-	-	-	-	-	-	-	-	-
H. lar	1.0000	-	-	-	-	-	-	-	-
P. abelii	ns	1.0000	-	-	-	-	-	-	-
P. pygmaeus	ns	ns	1.0000	-	-	-	-	-	-
G. beringei	ns	ns	ns	1.0000	-	-	-	-	-
G.g. gorilla	ns	ns	ns	ns	1.0000	-	-	-	-
G.b. graueri	ns	ns	ns	ns	ns	1.0000	-	-	-
P. paniscus	ns	ns	ns	ns	ns	ns	1.0000	-	-
P. troglodytes	ns	ns	ns	ns	ns	ns	ns	1.0000	-
H. sapiens	**<0.0001**	**<0.0001**	**<0.0001**	**<0.0001**	**<0.0001**	**<0.0001**	**<0.0001**	**<0.0001**	1.0000

Table 3.12: *Post-hoc* Tukey's HSD results on PC 1 comparing anthropoid genera following a MANOVA on MT 5 shape variables (PC 1 – PC 5). PC 2 principally tracked dorso-plantar MT head orientation. Bold = significance at $\alpha = 0.05$.

Species	*A. seniculus*	*A. fusciceps*	*C. apella*	*C. aethiops*	*E. patas*	*M. mulatta*	*M. nemestrina*	*M. fascicularis*	*P. ursinus*	*N. larvatus*	*P. rubicunda*
A. seniculus	1.0000	-	-	-	-	-	-	-	-	-	-
A. fusciceps	ns	1.0000	-	-	-	-	-	-	-	-	-
C. apella	ns	**<0.001**	1.0000	-	-	-	-	-	-	-	-
C. aethiops	ns	ns	ns	1.0000	-	-	-	-	-	-	-
E. patas	**<0.0001**	**<0.05**	**<0.0001**	**<0.001**	1.0000	-	-	-	-	-	-
M. mulatta	ns	ns	ns	ns	**<0.0001**	1.0000	-	-	-	-	-
M. nemestrina	ns	ns	ns	**<0.05**	ns	**<0.001**	1.0000	-	-	-	-
M. fascicularis	ns	ns	ns	ns	ns	**<0.05**	ns	1.0000	-	-	-
P. ursinus	**<0.05**	ns	ns	ns	ns	**<0.0001**	ns	ns	1.0000	-	-
N. larvatus	ns	ns	ns	ns	**<0.05**	**<0.001**	ns	ns	ns	1.0000	-
P. rubicunda	ns	ns	ns	ns	**<0.0001**	ns	ns	ns	**<0.0001**	**<0.05**	1.0000
H. lar	**<0.01**	ns	ns	ns	ns	**<0.0001**	**<0.05**	ns	ns	ns	**<0.0001**
P. abelii	ns	ns	ns	ns	ns	**<0.001**	ns	ns	ns	ns	ns
P. pygmaeus	**<0.01**	ns	ns	ns	ns	**<0.0001**	ns	ns	ns	ns	**<0.0001**
G. beringei	**<0.01**	ns	ns	ns	ns	**<0.0001**	ns	ns	ns	ns	**<0.0001**
G.g. gorilla	**<0.0001**	ns	**<0.001**	**<0.05**	ns	**<0.0001**	ns	ns	ns	ns	**<0.0001**
G.b. graueri	ns	ns	ns	ns	**<0.05**	ns	ns	ns	ns	ns	ns
P. paniscus	ns	ns	ns	ns	**<0.0001**	ns	ns	ns	ns	ns	ns
P. troglodytes	**<0.05**	ns	ns	**<0.005**	ns	**<0.0001**	ns	ns	ns	ns	**<0.0001**
H. sapiens	**<0.0001**	**<0.0001**	**<0.0001**	**<0.0001**	**<0.0001**	**<0.0001**	**<0.0001**	**<0.0001**	**<0.0001**	**<0.0001**	**<0.0001**

(Continued on next page)

Table 3.13: ***Post-hoc*** **Tukey's HSD results on PC 2 comparing anthropoid genera following a MANOVA on MT 5 shape variables (PC 1 – PC 5)**. PC 2 principally tracked dorso-plantar MT head orientation. Humans are unique on PC 2, with very high PC 2 scores. Bold = significance at $\alpha = 0.05$.

Species	*H. lar*	*P. abelii*	*P. pygmaeus*	*G. beringei*	*G.g. gorilla*	*G.g. graueri*	*P. paniscus*	*P. troglodytes*	*H. sapiens*
A. seniculus	-	-	-	-	-	-	-	-	-
A. fusciceps	-	-	-	-	-	-	-	-	-
C. apella	-	-	-	-	-	-	-	-	-
C. aethiops	-	-	-	-	-	-	-	-	-
E. patas	-	-	-	-	-	-	-	-	-
M. mulatta	-	-	-	-	-	-	-	-	-
M. nemestrina	-	-	-	-	-	-	-	-	-
M. fascicularis	-	-	-	-	-	-	-	-	-
P. ursinus	-	-	-	-	-	-	-	-	-
N. larvatus	-	-	-	-	-	-	-	-	-
P. rubicunda	-	-	-	-	-	-	-	-	-
H. lar	1.0000	-	-	-	-	-	-	-	-
P. abelii	ns	1.0000	-	-	-	-	-	-	-
P. pygmaeus	ns	ns	1.0000	-	-	-	-	-	-
G. beringei	ns	ns	ns	1.0000	-	-	-	-	-
G.g. gorilla	ns	ns	ns	ns	1.0000	-	-	-	-
G.b. graueri	ns	ns	ns	ns	**<0.05**	1.0000	-	-	-
P. paniscus	**<0.05**	ns	**<0.05**	**<0.0001**	**<0.0001**	ns	1.0000	-	-
P. troglodytes	ns	ns	ns	ns	ns	ns	ns	1.0000	-
H. sapiens	**<0.0001**	**<0.0001**	**<0.0001**	**<0.0001**	**<0.0001**	**<0.0001**	**<0.0001**	**<0.0001**	1.0000

Table 3.13: ***Post-hoc*** **Tukey's HSD results on PC 2 comparing anthropoid genera following a MANOVA on MT 5 shape variables (PC 1 – PC 5)**. PC 2 principally tracked dorso-plantar MT head orientation. Humans are unique on PC 2, with very high PC 2 scores. Bold = significance at $\alpha = 0.05$.

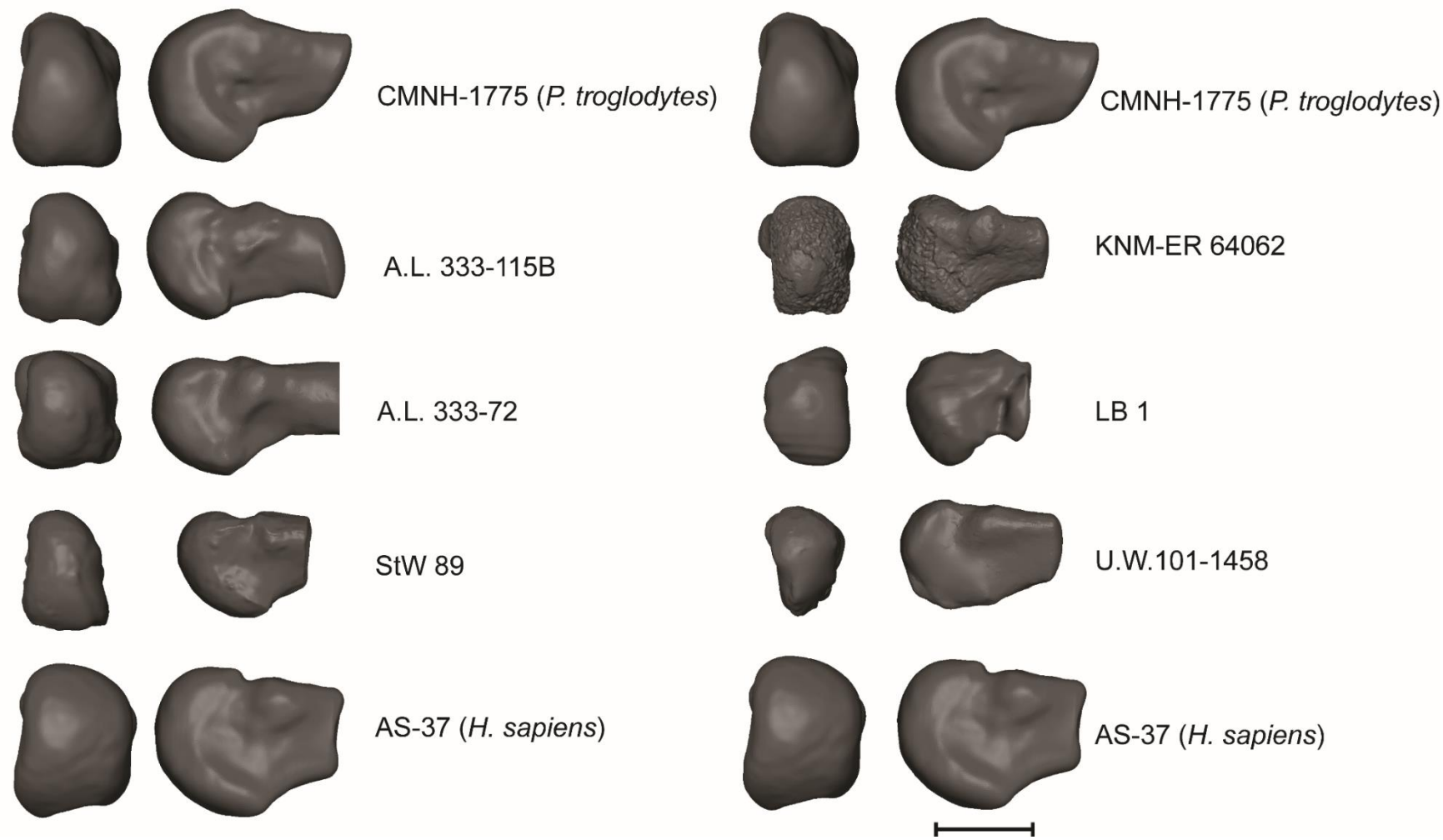

Figure 3.1: Comparative morphology of fossil second metatarsals (MT 2). Note that *Homo* is characterized by dorsal overlap of the distal articular surface onto the MT shaft and by wide flattening of the dorsal articular surface. Left column: distal views. Right column: lateral views. Bar: 1 cm.

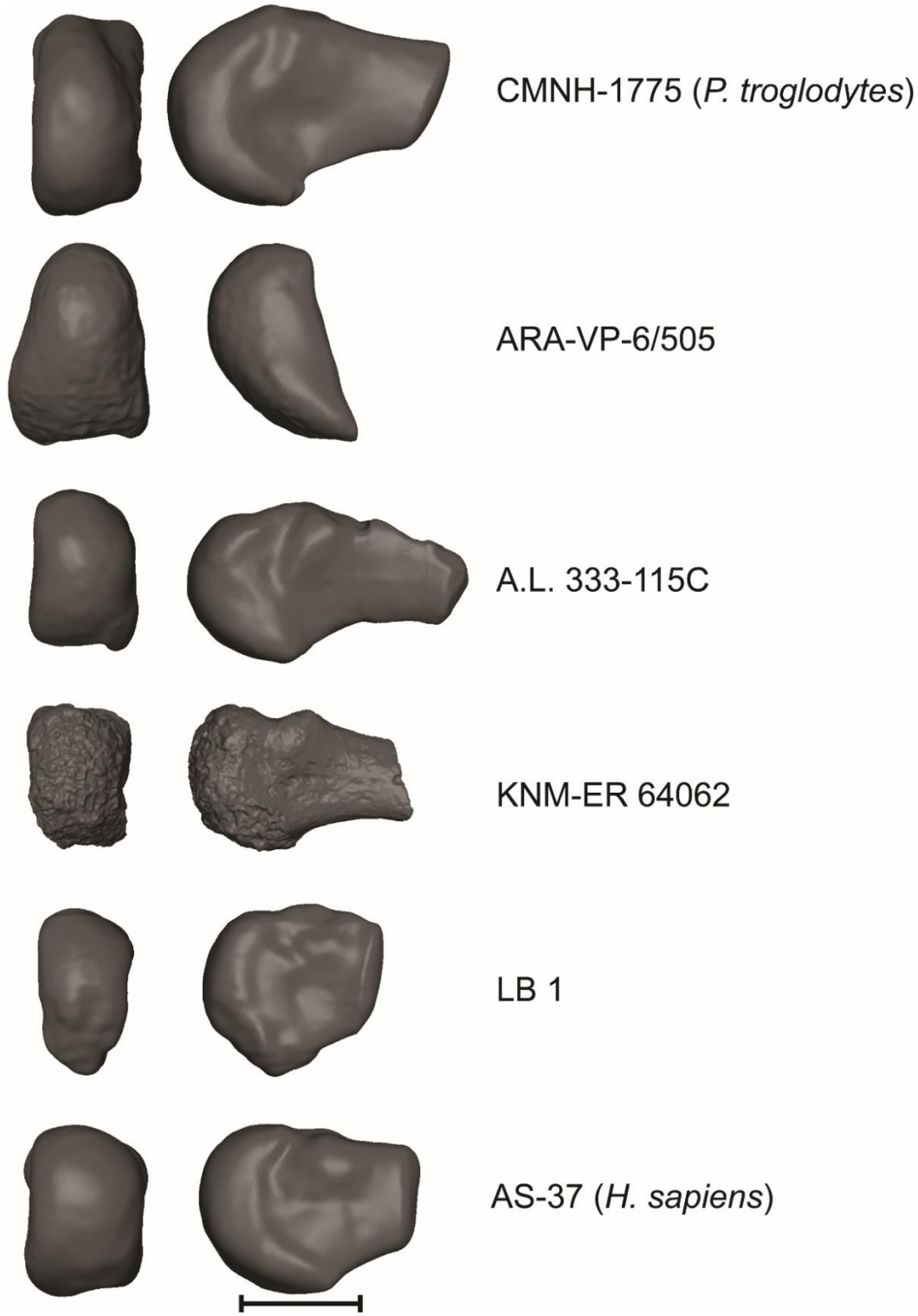

Figure 3.2: Comparative morphology of fossil third metatarsals (MT 3). Note that *Homo* is characterized by dorsal overlap of the distal articular surface onto the MT shaft and by wide flattening of the dorsal articular surface. Epicondylar surface landmarks were removed for MT 3 analyses in order to include ARA-VP-6/505 into the analysis Left column: distal views. Right column: lateral views. Bar: 1 cm.

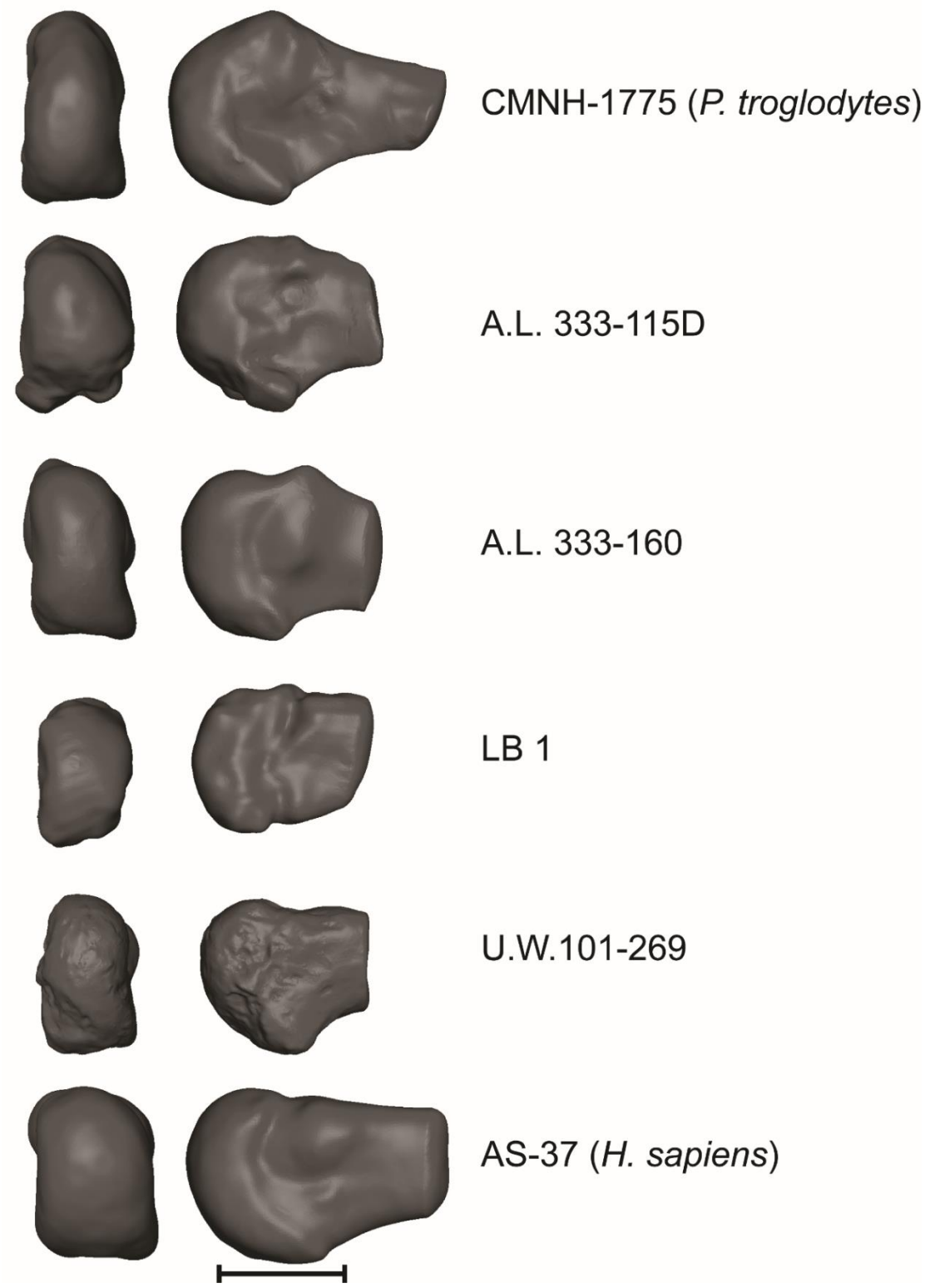

Figure 3.3: Comparative morphology of fossil fourth metatarsals (MT 4). Note that *Homo* is characterized by dorsal overlap of the distal articular surface onto the MT shaft and by wide flattening of the dorsal articular surface. Left column: distal views. Right column: lateral views. Bar: 1 cm.

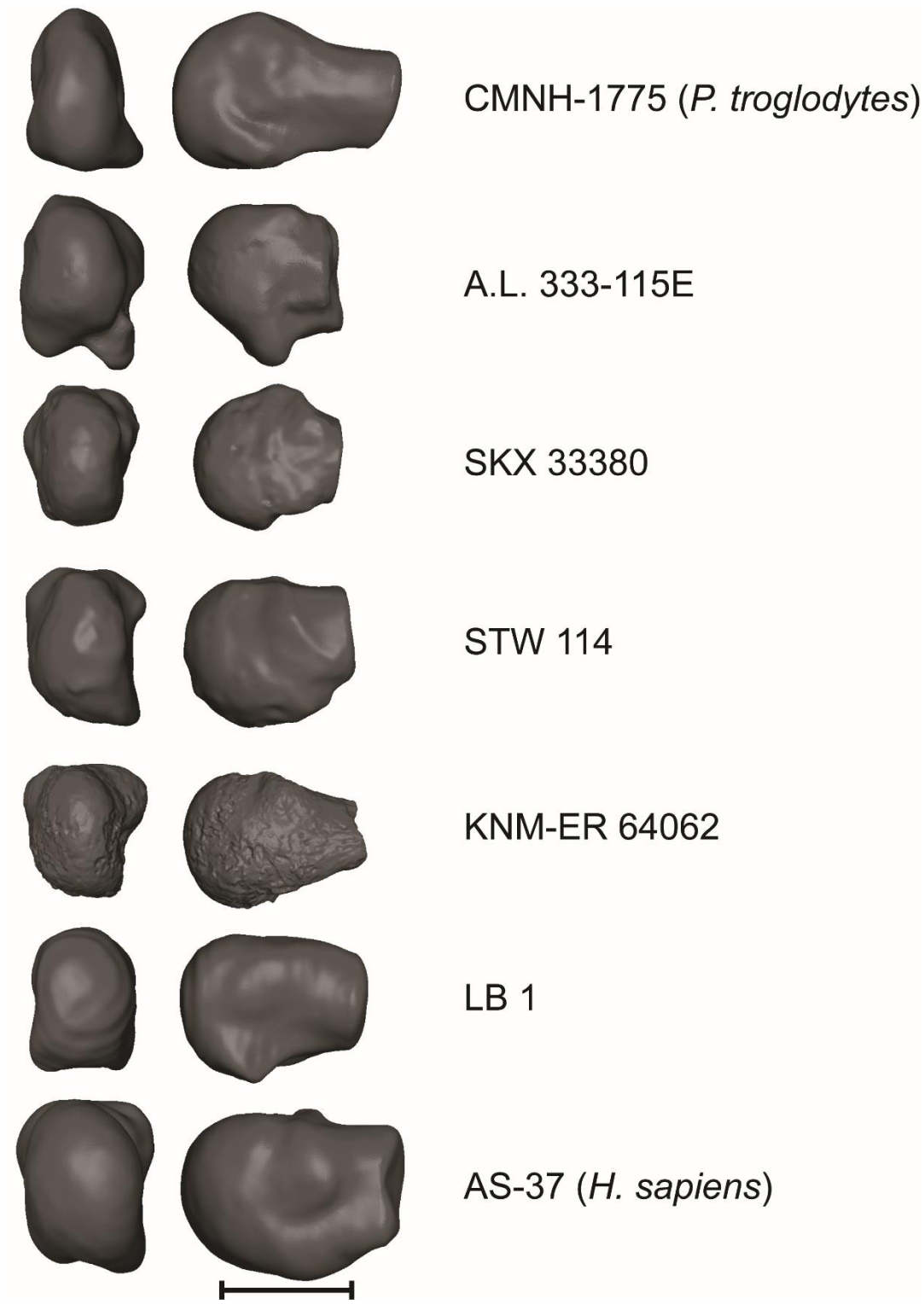

Figure 3.4: Comparative morphology of fossil fifth metatarsals (MT 5). Note that *Homo* is characterized by dorsal overlap of the distal articular surface onto the MT shaft and by wide flattening of the dorsal articular surface, although this is less pronounced in MT 5. Left column: distal views. Right column: lateral views. Bar: 1 cm.

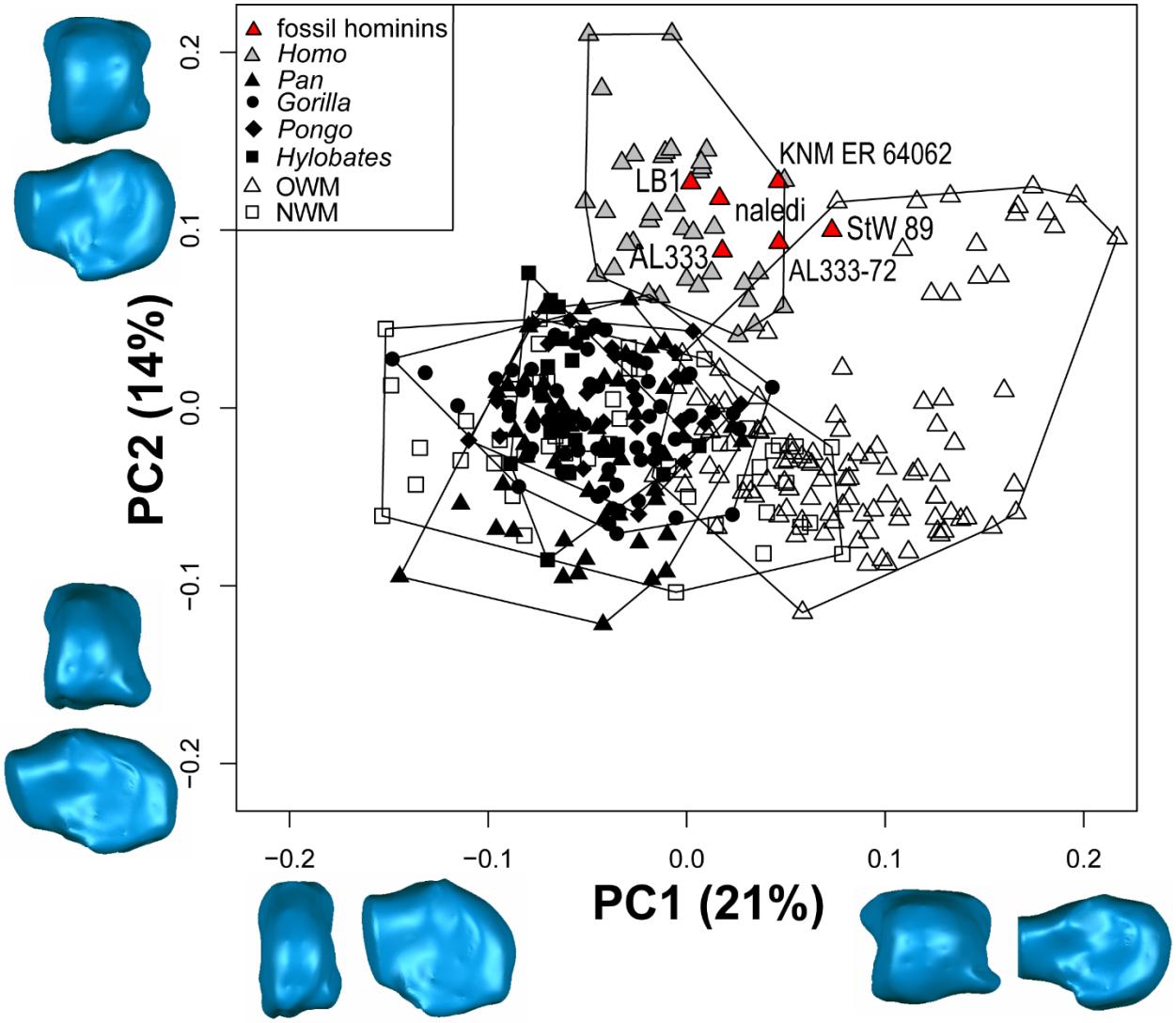

Figure 3.5: PCA scatterplot of PC 1 vs. PC 2 for MT 2. Note the general separation of monkeys (open rectangles), apes (filled shapes), and humans (gray triangles). Minimum convex polygons are constructed for these groups to illustrate their ranges in the morphospace. There is much overlap within apes, and between apes and NWMs. Fossil hominins (red triangles) primarily fall within the human polygon except for StW 89, which looks more similar to cercopithecoids with high PC 2 values (i.e., patas monkeys). PC 1 tracked mediolateral head robusticity and PC 2 strongly tracked dorso-plantar orientation of the MT head. 3D surface morphs in lateral and distal views represent articular shape differences of observed extremes (PC 1: -0.15 – 0.20; PC 2: -0.12 – 0.20).

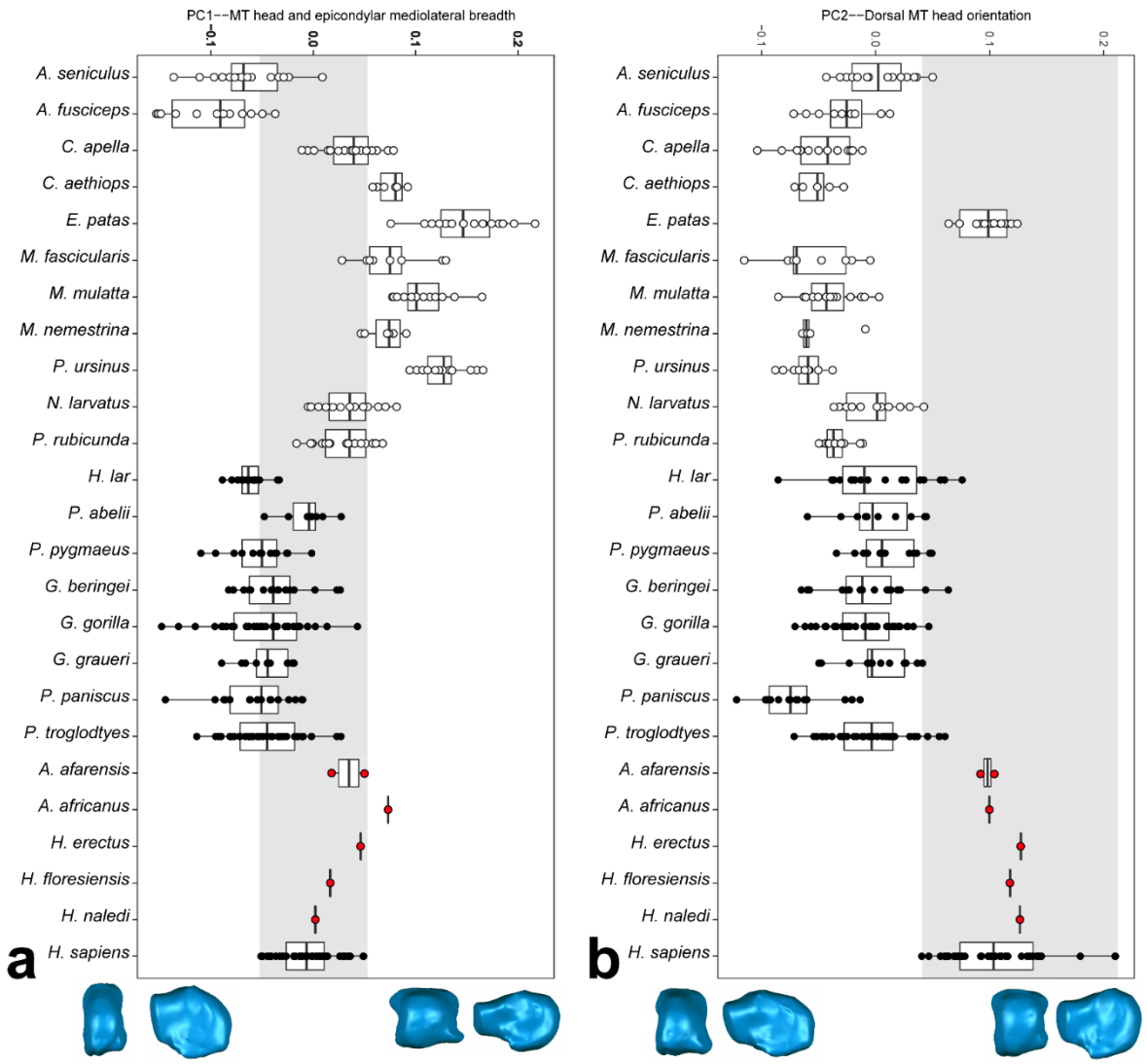

Figure 3.6: Cleveland box-and-whisker plots of PC 1 (a) and PC 2 (b) scores for the anthropoid MT 2. Generally, humans overlap with apes and hominins on PC 1 (MT head robusticity), and are unique on PC 2 (dorsal head orientation), except for patas monkeys, which show convergence with humans on PC 2 (see Results). StW 89 is not as human-like as the other hominins. Shaded bar: modern human range. 3D surface morphs in lateral and distal views represent articular shape differences of observed extremes (PC 1: -0.15 – 0.20; PC 2: -0.12 – 0.20). Vertical bars: median. Rectangles: interquartile range. Horizontal bars: range.

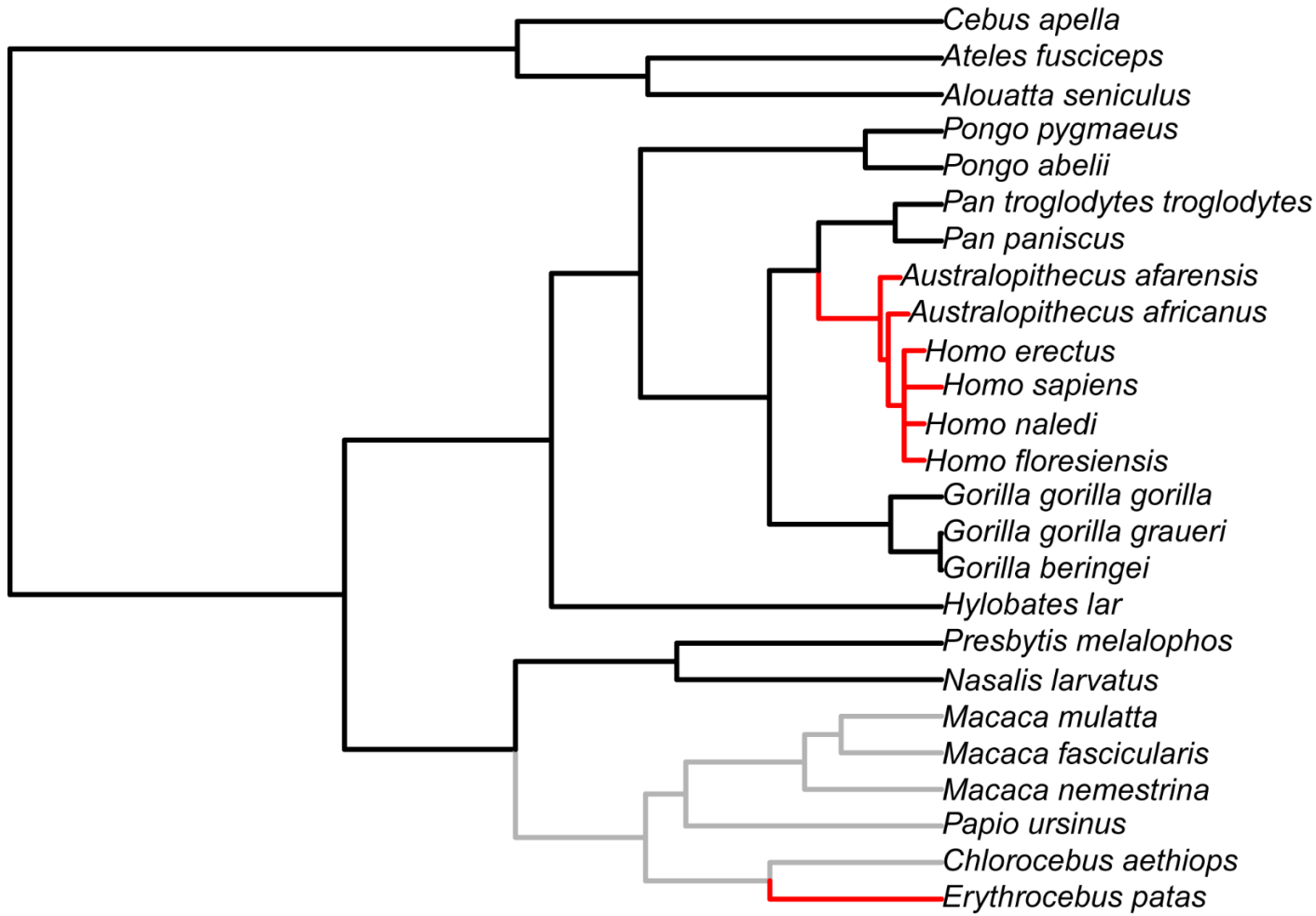

Figure 3.7: Time-calibrated phylogenetic tree with estimated adaptive regimes painted onto the tree branches for MT 2. Adaptive regimes are based on PC 1 (MT 2 head robusticity, plantar morphology) and PC 2 (MT 2 head orientation) scores. Convergent regimes are highlighted with red branches and non-convergent regimes are highlighted in gray branches. The three regime shifts towards different adaptive optima includes a convergent regime with hominins and patas monkeys (red), and non-convergent regimes with apes, colobines and cebids (black), and cercopithecines (gray).

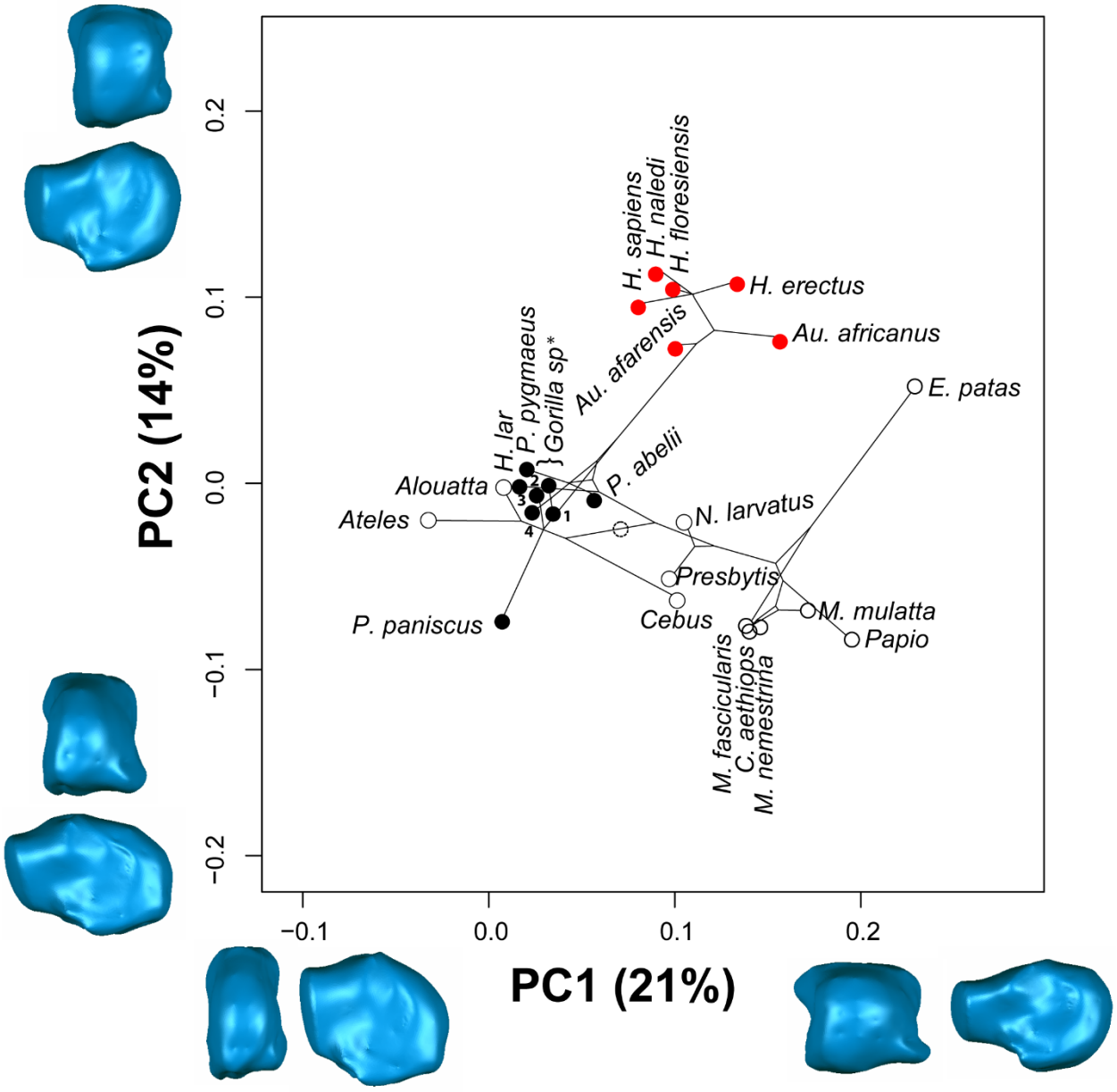

Figure 3.8: Phylomorphospace plot of the anthropoid molecular phylogeny superimposed upon a species-means bivariate PCA scatterplot of MT 2. Upon diverging towards their respective adaptive optima, cercopithecoids (open circles), and hominins (red circles) undergo relatively little evolutionary shape change in the MT 2 head compared to monkeys. Note major evolutionary shape changes in the hominin divergence from apes, and *E. patas* convergence with hominins on PC 2. Additionally, bonobos exhibit more evolutionary change than other apes studied. [1]*Pan troglodytes*; [2]*G. b. beringei;* [3]*G. b. graueri;* [4]*G. g. gorilla*.

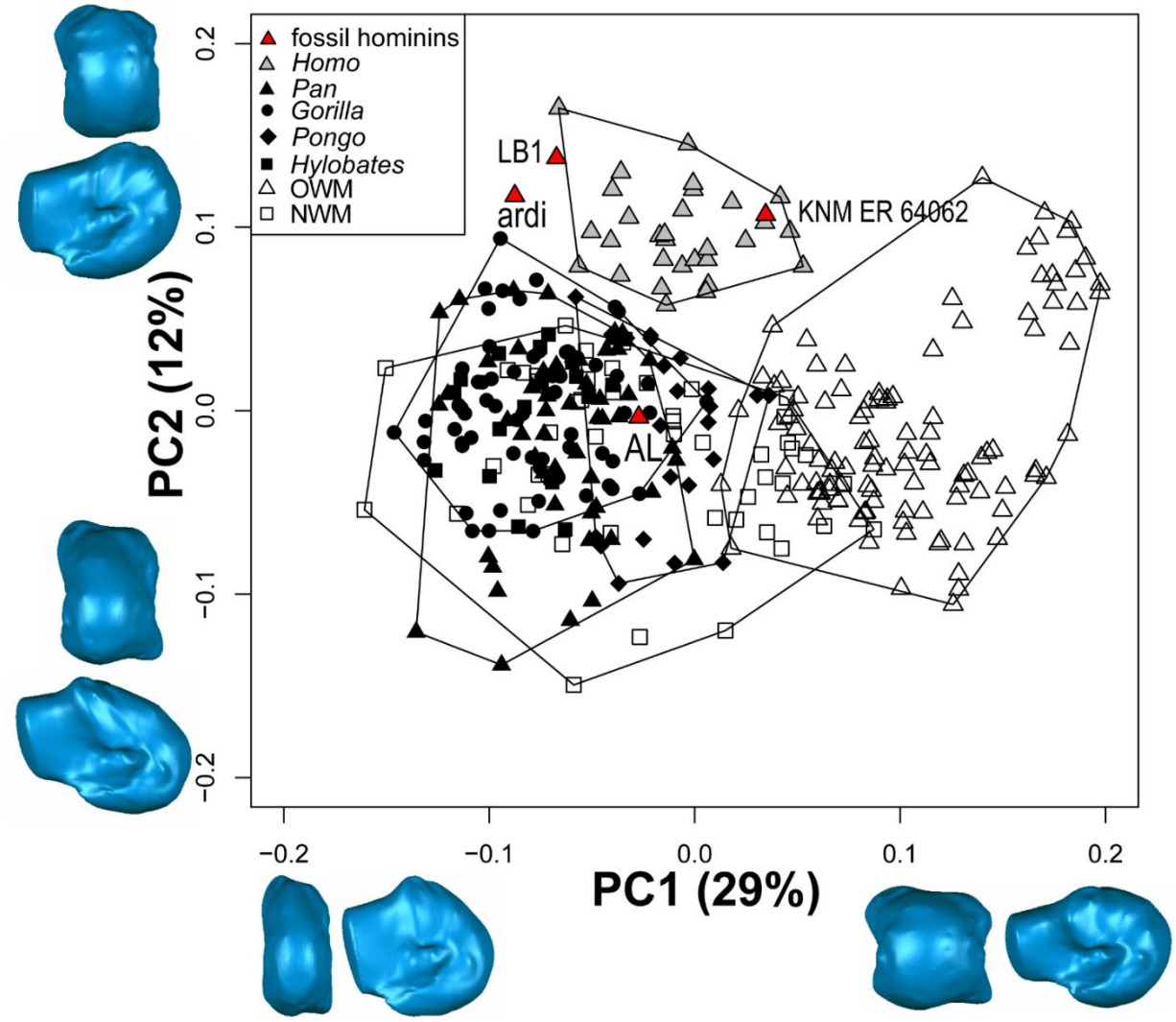

Figure 3.9: PCA scatterplot of PC 1 vs. PC 2 for MT 3. Note the general separation of monkeys (open rectangles), apes (filled shapes), and humans (gray triangles). Minimum convex polygons are constructed for these groups to illustrate their ranges in the morphospace. Apes overlap each other greatly, and NWM overlap both apes and OWMs. Fossil hominins (red triangles) fall within or around the human polygon except for A.L. 333-115C, which looks more similar to *Pan* or *Gorilla*. Epicondylar surface landmarks were removed to incorporate *Ar. ramidus* into the analysis (see Materials and Methods). PC 1 tracked mediolateral head robusticity and PC 2 strongly tracked dorso-plantar orientation of the MT head. 3D surface morphs in lateral and distal views represent articular shape differences of observed extremes (PC 1: -0.15 - 0.20; PC 2: -0.12 - 0.18).

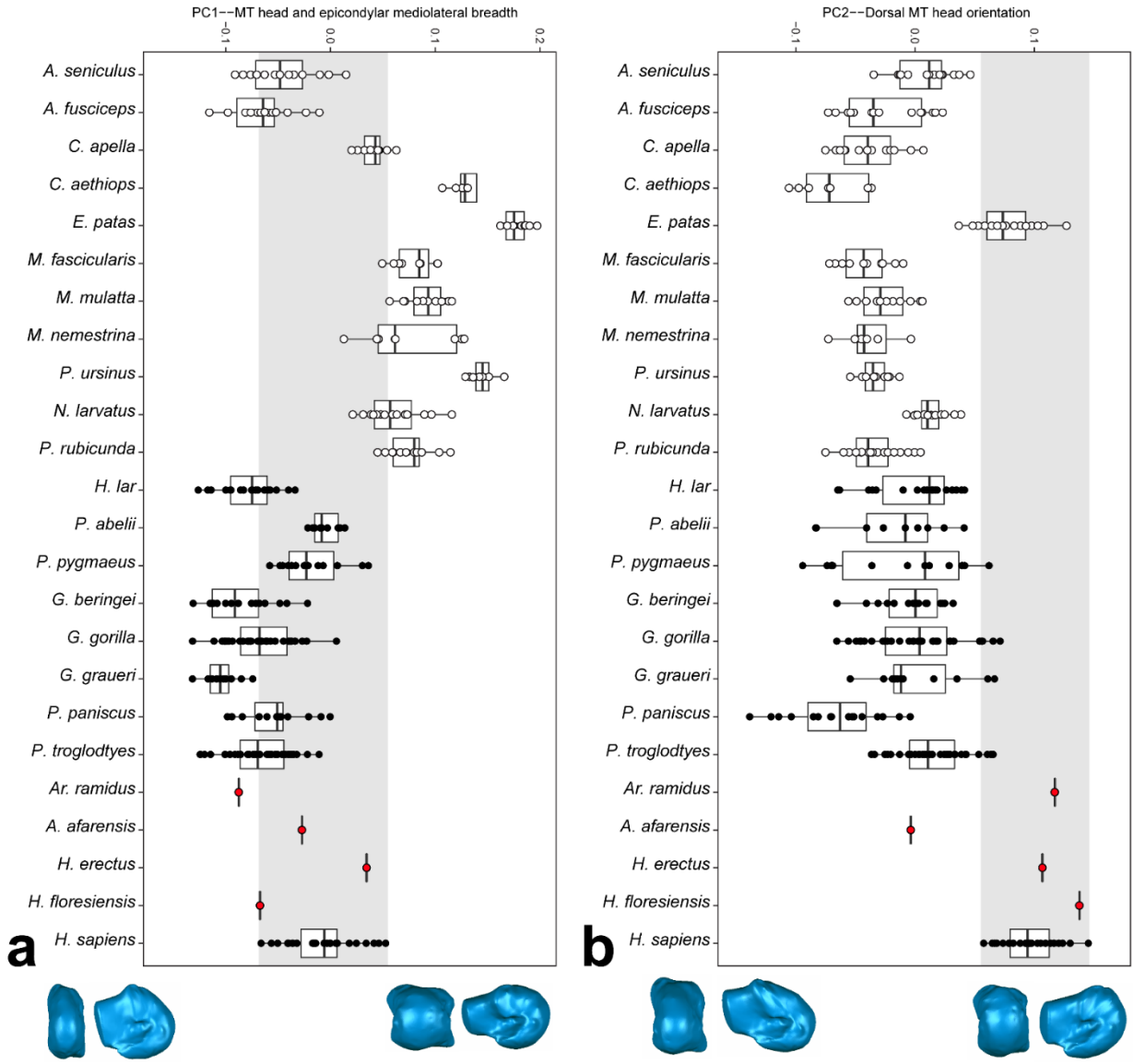

Figure 3.10: Cleveland box-and-whisker plots of PC 1 (a) and PC 2 (b) scores for the anthropoid MT 3. Generally, humans overlap with apes and hominins on PC 1 (MT head robusticity), and are unique on PC 2 (dorsal head orientation), except for patas monkeys, which show convergence with humans on PC 2 (see Results). Most hominins resemble modern-humans, except for A.L.-333C, which looks chimpanzee-like. Epicondylar surface landmarks were removed to incorporate *Ar. ramidus* into the analysis (see Materials and Methods). Shaded bar: modern human range. 3D surface morphs in lateral and distal views represent articular shape differences of observed extremes (PC 1: -0.15 - 0.20; PC 2: -0.12 - 0.18). Vertical bars: median. Rectangles: interquartile range. Horizontal bars: range.

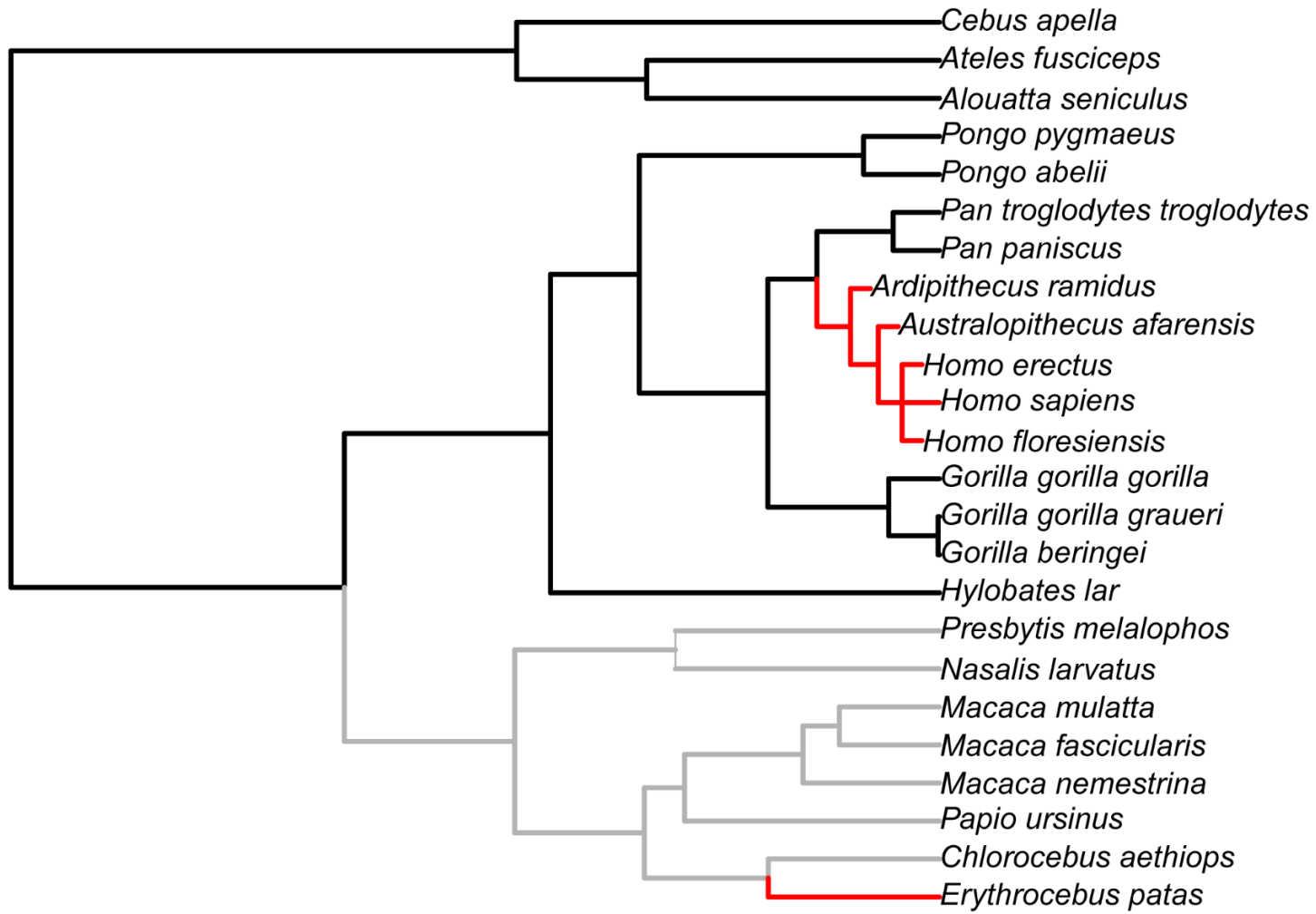

Figure 3.11: Time-calibrated phylogenetic tree with estimated adaptive regimes painted onto the tree branches for MT 3. Adaptive regimes are based on PC 1 (MT 3 head robusticity, plantar morphology) and PC 2 (MT 3 head orientation) scores. Convergent regimes are highlighted with red branches and non-convergent regimes are highlighted in gray branches. The three regime shifts towards different adaptive optima includes a convergent regime with hominins and patas monkeys (red), and non-convergent regimes with apes, colobines and cebids (black), and cercopithecines (gray).

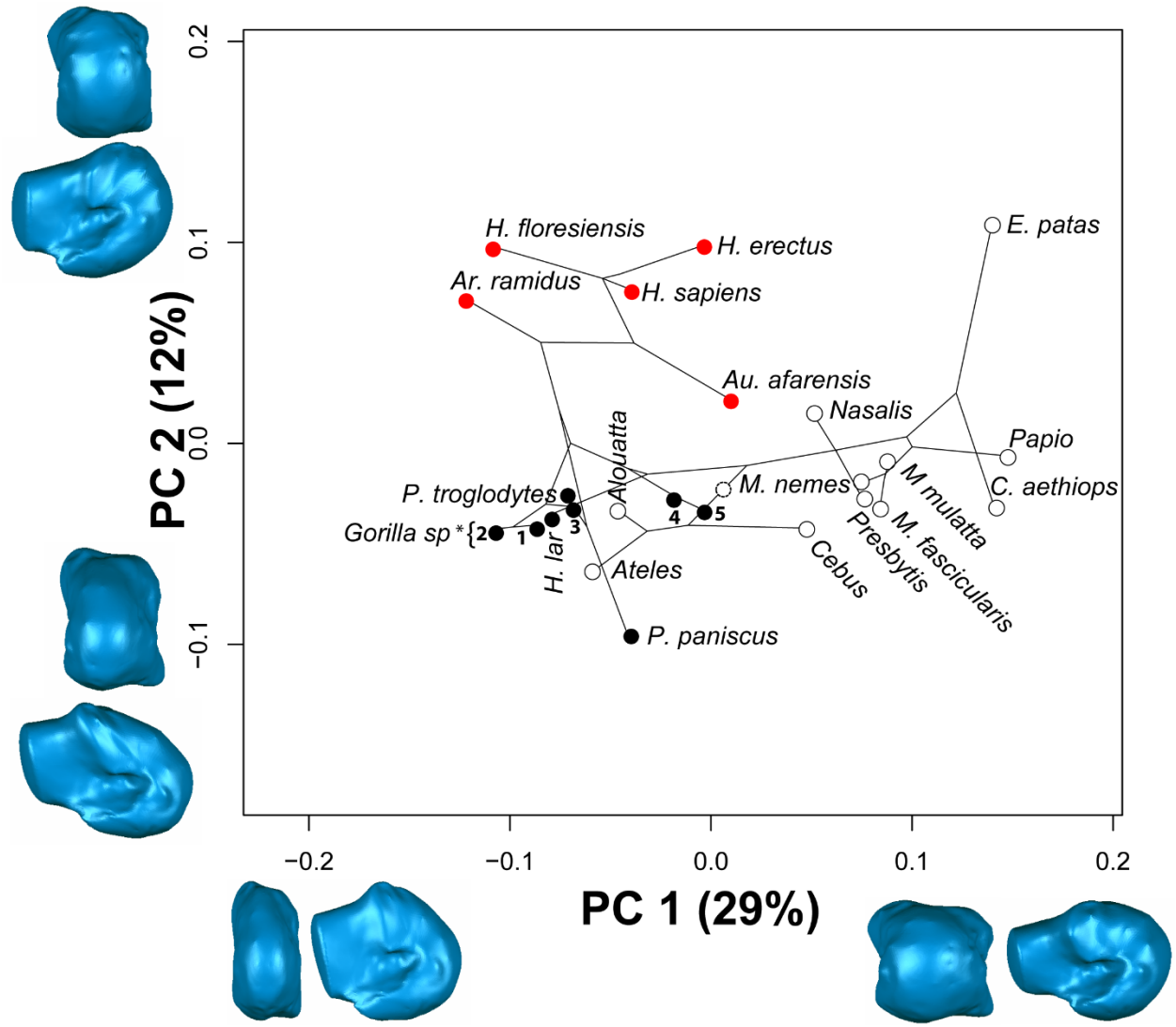

Figure 3.12: Phylomorphospace plot of the anthropoid molecular phylogeny superimposed upon a species-means bivariate PCA scatterplot of MT 3. Upon diverging towards their respective adaptive optima, cercopithecoids (open circles), hominins (red circles), and apes (black circles) all undergo significant evolutionary change in one or more lineages. Note major evolutionary shape changes in the hominin divergence from apes, and *E. patas* convergence with hominins on PC 2. Additionally, bonobos exhibit more evolutionary change than other apes studied. [1]*G. b. beringei*; [2]*G. b. graueri;* [3]*G. g. gorilla;* [4]*P. pygmaeus*; [5]*P. abelii*

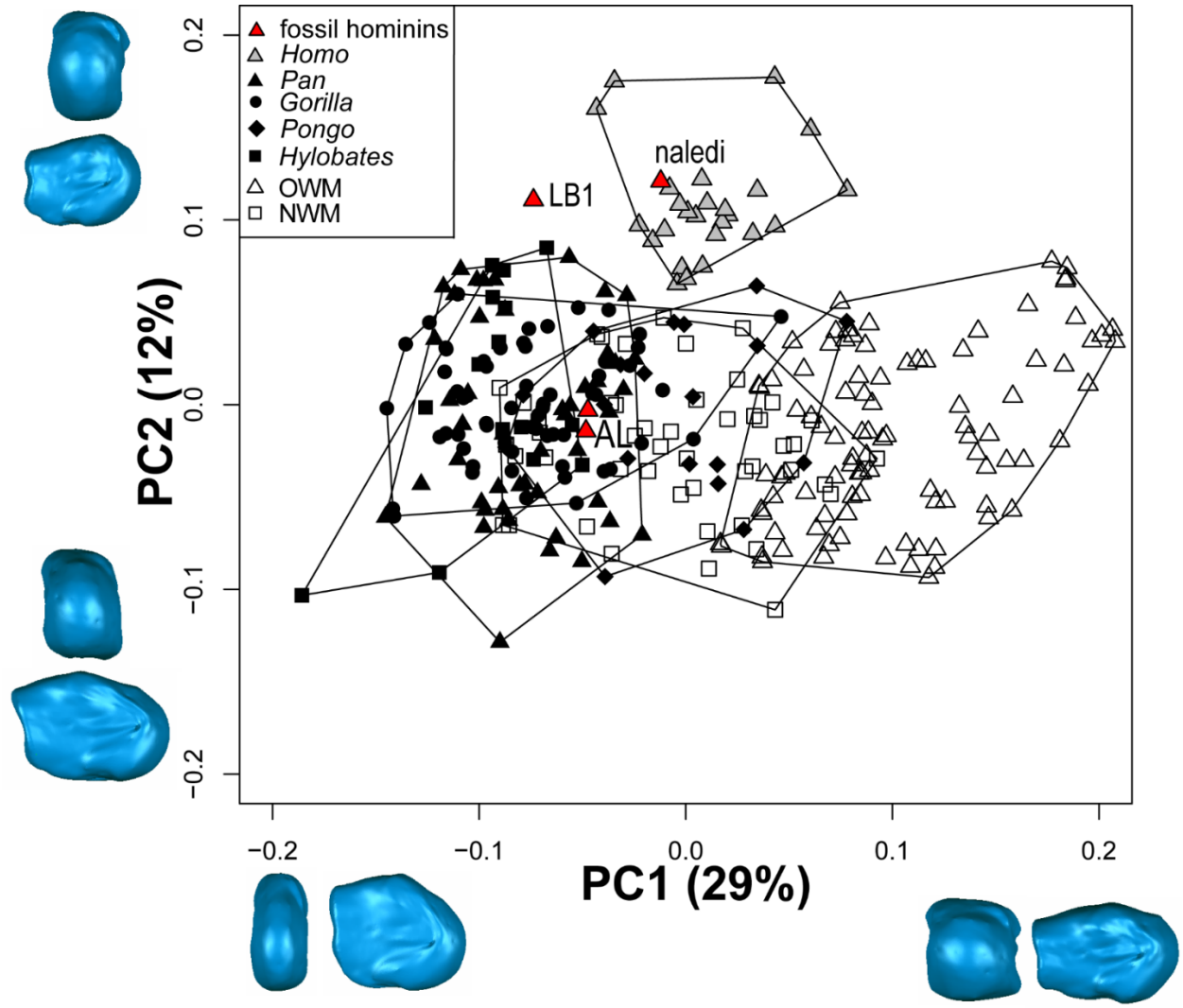

Figure 3.13: PCA scatterplot of PC 1 vs. PC 2 for MT 4. Note the general separation of monkeys (open rectangles), apes (filled shapes), and humans (gray triangles). Minimum convex polygons are constructed for these groups to illustrate their ranges in the morphospace. There is much overlap between all groups except humans. *H. naledi* looks most human-like, and LB 1 shows mosaic morphology. Both A.L. 333 specimens look more chimpanzee like in MT 4. PC 1 tracked mediolateral head robusticity and PC 2 strongly tracked dorso-plantar orientation of the MT head. 3D surface morphs in lateral and distal views represent articular shape differences of observed extremes (PC 1: -0.20 - 0.20; PC 2: -0.12 - 0.18).

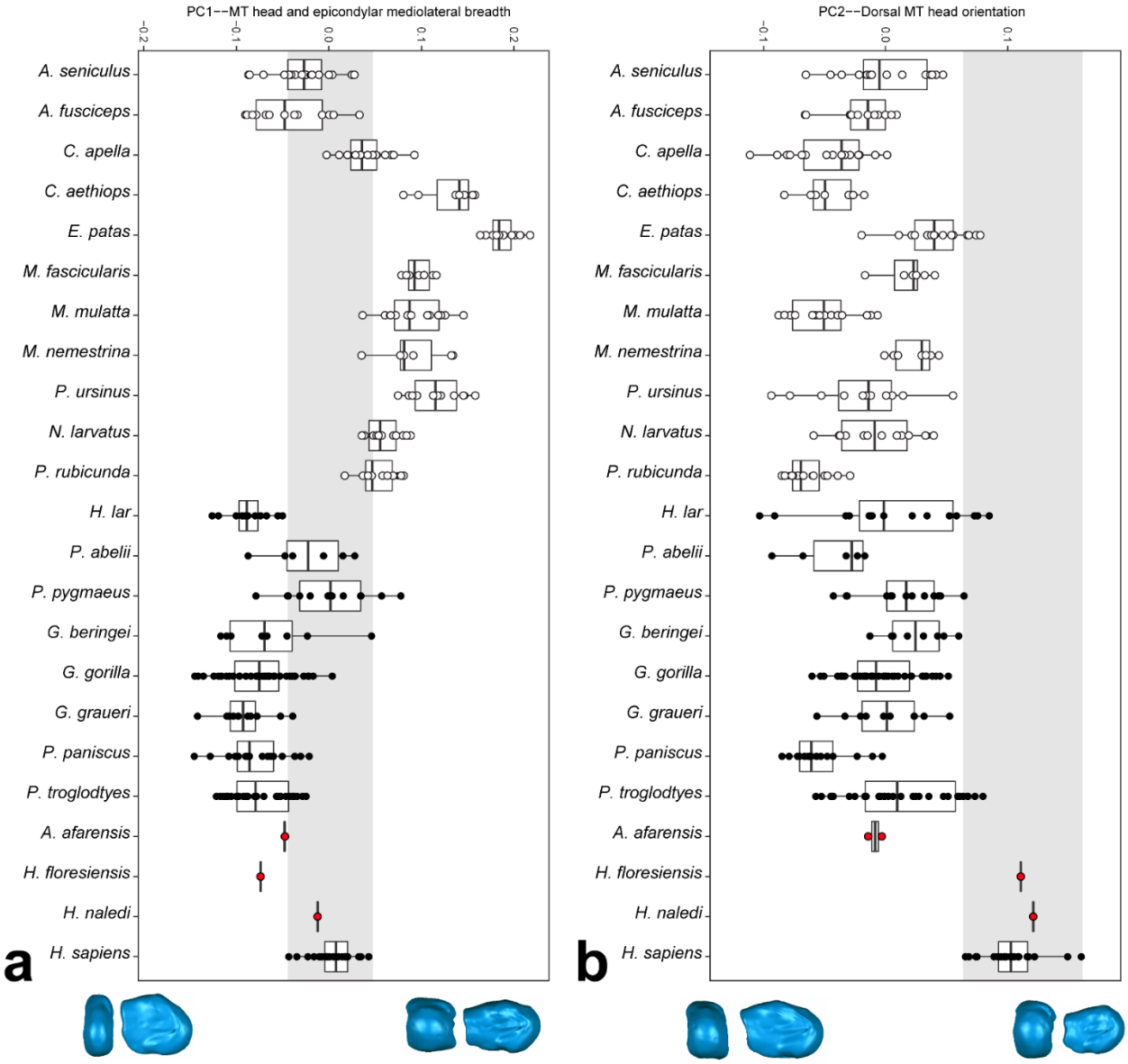

Figure 3.14: Cleveland box-and-whisker plots of PC 1 (a) and PC 2 (b) scores for the anthropoid MT 4. Generally, humans overlap with apes and hominins on PC 1 (MT head robusticity), and are unique on PC 2 (dorsal head orientation). *Au. afarensis* looks chimpanzee-like in its MT 4 morphology. Shaded bar: modern human range. 3D surface morphs in lateral and distal views represent articular shape differences of observed extremes (PC 1: -0.20 - 0.20; PC 2: -0.12 - 0.18). Vertical bars: median. Rectangles: interquartile range. Horizontal bars: range.

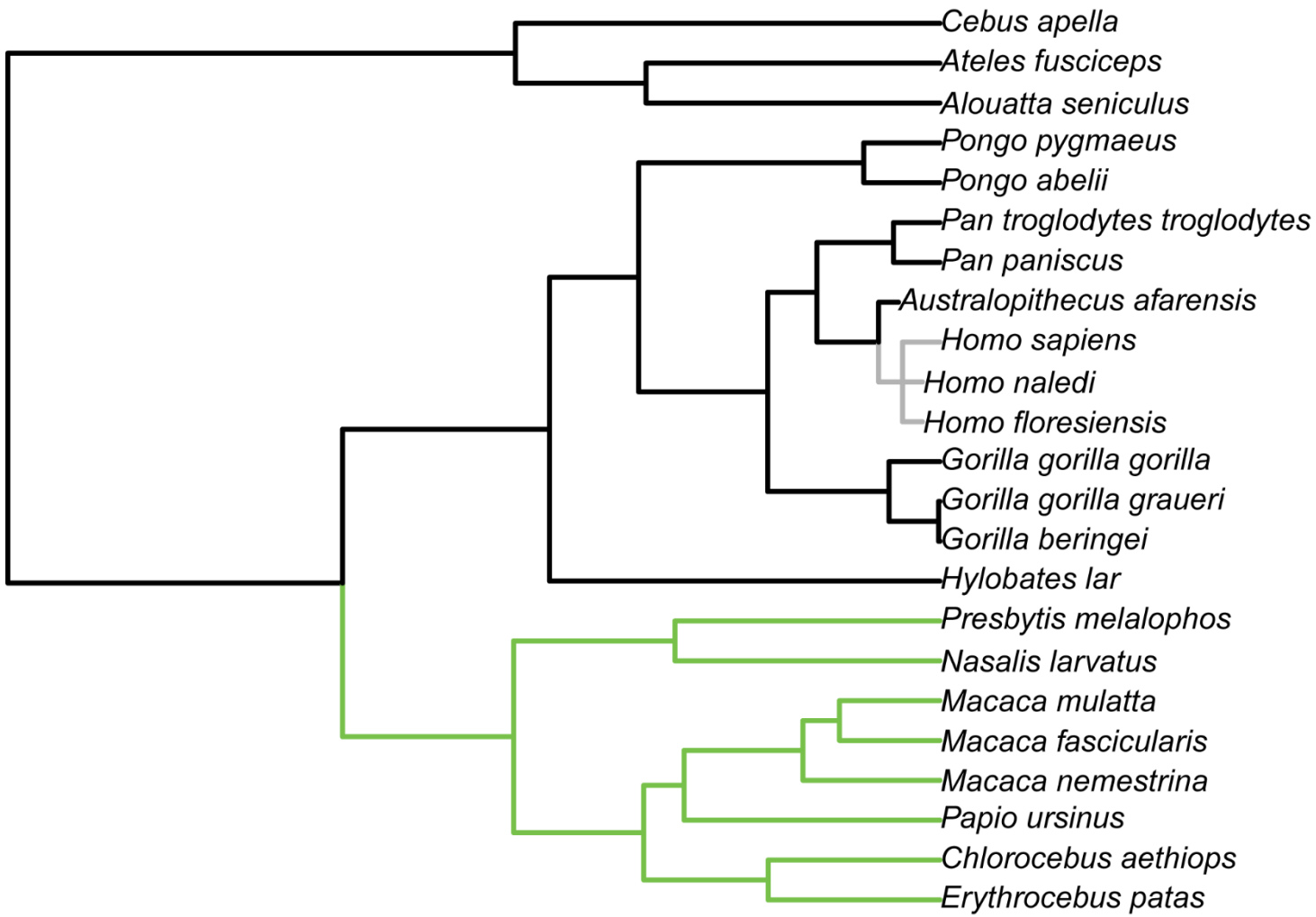

Figure 3.15: Time-calibrated phylogenetic tree with estimated adaptive regimes painted onto the tree branches for MT 4. Adaptive regimes are based on PC 1 (MT 4 head robusticity, plantar morphology) and PC 2 (MT 4 head orientation) scores. No evidence for convergence between anthropoid clades was found. The three regime shifts towards different adaptive optima includes apes, cebids, and australopithecines (black), cercopithecoids (green), and genus *Homo* (gray).

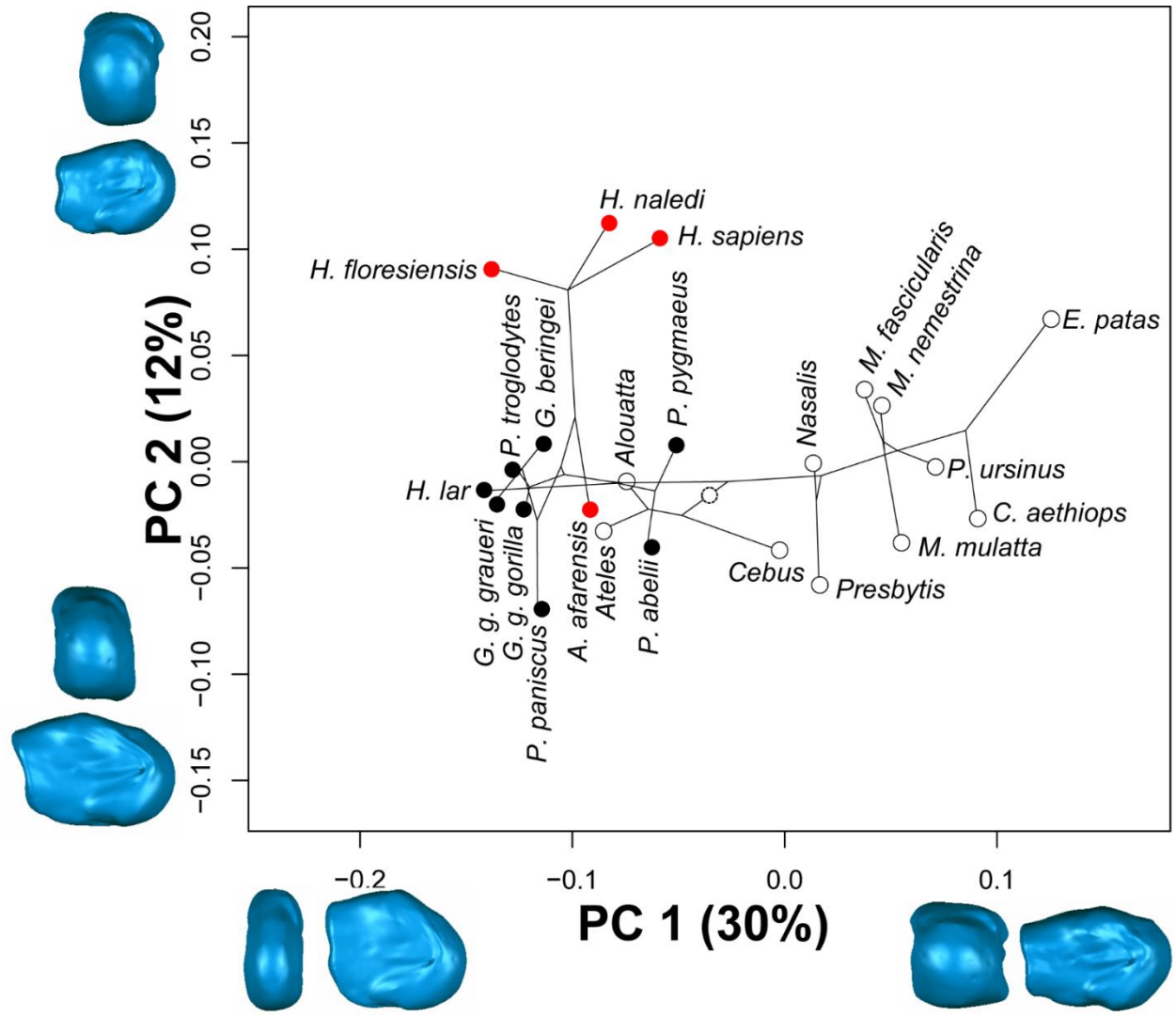

Figure 3.16: Phylomorphospace plot of the anthropoid molecular phylogeny superimposed upon a species-means bivariate PCA scatterplot of MT 4. Upon diverging towards their respective adaptive optima, cercopithecoids (open circles) experience relatively more evolutionary changes than apes (closed circles). Hominins (red circles) diverge greatly from apes on PC 2, but *Au. afarensis* retains the ape-like condition in MT 4. *Pongo* evolves a similar MT head shape to the more suspensory NWMs (e.g., *Alouatta, Ateles*). Within *Homo, H. naledi* is more similar to the modern condition than what is seen in LB 1.

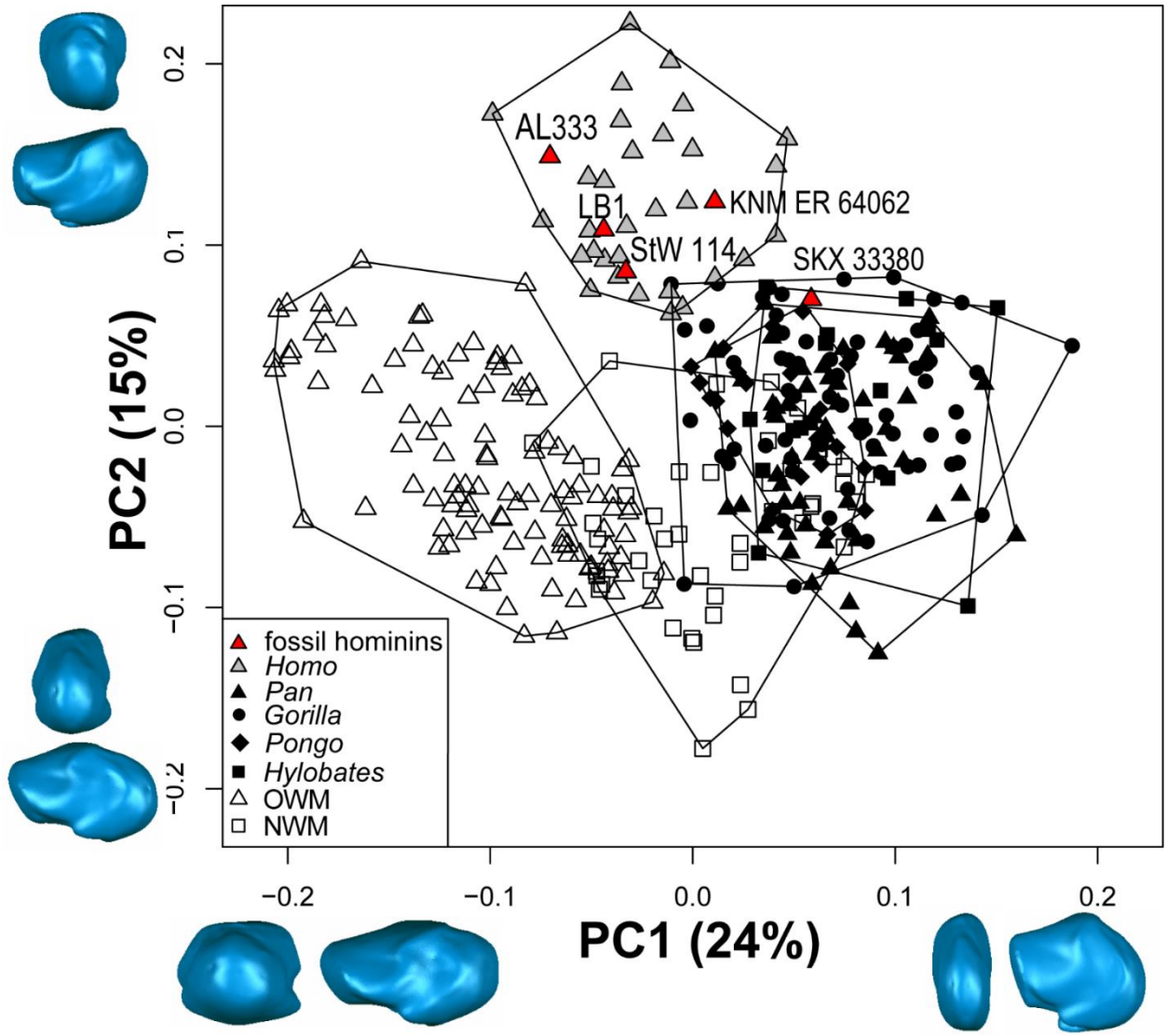

Figure 3.17: PCA scatterplot of PC 1 vs. PC 2 for MT 5. Note the general separation of monkeys (open rectangles), apes (filled shapes), and humans (gray triangles). Minimum convex polygons are constructed for these groups to illustrate their ranges in the morphospace. There is much overlap between all groups except humans. All hominins look similar to modern humans in MT 5, except for SKX 33380, a *Paranthropus* specimen, which is more similar to apes on PC 1, but overlaps apes and humans on PC 2. PC 1 tracked mediolateral head robusticity and PC 2 strongly tracked dorso-plantar orientation of the MT head. 3D surface morphs in lateral and distal views represent articular shape differences of observed extremes (PC 1: -0.20 - 0.20; PC 2: -0.18 - 0.20).

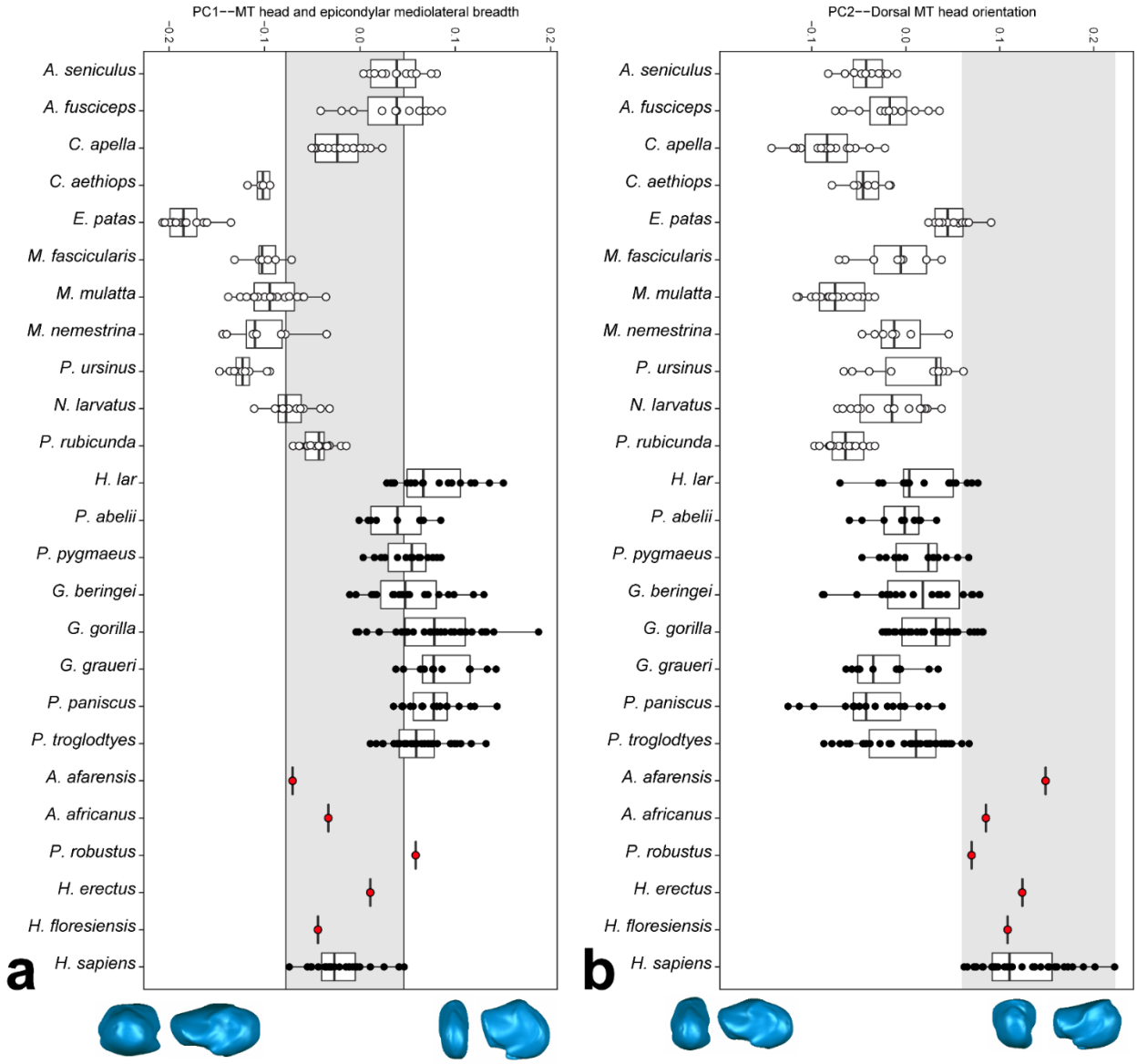

Figure 3.18: Cleveland box-and-whisker plots of PC 1 (a) and PC 2 (b) scores for the anthropoid MT 5. Generally, humans overlap with *Gorilla* and *Pongo* and hominins on PC 1 (MT head robusticity), and are unique on PC 2 (dorsal head orientation). Shaded bar: modern human range. 3D surface morphs in lateral and distal views represent articular shape differences of observed extremes (PC 1: -0.20 - 0.20; PC 2: -0.18 - 0.20). Vertical bars: median. Rectangles: interquartile range. Horizontal bars: range.

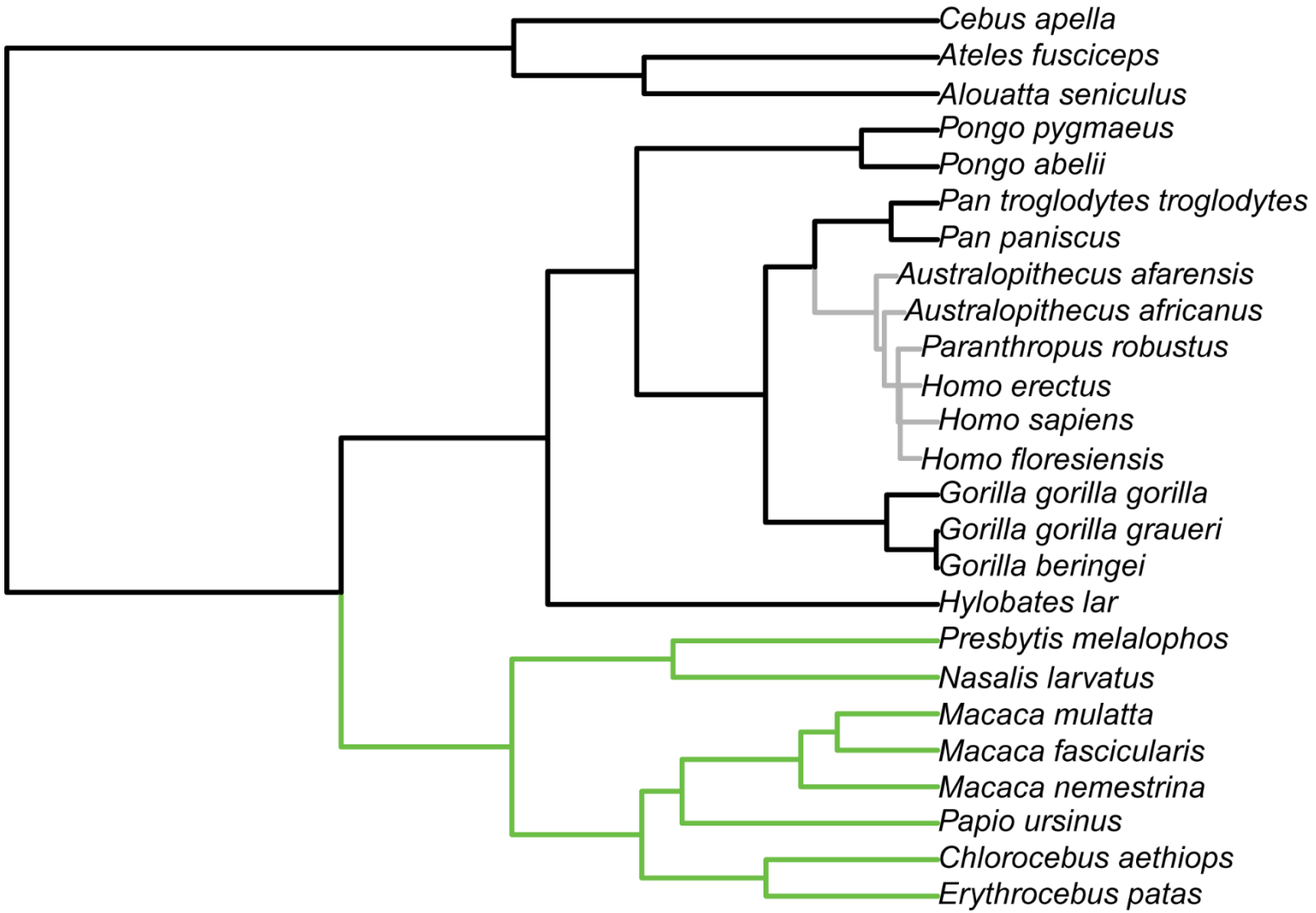

Figure 3.19: Time-calibrated phylogenetic tree with estimated adaptive regimes painted onto the tree branches for MT 5. Adaptive regimes are based on PC 1 (MT 5 head robusticity, plantar morphology) and PC 2 (MT 5 head orientation) scores. No evidence for convergence between anthropoid clades was found. The three regime shifts towards different adaptive optima includes apes, cebids, and australopithecines (black), cercopithecoids (green), and genus *Homo* (gray).

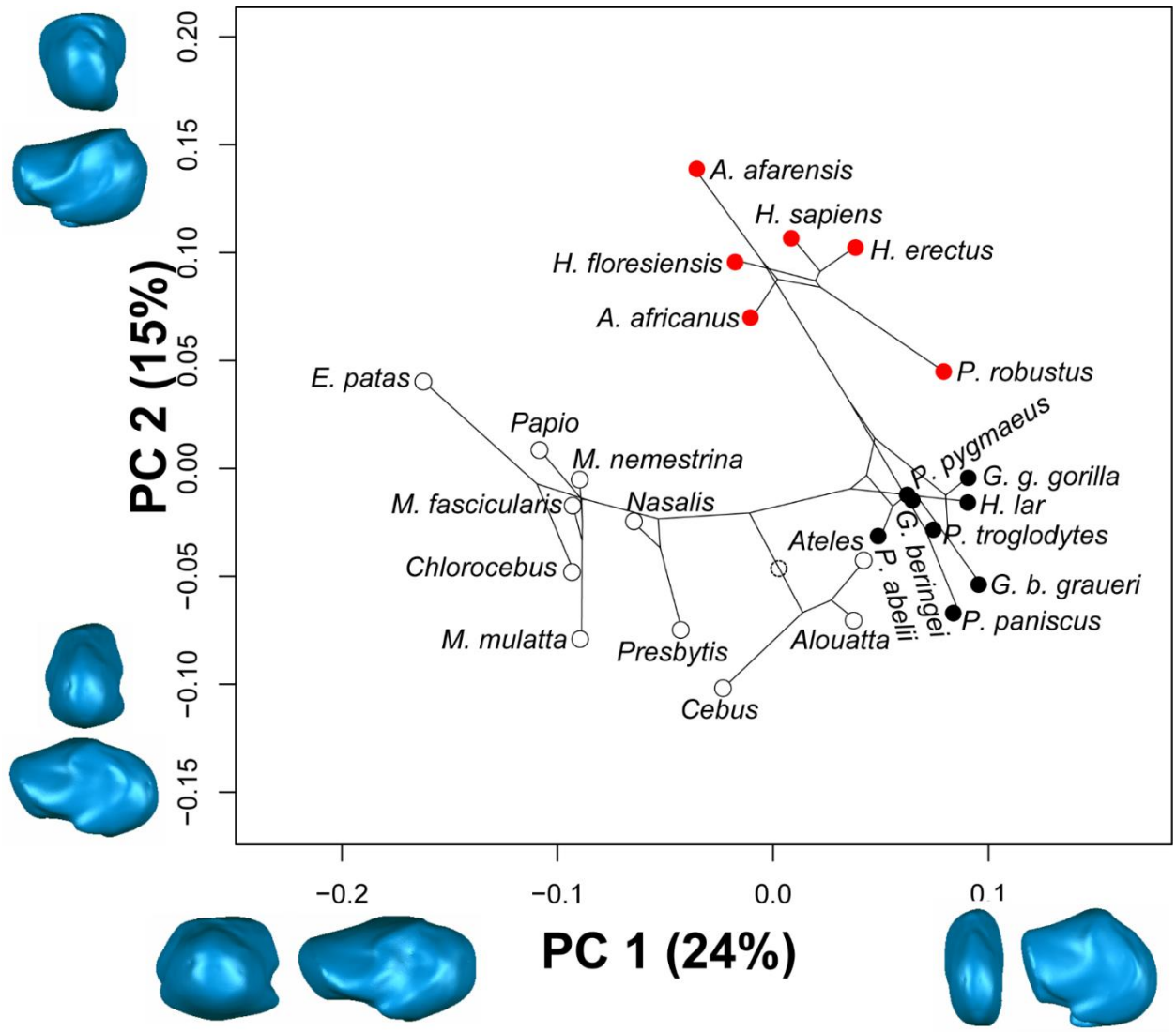

Figure 3.20: Phylomorphospace plot of the anthropoid molecular phylogeny superimposed upon a species-means bivariate PCA scatterplot of MT 5. Apes (black circles) undergo relatively little evolutionary change compared to monkeys (open circles) and hominins (red circles). The tree-like structure of the phylogeny is easily visualized in the MT 5 morphospace, suggesting strong phylogenetic signal in the shape data. Major evolutionary shape changes have occurred leading to the present hominin condition, in *Paranthropus*, *Cebus*, and *E. patas*.

Chapter 4

Shape Analysis of the Anthropoid Pedal Proximal Phalanges (PP 1, 3, 5)

4.1 Introduction

Morphological properties of the proximal phalanges (both pedal and manual) have long been thought to be reflective of substrate use in primates. Because of the frequent and repetitive contact with arboreal substrates, the anthropoid hand and foot must be able to resist bending strains incurred during both manual and pedal grasping and this is thought to be the mechanism which drives the increased phalangeal curvature (Preuschoft, 1970) seen in many extant and fossil hominoids. In addition to phalangeal curvature, different metrics capturing a variety of phalangeal morphological properties, including relative lengths, robusticities, and proportions have been used to infer the locomotor behavior of extinct hominins, hominoids, and primates more generally (Susman, 1979; Bush et al., 1982; Latimer et al., 1982; Stern and Susman, 1983; Latimer and Lovejoy, 1990a; Stern et al., 1995; Jungers et al., 1997; Alba et al., 2003; Almécija et al., 2007; Deane and Begun, 2008; Almécija et al., 2009; Patel, 2009; Alba et al., 2010; Almécija et al., 2015). In particular, the discovery of a largely intact *Australopithecus afarensis* forefoot in Hadar (A.L. 333-115; Latimer et al., 1982) has offered researchers opportunity to study metatarsal and phalangeal functional morphology in this Pliocene hominin. Some work has shown that the hominins represented at the 333 locality likely practiced both arboreal and terrestrial locomotion (Stern and Susman, 1983), but other workers have disagreed with this interpretation (Latimer and Lovejoy, 1990a; Ward, 2002). As part of their counterargument, Latimer and Lovejoy (1990a) remarked on the proximal phalangeal base orientation of the Hadar fossils, and how they, like human phalanges, possessed a pronounced dorsal slant (i.e., "dorsal canting"). This phalangeal property was not quantified until later (Duncan et al., 1994), and the results demonstrated some overlap between hominoids (e.g., *Gorilla*) and humans in terms of canting angle. The issue of dorsal phalangeal canting has since been revisited several times (Rein

and Harrison, 2007; Griffin and Richmond, 2010; Rein, 2011; Rein and McCarty, 2012) but has only been quantified using linear metrics that may not completely characterize complex joint surfaces (MacLatchy and Bossert, 1996). An additional confounding factor to the morphology of phalangeal canting is that although it is assumed that the dorsal orientation of the phalangeal base is predictive of human-like joint mechanics in the forefoot (i.e., high metatarsophalangeal joint [MTPJ] dorsiflexion angles at the end of stance phase), the phalangeal base orientation as measured in prior work (Duncan et al., 1994; Griffin and Richmond, 2010) is highly susceptible to phalangeal curvature. Indeed, dorsal canting as measured in previous work seems to be more an indirect measure of phalangeal curvature than of MTPJ orientation. If, for instance, the orangutan phalanx illustrated in Fig. 1c of Griffin and Richmond (2010: 117) was cut at midshaft and then laid on the substrate for measurement, their canting angular measurement (α) would undoubtedly increase. Therefore, it is unclear how this metric is much different than a measurement of phalangeal curvature, which is informative for inferring arboreal substrate use. However, as a proxy for human-like forefoot joint mechanics, a qualitative assessment (Latimer et al., 1982; Latimer and Lovejoy, 1990a) or measurement of angle of base orientation (Griffin and Richmond, 2010; Rein and McCarty, 2012) are both insufficient. With the expanding array of largely intact pedal material described in recent years since the fossil discoveries at Hadar (Jungers et al., 2009; Lovejoy et al., 2009; Haile-Selassie et al., 2012; Harcourt-Smith et al., 2015; Jungers et al., 2015), it is critical to use new methods for phalangeal base morphology quantification that are robust to other properties inherent to the element such as curvature. These methods would allow us to compare the joint surfaces of the phalangeal base with that of the corresponding metatarsal head, to get a better sense of what MTPJ mechanics can be inferred from hominin fossil material.

To that end, I present here a comprehensive 3-dimensional (3D) geometric morphometric (GM) shape analysis across select extant anthropoid and fossil hominin phalanges (PP 1, PP 3, PP 5). I hypothesize that morphological characters of the PP base (e.g., dorsal canting, PP base orientation) are functional. If dorsal phalangeal canting is important for MTPJ range of motion (ROM), then I predict that phalangeal base orientation will be one of the main shape changes captured by the eigenanalyses. Further, I predict that because humans dorsiflex their forefoot joints to significantly higher ROMs than extant apes (Griffin et al., 2010b; Holowka and Fernández, 2016), phalangeal canting should serve to significantly distinguish modern humans

from extant apes and other anthropoids. Some very terrestrial taxa (e.g., *E. patas*, *G. beringei*) are predicted to overlap with humans because they too habitually dorsiflex their forefoot joints on terrestrial substrates.

4.2 Materials and Methods

Phalangeal base morphology was quantified using a 7x7 3D surface patch with four user-defined landmarks (dorso-plantar height, medio-lateral breadth) and 45 semi-landmarks (Fig. 4.1). In addition to the automatically placed landmarks (Fig. 4.1; orange squares), the remaining boundary landmarks of the 7x7 surface patch (Fig. 4.1; blue squares) were also treated as sliding landmarks using the R package *Geomorph* version 3.0 (Adams and Otárola-Castillo, 2013; Adams et al., 2015). This semi-landmark patch density was used to increase the capture of subtle morphological differences in the phalangeal articular surfaces. Additionally, an error study was conducted to quantify measurement error using methodology described in previous work (Proctor, 2010b; Fernández et al., 2015). The error study was conducted on the hallucal phalanges and included ten randomly selected individuals from three genera (*Pan, Gorilla, Nasalis*). One of these ten phalanges, per genera, was repeatedly measured five times across five different days and the relative clustering of repeated measures versus non-repeated measures was assessed using a PCA scatterplot. The remaining methods are identical to those used in Chapter 2 and Chapter 3, with differences only in the sample as detailed below.

4.2.1 Extant Sample

I quantified shape differences in the proximal phalangeal base in 848 anthropoid PP 1, PP 3, and PP 5s. These phalanges were chosen as representative of the medial and lateral forefoot, and were the phalanges readily identifiable from disarticulated museum specimens (Table 4.1 – 4.3). The data were collected and processed from the same institutions and protocols listed in Chapter 2. As was the case for the metatarsal data, most of the cercopithecoid phalangeal data was already micro CT scanned by Dr. Biren Patel (see Chapter 2), who graciously provided me with this raw scan data for this dissertation. Likewise, Dr. Sergio Almécija provided some of the *Gorilla* and *Pan* phalanges used in these analyses. Identifying pedal proximal phalanges was not a trivial task like in the metatarsals, and I developed the following protocol for identifying pedal phalanges in museum collections or virtually in whole-foot micro CT scans: In cercopithecoids, PP 1 was the most robust, PP 3 was the longest, and PP 5 was the shortest. In most apes and

humans: PP 1 was the most robust, PP 3 was just smaller (e.g., shorter and more gracile) than PP 2, and PP 5 was the shortest. PP 3 and PP 5 elements were only selected when all of the pedal phalanges from the lesser toes were available for comparison. The PP 1 was obvious and readily identified even in partial specimens, and hence is the largest sample in this chapter. Pedal phalanges were distinguished from manual phalanges by their markedly more waisted appearance at the proximal end, with less developed digital flexor ridges than their manual phalangeal counterparts. This was especially obvious in apes, whose manual phalanges are far more robust than their pedal phalanges. In humans, the shaft of pedal phalanges is less mediolaterally compressed ("D" shaped) than their manual phalanges (White et al., 2011). Cercopithecoid manual and pedal phalanges are more similar, but in most cases it was still possible to identify the relatively more gracile pedal elements. In ambiguous cases, the PP 3 and PP 5s were not sampled. Siding pedal phalanges is difficult, and so to ensure that the proper side was used in the shape analyses, an additional reflection step was performed in addition to a standard generalized Procrustes analysis (GPA). GPA with reflection first reflects all configurations to one side (e.g., the right side this case) and then a standard Procrustes fit is performed on the landmark data afterwards. The resultant data is strictly "reflection shape" instead of shape (Dryden and Mardia, 1998) but the result is essentially the same as shape data (Klingenberg, 2011).

4.2.2 Fossil Sample

I analyzed 18 fossil phalangeal bases (Table 4.4; Figs. 4.2 – 4.4), mostly from fossil hominins described in Chapter 2 and Chapter 3; more specific information about the specimens analyzed is detailed as follows:

Ardipithecus kaddaba

A complete left proximal phalanx, AME-VP-1/71, was recovered by Leslia Hlusko in 1999 from the western margin of the Middle Awash sediments, most of which date to the late Miocene (5.2 – 5.8 Ma). The PP fossil dates to the younger end of that range ~ 5.2 Ma (Haile-Selassie, 2001) and displays mosaic morphology seen in both apes and hominins, including a high degree of phalangeal curvature, as well as a dorsally canted phalangeal base. The specimen was micro CT scanned by Dr. Gen Suwa and Dr. Tim White. These researchers and Dr. Haile-

Selassie graciously provided permission to use the *Ar. kadabba* PP scan for this dissertation. The specimen was analyzed with the PP 3 dataset.

Ardipithecus ramidus

Three fossils attributed to *Ardipithecus ramidus* were included in the phalangeal analyses. These specimens were recovered from Aramis, near the Daam Aatu Basaltic Tuff (~4.4 ma; White et al., 1994). ARA-VP-6/500-094 is a complete third or fourth proximal phalanx (listed as PP 4, Lovejoy et al., 2009) with high phalangeal curvature (included angle ~ 58°) and dorsal canting, similar to other fossil hominins. ARA-VP-6/500-008 was also included (listed as PP 3, Lovejoy et al., 2009). This fossil was not discussed in the main text of Lovejoy et al. (2009) but is included in one table in the supplementary material. It looks very similar to ARA-VP-6/500-094 but is broken around midshaft (Fig. 4.3, specimen d). Another phalanx was included, ARA-VP-6/500-1006, as a possible PP 5 based on its gracility and length compared to the other *Ar. ramidus* phalanges (Fig. 4.4), but is not described in Lovejoy et al. (2009) or listed in the supplemental material. The *Ardipithecus* phalangeal bases are both convexly deep with a pronounced dorsal rim, ellipsoid, and demonstrate well-developed plantar tubercles, which overall results in a mosaic of human-like and cercopithecoid-like features (see shape analysis results below). The *Ardipithecus* specimens was micro CT scanned by Dr. Gen Suwa and Dr. Tim White, who graciously provided the scans for this dissertation.

Australopithecus afarensis

Several fossil pedal phalanges from the A.L. 333 and A.L. 333w localities were included in the phalangeal analyses. First, A.L. 333-115F was included as the only hallucal phalanx from *Australopithecus* (Fig. 4.2). A.L. 333-115F is a partial left hallucal phalanx found with 17 other associated pedal remains in the Denan Dora member of the Hadar Formation (~3.0 Ma, Aronson et al., 1977), including a PP 3 (A.L. 333-115H) and PP 5 (A.L. 333-115J), which are both intact specimens (Figs. 4.3 – 4.4). Other probable PP 3s include A.L. 333-25 and A.L. 333w-51. Probable PP 5s included for analyses are A.L. 333w-26 and A.L. 333-71 (Fig. 4.4). All of these specimens were recovered from the Hadar Formation in the 1974 – 1977 field seasons (Latimer

et al., 1982). All of these specimens were laser scanned from high quality research casts except for A.L. 333-71, which was laser scanned from the original specimen at the National Ethiopian Museum, Addis Ababa, Ethiopia, by Drs. Caley Orr and Sergio Almécija.

Early *Homo*

In 2013, new fossil hominins were discovered from Kolom Odiet, near Ileret, West Turkana, Kenya (Jungers et al., 2015). Two partial skeletons were found, and one of these, KNM-ER 64062, preserves MT heads 1, 2, 3, 5, as well as the proximal hallucal phalanx. The MT heads were analyzed in Chapters 2 and 3. These elements were recovered just above the KBS Tuff, dated to 1.89 Ma. Here, the hallucal phalanx is included for analysis. The KNM-ER 64062 PP 1 base is human-like with a deep, concave and ovoid base (Fig. 4.2), but its overall robusticity is similar to other hominins, such as *H. floresiensis* (see below) but more gracile than modern humans.

Homo floresiensis

Pedal fossils from *Homo floresiensis* were first excavated from Liang Bua (LB1) in 2003, a limestone cave on the island of Flores, eastern Indonesia (Brown et al., 2004). Included in this analysis are proximal pedal phalanges described in Jungers et al. (2009); the probable PP 3s include LB1/36, LB1/38, and LB1/41 (Fig. 4.3). LB1/34 is included as a probable PP 5 (Fig. 4.4). In addition to these published pedal phalanges, two new hallucal phalanges were also included (See Dingwall et al., 2014 for an abstract). The first was found in Sector XVI, Spit 72 (hereafter: LB-XVI-72) and the second hallucal phalanx was found in Sector IV, Spit 42D (hereafter: LB-IV-42D). Both LB-XVI-72and LB-IV-42D are robust, short, and demonstrate little curvature (Fig. 4.2). The plantar tubercle is more developed on the left side in both specimens (Fig. 4.2). LB-XVI-72 is larger and more robust overall, but neither phalanx approaches the robusticity of a modern human phalanx. LB-IV-42D has an ovoid and very concave proximal articular surface, with a dorsally raised rim, similar to a modern human. LB-XVI-72 has a more ellipsoid and shallower proximal articular surface, and a present but more weakly expressed dorsal rim.

Homo naledi

Undated pedal fossils from a new hominin uncovered in the Rising Star cave system, Gauteng, South Africa (Berger et al., 2015) has yielded a largely complete right foot (Harcourt-Smith et al., 2015), and partial pedal remains of several other individuals. At least 40 proximal pedal phalanges have been recovered, 8 of which are hallucal phalanges (Harcourt-Smith et al., 2015). However, the only available specimen currently on MorphoSource is a right partial hallucal fragment that preserves the base, U.W. 101-1419. Qualitatively, U.W. 101-1419 looks very human-like—it is broadly ovoid, with a deep, convexly excavated base capped dorsally by a pronounced bony rim. In lateral view, the phalangeal base looks dorsally canted, but the overall robusticity of the phalanx is not like that seen in modern humans. The shaft is relatively gracile, and looks more similar to *H. floresiensis* or KNM-ER 64062 than to modern humans, which is unlike what was seen in its hallucal morphology. See Chapter 2 (Materials and Methods) for a more complete description of *H. naledi*.

4.3 Results

4.3.1 Error Study

Results from the repeatability experiment are shown graphically in Fig. 4.5. The relative grouping of the repeated specimens is evident in the *Pan*, *Gorilla*, and *Nasalis* morphospaces. In each instance, repeated measures formed a distinct cloud in the morphospace with relatively little variance. Overall, the results suggest that 3D landmark placement was very repeatable

4.3.2 Allometric regressions

Multivariate, phylogenetically corrected least-squares (PGLS) allometric regressions of size (logged centroid size) on shape (PCs and Procrustes coordinates) revealed that size was not a significant factor on PP base shape. These results suggest that shape differences observed in PP 1, PP 3, and PP 5 are being driven by phylogenetic and/or functional differences in the sample (see below).

4.3.3 PCA/MANOVA

Results from the PP shape analyses are similar to what was seen in both Chapter 2 and Chapter 3, with separations of ape, human, and monkey clusters. As in the metatarsal data, New World monkeys (NWMs) tended to overlap with the ape distributions, or occupy a position in the

tangent space intermediate between apes and Old World monkeys (OWMs). Humans often fell intermediate between monkeys and apes on one axis, and then discriminated from the rest of the sample on the other axis, a pattern also seen in the metatarsal data. Fossil hominins were generally found to look more ape-like, which is in contrast to the lesser metatarsal data (Chapter 3) but similar to what was seen in the hallux (Chapter 2). MANOVAs confirmed differences in PP 1, PP 3, and PP 5 shape variables among species and post-hoc tests further revealed significant differences among all of the groups in the sample. The results of these analyses are presented for each case in more detail below.

4.3.4 Comparative aspects of shape

In all cases, the first two principal components (PCs) explained the majority of the variance in the shape data (45 – 61 %), with PC 1 and PC 2 both tracking shape changes that have been theorized as functionally important for MTPJ function. In most cases, PC 1 tracked the depth (convexity) and ovoid form of the PP base, with low PC 1 scores demonstrating convexly deep and ovoid morphologies. Most great apes demonstrated this morphology. High PC 1 scores describe a very ellipsoid base with very large, pronounced plantar tubercles—a morphology typified by cercopithecoids. PC 2 also tracked ovoid versus ellipsoid configuration of the PP base along with information about phalangeal base joint orientation. High PC 2 scores had a strongly dorsal orientation to the PP base, and low PC 2 scores had PP bases whose orientation was more orthogonal to the substrate (i.e., not very dorsally canted). More detailed results regarding all eigenanalyses, MANOVA, and phylogenetic analyses are presented below for each proximal phalanx sampled.

4.3.5 PP 1

Extant anthropoids

In PP 1, PC 1 (25% variance explained) tracked the convexity and ovoid form of the phalangeal base, along with the presence of a pronounced rim at the dorsal perimeter of the bone, a morphology often seen in hominins (Latimer et al., 1982) and some hominoids (Duncan et al., 1994; Griffin and Richmond, 2010). Phalangeal bases with low PP 1 scores tended to be very convexly excavated (deep), more ovoid than ellipsoid in form, and had a robust dorsal rim present. High PC 1 scores were relatively flatter, more ellipsoid than ovoid in form, and lacked a

dorsal rim entirely. Additionally, those phalangeal bases with high PC 1 scores had markedly pronounced plantar tubercles.

Significant differences between species in hallucal phalangeal base shape variables are presented in Table 4.5 for PC 1 and Table 4.6 for PC 2. On PC 1, there is much overlap in the total range of variation between all great apes, and some overlap with *Homo*, which occupy low PC 1 values, and the monkey sample and *Hylobates*, which all have high PC 1 values (Fig. 4.6; 4.7a). Humans are on the far left of the PC 1 axis, overlapping only with *Gorilla*. *Post-hoc* tests with subspecies as a fixed factor on PC 1 revealed that within great apes, although there is much overlap in the total range of variation, there were still several significant differences between great ape taxa. Mountain gorillas (*G. beringei*) were significantly different from all groups including the closely related Grauer's gorilla (*G. b. graueri*), but did not differ from lowland gorillas ($p < 0.01$). Out of all non-human apes, mountain gorillas overlapped most extensively with modern humans, although humans were still significantly different from them ($p < 0.05$) as well the rest of the sample ($p < 0.0001$). Bonobos also separated from most other great apes, including chimpanzees ($p < 0.0001$), and tended to have somewhat higher, more monkey-like PC 1 values than other apes. Gibbons were very different from all other apes in PP 1 base morphology ($p < 0.0001$), and overlapped entirely with cercopithecoids on PC 1, except *Nasalis* ($p < 0.0001$). NWMs were not found to be significantly different from cercopithecoids on PC 1, but see the PC 2 results below. There was great overlap within the cercopithecoid sample, with no notable significant differences between groups.

In PP 1, PC 2 (20% variance explained) tracked ovoid versus ellipsoid configuration of the PP base along with information about phalangeal base joint orientation. High PC 2 scores had a strongly dorsal orientation to the PP base, and low PC 2 scores had PP bases whose orientation was more orthogonal to the substrate. *Post-hoc* tests revealed significant differences among and the groups studied (Fig 4.6; Fig 4.7b). PC 2 was essentially the discriminating axis of variation for NWMs. *Ateles* and *Alouatta*, and to a lesser extent *Cebus*, separated from most of the rest of the sample ($p < 0.05$) by having uniquely low PC 2 scores. The rest of the sample largely overlapped on this axis, and thus shape differences in PC 2 were generally less informative than PC 1 in the hallucal phalanx.

Fossil hominins

Results from the PP 1 base shape analysis reveal that in general, fossil hominin hallucal phalanges do not greatly resemble those of modern humans. The intact PP 1 from KNM-ER 64062 was the most human-like in its morphology, and did fall within the *Homo* minimum convex polygon. However, it did so while also overlapping with the *Gorilla* distribution, and gorillas have been known to demonstrate human-like phalangeal base morphology (Duncan et al., 1994; Griffin and Richmond, 2010). The new *H. floresiensis* fossils, LB-XVI-72 and LB-IV-42D, plotted very close to one another in the tangent space, squarely within the great ape distribution. Lastly, the *Au. afarensis* PP 1 specimen A.L. 333-115F also fell within the great ape distribution, but differed from the other fossil hominins by having a much lower PC 2 score. *Homo naledi*, despite looking very human-like qualitatively, fell just outside the human polygon on PC 1, and was found to be intermediate between *Homo* and *Gorilla*, similar to some of its ankle morphology and phalangeal curvature (Harcourt-Smith et al., 2015). On PC 2, *H. naledi* fell towards the maximum end of the human distribution, which also overlapped with *Pan* and *Gorilla*. Overall, only the hallucal phalanx from Ileret (KNM-ER 64062) resembled modern humans in hallucal base shape.

4.3.6 Phylogenetic comparative analyses

Permutation tests for phylogenetic signal did not reveal significant phylogenetic patterning in the anthropoid PP 1 shape data (p = ns; $K_{mult} \sim 0$). Results from the multi-regime OU modeling in *SURFACE* did not converge with the given PP 1 shape data, and returned nonsensical alpha values. These results suggest that the hallucal phalanx shape is likely driven more by functional than phylogenetic signals.

Phylomorphospace plots illustrated several broad patterns in the evolutionary shape change of the anthropoid PP 1 base (Fig. 4.8). Generally, apes and humans, cercopithecines, and NWMs/Colobines separated from each other in the phylomorphospace. The ancestral state reconstruction suggests that NWMs have not deviated much from the ancestral condition, whereas catarrhines have changed moreso on PC 2. On PC 1, all monkeys and lesser apes resemble the ancestral condition. Extant apes appear derived from the hominoid last common ancestor (LCA), but fossils hominoids are needed to calibrate this reconstruction. Branch lengths indicate that within apes, species of *Gorilla, Pan,* and *Hylobates* have undergone relatively large amounts of evolutionary shape change in the PP 1 base. Within hominins, the ancestral condition

appears to be ape-like with regards to phalangeal base morphology, with *H. floresiensis* retaining the ape and australopithecine-like PC 1 morphology, while east African early *Homo,* as well as modern humans diverge towards the left limit of the tangent space. Like what was seen in the MT 1 (see Chapter 2), the PP 1 shape data demonstrates that the modern human-like form did not appear until relatively late in human evolution.

4.3.7 PP 3

Extant anthropoids

In PP 3, PC 1 (53% variance explained) tracked the convexity and ovoid form of the phalangeal base, relative plantar tubercle size, as well as overall phalangeal base orientation. Like what was seen in PP 1, apes and humans overlap on this axis, with a very convexly deep, ovoid base that is often slanted dorsally—all of these morphologies are present in those specimens with low PC 1 scores. Phalanges with high PC 1 scores look entirely different (Fig. 4.9; Fig. 4.10a), with pronounced dorsal excavation of the phalangeal base. Pedal phalanges with high PC 1 scores have a base that recedes into the diaphysis without any pronounced boundary or dorsal rim, flanked on either side by large plantar tubercles that give the base a much more ellipsoid form compared to what is seen in humans and apes.

Post-hoc tests revealed significant differences among all the groups studied on PC 1 (Table 4.7; Fig 4.9; Fig 4.10b). All apes and monkeys do not overlap ($p < 0.0001$). Within apes, chimpanzees separated from all other apes ($p < 0.0001$) except for bonobos and gibbons. Unlike what was seen in the hallucal phalanx, gibbons do not appear monkey-like in their non-hallucal phalanges. Within monkeys, there was strong separation between Old World and New World groups, especially *Alouatta* and *Cebus*, who were significantly different from the Old World groups ($p < 0.0001$). *Cebus* was more intermediate and overlapped with many Old World taxa. This finding is similar to what was seen for *Cebus* in the lesser metatarsal data as well (see Chapter 3).

PC 2 (9% variance explained) was the discriminating axis that separated modern humans from the rest of the sample in PP 3. On this axis, shape changes were related to the expression of a pronounced dorsal ridge of bone on the dorsal perimeter of the proximal phalangeal articular surface. Those phalanges with high PC 2 scores did not express or weakly expressed this dorsal

rim of bone, even if the articular surface was canted dorsally. Low PC 2 scores strongly expressed this dorsal rim of bone, and this was essentially only seen in modern humans.

Post-hoc tests revealed significant differences among the groups studied on PC 2 (Table 4.8; Fig 4.9; Fig 4.10b). PC 2 was essentially the discriminating axis of variation for modern humans in the PP 3 data. Humans were significantly different from all other groups studied ($p < 0.01$) due to very low PC 2 scores. The rest of the sample largely overlapped on PC 2, with some minor exceptions (see Table 4.8). Within apes, mountain gorillas were significantly different from all other groups ($p < 0.05$) except for the other gorilla species.

Fossil hominins

Like the results in PP 1, the PP 3 fossil hominin shape data generally did not resemble the modern human condition (Fig. 4.9). Seven of the nine PP 3s studied in this dissertation fell directly within the chimpanzee minimum convex polygon on the morphospace. This includes phalanges from *Ar. kaddaba* (AME-VP-1/71), *Ar. ramidus* (ARA-VP-6/500-094, ARA-VP-6/500-008), *Au. afarensis* (A.L. 333-25, A.L. 333w-51), and *H. floresiensis* (LB1/38, LB1/41). All of these hominins plotted very closely to each other in the morphospace, within the variation of extant chimpanzees. Of these, however, two plotted just outside the range of modern humans, both specimens from Liang Bua (LB1/38, LB1/41). Both the *Ar. kadabba* and *Ar. ramidus* specimens fell deeper into the ape distribution, away from the human cloud, but the difference was subtle compared to some of the *Au. afarensis* specimens (see Fig. 4.9). Two exceptions that did look more human-like were A.L 333-115H (*Au. afarensis*) and LB1/36 (*H. floresiensis*). Note that multiple LB specimens were used in these analyses due to uncertainty of ray attribution in some of these elements (see Table 4.4). Neither the fossils of *Au. Afarensis* nor those of *H. floresiensis* looked exactly human-like, due to high PC 1 scores. The PC 2 scores for these two fossil specimens however are like those of modern humans, and likewise different from the rest of the sample. Overall, hominin PP 3 base morphology is mosaic, but still quite primitive.

4.3.8 Phylogenetic comparative analyses

Permutation tests for phylogenetic signal did reveal significant phylogenetic patterning in the anthropoid PP 3 shape data ($p = 0.0001$; $K_{mult} \sim 0.51$). Unlike the PP 1 results, results from the multi-regime OU modeling in *SURFACE* using PP 3 shape data did converge and provided

evidence for two non-convergent regime shifts towards different adaptive optima (Fig. 4.11). Non convergent regimes included a separate regime for monkeys (Fig. 4.11, black bars), and an ape/hominin regime (Fig. 4.11, grey bars).

Phylomorphospace plots illustrated several broad patterns in the evolutionary shape change of the anthropoid PP 1 base (Fig. 4.12). Generally, apes and humans, cercopithecines, and NWMs separated from each other in the phylomorphospace. The ancestral state reconstruction suggests that NWMs have not deviated much from the ancestral condition, whereas catarrhines have changed more so on PC 2. On PC 1, all monkeys and lesser apes resemble the ancestral condition. Extant apes appear derived from the hominoid last common ancestor (LCA), but fossils from stem hominoids are needed to calibrate this reconstruction. Branch lengths indicate that within apes, species of *Gorilla*, *Pan*, and *Hylobates* have undergone relatively large amounts of evolutionary shape change in the PP 1 base. Within hominins, the ancestral condition appears to be ape-like with regards to phalangeal base morphology, with *H. floresiensis* retaining the ape and australopithecine-like PC 1 morphology, while east African early *Homo*, as well as modern humans diverge towards the left limit of the tangent space. Similar to what was seen in the MT 1 (see Chapter 2), the PP 1 shape data demonstrates that the modern human-like form did not appear until relatively late in human evolution.

4.3.9 PP 5

Extant anthropoids

The shape changes captured by PC 1 (50% variance explained) and PC 2 (7% variance explained) in PP 5 are essentially identical (Figs. 4.13, 4.14a) to those discussed in the PP 3 data (see above). *Post-hoc* tests revealed significant differences among and the groups studied on PC 1 (Fig 4.13; Fig 4.14a) and PC 2 (Fig 4.3; Fig 4.14b). The PP 5 morphospace looks very similar to those of the lesser metatarsals (see Chapter 3), with distinct ape, monkey, and human clouds. PC 2 is again a discriminating axis for modern humans as in PP 3, but additionally, human PP 5 bases reside in a very constrained PC 1 range, which for the most part is intermediate between apes ($p < 0.0001$) and cercopithecoids ($p < 0.01$) with little overlap (Fig. 4.14a). Humans do however overlap with NWMs on PC 1. Within apes and monkeys, there is much overlap on PC 1 with very few significant differences (see Table 4.9). On PC 2, humans were found to be

significantly different from all other groups ($p < 0.01$), however the rest of the sample largely overlapped on PC 2, with very few exceptions (Table 4.10).

Fossil hominins

Generally, fossil hominins looked more human-like in PP 5 morphology than in either PP 3 or PP 1 (Fig. 4.13). Most specimens (e.g., A.L. 333-71, A.L. 333w-26, A.L. 333-115J, LB1/34) fell within the modern human minimum convex polygon, except for ARA-VP-6/500-1006, the *Ardipithecus* PP 5, which fell squarely within the cercopithecoid distribution. A.L. 333-115J fell on the cusp of the human distribution, and overlapped with *Pan* as well.

4.3.10 Phylogenetic comparative analyses

Permutation tests for phylogenetic signal did reveal significant phylogenetic patterning in the anthropoid PP 5 shape data ($p = 0.0001$; $K_{mult} \sim 0.55$). Results from the multi-regime OU modeling in *SURFACE* did not converge with the given PP 5 shape data, and returned nonsensical alpha values. The suspected lack of convergence seen in the PP 5 data is probably due to wide overlap between many groups in PC scores, and the relatively sparse sampling for the PP 5 compared to the other rays.

Phylomorphospace plots revealed several broad patterns in the evolutionary shape change of the anthropoid PP 5 base (Fig. 4.15). Generally, apes, hominins, cercopithecines, and NWMs separated from each other in the phylomorphospace. Additionally, all of the gorilla species and subspecies separated from the other apes, in a part of the morphospace intermediate between the remaining apes and hominins. The ancestral state reconstruction suggests that the LCA between chimpanzees and humans had a more monkey-like PP 5 base, and this is informed by the inclusion of the *Ardipithecus* PP 5. The results also suggest that the morphology in extant apes is quite derived, with much evolutionary shape change taking place between the hominoid LCA and extant African apes and humans. Monkeys, by comparison, have undergone relatively less evolutionary shape change than hominoids in the PP 5 base.

4.4 Discussion

Overall, I found mixed support for my hypotheses and predictions. Unlike in the metatarsal data, the majority of the shape variation in the phalangeal base shape data was well

captured on just the first two principal components, often with more than half of the variance explained with these two components. Although shape analyses did capture some functional signals in the phalangeal base, including the dorsal orientation of the base (i.e., dorsal canting), it was often not the discriminating factor between humans and other apes. Instead, the morphology most indicative of a human-like phalangeal base appeared to be a pronounced dorsal rim of bone buttressing the perimeter of a deeply convex base. This morphology is noted in the description of the Hadar material by Latimer et al. (1982), but here it has been quantified in a reliable manner. Interestingly, there is no single character of the phalangeal base that is entirely 'human-like', but a combination of several characters that yield an overall modern-human looking shape. While humans and apes often demonstrate varying degrees of dorsal canting, humans also have the pronounced, dorsally buttressed rim that has been hypothesized to limit extreme dorsiflexion during terrestrial bipedalism (Latimer and Lovejoy, 1990a). Regardless of whether or not this hypothesized function is accurate, this feature does seem to better characterize a human-like phalangeal base than dorsal canting. Thus, this metric may be more useful than the dorsal canting angle, especially in fragmentary fossil specimens.

Although the results of these analyses are similar to those of previous researchers (Duncan et al., 1994; Griffin and Richmond, 2010) in that some overlap between *Homo* and *Gorilla* was observed, results of these shape analyses are still informative because they demonstrate the particular shape changes that lead to this overlap. These taxa overlap not just because of phalangeal base orientation, but because some of these gorilla specimens present a pronounced dorsal rim, which was found to be a very human-like morphology. This was found only in the highly terrestrial mountain gorilla (*G. beringei*)—the taxon that overlapped most with humans in overall phalangeal shape, particularly in the hallucal proximal phalanx. This finding lends support to previous work on the ecological divergence of gorilla species (Tocheri et al., 2011; Dunn et al., 2014; Knigge et al., 2015; Tocheri et al., 2016), and may be indicative of increased terrestriality in mountain gorillas compared to western lowland and Grauer's gorillas.

One unexpected finding in the data is the shape of the gibbon hallucal proximal phalanx. The gibbon PP 1 greatly resembles cercopithecoids, but its lesser phalanges do not. I suspect that because gibbons have such forelimb dominated locomotion and only use hind limb propulsion for short distances (Fleagle, 1978; Gittins, 1983; Sati and Alfred, 2002), that the gibbon pedal

morphology, at least in the phalanges, has probably not changed much since the stem ape condition. Data from *Ekembo* sp. (McNulty et al., 2015) are needed to test this suspicion, and this will be pursued in future work. That said, it is known that *Ekembo* does resemble extant monkeys in some aspects of phalangeal morphology (Begun et al., 1994; Deane and Begun, 2008).

The multivariate shape data on the anthropoid phalangeal base describe more completely this half of the MTPJs than previous quantification attempts. However, the functional signals that can be drawn from the phalangeal base data alone are still ambiguous. Although there is clear separation of a human-like morphotype, especially in the more lateral digits, it is not clear how much of this separation is due to function versus phylogeny. Quantitative shape results did show however that apes and humans largely overlap in their canting morphology, and it is the expression of the dorsal bony rim (Latimer et al., 1982) that better distinguishes humans and some hominins from other anthropoids. Therefore, I conclude that dorsal canting alone is not informative of human-like midfoot stiffening and forefoot joint mechanics, contrary to what the general view of dorsal canting is currently (Latimer and Lovejoy, 1990a; Duncan et al., 1994; Griffin and Richmond, 2010; Rein and McCarty, 2012). The comparative sample and fossil data suggest that not just the orientation of the phalangeal base but several shape changes in the phalangeal base in addition to its orientation all contribute to a modern human-like morphology. This suite of features significantly distinguished humans from all other anthropoids sampled, but most hominins did not fully resemble a modern human phalangeal base shape. This finding weakens the "baggage" arguments and lends support to the hypothesis that arboreality played a major role in the positional behavior of early hominins. It is possible that in the forefoot, it is the metatarsal heads that bear the majority of the weight during locomotion, and that phalangeal morphology is more reflective of pedal grasping. If this was the case, then it would explain why the lesser MTs of hominins look more human-like, while their corresponding pedal proximal phalanges appear more ape-like. In any case, human-like phalangeal base shapes are not seen in the fossil record until early *Homo,* and even within genus *Homo* there is inconsistency (i.e., *H. floresiensis*). The consequences of this mixed forefoot shape pattern, and how it influences MTPJ morphology as a whole, was explored in the subsequent chapter (5).

4.5 References

Adams, D.C., Collyer, M.L., Otárola-Castillo, E., Sherratt, E., 2015. Geomorph: software for geometric morphometric analyses. R package version 2.1.2.

Adams, D.C., Otárola-Castillo, E., 2013. Geomorph: an R package for the collection and analysis of geometric morphometric shape data. Meth. Ecol. Evol. 4, 393-399.

Alba, D.M., Almécija, S., Moyà-Solà, S., 2010. Locomotor inferences *in Pierolapithecus* and *Hispanopithecus:* Reply to. J. Hum. Evol. 59, 143-149.

Alba, D.M., Moyà-Solà, S., Köhler, M., 2003. Morphological affinities of the *Australopithecus afarensis* hand on the basis of manual proportions and relative thumb length. J. Hum. Evol. 44, 225-254.

Almécija, S., Alba, D.M., Moyà-Solà, S., 2009. Pierolapithecus and the functional morphology of Miocene ape hand phalanges: paleobiological and evolutionary implications. J. Hum. Evol. 57, 284-297.

Almécija, S., Alba, D.M., Moyà-Solà, S., Köhler, M., 2007. Orang-like manual adaptations in the fossil hominoid *Hispanopithecus laietanus*: first steps towards great ape suspensory behaviours. Proc. Royal Soc. B. 274, 2375-2384.

Almécija, S., Smaers, J.B., Jungers, W.L., 2015. The evolution of human and ape hand proportions. Nat. Commun. 6.

Begun, D.R., Teaford, M.F., Walker, A., 1994. Comparative and functional anatomy of Proconsul phalanges from the Kaswanga Primate Site, Rusinga Island, Kenya. J. Hum. Evol. 26, 89-165.

Berillon, G., 1999. Geometric pattern of the hominoid hallucal tarsometatarsal complex. Quantifying the degree of hallux abduction in early hominids. C. R. Acad. Sci. Paris Séria IIa 328, 627-633.

Bojsen-Møller, F., 1979. Calcaneocuboid joint and stability of the longitudinal arch of the foot at high and low gear push off. J. Anat. 129, 165-176.

Brown, P., Sutikna, T., Morwood, M.J., Soejono, R.P., Jatmiko, Wayhu Saptomo, E., Awe Due, R., 2004. A new small-bodied hominin from the Late Pleistocene of Flores, Indonesia. Nature 431, 1055-1061.

Bush, M.E., Lovejoy, C.O., Johanson, D.C., Coppens, Y., 1982. Hominid carpal, metacarpal, and phalangeal bones recovered from the Hadar formation: 1974–1977 collections. Am. J. Phys. Anthropol. 57, 651-677.

Deane, A.S., Begun, D.R., 2008. Broken fingers: retesting locomotor hypotheses for fossil hominoids using fragmentary proximal phalanges and high-resolution polynomial curve fitting (HR-PCF). J. Hum. Evol. 55, 691-701.

Dingwall, H.L., Tocheri, M.W., Awe, R.D., Sutikna, T., Saptomo, E.W., Jatmiko, Wasisto, S., Jungers, W.L., 2014. Comparative morphology of the proximal hallucal phalanges of *Homo floresiensis*, Am. J. Phys. Anthropol., 106.

Dryden, I.L., Mardia, K.V., 1998. Statistical shape analysis. J. Wiley Chichester.

Duncan, A.S., Kappelman, J., Shapiro, L.J., 1994. Metatarsophalangeal joint function and positional behavior in *Australopithecus afarensis*. Am. J. Phys. Anthropol. 93, 67-81.

Dunn, R.H., Tocheri, M.W., Orr, C.M., Jungers, W.L., 2014. Ecological divergence and talar morphology in gorillas. Am. J. Phys. Anthropol. 153, 526-541.

Fernández, P.J., Almécija, S., Patel, B.A., Orr, C.M., Tocheri, M.W., Jungers, W.L., 2015. Functional aspects of metatarsal head shape in humans, apes, and Old World monkeys. J. Hum. Evol. 86, 136-146.

Fleagle, J.G., 1978. Locomotion, posture and habitat utilization of two sympatric Malaysian leaf-monkeys (*Presbytis obscura* and *Presbytis melalophos)*, in: Montgomery, G. (Ed.), Ecology of arboreal folivores. Smithsonian Press, Washington, D.C., pp. 243-251.

Gittins, S.P., 1983. Use of the forest canopy by the agile gibbon. Folia Primatol. 40, 134-144.

Griffin, N.L., D'Août, K., Richmond, B., Gordon, A., Aerts, P., 2010. Comparative in vivo forefoot kinematics of *Homo sapiens* and *Pan paniscus*. J. Hum. Evol. 59, 608-619.

Griffin, N.L., Richmond, B.G., 2010. Joint orientation and function in great ape and human proximal pedal phalanges. Am. J. Phys. Anthropol. 141, 116-123.

Haile-Selassie, Y., 2001. Late Miocene hominids from the Middle Awash, Ethiopia. Nature 412, 178-181.

Haile-Selassie, Y., Saylor, B.Z., Deino, A., Levin, N.E., Alene, M., Latimer, B.M., 2012. A new hominin foot from Ethiopia shows multiple Pliocene bipedal adaptations. Nature 483, 565-569.

Harcourt-Smith, W.E.H., Throckmorton, Z., Congdon, K.A., Zipfel, B., Deane, A.S., Drapeau, M.S.M., Churchill, S.E., Berger, L.R., DeSilva, J.M., 2015. The foot of *Homo naledi*. Nat. Commun. 6.

Hicks, J.H., 1954. The mechanics of the foot: II. the plantar aponeurosis and the arch. J. Anat. 88, 25-30.21.

Holowka, N.B., Fernández, P.J., 2016. Functional morphology of the metatarsophalangeal joints in chimpanzees and humans: a kinematic and morphometric approach. Am. J. Phys. Anthropol. 159, 176.

Indjeian, Vahan B., Kingman, Garrett A., Jones, Felicity C., Guenther, Catherine A., Grimwood, J., Schmutz, J., Myers, Richard M., Kingsley, David M., 2016. Evolving new skeletal traits by cis-regulatory changes in bone morphogenetic proteins. Cell 164, 45-56.

Jungers, W.L., Godfrey, L.R., Simons, E.L., Chatrath, P.S., 1997. Phalangeal curvature and positional behavior in extinct sloth lemurs (Primates, Palaeopropithecidae). Proc. Nat. Acad. Sci. 94, 11998-12001.

Jungers, W.L., Grine, F.E., Leakey, M.G., Leakey, L., Brown, F., Yang, D., Tocheri, M.W., 2015. New hominin fossils from Ileret (Kolom Odiet), Kenya. Am. J. Phys. Anthropol. 156, 181.

Jungers, W.L., Harcourt-Smith, W.E.H., Wunderlich, R.E., Tocheri, M.W., Larson, S.G., Sutikna, T., Due, R.A., Morwood, M.J., 2009. The foot of *Homo floresiensis*. Nature 459, 81-84.

Knigge, R.P., Tocheri, M.W., Orr, C.M., McNulty, K.P., 2015. Three-dimensional geometric morphometric analysis of talar morphology in extant gorilla taxa from highland and lowland habitats. Anat. Rec. 298, 277-290.

Latimer, B., Lovejoy, C.O., 1990a. Metatarsophalangeal joints of *Australopithecus afarensis*. Am. J. Phys. Anthropol. 83, 13-23.

Latimer, B.M., Lovejoy, C.O., 1990b. Hallucal tarsometatarsal joint in *Australopithecus afarensis*. Am. J. Phys. Anthropol. 82, 125-133.

Latimer, B.M., Lovejoy, C.O., Johanson, D.C., Coppens, Y., 1982. Hominid tarsal, metatarsal, and phalangeal bones recovered from the Hadar formation: 1974–1977 collections. Am. J. Phys. Anthropol. 57, 701-719.

Lovejoy, C.O., Latimer, B., Suwa, G., Asfaw, B., White, T.D., 2009. Combining prehension and propulsion: the foot of *Ardipithecus ramidus*. Science 326, 72, 72e71-72e78.

MacLatchy, L.M., Bossert, W.H., 1996. An analysis of the articular surface distribution of the femoral head and acetabulum in anthropoids, with implications for hip function in Miocene hominoids. J. Hum. Evol. 31, 425-453.

McNulty, K.P., Begun, D.R., Kelley, J., Manthi, F.K., Mbua, E.N., 2015. A systematic revision of Proconsul with the description of a new genus of early Miocene hominoid. J. Hum. Evol. 84, 42-61.

Patel, B.A., 2009. Not so fast: speed effects on forelimb kinematics in cercopithecine monkeys and implications for digitigrade postures in primates. Am. J. Phys. Anthropol. 140, 92-112.

Preuschoft, H., 1970. Functional anatomy of the lower extremity, in: Bourne, G.H. (Ed.), The chimpanzee, vol. 3. Karger, Basel, pp. 221-294.

Proctor, D.J., 2010. Three-dimensional morphometrics of the proximal metatarsal articular surfaces of *Gorilla, Pan, Hylobates*, and shod and unshod humans. University of Iowa.

Proctor, D.J., Broadfield, D., Proctor, K., 2008. Quantitative three-dimensional shape analysis of the proximal hallucial metatarsal articular surface in *Homo, Pan, Gorilla,* and *Hylobates*. Am. J. Phys. Anthropol. 135, 216-224.

Rein, T., Harrison, T., 2007. Quantifying the angle of orientation of the metatarsophalangeal joint surface of proximal phalanges in extant primates, Am. J. Phys. Anthropol. pp. 197-197.

Rein, T.R., 2011. The correspondence between proximal phalanx morphology and locomotion: implications for inferring the locomotor behavior of fossil catarrhines. Am. J. Phys. Anthropol. 146, 435-445.

Rein, T.R., McCarty, L.A., 2012. Metacarpophalangeal joint orientation in anthropoid manual phalanges. The Anatomical Record: Advances in Integrative Anatomy and Evolutionary Biology 295, 2057-2068.

Sati, J., Alfred, J., 2002. Locomotion and posture in Hoolock gibbon. Ann. For 10, 298-306.

Stern, J.T., 2000. Climbing to the top: a personal memoir of *Australopithecus afarensis*. Evol. Anthropol. 9, 111-148.

Stern, J.T., Jungers, W.L., Susman, R.L., 1995. Quantifying phalangeal curvature: An empirical comparison of alternative methods. Am. J. Phys. Anthropol. 97, 1-10.

Stern, J.T., Susman, R.L., 1983. The locomotor anatomy of *Australopithecus afarensis*. Am. J. Phys. Anthropol. 60, 279-317.

Susman, R.L., 1979. Comparative and functional morphology of hominoid fingers. Am. J. Phys. Anthropol. 50, 215-236.

Tocheri, M.W., Dommain, R., McFarlin, S.C., Burnett, S.E., Troy Case, D., Orr, C.M., Roach, N.T., Villmoare, B., Eriksen, A.B., Kalthoff, D.C., Senck, S., Assefa, Z., Groves, C.P., Jungers, W.L., 2016. The evolutionary origin and population history of the grauer gorilla. Am. J. Phys. Anthropol. 159, 4-18.

Tocheri, M.W., Solhan, C.R., Orr, C.M., Femiani, J., Frohlich, B., Groves, C.P., Harcourt-Smith, W.E., Richmond, B.G., Shoelson, B., Jungers, W.L., 2011. Ecological divergence and medial cuneiform morphology in gorillas. J. Hum. Evol. 60, 171-184.

Tuttle, R.H., 1981. Evolution of hominid bipedalism and prehensile capabilities. Philos. T. Roy. Soc. B. 292, 89-94.

Ward, C.V., 2002. Interpreting the posture and locomotion of *Australopithecus afarensis*: where do we stand? Am. J. Phys. Anthropol. 119, 185-215.

White, T.D., Black, M.T., Folkens, P.A., 2011. Human osteology. Academic press.

White, T.D., Suwa, G., Asfaw, B., 1994. *Australopithecus ramidus*, a new species of early hominid from Aramis, Ethiopia Nature 371, 306-312.

Taxon	**Locomotor Mode[1]**	**Foot Posture[2]**	**µCT**	**CT**	**Laser Scan**
Hominoids					
Homo sapiens	B	FCP	-	15	12
Gorilla beringei beringei	KW/C	IHSP	-	3	15
Gorilla beringei graueri	KW/C	IHSP	-	3	12
Gorilla gorilla gorilla	KW/C	IHSP	-	4	22
Pan paniscus	KW/C	IHSP	-	1	13
Pan troglodytes	KW/C	IHSP	-	7	35
Pongo abelii	S	IHSP	-	-	7
Pongo pygmaeus	S	IHSP	-	-	10
Hylobates lar	R	MFP	20	-	-
Cercopithecoids					
Chlorocebus aethiops	TQ	DG/SP	12	-	-
Erythrocebus patas	TQ	DG	17	-	-
Macaca fascicularis	TQ	DG/SP	11	-	-
Macaca mulatta	TQ	DG/SP	16	-	-
Macaca nemestrina	TQ	DG/SP	8	-	-
Papio ursinus	TQ	DG/SP	15	-	-
Nasalis larvatus	AQ	DG/SP	24	-	-
Presbytis rubicunda	AQ	DG/SP	-	-	15
Ceboids (NWMs)					
Alouatta seniculus	AQ	DG/SP	17	-	-
Ateles fusciceps	AQ/S	DG/SP	12	-	-
Cebus apella	AQ	DG/SP	5	-	-

Table 4.1. **Extant anthropoids included in PP 1 shape analyses**. See Table 2.1 for abbreviation key.

Taxon	**Locomotor Mode[1]**	**Foot Posture[2]**	**µCT**	**CT**	**Laser Scan**
Hominoids					
Homo sapiens	B	FCP	-	19	10
Gorilla beringei beringei	KW/C	IHSP	-	3	5
Gorilla beringei graueri	KW/C	IHSP	-	3	11
Gorilla gorilla gorilla	KW/C	IHSP	-	4	22
Pan paniscus	KW/C	IHSP	-	1	10
Pan troglodytes	KW/C	IHSP	-	7	28
Pongo abelii	S	IHSP	-	-	8
Pongo pygmaeus	S	IHSP	-	-	13
Hylobates lar	R	MFP	11	-	-
Cercopithecoids					
Chlorocebus aethiops	TQ	DG/SP	11	-	-
Erythrocebus patas	TQ	DG	17	-	-
Macaca fascicularis	TQ	DG/SP	11	-	-
Macaca mulatta	TQ	DG/SP	16	-	-
Macaca nemestrina	TQ	DG/SP	7	-	-
Papio ursinus	TQ	DG/SP	-	-	-
Nasalis larvatus	AQ	DG/SP	12	-	-
Presbytis rubicunda	AQ	DG/SP	-	-	19
Ceboids (NWMs)					
Alouatta seniculus	AQ	DG/SP	17	-	-
Ateles fusciceps	AQ/S	DG/SP	6	-	-
Cebus apella	AQ	DG/SP	5	-	-

Table 4.2. **Extant anthropoids included in PP 3 shape analyses**. See Table 2.1 for abbreviation key.

Taxon	**Locomotor Mode[1]**	**Foot Posture[2]**	**µCT**	**CT**	**Laser Scan**
Hominoids					
Homo sapiens	B	FCP	-	12	7
Gorilla beringei beringei	KW/C	IHSP	-		7
Gorilla beringei graueri	KW/C	IHSP	-	3	11
Gorilla gorilla gorilla	KW/C	IHSP	-	4	26
Pan paniscus	KW/C	IHSP	-	1	11
Pan troglodytes	KW/C	IHSP	-	7	28
Pongo abelii	S	IHSP	-	-	9
Pongo pygmaeus	S	IHSP	-	-	10
Cercopithecoids					
Chlorocebus aethiops	TQ	DG/SP	7	-	-
Erythrocebus patas	TQ	DG	16	-	-
Macaca fascicularis	TQ	DG/SP	7	-	-
Nasalis larvatus	AQ	DG/SP	3	-	-
Presbytis rubicunda	AQ	DG/SP	-	-	15
Ceboids (NWMs)					
Alouatta seniculus	AQ	DG/SP	4	-	-
Cebus apella	AQ	DG/SP	2	-	-

Table 4.3. **Extant anthropoids included in PP 5 shape analyses**. See Table 2.1 for abbreviation key.

Accession Number	Age (Ma)	Element	Taxon	Locality	Observation
AME-VP-1/71	5.2	PP 2 – 4*	*Ardipithecus kaddaba*	Middle Awash, Ethiopia	Original (μCT)
ARA-VP-6/500-008	4.4	PP 3	*Ardipithecus ramidus*	Aramis, Ethiopia	Original (μCT)
ARA-VP-6/500-094	4.4	PP 4	*Ardipithecus ramidus*	Aramis, Ethiopia	Original (μCT)
ARA-VP-6/500-1006	4.4	PP 5*	*Ardipithecus ramidus*	Aramis, Ethiopia	Original (μCT)
A.L. 333-25, w51	3.2 – 3.0	PP 2 – 4*	*Australopithecus afarensis*	Hadar, Ethiopia	Cast (LS)
A.L. 333-115 F, H, J	3.2 – 3.0	PP 1, 3, 5	*Australopithecus afarensis*	Hadar, Ethiopia	Cast (LS)
A.L. 333-71, w26	3.2 – 3.0	PP 5	*Australopithecus afarensis*	Hadar, Ethiopia	Original (LS)
KNM-ER 64062	1.88	PP 1	*Homo* sp. (cf. *erectus*)	Above KBS tuff, Ileret	Original (μCT)
LB-XVI-72, IV-42D	0.1 – 0.06	PP 1	*Homo floresiensis*	Liang Bua, Indonesia	Original (CT)
LB1/36, 38, 41,	0.1 – 0.06	PP 2 – 4*	*Homo floresiensis*	Liang Bua, Indonesia	Original (CT)
LB1/34	0.1 – 0.06	PP 5	*Homo floresiensis*	Liang Bua, Indonesia	Original (CT)
U.W. 101-1419	Undated	PP 1	*Homo naledi*	Gauteng, South Africa	Original (LS)

Table 4.4. **Fossil hominins included in the PP 1, 3, 5 shape analyses**. Please see text (Materials and Methods) for geological age estimates and taxonomic determinations. *Fragmentary or isolated pedal element that is unable to be attributed to a specific ray with certainty (Latimer et al., 1982). AME-VP-1/71 is listed as a PP 4 by Halie-Selassie (2001). See Materials and Methods for more information.

Species	*A. seniculus*	*A. fusciceps*	*C. apella*	*C. aethiops*	*E. patas*	*M. mulatta*	*M. nemestrina*	*M. fascicularis*	*P. ursinus*	*N. larvatus*	*P. rubicunda*
A. seniculus	1.0000	-	-	-	-	-	-	-	-	-	-
A. fusciceps	ns	1.0000	-	-	-	-	-	-	-	-	-
C. apella	ns	ns	1.0000	-	-	-	-	-	-	-	-
C. aethiops	ns	ns	ns	1.0000	-	-	-	-	-	-	-
E. patas	ns	ns	ns	ns	1.0000	-	-	-	-	-	-
M. mulatta	ns	ns	ns	ns	ns	1.0000	-	-	-	-	-
M. nemestr.	ns	ns	ns	ns	ns	ns	1.0000	-	-	-	-
M. fascicul.	**<0.01**	ns	ns	ns	ns	ns	ns	1.0000	-	-	-
P. ursinus	ns	ns	ns	ns	ns	ns	ns	**<0.05**	1.0000	-	-
N. larvatus	ns	ns	ns	ns	ns	ns	ns	**<0.0001**	ns	1.0000	-
P. rubicunda	ns	ns	ns	ns	ns	ns	ns	ns	ns	ns	1.0000
H. lar	**<0.05**	ns	ns	ns	ns	ns	ns	ns	ns	**<0.0001**	ns
P. abelii	**<0.0001**	**<0.0001**	**<0.0001**	**<0.0001**	**<0.0001**	**<0.0001**	**<0.0001**	**<0.0001**	**<0.0001**	**<0.0001**	**<0.0001**
P. pygmaeus	**<0.0001**	**<0.0001**	**<0.0001**	**<0.0001**	**<0.0001**	**<0.0001**	**<0.0001**	**<0.0001**	**<0.0001**	**<0.0001**	**<0.0001**
G. beringei	**<0.0001**	**<0.0001**	**<0.0001**	**<0.0001**	**<0.0001**	**<0.0001**	**<0.0001**	**<0.0001**	**<0.0001**	**<0.0001**	**<0.0001**
G.g. gorilla	**<0.0001**	**<0.0001**	**<0.0001**	**<0.0001**	**<0.0001**	**<0.0001**	**<0.0001**	**<0.0001**	**<0.0001**	**<0.0001**	**<0.0001**
G.g. graueri	**<0.0001**	**<0.0001**	**<0.0001**	**<0.0001**	**<0.0001**	**<0.0001**	**<0.0001**	**<0.0001**	**<0.0001**	**<0.0001**	**<0.0001**
P. paniscus	**<0.0001**	**<0.0001**	**<0.0001**	**<0.0001**	**<0.0001**	**<0.0001**	**<0.0001**	**<0.0001**	**<0.0001**	**<0.0001**	**<0.0001**
P. trogl.	**<0.0001**	**<0.0001**	**<0.0001**	**<0.0001**	**<0.0001**	**<0.0001**	**<0.0001**	**<0.0001**	**<0.0001**	**<0.0001**	**<0.0001**
H. sapiens	**<0.0001**	**<0.0001**	**<0.0001**	**<0.0001**	**<0.0001**	**<0.0001**	**<0.0001**	**<0.0001**	**<0.0001**	**<0.0001**	**<0.0001**

(Continued on next page)

Table 4.5: *Post-hoc* Tukey's HSD results on PC 1 comparing anthropoid genera following a MANOVA on PP 1 shape variables (PC 1 - 5). PC 1 principally tracked phalangeal base convexity, ovoid form, and the expression of a dorsal rim of bone at the perimeter of the proximal articular surface. Humans are unique amongst anthropoids on PC 1. Bold = significance at $\alpha = 0.05$.

Species	*H. lar*	*P. abelii*	*P. pygmaeus*	*G. beringei*	*G.g. gorilla*	*G.g. graueri*	*P. paniscus*	*P. troglodytes*	*H. sapiens*
A. seniculus	-	-	-	-	-	-	-	-	-
A. fusciceps	-	-	-	-	-	-	-	-	-
C. apella	-	-	-	-	-	-	-	-	-
C. aethiops	-	-	-	-	-	-	-	-	-
E. patas	-	-	-	-	-	-	-	-	-
M. mulatta	-	-	-	-	-	-	-	-	-
M. nemestrina	-	-	-	-	-	-	-	-	-
M. fascicularis	-	-	-	-	-	-	-	-	-
P. ursinus	-	-	-	-	-	-	-	-	-
N. larvatus	-	-	-	-	-	-	-	-	-
P. rubicunda	-	-	-	-	-	-	-	-	-
H. lar	1.0000	-	-	-	-	-	-	-	-
P. abelii	**<0.0001**	1.0000	-	-	-	-	-	-	-
P. pygmaeus	**<0.0001**	ns	1.0000	-	-	-	-	-	-
G. beringei	**<0.0001**	**<0.05**	**<0.01**	1.0000	-	-	-	-	-
G.g. gorilla	**<0.0001**	ns	ns	ns	1.0000	-	-	-	-
G.g. graueri	**<0.0001**	ns	ns	**<0.01**	ns	1.0000	-	-	-
P. paniscus	**<0.0001**	ns	**<0.05**	**<0.0001**	**<0.0001**	**<0.0001**	1.0000	-	-
P. troglodytes	**<0.0001**	ns	ns	**<0.0001**	ns	ns	**<0.0001**	1.0000	-
H. sapiens	**<0.0001**	**<0.0001**	**<0.0001**	**<0.05**	**<0.0001**	**<0.0001**	**<0.0001**	**<0.0001**	1.0000

Table 4.5: *Post-hoc* Tukey's HSD results on PC 1 comparing anthropoid genera following a MANOVA on PP 1 shape variables (PC 1 - 5). PC 1 principally tracked phalangeal base convexity, ovoid form, and the expression of a dorsal rim of bone at the perimeter of the proximal articular surface. Humans are unique amongst anthropoids on PC 1. Bold = significance at $\alpha = 0.05$.

Species	*A. seniculus*	*A. fusciceps*	*C. apella*	*C. aethiops*	*E. patas*	*M. mulatta*	*M. nemestrina*	*M. fascicularis*	*P. ursinus*	*N. larvatus*	*P. rubicunda*
A. seniculus	1.0000	-	-	-	-	-	-	-	-	-	-
A. fusciceps	ns	1.0000	-	-	-	-	-	-	-	-	-
C. apella	ns	ns	1.0000	-	-	-	-	-	-	-	-
C. aethiops	ns	**<0.01**	ns	1.0000	-	-	-	-	-	-	-
E. patas	**<0.0001**	**<0.0001**	ns	ns	1.0000	-	-	-	-	-	-
M. mulatta	**<0.0001**	**<0.0001**	**<0.05**	ns	ns	1.0000	-	-	-	-	-
M. nemestr.	**<0.0001**	**<0.0001**	**<0.01**	ns	ns	ns	1.0000	-	-	-	-
M. fascicul.	**<0.01**	**<0.0001**	ns	ns	ns	ns	ns	1.0000	-	-	-
P. ursinus	**<0.0001**	**<0.0001**	**<0.01**	**<0.01**	ns	ns	ns	ns	1.0000	-	-
N. larvatus	**<0.0001**	**<0.0001**	ns	ns	ns	ns	ns	ns	ns	1.0000	-
P. rubicunda	**<0.0001**	**<0.0001**	**<0.0001**	**<0.0001**	**<0.01**	ns	ns	ns	ns	**<0.05**	1.0000
H. lar	**<0.0001**	**<0.0001**	**<0.01**	ns	ns	ns	ns	ns	ns	ns	ns
P. abelii	ns	**<0.01**	ns	ns	ns	ns	ns	ns	ns	ns	**<0.01**
P. pygmaeus	**<0.0001**	**<0.0001**	ns	ns	ns	ns	ns	ns	ns	ns	ns
G. beringei	**<0.01**	**<0.0001**	ns	ns	ns	ns	ns	ns	**<0.05**	ns	**<0.0001**
G.g. gorilla	**<0.0001**	**<0.0001**	ns	ns	ns	ns	ns	ns	ns	ns	**<0.01**
G.g. graueri	**<0.0001**	**<0.0001**	**<0.05**	ns	ns	ns	ns	ns	ns	ns	ns
P. paniscus	**<0.0001**	**<0.0001**	**<0.01**	ns	ns	ns	ns	ns	ns	ns	ns
P. troglod.	**<0.05**	**<0.0001**	ns	ns	ns	ns	**<0.05**	ns	**<0.0001**	ns	**<0.0001**
H. sapiens	**<0.0001**	**<0.0001**	ns	ns	ns	ns	ns	ns	ns	ns	**<0.05**

(Continued on next page)

Table 4.6: *Post-hoc* Tukey's HSD results on PC 2 comparing anthropoid genera following a MANOVA on PP 1 shape variables (PC 1 - 5). PC 2 principally tracked the dorsal orientation of the phalangeal base. NWMs and presbytis separate from most groups. Bold = significance at $\alpha = 0.05$.

Species	*H. lar*	*P. abelii*	*P. pygmaeus*	*G. beringei*	*G.g. gorilla*	*G.g. graueri*	*P. paniscus*	*P. troglodytes*	*H. sapiens*
A. seniculus	-	-	-	-	-	-	-	-	-
A. fusciceps	-	-	-	-	-	-	-	-	-
C. apella	-	-	-	-	-	-	-	-	-
C. aethiops	-	-	-	-	-	-	-	-	-
E. patas	-	-	-	-	-	-	-	-	-
M. mulatta	-	-	-	-	-	-	-	-	-
M. nemestrina	-	-	-	-	-	-	-	-	-
M. fascicular.	-	-	-	-	-	-	-	-	-
P. ursinus	-	-	-	-	-	-	-	-	-
N. larvatus	-	-	-	-	-	-	-	-	-
P. rubicunda	-	-	-	-	-	-	-	-	-
H. lar	1.0000	-	-	-	-	-	-	-	-
P. abelii	ns	1.0000	-	-	-	-	-	-	-
P. pygmaeus	ns	ns	1.0000	-	-	-	-	-	-
G. beringei	ns	ns	ns	1.0000	-	-	-	-	-
G.g. gorilla	ns	ns	ns	ns	1.0000	-	-	-	-
G.g. graueri	ns	ns	ns	ns	ns	1.0000	-	-	-
P. paniscus	ns	ns	ns	ns	ns	ns	1.0000	-	-
P. troglodytes	**<0.01**	ns	ns	ns	ns	**<0.05**	**<0.01**	1.0000	-
H. sapiens	ns	ns	ns	ns	ns	ns	ns	ns	1.0000

Table 4.6: *Post-hoc* Tukey's HSD results on PC 2 comparing anthropoid genera following a MANOVA on PP 1 shape variables (PC 1 - 5). PC 2 principally tracked the dorsal orientation of the phalangeal base. NWMs and presbytis separate from most groups. Bold = significance at $\alpha = 0.05$.

Species	*A. seniculus*	*A. fusciceps*	*C. apella*	*C. aethiops*	*E. patas*	*M. mulatta*	*M. nemestrina*	*M. fascicularis*	*N. larvatus*	*P. rubicunda*
A. seniculus	1.0000	-	-	-	-	-	-	-	-	-
A. fusciceps	ns	1.0000	-	-	-	-	-	-	-	-
C. apella	**<0.01**	**<0.01**	1.0000	-	-	-	-	-	-	-
C. aethiops	**<0.0001**	**<0.0001**	ns	1.0000	-	-	-	-	-	-
E. patas	**<0.0001**	**<0.0001**	ns	ns	1.0000	-	-	-	-	-
M. mulatta	**<0.0001**	**<0.0001**	ns	ns	ns	1.0000	-	-	-	-
M. nemestrina	**<0.0001**	**<0.01**	ns	ns	ns	ns	1.0000	-	-	-
M. fascicularis	**<0.0001**	**<0.0001**	ns	ns	ns	ns	ns	1.0000	-	-
N. larvatus	**<0.01**	ns	ns	**<0.0001**	ns	ns	ns	ns	1.0000	-
P. rubicunda	**<0.0001**	**<0.0001**	ns	ns	ns	ns	ns	ns	**<0.01**	1.0000
H. lar	**<0.0001**	**<0.01**	**<0.0001**	**<0.0001**	**<0.0001**	**<0.0001**	**<0.0001**	**<0.0001**	**<0.0001**	**<0.0001**
P. abelii	**<0.0001**	**<0.0001**	**<0.0001**	**<0.0001**	**<0.0001**	**<0.0001**	**<0.0001**	**<0.0001**	**<0.0001**	**<0.0001**
P. pygmaeus	**<0.0001**	**<0.0001**	**<0.0001**	**<0.0001**	**<0.0001**	**<0.0001**	**<0.0001**	**<0.0001**	**<0.0001**	**<0.0001**
G. beringei	**<0.0001**	**<0.0001**	**<0.0001**	**<0.0001**	**<0.0001**	**<0.0001**	**<0.0001**	**<0.0001**	**<0.0001**	**<0.0001**
G.g. gorilla	**<0.0001**	**<0.0001**	**<0.0001**	**<0.0001**	**<0.0001**	**<0.0001**	**<0.0001**	**<0.0001**	**<0.0001**	**<0.0001**
G.g. graueri	**<0.0001**	**<0.0001**	**<0.0001**	**<0.0001**	**<0.0001**	**<0.0001**	**<0.0001**	**<0.0001**	**<0.0001**	**<0.0001**
P. paniscus	**<0.0001**	**<0.0001**	**<0.0001**	**<0.0001**	**<0.0001**	**<0.0001**	**<0.0001**	**<0.0001**	**<0.0001**	**<0.0001**
P. troglodytes	**<0.0001**	**<0.0001**	**<0.0001**	**<0.0001**	**<0.0001**	**<0.0001**	**<0.0001**	**<0.0001**	**<0.0001**	**<0.0001**
H. sapiens	**<0.0001**	**<0.0001**	**<0.0001**	**<0.0001**	**<0.0001**	**<0.0001**	**<0.0001**	**<0.0001**	**<0.0001**	**<0.0001**

(Continued on next page)

Table 4.7: *Post-hoc* Tukey's HSD results on PC 1 comparing anthropoid genera following a MANOVA on PP 3 shape variables (PC 1 - 5). PC 1 principally tracked phalangeal base convexity, phalangeal base ovoid form, and plantar tubercle morphology. Apes and monkeys are completely different from each other on this axis. Bold = significance at $\alpha = 0.05$.

Species	*H. lar*	*P. abelii*	*P. pygmaeus*	*G. beringei*	*G.g. gorilla*	*G.g. graueri*	*P. paniscus*	*P. troglodytes*	*H. sapiens*
A. seniculus	-	-	-	-	-	-	-	-	-
A. fusciceps	-	-	-	-	-	-	-	-	-
C. apella	-	-	-	-	-	-	-	-	-
C. aethiops	-	-	-	-	-	-	-	-	-
E. patas	-	-	-	-	-	-	-	-	-
M. mulatta	-	-	-	-	-	-	-	-	-
M. nemestrina	-	-	-	-	-	-	-	-	-
M. fascicul.	-	-	-	-	-	-	-	-	-
P. ursinus	-	-	-	-	-	-	-	-	-
N. larvatus	-	-	-	-	-	-	-	-	-
P. rubicunda	-	-	-	-	-	-	-	-	-
H. lar	1.0000	-	-	-	-	-	-	-	-
P. abelii	**<0.01**	1.0000	-	-	-	-	-	-	-
P. pygmaeus	ns	ns	1.0000	-	-	-	-	-	-
G. beringei	**<0.0001**	ns	ns	1.0000	-	-	-	-	-
G.g. gorilla	ns	ns	ns	ns	1.0000	-	-	-	-
G.g. graueri	**<0.0001**	ns	ns	ns	ns	1.0000	-	-	-
P. paniscus	ns	ns	ns	ns	ns	ns	1.0000	-	-
P. troglodytes	ns	**<0.0001**	**<0.0001**	**<0.0001**	**<0.0001**	**<0.0001**	ns	1.0000	-
H. sapiens	ns	ns	ns	**<0.05**	ns	**<0.05**	ns	**<0.0001**	1.0000

Table 4.7: *Post-hoc* Tukey's HSD results on PC 1 comparing anthropoid genera following a MANOVA on PP 3 shape variables (PC 1 - 5). PC 1 principally tracked phalangeal base convexity, phalangeal base ovoid form, and plantar tubercle morphology. Apes and monkeys are completely different from each other on this axis. Bold = significance at $\alpha = 0.05$.

Species	*A. seniculus*	*A. fusciceps*	*C. apella*	*C. aethiops*	*E. patas*	*M. mulatta*	*M. nemestrina*	*M. fascicularis*	*N. larvatus*	*P. rubicunda*
A. seniculus	1.0000	-	-	-	-	-	-	-	-	-
A. fusciceps	**<0.0001**	1.0000	-	-	-	-	-	-	-	-
C. apella	ns	ns	1.0000	-	-	-	-	-	-	-
C. aethiops	ns	**<0.0001**	ns	1.0000	-	-	-	-	-	-
E. patas	ns	**<0.0001**	ns	ns	1.0000	-	-	-	-	-
M. mulatta	**<0.05**	ns	ns	ns	**<0.01**	1.0000	-	-	-	-
M. nemestrina	ns	ns	ns	ns	**<0.05**	ns	1.0000	-	-	-
M. fascicularis	ns	ns	ns	ns	ns	ns	ns	1.0000	-	-
N. larvatus	ns	**<0.01**	ns	ns	ns	ns	ns	ns	1.0000	-
P. rubicunda	ns	**<0.0001**	ns	ns	ns	**<0.0001**	**<0.0001**	**<0.01**	ns	1.0000
H. lar	**<0.01**	ns	ns	**<0.01**	**<0.0001**	ns	ns	ns	ns	**<0.0001**
P. abelii	ns	**<0.05**	ns	ns	ns	ns	ns	ns	ns	ns
P. pygmaeus	ns	**<0.0001**	ns	ns	ns	ns	ns	ns	ns	ns
G. beringei	**<0.0001**	ns	ns	**<0.01**	**<0.0001**	ns	ns	ns	**<0.05**	**<0.0001**
G.g. gorilla	**<0.05**	ns	ns	ns	**<0.01**	ns	ns	ns	ns	**<0.0001**
G.g. graueri	ns	ns	ns	ns	**<0.01**	ns	ns	ns	ns	**<0.0001**
P. paniscus	ns	**<0.0001**	ns	ns	ns	**<0.0001**	**<0.01**	**<0.05**	ns	ns
P. troglodytes	ns	**<0.0001**	ns	ns	ns	ns	ns	ns	ns	**<0.05**
H. sapiens	**<0.0001**	**<0.0001**	**<0.0001**	**<0.0001**	**<0.0001**	**<0.0001**	**<0.0001**	**<0.0001**	**<0.0001**	**<0.0001**

(Continued on next page)

Table 4.8: *Post-hoc* Tukey's HSD results on PC 2 comparing anthropoid genera following a MANOVA on PP 3 shape variables (PC 1 - 5). PC 2 principally tracked the expression of a dorsal rim of bone at the perimeter of the proximal articular surface. Humans are unique amongst anthropoids on PC 1. Bold = significance at $\alpha = 0.05$.

Species	*H. lar*	*P. abelii*	*P. pygmaeus*	*G. beringei*	*G.g. gorilla*	*G.g. graueri*	*P. paniscus*	*P. troglodytes*	*H. sapiens*
A. seniculus	-	-	-	-	-	-	-	-	-
A. fusciceps	-	-	-	-	-	-	-	-	-
C. apella	-	-	-	-	-	-	-	-	-
C. aethiops	-	-	-	-	-	-	-	-	-
E. patas	-	-	-	-	-	-	-	-	-
M. mulatta	-	-	-	-	-	-	-	-	-
M. nemestrina	-	-	-	-	-	-	-	-	-
M. fascicularis	-	-	-	-	-	-	-	-	-
P. ursinus	-	-	-	-	-	-	-	-	-
N. larvatus	-	-	-	-	-	-	-	-	-
P. rubicunda	-	-	-	-	-	-	-	-	-
H. lar	1.0000	-	-	-	-	-	-	-	-
P. abelii	ns	1.0000	-	-	-	-	-	-	-
P. pygmaeus	**<0.01**	ns	1.0000	-	-	-	-	-	-
G. beringei	ns	**<0.05**	**<0.0001**	1.0000	-	-	-	-	-
G.g. gorilla	ns	ns	ns	ns	1.0000	-	-	-	-
G.g. graueri	ns	ns	ns	ns	ns	1.0000	-	-	-
P. paniscus	**<0.0001**	ns	ns	**<0.0001**	**<0.0001**	**<0.01**	1.0000	-	-
P. troglodytes	**<0.01**	ns	ns	**<0.0001**	**<0.05**	ns	ns	1.0000	-
H. sapiens	**<0.0001**	**<0.0001**	**<0.0001**	**<0.0001**	**<0.0001**	**<0.0001**	**<0.01**	**<0.0001**	1.0000

Table 4.8: *Post-hoc* Tukey's HSD results on PC 2 comparing anthropoid genera following a MANOVA on PP 3 shape variables (PC 1 - 5). PC 2 principally tracked the expression of a dorsal rim of bone at the perimeter of the proximal articular surface. Humans are unique amongst anthropoids on PC 1. Bold = significance at $\alpha = 0.05$.

Species	*A. seniculus*	*C. apella*	*C. aethiops*	*E. patas*	*M. fascicularis*	*N. larvatus*	*P. rubicunda*
A. seniculus	1.0000	-	-	-	-	-	-
C. apella	ns	1.0000	-	-	-	-	-
C. aethiops	**<0.0001**	ns	1.0000	-	-	-	-
E. patas	**<0.0001**	ns	ns	1.0000	-	-	-
M. fascicularis	**<0.0001**	**<0.05**	ns	ns	1.0000	-	-
N. larvatus	**<0.05**	ns	ns	ns	ns	1.0000	-
P. rubicunda	**<0.0001**	**<0.05**	ns	ns	ns	ns	1.0000
P. abelii	**<0.05**	**<0.0001**	**<0.0001**	**<0.0001**	**<0.0001**	**<0.0001**	**<0.0001**
P. pygmaeus	**<0.01**	**<0.0001**	**<0.0001**	**<0.0001**	**<0.0001**	**<0.0001**	**<0.0001**
G. beringei	**<0.0001**	**<0.0001**	**<0.0001**	**<0.0001**	**<0.0001**	**<0.0001**	**<0.0001**
G.g. gorilla	**<0.0001**	**<0.0001**	**<0.0001**	**<0.0001**	**<0.0001**	**<0.0001**	**<0.0001**
G.g. graueri	**<0.0001**	**<0.0001**	**<0.0001**	**<0.0001**	**<0.0001**	**<0.0001**	**<0.0001**
P. paniscus	ns	**<0.05**	**<0.0001**	**<0.0001**	**<0.0001**	**<0.0001**	**<0.0001**
P. troglodytes	**<0.0001**	**<0.0001**	**<0.0001**	**<0.0001**	**<0.0001**	**<0.0001**	**<0.0001**
H. sapiens	ns	ns	**<0.0001**	**<0.0001**	**<0.0001**	**<0.01**	**<0.0001**

(Continued on next page)

Table 4.9: *Post-hoc* Tukey's HSD results on PC 1 comparing anthropoid genera following a MANOVA on PP 5 shape variables (PC 1 - 5). PC 1 principally tracked phalangeal base convexity, phalangeal base ovoid form, and plantar tubercle morphology. Apes and monkeys are completely different from each other on this axis. Bold = significance at $\alpha = 0.05$.

Species	*P. abelii*	*P. pygmaeus*	*G. beringei*	*G.g. gorilla*	*G.g. graueri*	*P. paniscus*	*P. troglodytes*	*H. sapiens*
A. seniculus	-	-	-	-	-	-	-	-
C. apella	-	-	-	-	-	-	-	-
C. aethiops	-	-	-	-	-	-	-	-
E. patas	-	-	-	-	-	-	-	-
N. larvatus	-	-	-	-	-	-	-	-
P. rubicunda	-	-	-	-	-	-	-	-
P. abelii	1.0000	-	-	-	-	-	-	-
P. pygmaeus	ns	1.0000	-	-	-	-	-	-
G. beringei	ns	ns	1.0000	-	-	-	-	-
G.g. gorilla	ns	ns	ns	1.0000	-	-	-	-
G.g. graueri	ns	ns	ns	ns	1.0000	-	-	-
P. paniscus	ns	ns	**<0.01**	**<0.01**	**<0.05**	1.0000	-	-
P. troglodytes	ns	ns	ns	ns	ns	**<0.01**	1.0000	-
H. sapiens	**<0.0001**	**<0.0001**	**<0.0001**	**<0.0001**	**<0.0001**	**<0.0001**	**<0.0001**	1.0000

Table 4.9: *Post-hoc* Tukey's HSD results on PC 1 comparing anthropoid genera following a MANOVA on PP 5 shape variables (PC 1 - 5). PC 1 principally tracked phalangeal base convexity, phalangeal base ovoid form, and plantar tubercle morphology. Apes and monkeys are completely different from each other on this axis. Bold = significance at $\alpha = 0.05$.

Species	*A. seniculus*	*C. apella*	*C. aethiops*	*E. patas*	*M. fascicularis*	*N. larvatus*	*P. rubicunda*
A. seniculus	1.0000	-	-	-	-	-	-
C. apella	ns	1.0000	-	-	-	-	-
C. aethiops	ns	ns	1.0000	-	-	-	-
E. patas	ns	ns	ns	1.0000	-	-	-
M. fascicularis	ns	ns	ns	**<0.05**	1.0000	-	-
N. larvatus	ns	ns	ns	ns	ns	1.0000	-
P. rubicunda	ns	ns	ns	ns	ns	ns	1.0000
P. abelii	ns	ns	ns	ns	ns	ns	ns
P. pygmaeus	ns	ns	ns	ns	ns	ns	ns
G. beringei	ns	ns	ns	ns	ns	ns	ns
G.g. gorilla	**<0.01**	ns	ns	ns	ns	ns	ns
G.g. graueri	ns	ns	ns	ns	ns	ns	ns
P. paniscus	ns	ns	ns	**<0.01**	ns	ns	ns
P. troglodytes	ns	ns	ns	**<0.05**	ns	ns	ns
H. sapiens	**<0.0001**	**<0.01**	**<0.0001**	**<0.0001**	**<0.0001**	**<0.01**	**<0.0001**

(Continued on next page)

Table 4.10: *Post-hoc* Tukey's HSD results on PC 2 comparing anthropoid genera following a MANOVA on PP 5 shape variables (PC 1 - 5). PC 2 principally tracked the expression of a dorsal rim of bone at the perimeter of the proximal articular surface. Humans are unique amongst anthropoids on PC 1. Bold = significance at $\alpha = 0.05$.

Species	*P. abelii*	*P. pygmaeus*	*G. beringei*	*G.g. gorilla*	*G.g. graueri*	*P. paniscus*	*P. troglodytes*	*H. sapiens*
A. seniculus	-	-	-	-	-	-	-	-
C. apella	-	-	-	-	-	-	-	-
C. aethiops	-	-	-	-	-	-	-	-
E. patas	-	-	-	-	-	-	-	-
N. larvatus	-	-	-	-	-	-	-	-
P. rubicunda	-	-	-	-	-	-	-	-
P. abelii	1.0000	-	-	-	-	-	-	-
P. pygmaeus	ns	1.0000	-	-	-	-	-	-
G. beringei	ns	ns	1.0000	-	-	-	-	-
G.g. gorilla	ns	ns	ns	1.0000	-	-	-	-
G.g. graueri	ns	ns	ns	ns	1.0000	-	-	-
P. paniscus	ns	ns	ns	**<0.0001**	**<0.05**	1.0000	-	-
P. troglodytes	ns	ns	ns	**<0.0001**	ns	ns	1.0000	-
H. sapiens	**<0.0001**	**<0.0001**	**<0.0001**	**<0.0001**	**<0.0001**	**<0.0001**	**<0.0001**	1.0000

Table 4.10: ***Post-hoc*** **Tukey's HSD results on PC 2 comparing anthropoid genera following a MANOVA on PP 3 shape variables (PC 1 - 5)**. PC 2 principally tracked the expression of a dorsal rim of bone at the perimeter of the proximal articular surface. Humans are unique amongst anthropoids on PC 1. Bold = significance at $\alpha = 0.05$.

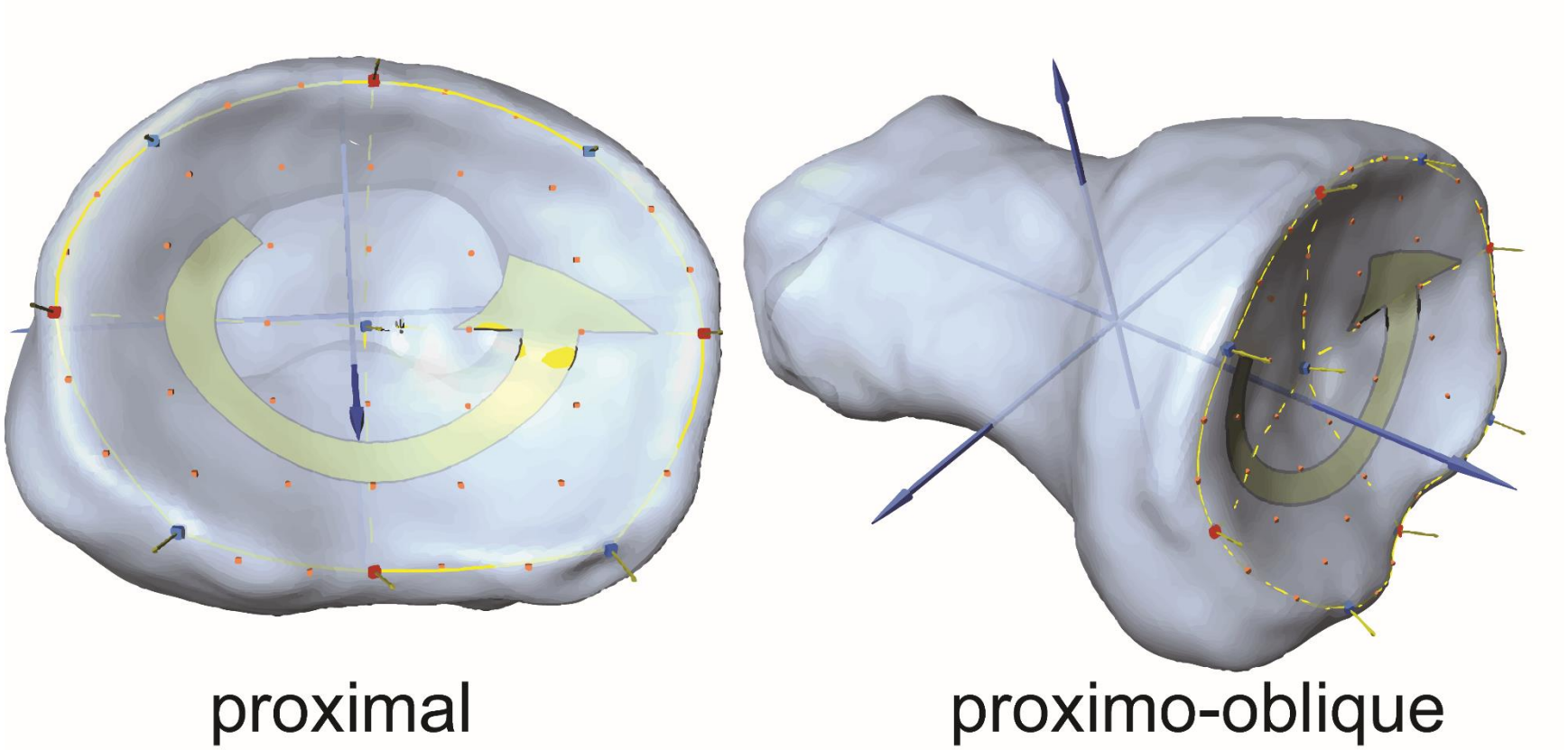

Figure 4.1: 3D landmark surface patch boundaries. A Homo sapiens right hallucal phalanx with a 7x7 landmark patch applied to the proximal articular surface is presented in two views. Red rectangles: user-defined landmarks (D-P height, M-L breadth); orange rectangles: sliding semi-landmarks, blue rectangles: surface patch boundary landmarks, treated as sliding semi-landmarks; solid yellow lines: approximate surface patch boundaries; yellow arrow: order in which landmarks are collected (counter-clockwise). Semi-landmarks are placed automatically between landmark positions and are evenly spaced using minimized Procrustes distances.

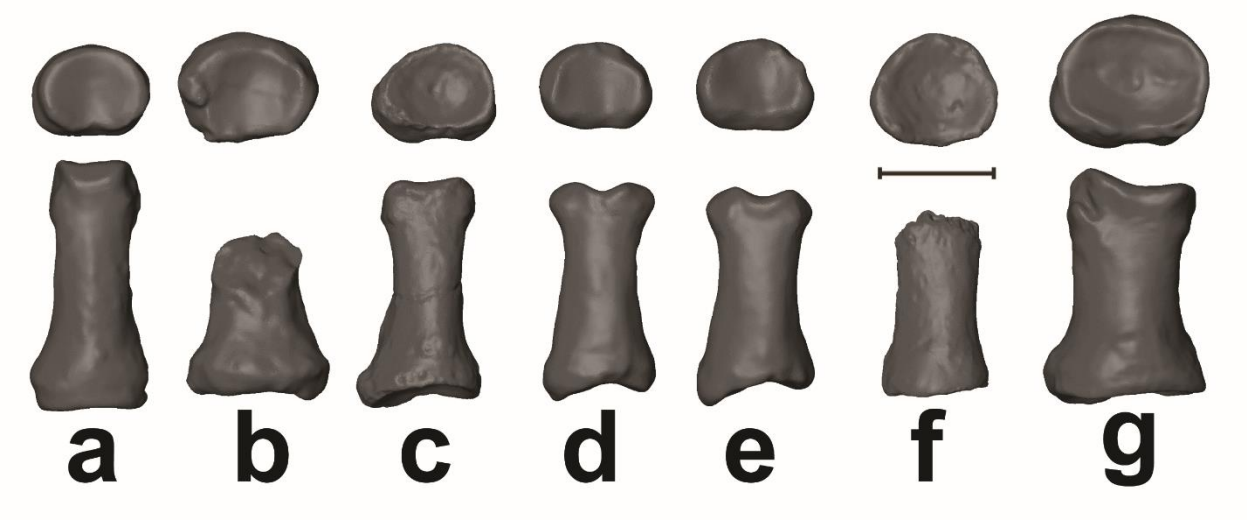

Figure 4.2: Comparative morphology of the hallucal phalanx (PP 1). *Homo* is characterized by a short, robust hallucal phalanx with a deeply convexly excavated base, and the presence of a pronounced rim of bone lining the perimeter of the articular surface, with the marked rim projecting dorso-proximally. **a**: *Pan troglodytes*; **b**: A.L. 333-115F; **c**: KNM-ER 64062; **d**: LB-IV-42D; **e**: LB/82; **f**: U.W. 101-1419; **g**: *Homo sapiens*. Top: proximal view. Bottom: plantar view. Bar: 1 cm.

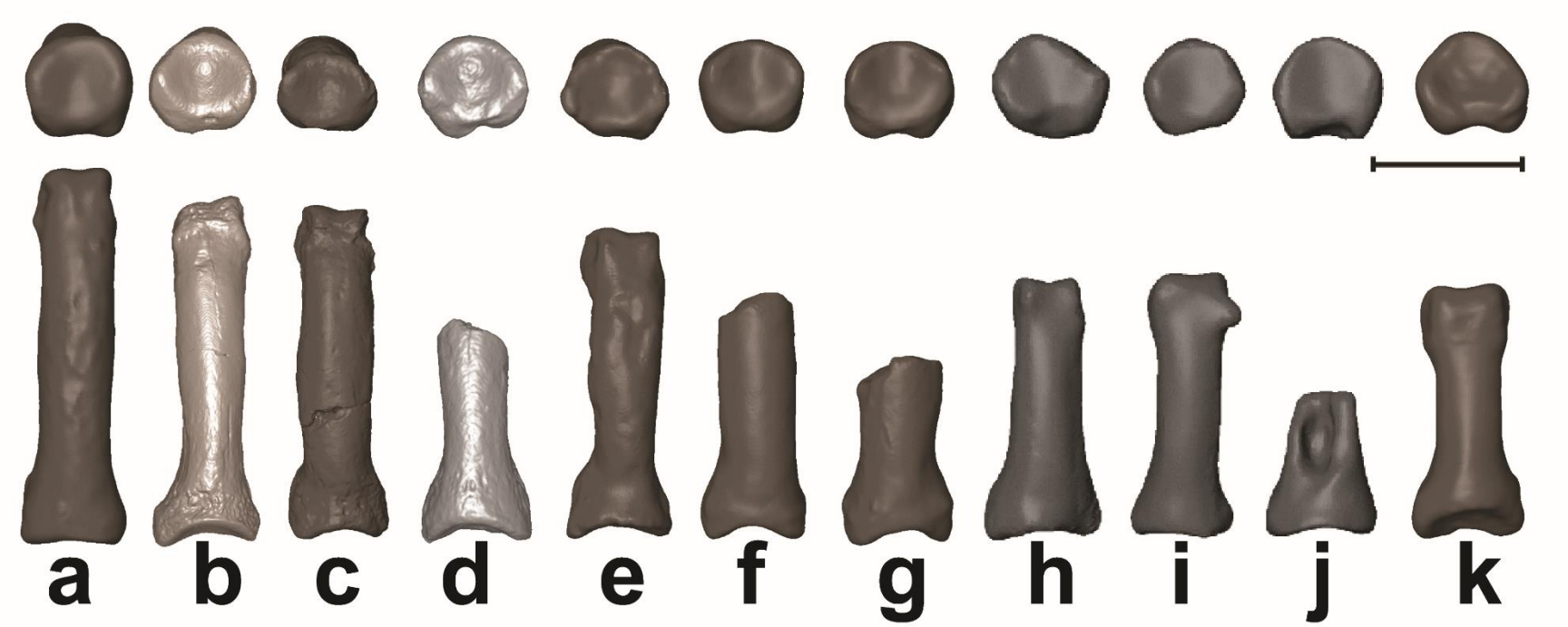

Figure 4.3: Comparative morphology of the third pedal proximal phalanx (PP 3). *Homo* is characterized by a short, robust PP 3 with a deeply convexly excavated base, and the presence of a pronounced rim of bone lining the perimeter of the articular surface, with the marked rim projecting dorso-proximally. **a**: *Pan troglodytes*; **b**: AME-VP-1/71; **c**: ARA-VP-6/500-094; **d**: ARA-VP-6/500-008; **e**: A.L. 333-115H; **f**: A.L. 333-25; **g**: A.L. 333w-51; **h**: LB1/36; **i**: LB1/38; **j**: LB1/41; **k**: *Homo sapiens* Top: proximal view. Bottom: plantar view. Bar: 1 cm.

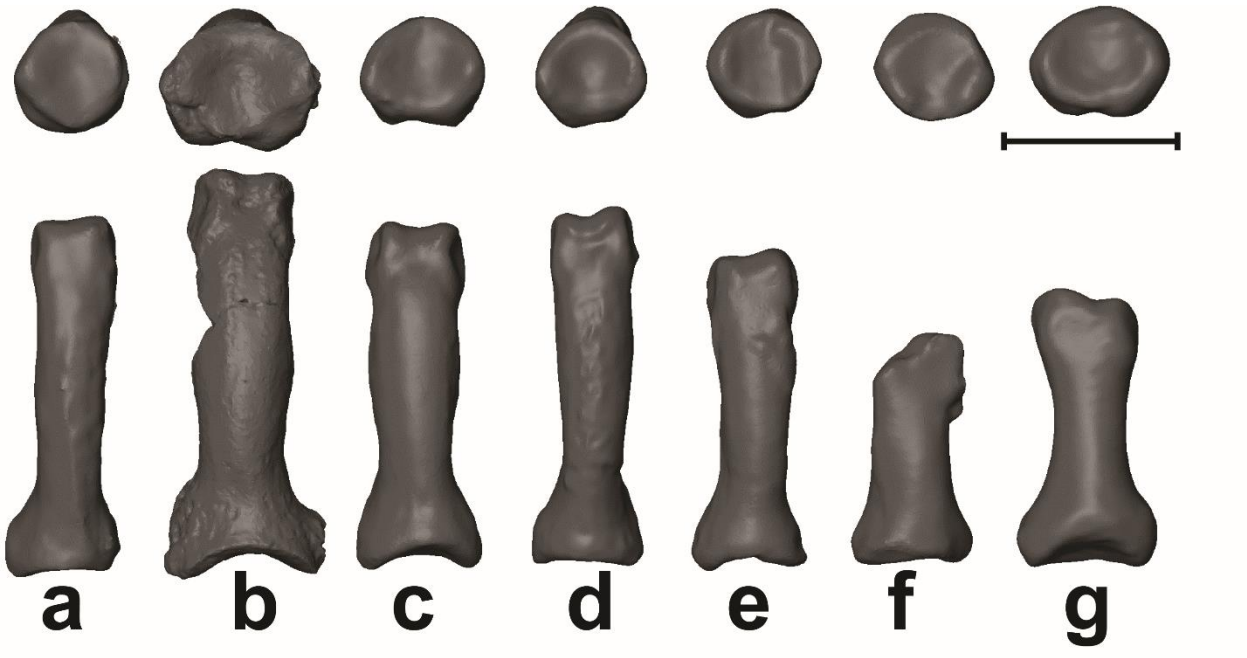

Figure 4.4: Comparative morphology of the fifth pedal proximal phalanx (PP 5). *Homo* is characterized by a short, robust PP 5 with a deeply convexly excavated base, and the presence of a pronounced rim of bone lining the perimeter of the articular surface, with the marked rim projecting dorso-proximally. **a**: *Pan troglodytes*; **b**: ARA-VP-6/500-1006; **c**: A.L. 333w-26; **d**: A.L. 333-71; **e**: A.L. 333-115J; **f**: LB1/34; **g**: *Homo sapiens*. Top: proximal view. Bottom: plantar view. Bar: 1 cm.

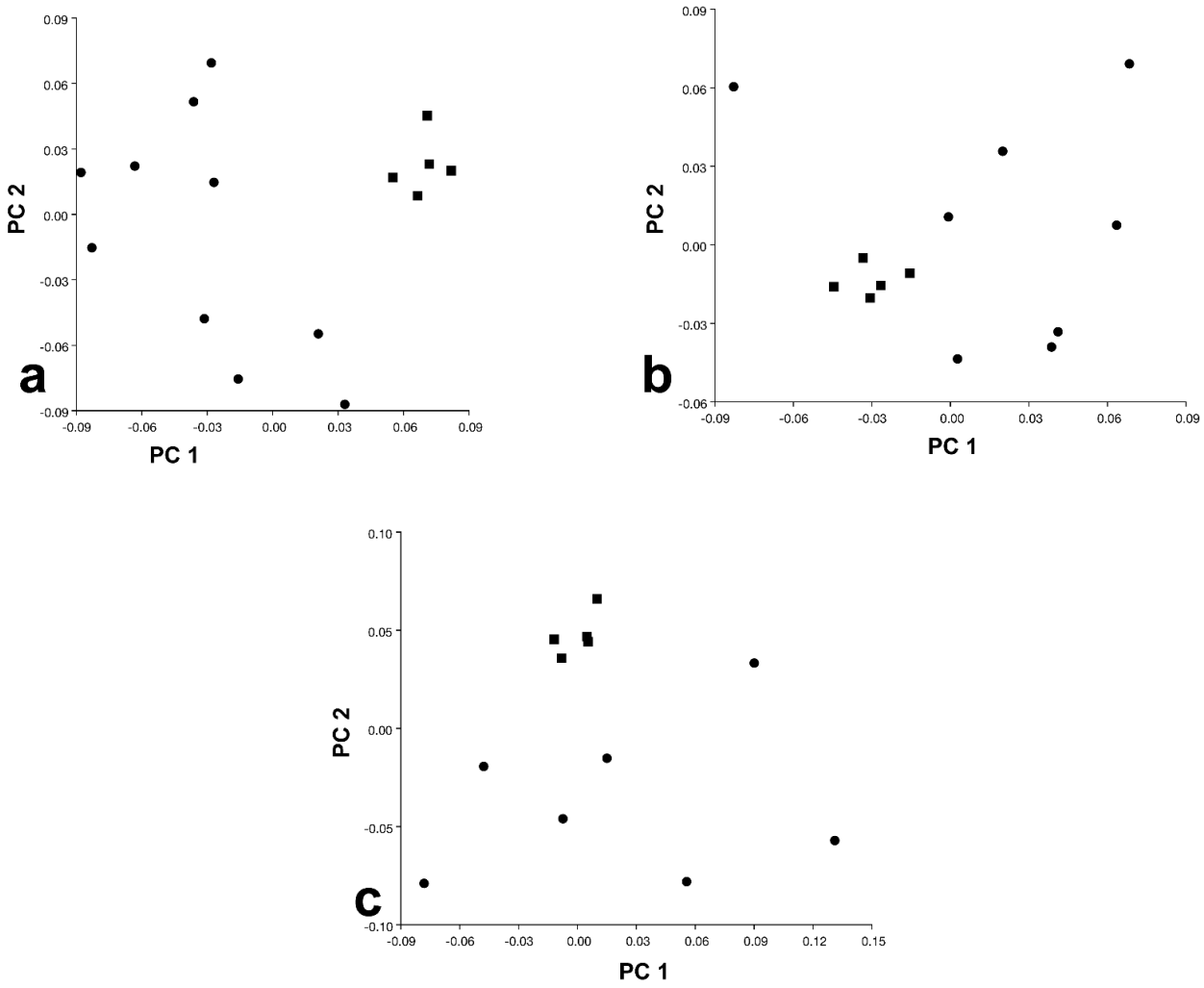

Figure 4.5: Graphical results of the phalangeal error study. PCA scatterplots of PC 1 vs. PC 2 for repeated measures on PP 1. Circles: individuals, rectangles: repeated measures. The relative clustering of repeated measures demonstrates that the landmarks chosen are very repeatable. **a**: *Pan*; **b**: *Gorilla*; **c**: *Nasalis*.

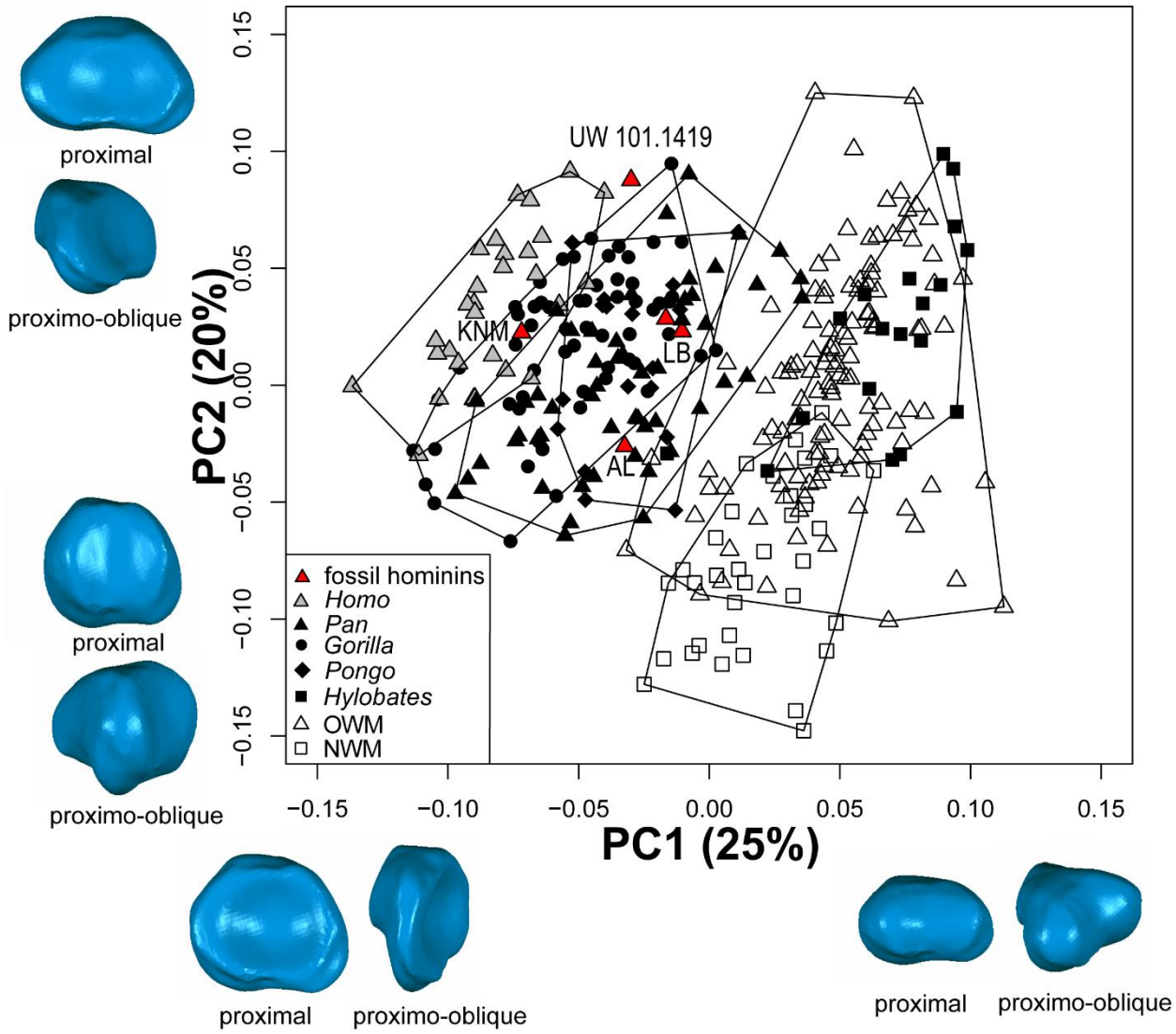

Figure 4.6: PCA scatterplot of PC 1 vs. PC 2 for PP 1. Note the general separation of monkeys (open rectangles), apes (filled shapes), and humans (gray triangles). Minimum convex polygons are constructed for these groups to illustrate their ranges in the morphospace. There is much overlap within apes and cercopithecoids, but NWMs separate from the sample on PC 2. Humans overlap in total range with *Gorilla*. Of all fossil hominins (red triangles), KNM-ER 64062 was the most human-like hallucal phalanx, the rest looked ape-like in the eigenanalyses. PC 1 principally tracked phalangeal base convexity, ovoid form, and the expression of a dorsal rim of bone at the perimeter of the proximal articular surface. 3D surface morphs in proximal and proximo-oblique views represent articular shape differences of observed extremes (PC 1: -0.15 – 0.15; PC 2: -0.15 – 0.15).

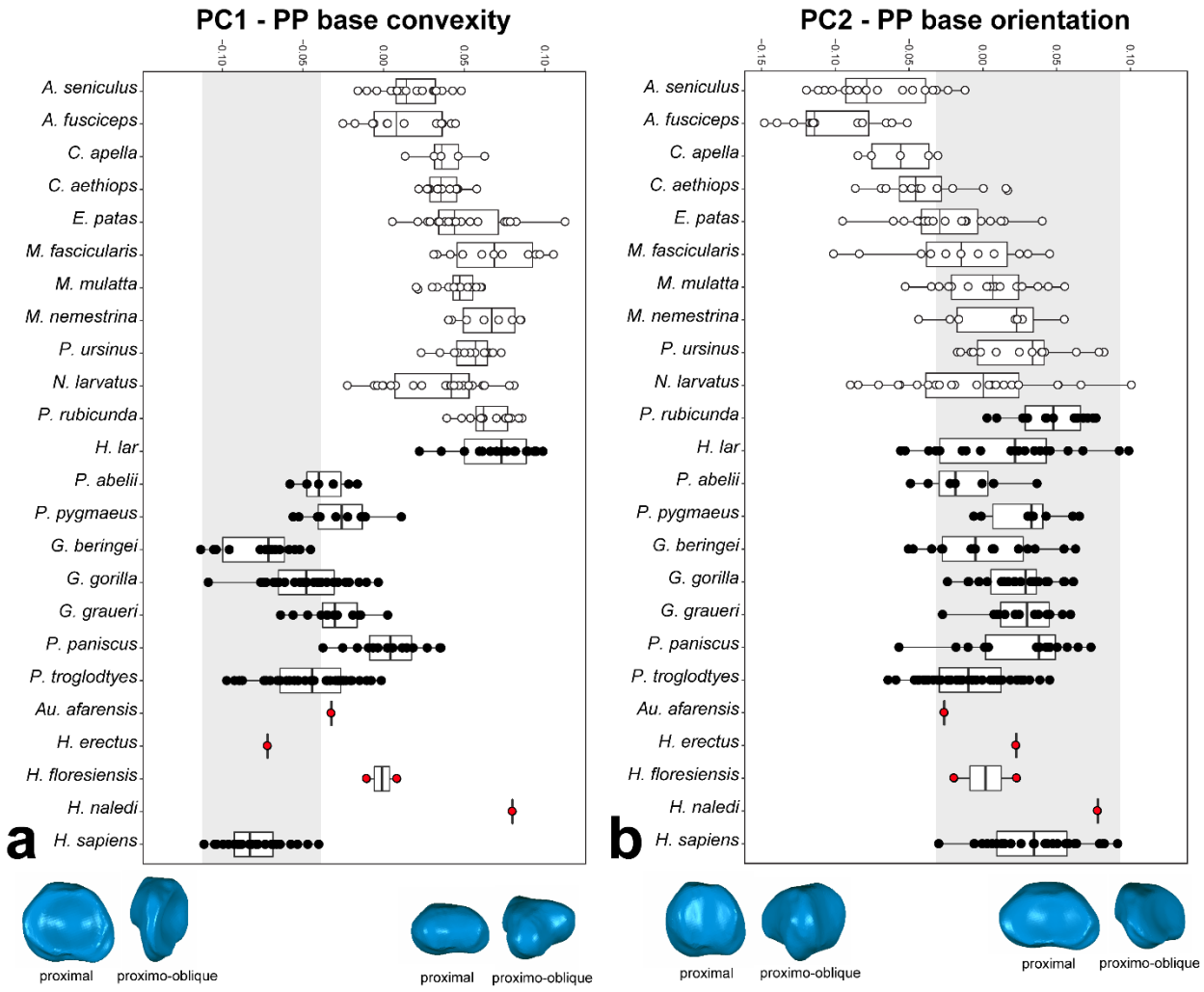

Figure 4.7: Cleveland box-and-whisker plots of PC 1 (a) and PC 2 (b) scores for the anthropoid PP 1. Although humans overlap with the total range of variation in chimpanzees and gorillas, they are significantly different from all groups on PC 1. KNM-ER 64062 is most similar to humans in overall morphology. Shaded bar: modern human range. 3D surface morphs in proximal and proximo-oblique views represent articular shape differences of observed extremes (PC 1: -0.15 – 0.15; PC 2: -0.15 – 0.15).Vertical bars: median. Rectangles: interquartile range. Horizontal bars: range.

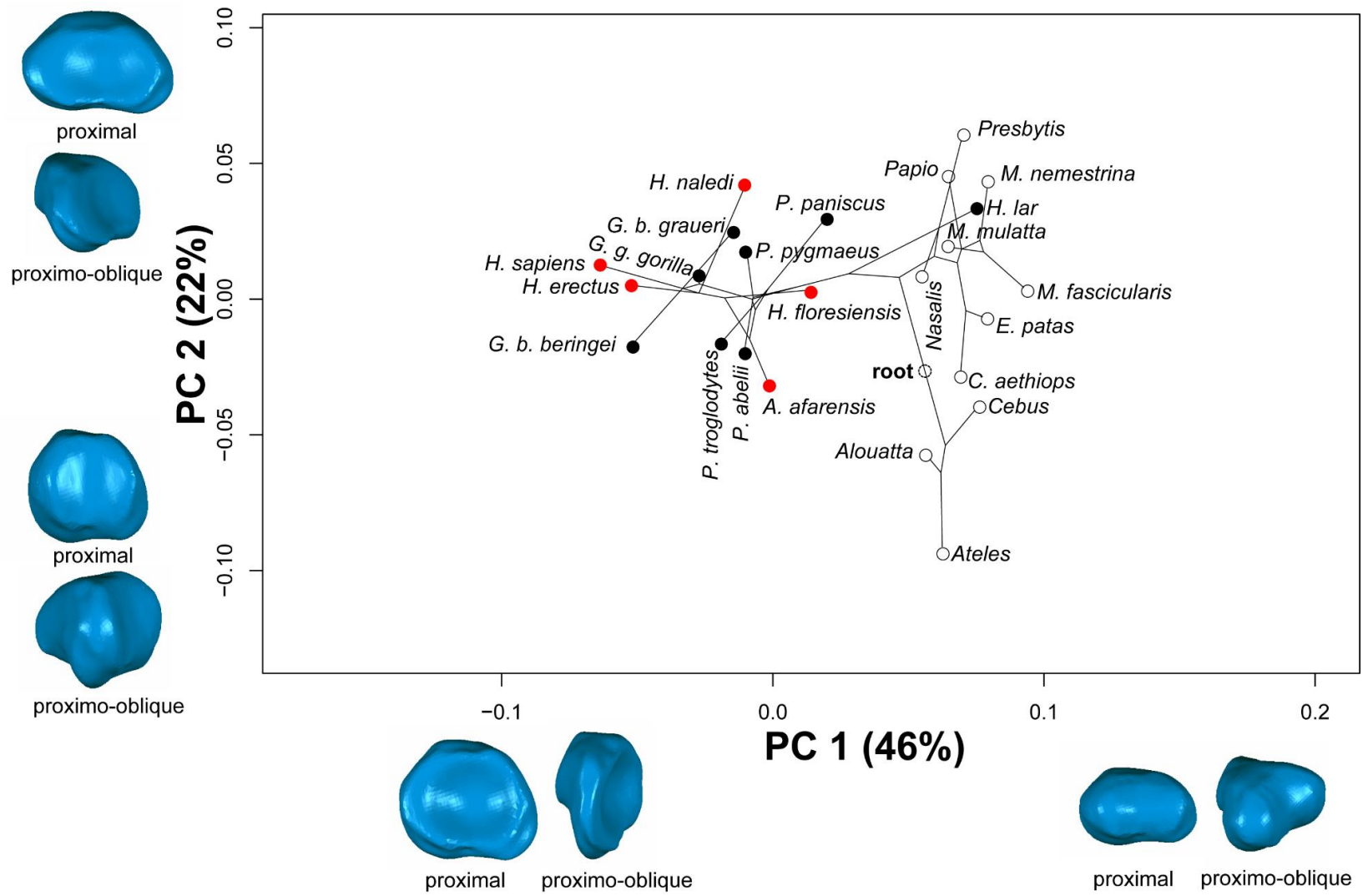

Figure 4.8: Phylomorphospace plot of the anthropoid molecular phylogeny superimposed upon a species-means bivariate PCA scatterplot of PP 1. Hominoids, cercopithecoids, and NWMs generally separate into different regions of the tangent shape space. Note however that gibbons look cercopithecoid-like in hallucal phalangeal morphology, and this is perhaps similar to the condition found in the hominoid LCA. Red circles: hominins; filled circles: apes; open circles: monkeys.

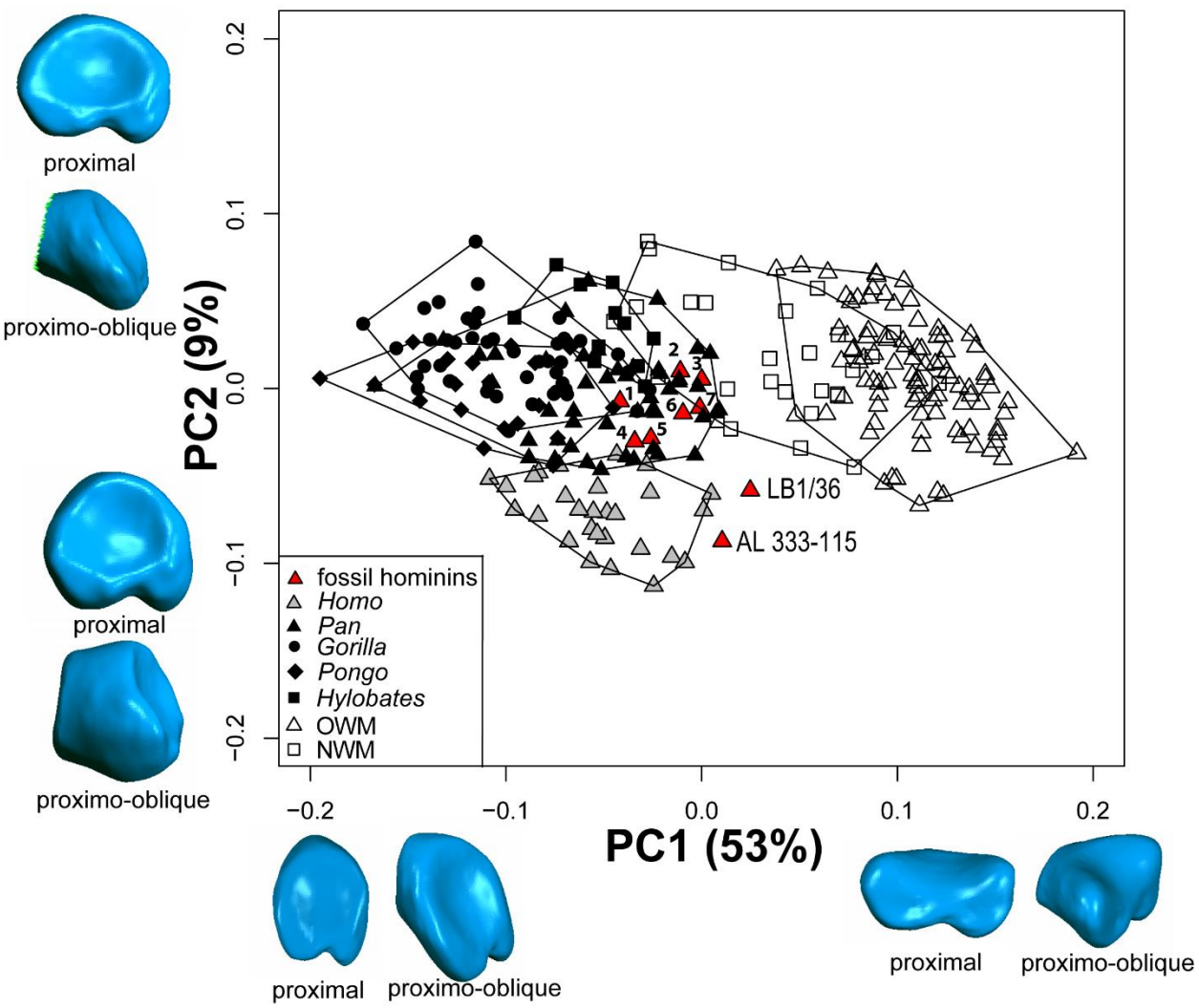

Figure 4.9: PCA scatterplot of PC 1 vs. PC 2 for PP 3. Note the general separation of monkeys (open shapes), apes (filled shapes), and humans (gray triangles). Minimum convex polygons are constructed for these groups to illustrate their ranges in the morphospace. There is much overlap within apes and cercopithecoids, but NWMs separate from the sample on PC 2. Humans overlap in total range with *Gorilla.* Of all fossil hominins (red triangles), KNM-ER 64062 was the most human-like hallucal phalanx, the rest looked ape-like in the eigenanalyses. PC 1 principally tracked phalangeal base convexity, ovoid form, and the expression of a dorsal rim of bone at the perimeter of the proximal articular surface. 3D surface morphs in proximal and proximo-oblique views represent articular shape differences of observed extremes (PC 1: -0.20 – 0.20; PC 2: -0.10 – 0.10). **1**: AME-VP-1/71; **2**: ARA-VP-6/500-094; **3**: A.L. 333-25; **4**: LB1/41 **5**: LB1/38 **6**: ARA-VP-6/500-008; **7**: A.L. 333w-51.

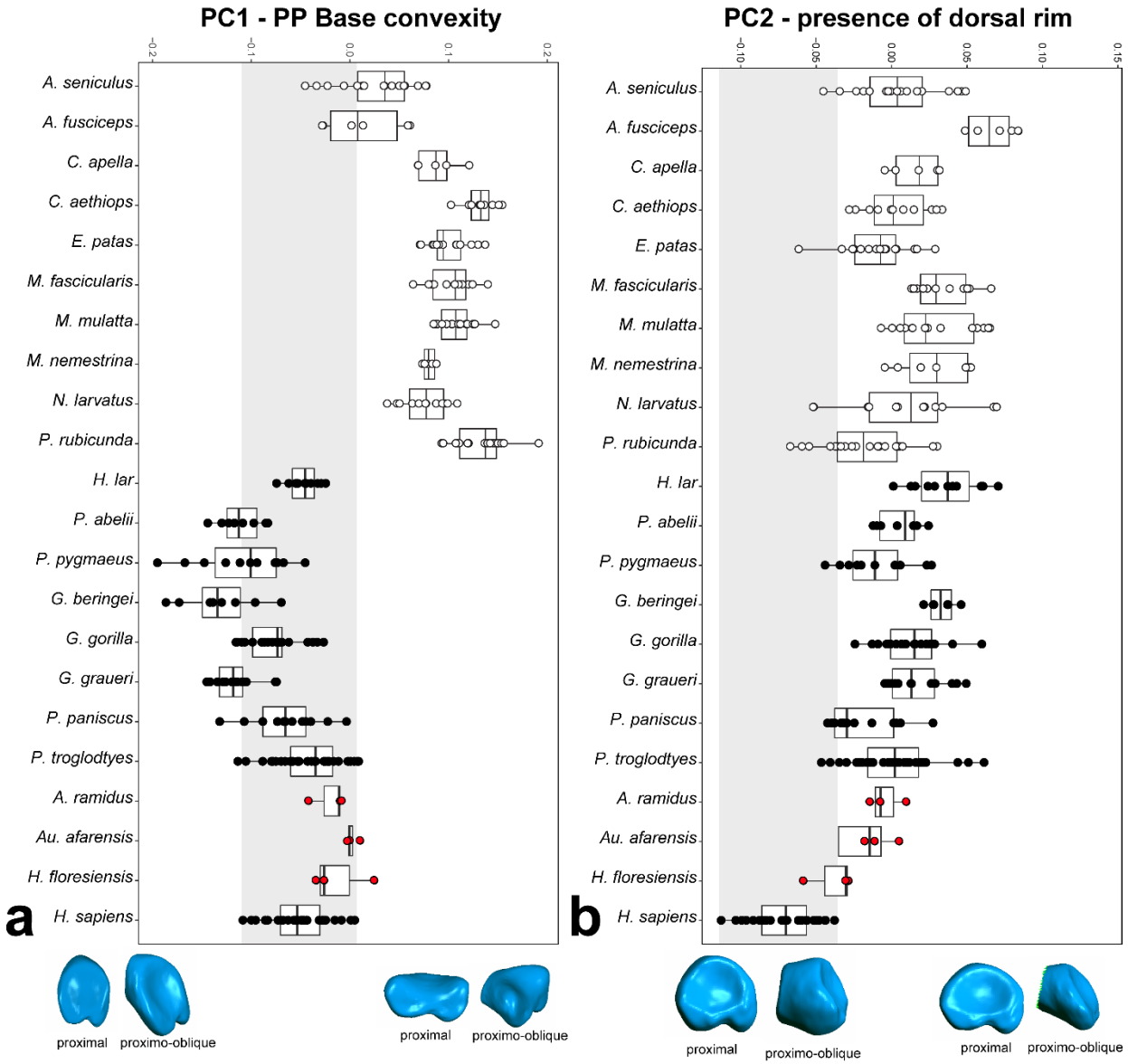

Figure 4.10: Cleveland box-and-whisker plots of PC 1 (a) and PC 2 (b) scores for the anthropoid PP 3. Apes and cercopithecoids do not overlap on PC 1 at all and have a dramatically different form in PP 3 on this axis from the monkey condition. PC 2 is the discriminating axis of variation for *Homo*, marked by the strong presence of a dorsal rim of bone in addition to dorsal orientation of the proximal phalangeal base. This morphology is expressed in fossil hominins, but at a level intermediate between that of chimpanzees and humans. *Ardipithecus*, however, appears entirely chimpanzee-like. Shaded bar: modern human range. 3D surface morphs in proximal and proximo-oblique views represent articular shape differences of observed extremes (PC 1: -0.15 – 0.15; PC 2: -0.15 – 0.15).Vertical bars: median. Rectangles: interquartile range. Horizontal bars: range.

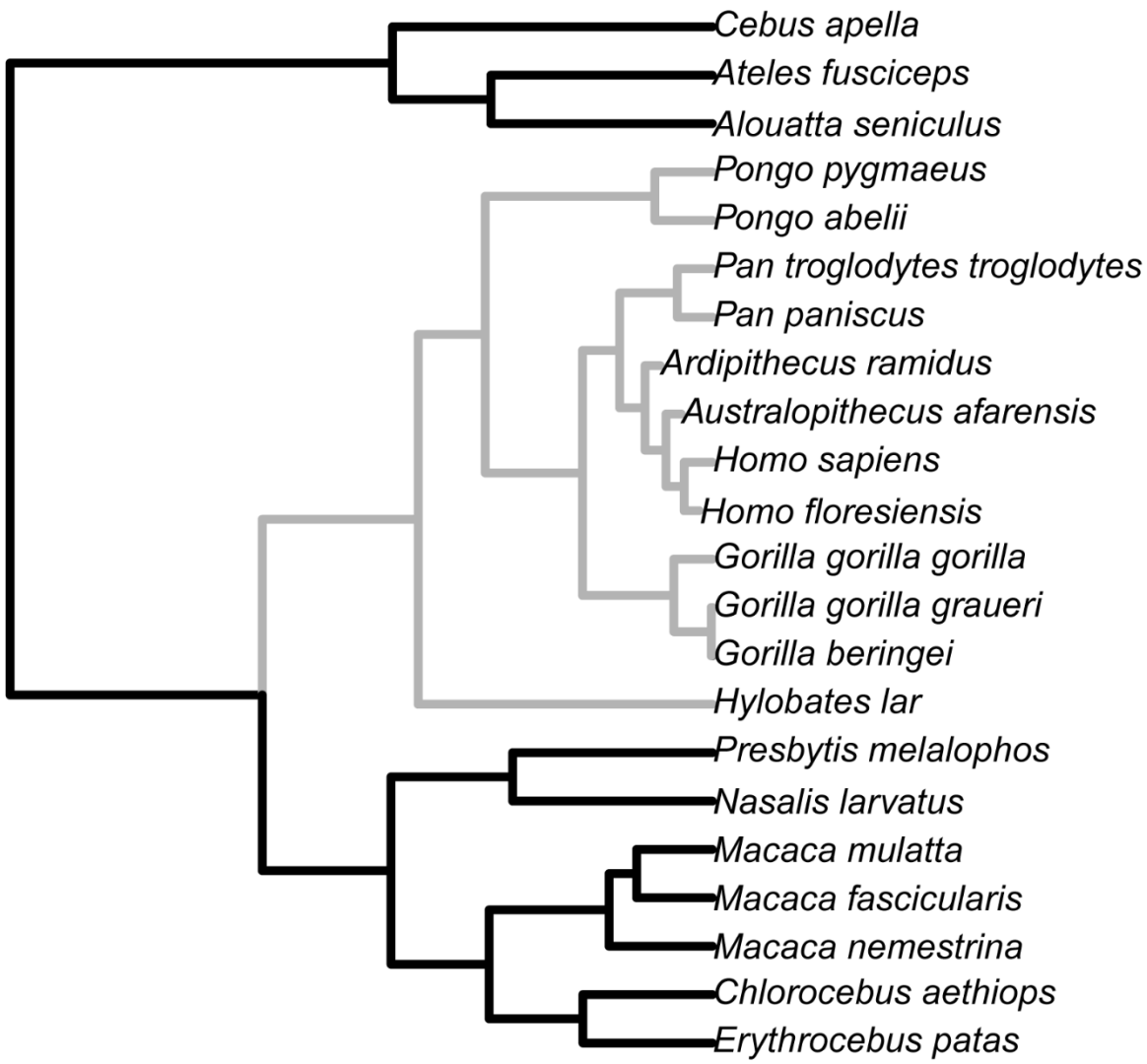

Figure 4.11: Time-calibrated phylogenetic tree with estimated adaptive regimes painted onto the tree branches for PP 3. Adaptive regimes are based on PC 1 (base convexity and form) and PC 2 (phalangeal base orientation and presence of dorsal rim) scores. The two regime shifts found includes a non-convergent regime found in hominoids (gray branches) separate from a second regime encapsulating monkeys (black branches).

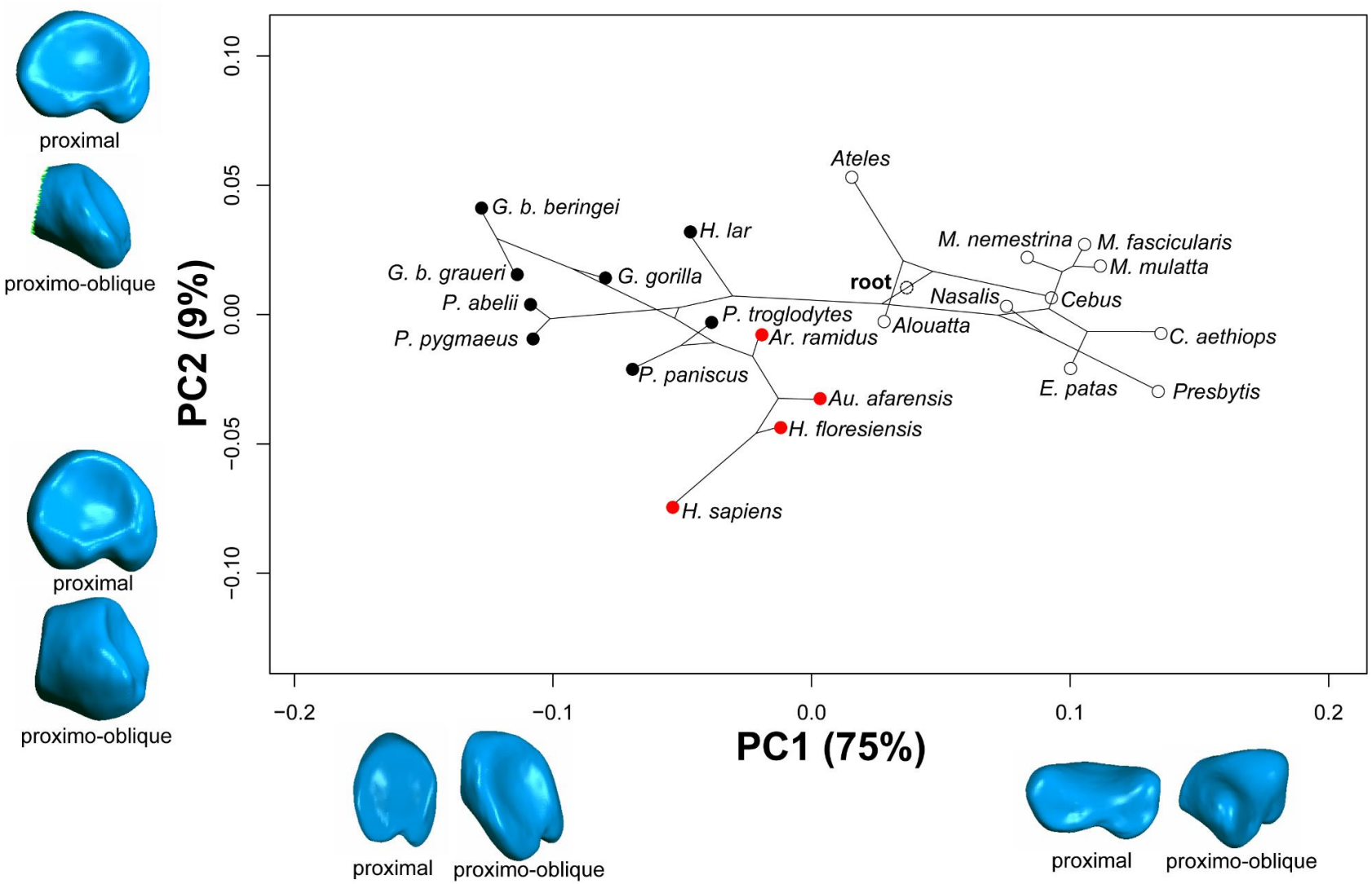

Figure 4.12: Phylomorphospace plot of the anthropoid molecular phylogeny superimposed upon a species-means bivariate PCA scatterplot of PP 3. Apes, monkeys, and hominins all separate into different regions of the morphospace. *Ardipithecus* looks more similar to *Pan* than extant *Homo*, but all fossil hominins exhibit some signal of human-like morphology in the PP 3 base. Red circles: hominins; filled circles: apes; open circles: monkeys.

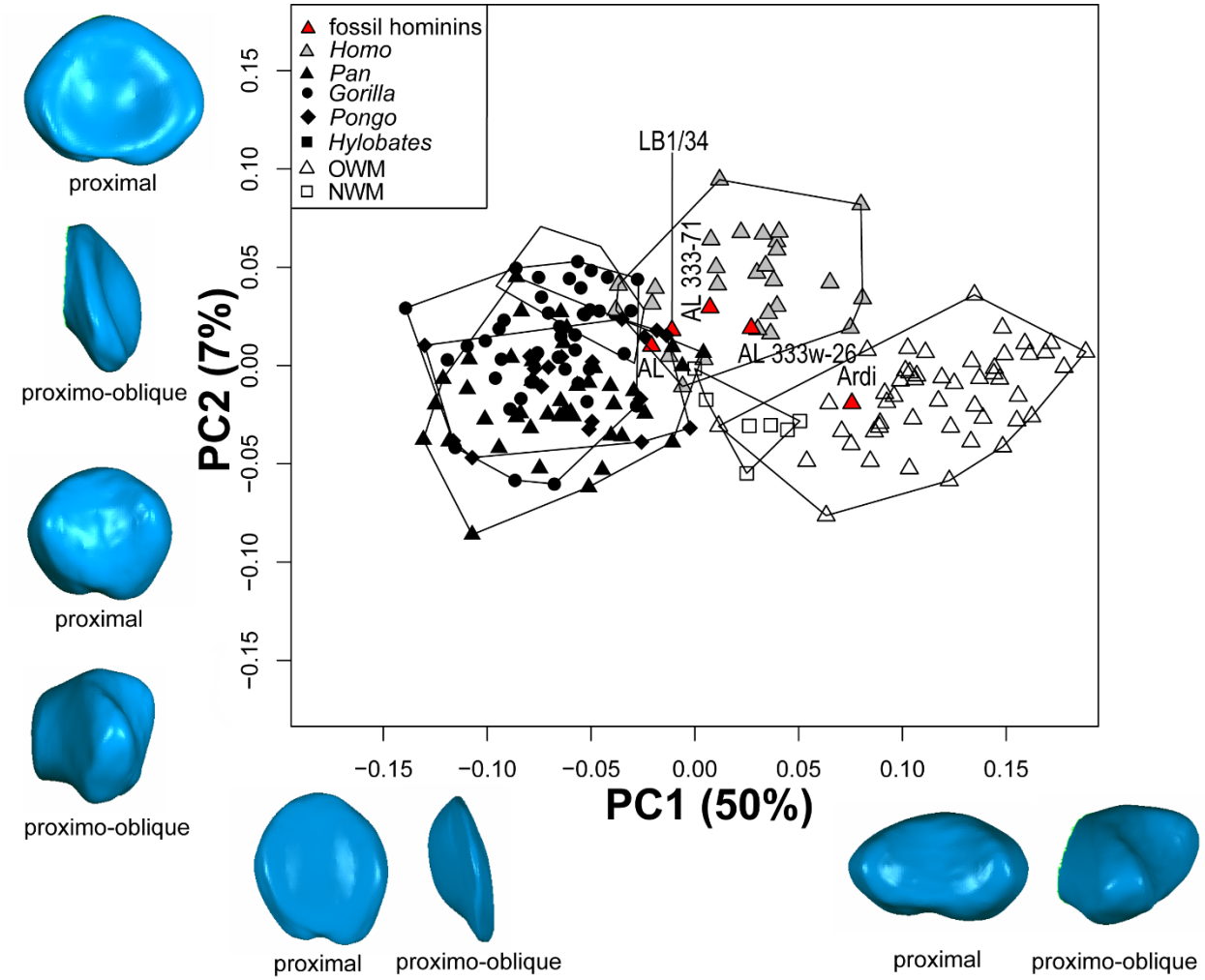

Figure 4.13: PCA scatterplot of PC 1 vs. PC 2 for PP 5. Note the general separation of monkeys (open rectangles), apes (filled shapes), and humans (gray triangles). Minimum convex polygons are constructed for these groups to illustrate their ranges in the morphospace. The tangent space is reminiscent of those seen in the lesser metatarsals (e.g., Fig. 3.5), with humans intermediate between apes and monkeys on PC 1, but separating on PC 2. Fossil hominins (red triangles) look more derived in their PP 5 morphology, except for *Ardipithecus*, which has a cercopithecoid-like shape in the PP 5 phalangeal base. PC 1 principally tracked phalangeal base convexity, ovoid form, and the expression of a dorsal rim of bone at the perimeter of the proximal articular surface. 3D surface morphs in proximal and proximo-oblique views represent articular shape differences of observed extremes (PC 1: -0.15 – 0.15; PC 2: -0.10 – 0.10).

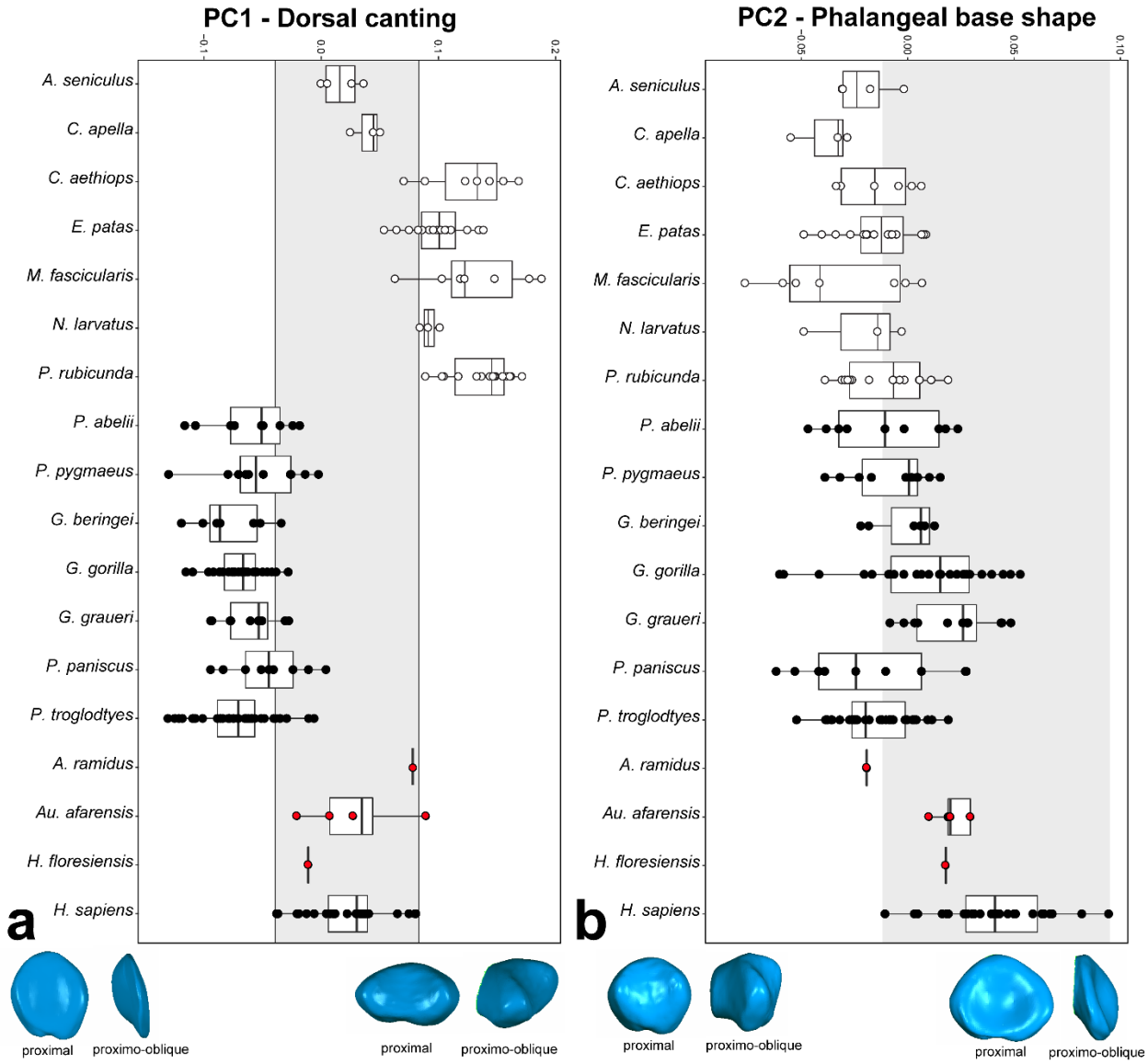

Figure 4.14: Cleveland box-and-whisker plots of PC 1 (a) and PC 2 (b) scores for the anthropoid PP 5. Humans and fossil hominins share a mostly unique position between apes and cercopithecoids on PC 1 (although with overlap from NWMs). On PC 2, humans are distinguished notably high PC 2 scores that are mostly outside the interquartile range of most groups except gorillas. Fossil hominins lie between gorillas and humans on PC 2. 3D surface morphs in lateral and distal views represent articular shape differences of observed extremes (PC 1: -0.15 – 0.15; PC 2: -0.10 – 0.10). Vertical bars: median. Rectangles: interquartile range. Horizontal bars: range.

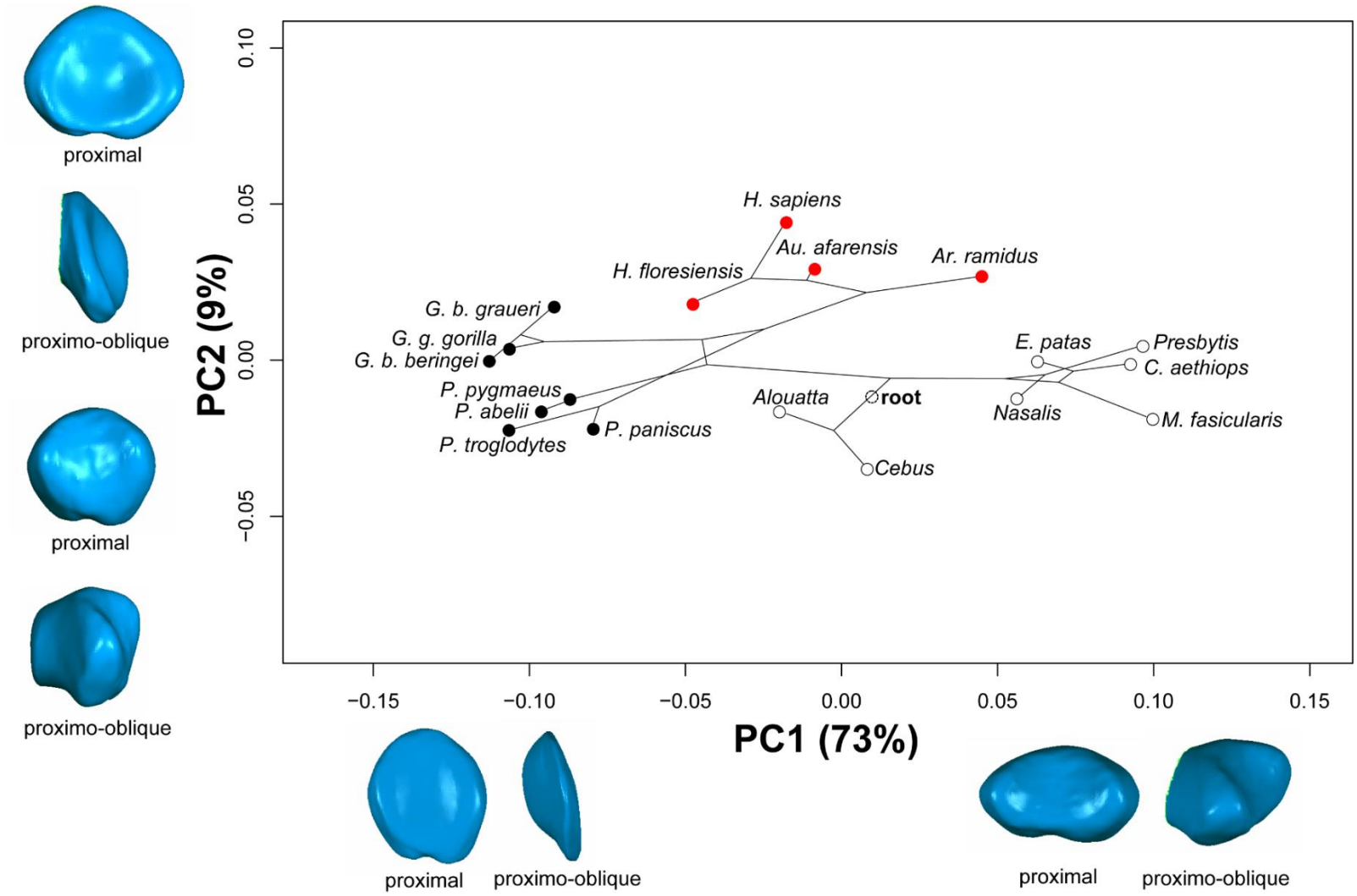

Figure 4.15: Phylomorphospace plot of the anthropoid molecular phylogeny superimposed upon a species-means bivariate PCA scatterplot of PP 5. In the PP 5, the *Pan-Homo* LCA is reconstructed as possessing a PP 5 base morphology more like that seen in hominins than that seen in extant apes. Apes and hominins have undergone more shape evolution than monkeys, as indicated by relative branch lengths. Red circles: hominins; filled circles: apes; open circles: monkeys.

Chapter 5

The Anthropoid Metatarsophalangeal Joints: Total Morphological Pattern

5.1 Introduction

The degree to which two appositional subchondral bony surfaces match each other at a given synovial joint can be thought of as the level of congruence that exists between those mated surfaces. In this way, some joints may be described as quite incongruent such that the two appositional surfaces do not match very well (e.g., knee and shoulder [glenohumeral] joints; Kelkar et al., 2001), and other joints can be described as highly congruent such that the appositional surfaces match quite well (e.g., the talocrural, metacarpophalangeal, and elbow joint complex; Waide et al., 2000; Turley and Frost, 2014). The congruence between mated appositional surfaces is an important property of synovial joints because the level of congruence is thought to play a role in performance variables such as joint range of motion and stability (MacLatchy, 1996; MacLatchy and Bossert, 1996; Waide et al., 2000; Kelkar et al., 2001; Hammond et al., 2010) at any given synovial joint. Indeed, many studies of prosthesis design and skeletal pathology have correlated a reduction in joint covariance with that of impaired performance or reduced prosthesis lifespan (Hlaváček and Vokoun, 1998; Waide et al., 2000; Kelkar et al., 2001; Laroche et al., 2006; Peeters et al., 2013; Halilaj et al., 2014), thus providing additional support for this notion. Generally, incongruent joints are thought to provide more mobility at the cost of stability (e.g., shoulder/glenohumeral) whereas other, more congruent joints are thought to sacrifice mobility in exchange for increased stability (MacConaill and Basmajian, 1969). Previous research seems to agree with this theoretical framework. Although the glenohumeral joint is largely incongruent and highly mobile, increased stability with relatively higher joint congruence at this joint has been observed in that more congruent joints showed less infero-superior translation of the humeral head during arm elevation (Kelkar et al.,

2001). Other studies of the complex elbow articular surfaces and other joints have reported relationships between congruence and even load distributions and range of motion (Waide et al., 2000). Physical anthropologists have focused on joint congruence in the hip as measured by less femoral head coverage of the acetabulum. Less acetabular coverage has been hypothesized to increase hip mobility, which is important for negotiating arboreal substrates. It has recently been shown that more suspensory anthropoids have greater ranges of motion than their terrestrial counterparts in hip abduction and external rotation, which is correlated with areas of less femoral head coverage of the acetabulum (dorsally and caudally; Hammond, 2014). In addition to the evolutionary remodeling of the hip joint and its impact on congruence, physical anthropologists have also discussed joint congruence observed in the forefoot at the metatarsophalangeal joints (MTPJs). It has been argued that the ape pedal forefoot, similar to that of the human hand, achieves maximal congruency at the MTPJs (i.e., the closed-packed position—CPP) during flexion (i.e., plantarflexion) of the digits (Susman, 1983) such that the joints are most stable during pedal grasping. This has been theorized on the basis of ape MTPJ joint orientation (Hamrick, 1996), joint shape, and hypotheses about the role of soft tissue during the close-packing process (Watson and Weinzweig, 1998; Fig. 5.1). Given these factors, the human forefoot is thought to achieve the CPP when the digits are in maximal extension (i.e., dorsiflexion). This argument is supported by kinematic and kinetic experiments that show human MTPJs achieve maximal dorsiflexion when peak plantar pressures under the forefoot occur just prior to push off at the end (96%) of stance phase (Vereecke et al., 2003; Griffin et al., 2010a). Moreover, it is thought that the derived morphology seen in several hominin forefoot elements has evolved to help achieve maximum congruency in dorsiflexion as opposed to plantarflexion (Susman and Brain, 1988; Susman and de Ruiter, 2004) early in the hominin lineage as an adaptation to increased terrestriality in their locomotor behavior.

In an attempt to quantify the level of joint congruence that exists in the hominin MTPJs, I present here a detailed morphometric analysis that utilizes statistical measures of covariance on multivariate, 3-dimensional (3D) measures of shape on appositional shapes in a mean-centered orientation to serve as proxies for joint congruency (Harcourt-Smith et al., 2008; Turley and Frost, 2014). The subchondral articular surfaces of the metatarsal head and phalangeal base were quantified using 3D geometric morphometric techniques and then their covariance was measured. Although this approach does not consider the effect of soft tissue elements in joint

function, it is an approach that can serve as a proxy for joint interface shape and function (Hamrick, 1999; Harcourt-Smith et al., 2008; Hammond et al., 2010; Turley and Frost, 2014) and lends itself well to the comparative morphology approach due to the relatively wide availability of subchondral versus soft tissue specimens available in collections. As a functional ellipsoidal joint, it is hypothesized that the anthropoid MTPJs must exhibit some baseline level of covariance, and it is predicted that there will be a significant covariation between the joint shape of the MT head and the phalangeal base. Based on hypotheses about joint range of motion versus joint stability (MacConaill and Basmajian, 1969), I predict that those species with highly variable positional behavior (i.e., semi-terrestrial monkeys; African apes) will show less covariance than those species with very stereotypical positional behavior (i.e., bipedal modern humans). Likewise, fossil hominins, because of their likely (i.e., *Ardipithecus*) and debated (*Australopithecus*) mixed substrate use, should exhibit less MTPJ covariance relative to modern humans as well because these species are evolving to accommodate increased terrestriality in their locomotor behavior.

5.2 Materials and Methods

The MTPJ covariation analyses utilize the 3D shape data gathered in the previous chapters to explore total morphological patterns in the anthropoid forefoot (see Chapters 2 – 4 for more detail regarding data collection/processing protocols). A combined, "within ray" PCA was performed using the Procrustes coordinates of the MT head and PP base in order to visualize patterns in total MTPJ shape across anthropoids. Statistical tests on the shape variables follows that of previous chapters (e.g., MANOVA, *post hoc* Tukey's HSD).Polygonal surface morphs could not be generated for the PCA plots because of the inclusion of multiple articular surfaces. Likewise, while wireframes representing articular surface shapes could potentially be generated for the combined PCA plots, the mean-centered orientation of the MT head and PP base cause the two wireframe meshes to clip and occlude one another, making shape change determinations from static images impossible. Therefore, I include detailed descriptions of the shape changes along each functional axis, but do not include wireframes or polygonal shape morph images along the PCA axes in this chapter. To statistically assess patterns of MTPJ covariation, a 2-block partial least squares analysis (2B-PLS) (Rohlf and Corti, 2000) was performed on the forefoot shape data in *Geomorph*. The first block consisted of the metatarsal shape data analyzed

in chapters 2 and 3, and the second block contained the phalangeal base shape data analyzed in chapter 4. More specifically, each shape block contained the Procrustes residuals data for each specimen (Bookstein et al., 2003) which are aligned coordinates mean-centered on their corresponding landmarks in the consensus configuration (Dryden and Mardia, 1998; McNulty, 2009). When blocks consist of Procrustes residuals, the 2B-PLS analysis is referred to as a singular warps analysis (Bookstein et al., 2003; Turley and Frost, 2014). The Procrustes residuals were computed in the R package *Evomorph* (Diawol et al., 2015) using GPA-aligned coordinates computed in *Geomorph* (Adams et al., 2015) and a landmark configuration file exported from *Landmark Editor* (Wiley et al., 2005). Using Procrustes residuals avoids problems in the generation of the cross-covariance matrix inherent to covariance analyses that use GPA-aligned coordinates instead of mean-centered data (McNulty, 2009), which can then lead to problems in data interpretation. Both blocks came from matched metatarsal-proximal phalangeal pairs from the same individual. In total, 316 matched MT 1 – PP 1 pairs (Table 5.1), 264 matched MT 3 – PP 3 pairs (Table 5.2), and 180 matched MT 5 – PP 5 pairs (Table 5.3) were included in the anthropoid forefoot covariance analyses (n = 1520 forefoot bones in total). Additionally, fossil hominin matched MTPJ pairs were also included for those groups that had preserved associated MTPJ fossil subchondral surfaces in the first (n = 4), third (n = 4), and fifth (n = 2) pedal rays (Table 5.4). Each block contained shape data from 7x7 surface landmark patches applied in *Landmark Editor*. Including semi-landmarks, 149 landmarks were used to capture MT and PP articular surfaces, and these went into block 1 (MT shape) and block 2 (PP shape) of the 2B-PLS analysis. To explore the effects of overall size and shape on covariation, a Procrustes form space (Mitteroecker and Gunz, 2009) was also constructed by including the log of centroid size for each specimen along with the Procrustes coordinates in the cross-covariance matrix. Procrustes form space is useful when both size and shape are of interest in an analysis, such as in fossil classification studies (e.g. Harcourt-Smith et al., 2008).

The purpose of a 2B-PLS is to find pairs of linear combinations of variables that account for the observed covariances (or correlations) between two sets (blocks) of variables. PLS axis 1 is the axis that best explains the variance in both data sets (blocks) 1 and 2. The method quantifies the degree of association between two blocks of shape data as defined by the 3D landmark coordinate surface patches using a partial least squares approach and the significance of the correlation between the two blocks is assessed using a permutation test (n = 10,000

iterations); this differs from regression in that both blocks of shape data are considered equally (e.g., one block is not considered to be a set of independent variables measured without error). When given blocks of appositional joint surface data as input, the 2B-PLS statistic can be interpreted as a measure of joint covariance—a measurement of two opposing joint surfaces as they relate to one another considering the 3D surface shape contours of each bone at their interface without imposing assumptions about habitual joint posture, range of motion at the joints, or any assessment of volume separating presumably "optimally" positioned surfaces (Harcourt-Smith et al., 2008). However, this approach is limited by orienting both joint surfaces in a mean-centered orientation, which may not be anatomically functional. However, the orientation process is automated during the eigenanalyses, and removes any bias that may be introduced by manually registering joint surfaces in any sort of hypothesized functionally important configuration. To assess the strength of MTPJ covariation, the r-PLS correlation coefficient for the main axes of variation was used. This is the strength of the association between PLS axis 1 in block 1 and PLS axis 1 in block 2. This was used instead of overall measures of covariation (e.g., RV coefficient, CR coefficient; Adams, 2016) because interpretations of covariation were limited to those axes which were functionally interpretable, and because PLS axis 1 often explained a disproportionate (> 50%) of the variance in the dataset.

5.3 Results

Results from the within-ray PCAs demonstrate better group separation between shape variables ($p < 0.0001$) than the single-element PCAs (see Chapters 2 – 4), especially in distinguishing modern humans from other anthropoids (Fig. 5.2 – Fig. 5.5). In the hallucal ray, the first three PCs captured functional signals of anthropoid MTPJ shape, whereas the first two PCs captured functional signals in the third and fifth ray datasets.

For the hallucal ray, PC 1 (18% variance explained) seemed to be similar to PC 1 from the PP base shape analyses (see Chapter 4), which was related to dorsal canting. Like in the phalangeal data, here PC 1 separated great apes from OWMs, NWMs, and gibbons ($p < 0.0001$). Great apes, who demonstrated variable amounts of dorsal canting in their proximal phalanges, overlapped each other with low PC 1 scores. All monkeys and gibbons, who lacked dorsal canting entirely, occupied high PC 1 scores. Within this overall separation, modern humans were significantly different from all groups except mountain gorillas (*G. b. beringei*) ($p <$

0.0001; Table 5.5), with the lowest PC 1 scores on average. Hominins overlapped with humans on PC 1 except for *Au. afarensis*, which fell close to the mean of the bonobo distribution (Fig. 5.6a). PC 2 (11% variance explained) appeared to be driven mostly by MT head dorsal robusticity and epicondylar breadth. Low PC 2 scores were more dorsally robust with wide, pronounced epicondyles, whereas high PC 2 scores were more dorsally gracile with weakly developed MT epicondyles. On this axis, humans overlapped extensively with the more terrestrial cercopithecoids to the exclusion of all other apes and the more arboreal colobines and NWM groups ($p < 0.0001$; Fig. 5.6b; Table 5.6). PC 3 (8% variance explained) appeared to be partly related to dorsal orientation of the MT head with positive PC 3 scores being more dorsally oriented, and negative PC 3 scores being more plantarly oriented. This likely drove the overlap observed between modern humans all hominins. However, the high overlap between humans and arboreal monkeys (Fig. 5.6c; Table 5.7) on this axis was unusual and indicative of other correlated shape changes that occurred on PC 3. Regardless, the combination of PC 1 and PC 3 MTPJ morphology was a good distinguisher of human and hominin forefoot morphology (Fig. 5.3), which was not achieved in single-element PCA analyses for the hallucal ray in previous analyses (Chapters 2, 4).

Combined PCA results for MTPJs 3 and 5 were similar. For MTPJ 3, PC 1 (34% variance explained) again was related to PP base canting, with complete separation between hominoids at the positive PC 1 spectrum, and monkeys at the negative PC 1 spectrum ($p < 0.0001$; Table 5.8; Fig. 5.7a). PC 2 (10% variance explained) was related to MT head orientation, with high PC 2 scores being more dorsally oriented, and low PC 2 scores being more plantarly oriented. Like in the MT 2 and MT 3 datasets (see Chapter 3), considerable overlap was found between humans and patas monkeys, to the exclusion of all other groups on this axis ($p < 0.0001$; Table 5.9; Fig. 5.7b). The Liang Bua elements (LB1/21 and LB42D; see Table 5.4) fell within the human polygon, *Ardipithecus* MTPJ morphology was intermediate between humans and apes on PC 2, and *Au. afarensis* was more chimpanzee-like overall on both axes. In MTPJ 5, the ordination was very similar to what was seen in MTPJ 3 but humans were more intermediate between monkeys and apes on PC 1 (28% variance explained; Fig 5.8a). PC 2 (12% variance explained) results were also similar to those in MTPJ 3, again with humans separating from the sample with high PC 2 scores ($p < 0.0001$; Fig 5.8b). Hominin MTPJs from *Au. afarensis* and *H. floresiensis* both fell within the human range of variation in MTPJ 5.

Results from the 2B-PLS analyses found a significant covariation of Block 1 and Block 2 PLS axes 1 in the hallucal ray ($p < 0.0001$; r-PLS = 0.744; Fig. 5.9), the third pedal ray ($p<0.001$; r-PLS = 0.799; Fig. 5.10), and in the fifth pedal ray ($p < 0.001$; r-PLS =0.786; Fig. 5.11). The results offer evidence of strong forefoot (MT head and PP base) shape covariance in anthropoids. When within-species forefoot covariance was explored, the results found similar r-PLS values for most taxa, but the covariance between blocks was often not significant (Table 5.10 – Table 5.11) Within-species r-PLS values are not reported for MTPJ 5 due to low sample sizes for most groups. In the hallux, the significance of the covariance signal was found to be significant in the ape ($p < 0.0001$) but not monkey groups; in the third and fifth pedal rays the correlation between major block PLS axes was similar but no correlation was found to be statistically significant after the permutation test was performed. When the Procrustes form matrix (Mitteroecker and Gunz, 2009) was used in Blocks 1 and 2 instead of the Procrustes residuals, the covariation signals improved dramatically in the hallucal ray ($p < 0.0001$; r-PLS = 0.975; >99% covariance explained), the third pedal ray ($p < 0.0001$; r-PLS = 0.988; >99% covariance explained), and the fifth pedal ray ($p < 0.0001$; r-PLS = 0.966; >99% covariance explained) (Fig. 5.12). The difference between the Procrustes shape and Procrustes form matrix covariance signals indicate that both size and shape play important roles in anthropoid forefoot covariance.

5.4 Discussion

When both forefoot elements are including in the PCA analyses, the resultant morphospace characterized the total morphological pattern of the anthropoid MTPJs. The axes simultaneously characterized shape variation in the proximal phalangeal base and metatarsal head, with patterns that echoed the functional signals discussed in Chapters 2 – 4, although with somewhat different implications for fossil hominins. When fossils were plotted against extant anthropoid MTPJ shape variables, hominins appeared more human-like in MTPJ 1, in contrast to what the hallucal head or phalanx results demonstrated alone. The MTPJ 3 results were more mixed, primarily due to the mosaic nature of the hominin PP base. In MTPJ 5, hominin morphology was indistinguishable from that of modern humans. One salient feature was the range of variation in modern human MTPJ 1 morphology compared to other anthropoids. Humans were characterized by a very narrow range of variation in MTPJ morphology, and this was apparent both in the area of the human polygon in the MTPJ 1 morphospace (Fig. 5.2) and

the human MTPJ 1 PC score interquartile range (Fig. 5.6b). If one takes the range of MTPJ 1 variation to be a proxy for hallucal joint covariation, then it would appear that humans, who have very stereotypical foot postures and joint loading regimes compared to other anthropoids, correspondingly have a very tight covariation in MTPJ 1 appositional articular surface shape compared to other anthropoids. This result lends some support to my hypothesis that humans should have a tighter relationship between MT head and PP base morphology than other anthropoids due to their stereotypied locomotor and foot posture patterns. Humans were unique in their narrow range of variation on MTPJ 1 compared to other anthropoids, and this perhaps reflected arboreal pedal grasping employed at least in part by the non-human anthropoid groups, or, in the case of gibbons, very little reliance on hind limb driven locomotion (Hunt, 1991). This finding was not found in MTPJ 3 and MTPJ 5, perhaps reflecting the importance of the unique hallucal MTPJ in humans, whose articular surfaces likely must covary very tightly in order to maintain this joint's important biomechanical role in bipedalism.

2B-PLS results were indicative of a high association between metatarsal head shape and phalangeal base shape in anthropoids. The overall degree of association between the two datasets (e.g., RV or preferably the CR coefficient; Adams, 2016) was not performed because the question of modularity and evolvable units was not explored here, rather I sought to explore the association between a specific set of functionally interpretably morphologies at the forefoot joints, such as metatarsal and phalangeal base orientation, MT head robusticity, and the presence of bony correlates associated with "dorsal canting" (see Chapter 4). Since these morphologies were all captured by the largest eigenvectors in the Procrustes analyses, it is likely that these shape changes are those which are summarized in the main PLS axes of both data blocks, which harbor the grand majority of the within and between-block shape variation (> 80% in all cases) in both the metatarsal and phalangeal datasets. For this reason, I relied on the covariance coefficient between the main PLS axes between both blocks, r-PLS. However, within-species r-PLS results tests were all very similar but largely not significant (Table 5.10 – Table 5.11) and did not support my predictions about MTPJ forefoot covariation and locomotor behavior. This may be due to a limitation with this method (and within-species sample sizes for some groups) in that it cannot measure articular surface covariation in functionally meaningful joint postures. In a neutral, mean-centered orientation, it was found that the MTPJs do strongly covary, but the pattern of covariance was not different when group structure was taken into account.

In this way, it can be said that 2B-PLS on multivariate 3D shape data can provide some insight into appositional joint surface covariance in the lower limb like in prior work (Harcourt-Smith et al., 2008; Turley and Frost, 2014), but the functional interpretations stemming from this covariance as measured by 2B-PLS analyses alone are unclear. While this method may have some application for fossil specimen assessment, this usefulness is marred because covariance between block PLS axes rises dramatically when a size proxy (log centroid size) is factored into the cross-covariance matrix. The quantitative finding that larger elements go with correspondingly larger elements is not especially useful in determining fossil specimen associations. Overall, although it has been claimed that 2B-PLS analyses on shape data blocks can serve as a strong proxy for joint congruence (Harcourt-Smith et al., 2008; Turley and Frost, 2014), it is not an especially useful measure of congruence because eigenanalyses don't consider loose and close-packed positions of the joints in question, and the PLS axes are difficult to interpret functionally unlike the linearly uncorrelated axes of a PCA. Therefore, even if the shape covariance data were to equate closely with joint congruence, the covariance data does not allow one to extrapolate in a more detailed manner on the nature of the congruence analysis.

Because relative levels of joint congruence in the foot are of keen interest to hypotheses of pedal functional morphology and evolution (Susman, 1983; Lovejoy et al., 2009), what is needed is an approach that will allow for a more detailed view into joint contact during locomotion. Other novel morphometric techniques have been developed recently and attempts made to quantify joint congruence have included ratios of curvatures and dimensions between appositional surfaces (Peeters et al., 2013) and a polar coordinate approach using a modified Bhattacharyaa distance criterion (Halilaj et al., 2014). While these methodologies are promising, they are sensitive to resolving the proper reference frame of the element, which is not trivial in a comparative morphology study. Ultimately, in order to best examine forefoot joint congruence, cineradiographic and computed tomography (CT) data are needed to visualize joint motion and morphology. New kinematic techniques recently developed such as X-Ray Reconstruction of Moving Morphology (XROMM) would allow for pinpointing that moment in the gait cycle where maximum joint congruency is achieved between the distal metatarsus and the phalangeal base, and it is predicted that this would occur at around the end of stance phase during lift-off. Since it is already known that maximum plantar pressure under the MTPJs is achieved at this time (Vereecke et al., 2003; Griffin et al., 2010a), such a study could potentially tie maximum

plantar pressure and maximum dorsiflexion angle excursions to maximum achieved joint congruency in the MTPJs—a finding that would provide robust support for the hypothesis that maximal joint congruence (i.e., the closed-packed position; MacConaill and Basmajian, 1969) is a critical component of joint stability in the hominin forefoot as some researchers have suggested (Susman, 1983; Susman and Brain, 1988; Susman and de Ruiter, 2004). It is my hope to pursue such an experimental design to help answer these questions about forefoot evolution in forthcoming work. For now, however, morphological correlates of function suggest important and co-evolving roles of the MT head and phalangeal base, and a constrained hallucal MTPJ range of covariation that seems unique to modern humans. Lastly, combined PCAs on multiple forefoot elements allowed for a more complete comparison of MTPJ shape than single element PCAs alone, and ultimately provides a more complete picture of forefoot joint functional morphology.

5.5 References

Adams, D.C., Collyer, M.L., Otárola-Castillo, E., Sherratt, E., 2015. Geomorph: software for geometric morphometric analyses. R package version 3.2.2.

Adams, D.C., 2016. Evaluating modularity in morphometric data: challenges with the RV coefficient and a new test measure. Meth. Ecol. Evol., n/a-n/a.

Almécija, S., Smaers, J.B., Jungers, W.L., 2015. The evolution of human and ape hand proportions. Nat. Commun. 6.

Almécija, S., Tallman, M., Alba, D.M., Pina, M., Moyà-Solà, S., Jungers, W.L., 2013. The femur of *Orrorin tugenensis* exhibits morphometric affinities with both Miocene apes and later hominins. Nat. Commun. 4, 2888.

Bookstein, F.L., Gunz, P., Mitterœcker, P., Prossinger, H., Schæfer, K., Seidler, H., 2003. Cranial integration in *Homo*: singular warps analysis of the midsagittal plane in ontogeny and evolution. J. Hum. Evol. 44, 167-187.

Diawol, V.P., Giri, F., Collins, P.A., 2015. Shape and size variations of *Aegla uruguayana* (Anomura, Aeglidae) under laboratory conditions: a geometric morphometric approach to the growth. Iheringia. Série Zoologia 105, 76-83.

Dryden, I.L., Mardia, K.V., 1998. Statistical shape analysis. J. Wiley Chichester.

Dunbar, R.I.M., Dunbar, E.P., 1974. Ecological relations and niche separation between sympatric terrestrial primates in Ethiopia. Folia Primatol. 21, 36-60.

Griffin, N.L., D'Août, K., Richmond, B., Gordon, A., Aerts, P., 2010. Comparative in vivo forefoot kinematics of *Homo sapiens* and *Pan paniscus*. J. Hum. Evol. 59, 608-619.

Halilaj, E., Laidlaw, D.H., Moore, D.C., Crisco, J.J., 2014. Polar histograms of curvature for quantifying skeletal joint shape and congruence. Journal of Biomechanical Engineering 136, 094503-094503.

Hammond, A.S., 2014. In vivo baseline measurements of hip joint range of motion in suspensory and nonsuspensory anthropoids. Am. J. Phys. Anthropol. 153, 417-434.

Hammond, A.S., Ning, J., Ward, C.V., Ravosa, M.J., 2010. Mammalian limb loading and chondral modeling during ontogeny. The Anatomical Record: Advances in Integrative Anatomy and Evolutionary Biology 293, 658-670.

Hamrick, M.W., 1996. Articular size and curvature as determinants of carpal joint mobility and stability in strepsirhine primates. J. Morphol. 230, 113-127.

Hamrick, M.W., 1999. A chondral modeling theory revisited. Journal of Theoretical Biology 201, 201-208.

Harcourt-Smith, W.E.H., Tallman, M., Frost, S.R., Wiley, D.F., Rohlf, F.J., Delson, E., 2008. Analysis of selected hominoid joint surfaces using laser scanning and geometric morphometrics: a preliminary report, in: Sargis, E.J., Dagosto, M. (Eds.), Mammalian Evolutionary Morphology: A Tribute to Frederick S. Szalay. Springer Netherlands, Dordrecht, pp. 373-383.

Hlaváček, M., Vokoun, D., 1998. The influence of articular surface incongruity on lubrication and contact pressure distribution of loaded synovial joints. Proceedings of the Institution of Mechanical Engineers, Part H: Journal of Engineering in Medicine 212, 11-22.

Holowka, N.B., Fernández, P.J., 2016. Functional morphology of the metatarsophalangeal joints in chimpanzees and humans: a kinematic and morphometric approach. Am. J. Phys. Anthropol. 159, 176.

Hunt, K.D., 1991. Positional behavior in the hominoidea. Int J Primatol 12, 95-118.

Jungers, W.L., Harcourt-Smith, W.E.H., Wunderlich, R.E., Tocheri, M.W., Larson, S.G., Sutikna, T., Due, R.A., Morwood, M.J., 2009. The foot of *Homo floresiensis*. Nature 459, 81-84.

Kelkar, R., Wang, V.M., Flatow, E.L., Newton, P.M., Ateshian, G.A., Bigliani, L.U., Pawluk, R.J., Mow, V.C., 2001. Glenohumeral mechanics: A study of articular geometry, contact, and kinematics. Journal of Shoulder and Elbow Surgery 10, 73-84.

Laroche, D., Pozzo, T., Ornetti, P., Tavernier, C., Maillefert, J.F., 2006. Effects of loss of metatarsophalangeal joint mobility on gait in rheumatoid arthritis patients. Rheumatology 45, 435-440.

Lewis, O.J., 1972. The evolution of the hallucial tarsometatarsal joint in the anthropoidea. Am. J. Phys. Anthropol. 37, 13-33.

Lovejoy, C.O., Latimer, B., Suwa, G., Asfaw, B., White, T.D., 2009. Combining prehension and propulsion: the foot of *Ardipithecus ramidus*. Science 326, 72, 72e71-72e78.

MacConaill, M.A., Basmajian, J.V., 1969. Muscles and movements. Williams & Williams Baltimore.

MacLatchy, L.M., 1996. Another look at the australopithecine hip. J. Hum. Evol. 31, 455-476.

MacLatchy, L.M., Bossert, W.H., 1996. An analysis of the articular surface distribution of the femoral head and acetabulum in anthropoids, with implications for hip function in Miocene hominoids. J. Hum. Evol. 31, 425-453.

McNulty, K.P., 2009. Computing singular warps from Procrustes aligned coordinates. J. Hum. Evol. 57, 191-194.

Meldrum, D.J., 1991. Kinematics of the cercopithecine foot on arboreal and terrestrial substrates with implications for the interpretation of hominid terrestrial adaptations. Am. J. Phys. Anthropol. 84, 273-289.

Mitteroecker, P., Gunz, P., 2009. Advances in geometric morphometrics. Evolutionary Biology 36, 235-247.

Nakagawa, N., 1989. Activity budget and diet of patas monkeys in Kala Maloue National Park, Cameroon: a preliminary report. Primates 30, 27-34.

Orr, C.M., 2005. Knuckle-walking anteater: a convergence test of adaptation for purported knuckle-walking features of african Hominidae. Am. J. Phys. Anthropol. 128, 639-658.

Patel, B., Polk, J., 2010. Distal forelimb kinematics in *Erythrocebus patas* and *Papio anubis* during walking and galloping. International Journal of Primatology 31, 191-207.

Patel, B.A., 2009. Not so fast: speed effects on forelimb kinematics in cercopithecine monkeys and implications for digitigrade postures in primates. Am. J. Phys. Anthropol. 140, 92-112.

Peeters, K., Schreuer, J., Burg, F., Behets, C., Van Bouwel, S., Dereymaeker, G., Sloten, J.V., Jonkers, I., 2013. Alterated talar and navicular bone morphology is associated with pes planus deformity: a CT-scan study. Journal of Orthopaedic Research 31, 282-287.

Rohlf, F.J., Corti, M., 2000. Use of two-block partial least-squares to study covariation in shape. Sys. Biol. 49, 740-753.

Schmitt, D., Larson, S.G., 1995. Heel contact as a function of substrate type and speed in primates. Am. J. Phys. Anthropol. 96, 39-50.

Seiffert, E.R., Perry, J.M.G., Simons, E.L., Boyer, D.M., 2009. Convergent evolution of anthropoid-like adaptations in Eocene adapiform primates. Nature 461, 1118-1121.

Susman, R.L., 1983. Evolution of the human foot: evidence from Plio-Pleistocene hominids. Foot Ankle 3, 365-376.

Susman, R.L., Brain, T.M., 1988. New first metatarsal (SKX 5017) from Swartkrans and the gait of *Paranthropus robustus*. Am. J. Phys. Anthropol. 77, 7-15.

Susman, R.L., de Ruiter, D.J., 2004. New hominin first metatarsal (SK 1813) from Swartkrans. J. Hum. Evol. 47, 171-181.

Turley, K., Frost, S.R., 2014. The appositional articular morphology of the talo-crural joint: the influence of substrate use on joint shape. Anat. Rec. 297, 618-629.

Vereecke, E., D'Août, K., De Clercq, D., Van Elsacker, L., Aerts, P., 2003. Dynamic plantar pressure distribution during terrestrial locomotion of bonobos (*Pan paniscus*). Am. J. Phys. Anthropol. 120, 373-383.

Waide, D.V., Lawlor, G.J., McCormack, B.A.O., Carr, A.J., 2000. The relationship between surface topography and contact in the elbow joint: development of a two-dimensional geometrical model in the coronal plane. Proceedings of the Institution of Mechanical Engineers, Part H: Journal of Engineering in Medicine 214, 413-423.

Watson, H., Weinzweig, J., 1998. Stiff joints, in: Green, D. (Ed.), Operative hand surgery. Churchill Livingstone New York, pp. 552-562.

Wiley, D.F., Amenta, N., Alcantara, D.A., Ghosh, D., Kil, Y.J., Delson, E., Harcourt-Smith, W.E.H., Rohlf, F.J., John, K.S., Hamann, B., 2005. Evolutionary morphing IEEE Visualization Conference, Minneapolis, MN, 431-438.

Taxon	**Locomotor Mode[1]**	**Foot Posture[2]**	**µCT**	**CT**	**Laser Scan**
Hominoids					
Homo sapiens	B	FCP	-	21	18
Gorilla beringei beringei	KW/C	IHSP	-	3	12
Gorilla beringei graueri	KW/C	IHSP	-	1	11
Gorilla gorilla gorilla	KW/C	IHSP	-	4	26
Pan paniscus	KW/C	IHSP	-	1	17
Pan troglodytes	KW/C	IHSP	-	5	30
Pongo abelii	S	IHSP	-	-	5
Pongo pygmaeus	S	IHSP	-	-	9
Hylobates lar	R	MFP	16	-	-
Cercopithecoids (OWMs)					
Chlorocebus aethiops	TQ	DG/SP	9	-	-
Erythrocebus patas	TQ	DG	17	-	-
Macaca fascicularis	TQ	DG/SP	10	-	-
Macaca mulatta	TQ	DG/SP	16	-	-
Macaca nemestrina	TQ	DG/SP	7	-	-
Papio ursinus	TQ	DG/SP	12	-	-
Nasalis larvatus	AQ	DG/SP	16	-	-
Presbytis rubicunda	AQ	DG/SP	-	-	13
Ceboids (NWMs)					
Alouatta seniculus	AQ	DG/SP	16	-	-
Ateles fusciceps	AQ/S	DG/SP	13	-	-
Cebus apella	AQ	DG/SP	6	-	-

Table 5.1. **Extant anthropoids included in MTPJ 1 shape analyses.** See Table 2.1 for abbreviation key.

Taxon	**Locomotor Mode[1]**	**Foot Posture[2]**	**µCT**	**CT**	**Laser Scan**
Hominoids					
Homo sapiens	B	FCP	-	15	13
Gorilla beringei beringei	KW/C	IHSP	-	2	5
Gorilla beringei graueri	KW/C	IHSP	-	3	11
Gorilla gorilla gorilla	KW/C	IHSP	-	4	22
Pan paniscus	KW/C	IHSP	-	1	13
Pan troglodytes	KW/C	IHSP	-	7	27
Pongo abelii	S	IHSP	-	-	9
Pongo pygmaeus	S	IHSP	-	-	11
Hylobates lar	R	MFP	9	-	-
Cercopithecoids (OWMs)					
Chlorocebus aethiops	TQ	DG/SP	7	-	-
Erythrocebus patas	TQ	DG	16	-	-
Macaca fascicularis	TQ	DG/SP	10	-	-
Macaca mulatta	TQ	DG/SP	16	-	-
Macaca nemestrina	TQ	DG/SP	6	-	-
Papio ursinus	TQ	DG/SP	-	-	-
Nasalis larvatus	AQ	DG/SP	10	-	-
Presbytis rubicunda	AQ	DG/SP	-	-	20
Ceboids (NWMs)					
Alouatta seniculus	AQ	DG/SP	13	-	-
Ateles fusciceps	AQ/S	DG/SP	5	-	-
Cebus apella	AQ	DG/SP	4	-	-

Table 5.2. Extant anthropoids included in MTPJ 3 shape analyses. See Table 2.1 for abbreviation key.

Taxon	**Locomotor Mode[1]**	**Foot Posture[2]**	**µCT**	**CT**	**Laser Scan**
Hominoids					
Homo sapiens	B	FCP	-	15	8
Gorilla beringei beringei	KW/C	IHSP	-	2	5
Gorilla beringei graueri	KW/C	IHSP	-	2	10
Gorilla gorilla gorilla	KW/C	IHSP	-	4	22
Pan paniscus	KW/C	IHSP	-	1	11
Pan troglodytes	KW/C	IHSP	-	7	27
Pongo abelii	S	IHSP	-	-	8
Pongo pygmaeus	S	IHSP	-	-	10
Cercopithecoids (OWMs)					
Chlorocebus aethiops	TQ	DG/SP	5	-	-
Erythrocebus patas	TQ	DG	14	-	-
Macaca fascicularis	TQ	DG/SP	5	-	-
Nasalis larvatus	AQ	DG/SP	2	-	-
Presbytis rubicunda	AQ	DG/SP	-	-	15
Ceboids (NWMs)					
Alouatta seniculus	AQ	DG/SP	3	-	-
Cebus apella	AQ	DG/SP	2	-	-

Table 5.3. Extant anthropoids included in MTPJ 5 shape analyses. See Table 2.1 for abbreviation key.

MT Accession Number	PP Accession Number	Ray	Taxon	Locality	Observation
A.L. 333-115 (A)	A.L. 333-115 (F)	1	*Au. afarensis*	Hadar, Ethiopia	Cast (LS)
LB1/21	LB1/42D*	1	*Au. afarensis*	Liang Bua, Indonesia	Original (CT)
U.W.101-1443	U.W.101-1419	1	*H. naledi*	Gauteng, South Africa	Original (CT)
KNM-ER 64062	KNM-ER 64062	1	*H.* sp. (cf. *erectus*)	Hadar, Ethiopia	Original (μCT)
ARA-VP-6/500-505	ARA-VP-6/500-008	3	*Ar. ramidus*	Aramis, Ethiopia	Original (μCT)
A.L. 333-115 (C)	A.L. 333-115 (H)	3	*Au. afarensis*	Hadar, Ethiopia	Cast (LS)
A.L. 333-72	A.L. 333w-51*	3	*Au. afarensis*	Above KBS tuff, Ileret	Original (μCT)
LB1/23	LB1/36	3	*Homo floresiensis*	Liang Bua, Indonesia	Original (CT)
A.L. 333-115 (E)	A.L. 333-115 (J)	5	*Au. afarensis*	Aramis, Ethiopia	Cast (LS)
LB1/25	LB1/34	5	*Homo floresiensis*	Liang Bua, Indonesia	Original (CT)

Table 5.4. **Fossil hominins included in the MTPJ shape covariance analyses.** Please see text (Materials and Methods) for geological age estimates and taxonomic determinations. *Chimeric specimen. LB1/42D is an unpublished hallucal phalanx from Liang Bua (Dingwall et al., 2014), see Chapter 4 for details. See Chapters 2-4 (Materials and Methods) for age estimates and taxonomic affiliation justifications. Other fossils described elsewhere (Latimer et al., 1982; Jungers et al., 2009 Lovejoy et al., 2009; Jungers et al., 2015; Harcourt-Smith et al., 2015).

Species	*A. seniculus*	*A. fusciceps*	*C. apella*	*C. aethiops*	*E. patas*	*M. mulatta*	*M. nemestrina*	*M. fascicularis*	*P. ursinus*	*N. larvatus*	*P. rubicunda*
A. seniculus	1.0000	-	-	-	-	-	-	-	-	-	-
A. fusciceps	ns	1.0000	-	-	-	-	-	-	-	-	-
C. apella	ns	ns	1.0000	-	-	-	-	-	-	-	-
C. aethiops	ns	ns	**<0.05**	1.0000	-	-	-	-	-	-	-
E. patas	**<0.0001**	**<0.0001**	**<0.0001**	**<0.01**	1.0000	-	-	-	-	-	-
M. mulatta	**<0.05**	ns	**<0.01**	ns	**<0.0001**	1.0000	-	-	-	-	-
M. nemestrina	**<0.0001**	**<0.0001**	**<0.0001**	**<0.01**	ns	**<0.0001**	1.0000	-	-	-	-
M. fascicularis	**<0.05**	ns	**<0.01**	ns	**<0.01**	ns	**<0.05**	1.0000	-	-	-
P. ursinus	**<0.0001**	**<0.0001**	**<0.0001**	**<0.05**	ns	**<0.01**	ns	ns	1.0000	-	-
N. larvatus	**<0.0001**	**<0.0001**	**<0.0001**	**<0.0001**	ns	**<0.0001**	ns	**<0.0001**	ns	1.0000	-
P. rubicunda	**<0.0001**	**<0.05**	**<0.0001**	ns	ns	ns	ns	ns	ns	ns	1.0000
H. lar	**<0.0001**	**<0.0001**	**<0.0001**	ns	ns	**<0.05**	ns	ns	ns	ns	ns
P. abelii	**<0.0001**	**<0.0001**	**<0.0001**	**<0.0001**	ns	**<0.0001**	ns	**<0.0001**	ns	ns	**<0.05**
P. pygmaeus	**<0.0001**	**<0.0001**	**<0.0001**	**<0.0001**	**<0.0001**	**<0.0001**	**<0.05**	**<0.0001**	**<0.0001**	**<0.01**	**<0.0001**
G.b. beringei	**<0.0001**	**<0.0001**	**<0.0001**	**<0.0001**	**<0.0001**	**<0.0001**	**<0.0001**	**<0.0001**	**<0.0001**	**<0.0001**	**<0.0001**
G.g. gorilla	**<0.0001**	**<0.0001**	**<0.0001**	**<0.0001**	**<0.0001**	**<0.0001**	**<0.0001**	**<0.0001**	**<0.0001**	**<0.0001**	**<0.0001**
G.b. graueri	**<0.0001**	**<0.0001**	**<0.0001**	**<0.0001**	**<0.0001**	**<0.0001**	**<0.0001**	**<0.0001**	**<0.0001**	**<0.0001**	**<0.0001**
P. paniscus	**<0.0001**	**<0.0001**	**<0.0001**	**<0.0001**	ns	**<0.0001**	ns	**<0.0001**	ns	ns	**<0.05**
P. troglodytes	**<0.0001**	**<0.0001**	**<0.0001**	**<0.0001**	**<0.05**	**<0.0001**	ns	**<0.0001**	**<0.0001**	ns	**<0.0001**
H. sapiens	**<0.0001**	**<0.0001**	**<0.0001**	**<0.0001**	**<0.0001**	**<0.0001**	**<0.0001**	**<0.0001**	**<0.0001**	**<0.0001**	**<0.0001**

(Continued on next page)

Table 5.5 ***Post-hoc*** **Tukey's HSD results on PC 1 comparing anthropoid genera following a MANOVA on MTPJ 1 shape variables (PC 1 - 5)**. PC 1 principally tracked phalangeal base convexity, phalangeal base ovoid form, and plantar tubercle morphology. Apes and monkeys are completely different from each other on this axis. Bold = significance at $\alpha = 0.05$.

Species	*H. lar*	*P. abelii*	*P. pygmaeus*	*G. b. beringei*	*G.g. gorilla*	*G.b. graueri*	*P. paniscus*	*P. troglodytes*	*H. sapiens*
A. seniculus	-	-	-	-	-	-	-	-	-
A. fusciceps	-	-	-	-	-	-	-	-	-
C. apella	-	-	-	-	-	-	-	-	-
C. aethiops	-	-	-	-	-	-	-	-	-
E. patas	-	-	-	-	-	-	-	-	-
M. mulatta	-	-	-	-	-	-	-	-	-
M. nemestrina	-	-	-	-	-	-	-	-	-
M. fascicularis	-	-	-	-	-	-	-	-	-
P. ursinus	-	-	-	-	-	-	-	-	-
N. larvatus	-	-	-	-	-	-	-	-	-
P. rubicunda	-	-	-	-	-	-	-	-	-
H. lar	1.0000	-	-	-	-	-	-	-	-
P. abelii	ns	1.0000	-	-	-	-	-	-	-
P. pygmaeus	**<0.0001**	ns	1.0000	-	-	-	-	-	-
G. b. beringei	**<0.0001**	**<0.0001**	**<0.01**	1.0000	-	-	-	-	-
G.b. gorilla	**<0.0001**	**<0.01**	ns	ns	1.0000	-	-	-	-
G.g. graueri	**<0.0001**	ns	ns	ns	ns	1.0000	-	-	-
P. paniscus	ns	ns	**<0.01**	**<0.0001**	**<0.0001**	**<0.0001**	1.0000	-	-
P. troglodytes	**<0.0001**	ns	ns	**<0.0001**	**<0.0001**	**<0.0001**	ns	1.0000	-
H. sapiens	**<0.0001**	**<0.0001**	**<0.0001**	ns	**<0.0001**	**<0.0001**	**<0.0001**	**<0.0001**	1.0000

Table 5.5 *Post-hoc* Tukey's HSD results on PC 1 comparing anthropoid genera following a MANOVA on MTPJ 1 shape variables (PC 1 - 5). PC 1 principally tracked phalangeal base convexity, phalangeal base ovoid form, and plantar tubercle morphology. Apes and monkeys are completely different from each other on this axis. Bold = significance at $\alpha = 0.05$.

Species	*A. seniculus*	*A. fusciceps*	*C. apella*	*C. aethiops*	*E. patas*	*M. mulatta*	*M. nemestrina*	*M. fascicularis*	*P. ursinus*	*N. larvatus*	*P. rubicunda*
A. seniculus	1.0000	-	-	-	-	-	-	-	-	-	-
A. fusciceps	ns	1.0000	-	-	-	-	-	-	-	-	-
C. apella	ns	ns	1.0000	-	-	-	-	-	-	-	-
C. aethiops	ns	**<0.01**	**<0.05**	1.0000	-	-	-	-	-	-	-
E. patas	**<0.0001**	**<0.0001**	**<0.0001**	ns	1.0000	-	-	-	-	-	-
M. mulatta	ns	**<0.01**	ns	ns	ns	1.0000	-	-	-	-	-
M. nemestrina	**<0.01**	**<0.0001**	**<0.01**	ns	ns	ns	1.0000	-	-	-	-
M. fascicularis	ns	**<0.05**	ns	ns	ns	ns	ns	1.0000	-	-	-
P. ursinus	**<0.05**	**<0.01**	**<0.05**	ns	ns	ns	ns	ns	1.0000	-	-
N. larvatus	ns	ns	ns	ns	**<0.05**	ns	ns	ns	ns	1.0000	-
P. rubicunda	ns	ns	ns	**<0.01**	**<0.0001**	**<0.01**	**<0.0001**	**<0.05**	**<0.0001**	ns	1.0000
H. lar	ns	ns	ns	**<0.05**	**<0.0001**	**<0.05**	**<0.0001**	ns	**<0.01**	ns	ns
P. abelii	ns	ns	ns	**<0.0001**	**<0.0001**	**<0.0001**	**<0.0001**	**<0.0001**	**<0.0001**	**<0.01**	ns
P. pygmaeus	**<0.0001**	**<0.01**	ns	**<0.0001**	**<0.0001**	**<0.0001**	**<0.0001**	**<0.0001**	**<0.0001**	**<0.0001**	**<0.01**
G. b. beringei	**<0.05**	ns	ns	**<0.0001**	**<0.0001**	**<0.0001**	**<0.0001**	**<0.0001**	**<0.0001**	**<0.0001**	ns
G.g. gorilla	**<0.0001**	**<0.01**	ns	**<0.0001**	**<0.0001**	**<0.0001**	**<0.0001**	**<0.0001**	**<0.0001**	**<0.0001**	**<0.05**
G.b. graueri	ns	ns	ns	ns	**<0.0001**	ns	**<0.01**	ns	ns	ns	ns
P. paniscus	**<0.0001**	**<0.01**	ns	**<0.0001**	**<0.0001**	**<0.0001**	**<0.0001**	**<0.0001**	**<0.0001**	**<0.0001**	**<0.01**
P. troglodytes	ns	ns	ns	**<0.01**	**<0.0001**	**<0.01**	**<0.0001**	**<0.05**	**<0.0001**	ns	ns
H. sapiens	**<0.0001**	**<0.0001**	**<0.0001**	ns	ns	ns	ns	ns	ns	**<0.05**	**<0.0001**

(Continued on next page)

Table 5.6 ***Post-hoc*** **Tukey's HSD results on PC 2 comparing anthropoid genera following a MANOVA on MTPJ 1 shape variables (PC 1 - 5)**. PC 2 principally tracked MT head robusticity. Humans overlap with the more terrestrial cercopithecoids on this axis, to the exclusion of NWMs and apes. Bold = significance at $\alpha = 0.05$.

Species	*H. lar*	*P. abelii*	*P. pygmaeus*	*G. b. beringei*	*G.g. gorilla*	*G.b. graueri*	*P. paniscus*	*P. troglodytes*	*H. sapiens*
A. seniculus	-	-	-	-	-	-	-	-	-
A. fusciceps	-	-	-	-	-	-	-	-	-
C. apella	-	-	-	-	-	-	-	-	-
C. aethiops	-	-	-	-	-	-	-	-	-
E. patas	-	-	-	-	-	-	-	-	-
M. mulatta	-	-	-	-	-	-	-	-	-
M. nemestrina	-	-	-	-	-	-	-	-	-
M. fascicularis	-	-	-	-	-	-	-	-	-
P. ursinus	-	-	-	-	-	-	-	-	-
N. larvatus	-	-	-	-	-	-	-	-	-
P. rubicunda	-	-	-	-	-	-	-	-	-
H. lar	1.0000	-	-	-	-	-	-	-	-
P. abelii	ns	1.0000	-	-	-	-	-	-	-
P. pygmaeus	**<0.0001**	ns	1.0000	-	-	-	-	-	-
G. b. beringei	ns	ns	ns	1.0000	-	-	-	-	-
G.g. gorilla	**<0.0001**	ns	ns	ns	1.0000	-	-	-	-
G.b. graueri	ns	ns	**<0.0001**	**<0.05**	**<0.0001**	1.0000	-	-	-
P. paniscus	**<0.0001**	ns	ns	ns	ns	**<0.0001**	1.0000	-	-
P. troglodytes	ns	ns	**<0.0001**	ns	**<0.0001**	ns	**<0.0001**	1.0000	-
H. sapiens	**<0.0001**	**<0.0001**	**<0.0001**	**<0.0001**	**<0.0001**	**<0.0001**	**<0.0001**	**<0.0001**	1.0000

Table 5.6 *Post-hoc* Tukey's HSD results on PC 2 comparing anthropoid genera following a MANOVA on MTPJ 1 shape variables (PC 1 - 5). PC 2 principally tracked MT head robusticity. Humans overlap with the more terrestrial cercopithecoids on this axis, to the exclusion of NWMs and apes. Bold = significance at $\alpha = 0.05$.

.

Species	*A. seniculus*	*A. fusciceps*	*C. apella*	*C. aethiops*	*E. patas*	*M. mulatta*	*M. nemestrina*	*M. fascicularis*	*P. ursinus*	*N. larvatus*	*P. rubicunda*
A. seniculus	1.0000	-	-	-	-	-	-	-	-	-	-
A. fusciceps	ns	1.0000	-	-	-	-	-	-	-	-	-
C. apella	ns	**<0.0001**	1.0000	-	-	-	-	-	-	-	-
C. aethiops	**<0.0001**	**<0.0001**	ns	1.0000	-	-	-	-	-	-	-
E. patas	**<0.0001**	**<0.0001**	ns	ns	1.0000	-	-	-	-	-	-
M. mulatta	**<0.0001**	**<0.0001**	**<0.01**	ns	ns	1.0000	-	-	-	-	-
M. nemestrina	**<0.0001**	**<0.0001**	ns	ns	ns	ns	1.0000	-	-	-	-
M. fascicularis	ns	**<0.0001**	ns	ns	ns	**<0.0001**	ns	1.0000	-	-	-
P. ursinus	**<0.0001**	**<0.0001**	ns	ns	ns	**<0.05**	ns	ns	1.0000	-	-
N. larvatus	ns	**<0.05**	ns	**<0.01**	**<0.0001**	**<0.0001**	**<0.01**	ns	**<0.05**	1.0000	-
P. rubicunda	**<0.01**	**<0.0001**	ns	ns	ns	**<0.0001**	ns	ns	ns	ns	1.0000
H. lar	**<0.0001**	**<0.0001**	ns	ns	ns	**<0.01**	ns	ns	ns	**<0.05**	ns
P. abelii	ns	**<0.01**	ns	ns	ns	**<0.01**	ns	ns	ns	ns	ns
P. pygmaeus	**<0.0001**	**<0.0001**	ns	ns	ns	ns	ns	ns	ns	**<0.01**	ns
G.b. beringei	**<0.0001**	**<0.0001**	ns	ns	ns	**<0.0001**	ns	ns	ns	ns	ns
G.g. gorilla	**<0.0001**	**<0.0001**	ns	ns	ns	**<0.01**	ns	ns	ns	**<0.0001**	ns
G.b. graueri	**<0.0001**	**<0.0001**	ns	ns	ns	**<0.01**	ns	ns	ns	ns	ns
P. paniscus	**<0.01**	**<0.0001**	ns	ns	ns	**<0.0001**	ns	ns	ns	ns	ns
P. troglodytes	**<0.0001**	**<0.0001**	ns	ns	ns	**<0.0001**	ns	ns	ns	ns	ns
H. sapiens	ns	**<0.01**	ns	**<0.0001**	**<0.0001**	**<0.0001**	**<0.0001**	ns	**<0.0001**	ns	**<0.01**

(Continued on next page)

Table 5.7 *Post-hoc* Tukey's HSD results on PC 3 comparing anthropoid genera following a MANOVA on MTPJ 1 shape variables (PC 1 - 5). PC 3 principally tracked MT head orientation, amongst other shape changes. The linear combination of shape variables PC 1 and PC 3 serve to separate modern humans and hominins from the rest of the anthropoid sample. Bold = significance at $\alpha = 0.05$.

Species	*H. lar*	*P. abelii*	*P. pygmaeus*	*G.b. beringei*	*G.g. gorilla*	*G.b. graueri*	*P. paniscus*	*P. troglodytes*	*H. sapiens*
A. seniculus	-	-	-	-	-	-	-	-	-
A. fusciceps	-	-	-	-	-	-	-	-	-
C. apella	-	-	-	-	-	-	-	-	-
C. aethiops	-	-	-	-	-	-	-	-	-
E. patas	-	-	-	-	-	-	-	-	-
M. mulatta	-	-	-	-	-	-	-	-	-
M. nemestrina	-	-	-	-	-	-	-	-	-
M. fascicularis	-	-	-	-	-	-	-	-	-
P. ursinus	-	-	-	-	-	-	-	-	-
N. larvatus	-	-	-	-	-	-	-	-	-
P. rubicunda	-	-	-	-	-	-	-	-	-
H. lar	1.0000	-	-	-	-	-	-	-	-
P. abelii	ns	1.0000	-	-	-	-	-	-	-
P. pygmaeus	ns	ns	1.0000	-	-	-	-	-	-
G b.. beringei	ns	ns	ns	1.0000	-	-	-	-	-
G.g. gorilla	ns	ns	ns	ns	1.0000	-	-	-	-
G.b. graueri	ns	ns	ns	ns	ns	1.0000	-	-	-
P. paniscus	ns	ns	ns	ns	ns	ns	1.0000	-	-
P. troglodytes	ns	ns	ns	ns	ns	ns	ns	1.0000	-
H. sapiens	**<0.0001**	ns	**<0.0001**	**<0.0001**	**<0.0001**	**<0.0001**	**<0.0001**	**<0.0001**	1.0000

Table 5.7 ***Post-hoc*** **Tukey's HSD results on PC 3 comparing anthropoid genera following a MANOVA on MTPJ 1 shape variables (PC 1 - 5)**. PC 3 principally tracked MT head orientation, amongst other shape changes. The linear combination of shape variables PC 1 and PC 3 serve to separate modern humans and hominins from the rest of the anthropoid sample. Bold = significance at $\alpha = 0.05$.

Species	*A. seniculus*	*A. fusciceps*	*C. apella*	*C. aethiops*	*E. patas*	*M. mulatta*	*M. nemestrina*	*M. fascicularis*	*N. larvatus*	*P. rubicunda*
A. seniculus	1.0000	-	-	-	-	-	-	-	-	-
A. fusciceps	ns	1.0000	-	-	-	-	-	-	-	-
C. apella	**<0.0001**	**<0.0001**	1.0000	-	-	-	-	-	-	-
C. aethiops	**<0.0001**	**<0.0001**	**<0.0001**	1.0000	-	-	-	-	-	-
E. patas	**<0.0001**	**<0.0001**	**<0.0001**	ns	1.0000	-	-	-	-	-
M. mulatta	**<0.0001**	**<0.0001**	ns	ns	**<0.01**	1.0000	-	-	-	-
M. nemestrina	**<0.0001**	**<0.0001**	ns	**<0.01**	**<0.0001**	ns	1.0000	-	-	-
M. fascicularis	**<0.0001**	**<0.0001**	ns	**<0.01**	**<0.01**	ns	ns	1.0000	-	-
N. larvatus	**<0.0001**	**<0.0001**	ns	**<0.0001**	**<0.0001**	**<0.05**	ns	ns	1.0000	-
P. rubicunda	**<0.0001**	**<0.0001**	ns	ns	ns	ns	ns	ns	**<0.01**	1.0000
H. lar	**<0.0001**	**<0.01**	**<0.0001**	**<0.0001**	**<0.0001**	**<0.0001**	**<0.0001**	**<0.0001**	**<0.0001**	**<0.0001**
P. abelii	**<0.0001**	**<0.01**	**<0.0001**	**<0.0001**	**<0.0001**	**<0.0001**	**<0.0001**	**<0.0001**	**<0.0001**	**<0.0001**
P. pygmaeus	**<0.0001**	**<0.0001**	**<0.0001**	**<0.0001**	**<0.0001**	**<0.0001**	**<0.0001**	**<0.0001**	**<0.0001**	**<0.0001**
G.b. beringei	**<0.0001**	**<0.0001**	**<0.0001**	**<0.0001**	**<0.0001**	**<0.0001**	**<0.0001**	**<0.0001**	**<0.0001**	**<0.0001**
G.g. gorilla	**<0.0001**	**<0.0001**	**<0.0001**	**<0.0001**	**<0.0001**	**<0.0001**	**<0.0001**	**<0.0001**	**<0.0001**	**<0.0001**
G.b. graueri	**<0.0001**	**<0.0001**	**<0.0001**	**<0.0001**	**<0.0001**	**<0.0001**	**<0.0001**	**<0.0001**	**<0.0001**	**<0.0001**
P. paniscus	**<0.0001**	ns	**<0.0001**	**<0.0001**	**<0.0001**	**<0.0001**	**<0.0001**	**<0.0001**	**<0.0001**	**<0.0001**
P. troglodytes	**<0.0001**	**<0.01**	**<0.0001**	**<0.0001**	**<0.0001**	**<0.0001**	**<0.0001**	**<0.0001**	**<0.0001**	**<0.0001**
H. sapiens	**<0.0001**	ns	**<0.0001**	**<0.0001**	**<0.0001**	**<0.0001**	**<0.0001**	**<0.0001**	**<0.0001**	**<0.0001**

(Continued on next page)

Table 5.8 *Post-hoc* Tukey's HSD results on PC 1 comparing anthropoid genera following a MANOVA on MTPJ 3 shape variables (PC 1 - 5). PC 1 principally tracked phalangeal base convexity, phalangeal base ovoid form, and plantar tubercle morphology. Apes and monkeys are completely different from each other on this axis. Bold = significance at $\alpha = 0.05$.

Species	*H. lar*	*P. abelii*	*P. pygmaeus*	*G b.. beringei*	*G.b. gorilla*	*G.g. graueri*	*P. paniscus*	*P. troglodytes*	*H. sapiens*
A. seniculus	-	-	-	-	-	-	-	-	-
A. fusciceps	-	-	-	-	-	-	-	-	-
C. apella	-	-	-	-	-	-	-	-	-
C. aethiops	-	-	-	-	-	-	-	-	-
E. patas	-	-	-	-	-	-	-	-	-
M. mulatta	-	-	-	-	-	-	-	-	-
M. nemestrina	-	-	-	-	-	-	-	-	-
M. fascicularis	-	-	-	-	-	-	-	-	-
P. ursinus	-	-	-	-	-	-	-	-	-
N. larvatus	-	-	-	-	-	-	-	-	-
P. rubicunda	-	-	-	-	-	-	-	-	-
H. lar	1.0000	-	-	-	-	-	-	-	-
P. abelii	ns	1.0000	-	-	-	-	-	-	-
P. pygmaeus	ns	ns	1.0000	-	-	-	-	-	-
G.b. beringei	**<0.01**	ns	ns	1.0000	-	-	-	-	-
G.g. gorilla	ns	ns	ns	ns	1.0000	-	-	-	-
G.b. graueri	**<0.0001**	**<0.0001**	**<0.0001**	ns	**<0.0001**	1.0000	-	-	-
P. paniscus	ns	ns	ns	**<0.0001**	**<0.01**	**<0.0001**	1.0000	-	-
P. troglodytes	ns	ns	ns	**<0.0001**	**<0.01**	**<0.0001**	ns	1.0000	-
H. sapiens	ns	ns	**<0.05**	**<0.0001**	**<0.0001**	**<0.0001**	ns	ns	1.0000

Table 5.8 *Post-hoc* Tukey's HSD results on PC 1 comparing anthropoid genera following a MANOVA on MTPJ 3 shape variables (PC 1 - 5). PC 1 principally tracked phalangeal base convexity, phalangeal base ovoid form, and plantar tubercle morphology. Apes and monkeys are completely different from each other on this axis. Bold = significance at $\alpha = 0.05$.

Species	*A. seniculus*	*A. fusciceps*	*C. apella*	*C. aethiops*	*E. patas*	*M. mulatta*	*M. nemestrina*	*M. fascicularis*	*N. larvatus*	*P. rubicunda*
A. seniculus	1.0000	-	-	-	-	-	-	-	-	-
A. fusciceps	ns	1.0000	-	-	-	-	-	-	-	-
C. apella	ns	ns	1.0000	-	-	-	-	-	-	-
C. aethiops	ns	ns	ns	1.0000	-	-	-	-	-	-
E. patas	**<0.0001**	**<0.0001**	**<0.0001**	**<0.0001**	1.0000	-	-	-	-	-
M. mulatta	ns	ns	ns	ns	**<0.0001**	1.0000	-	-	-	-
M. nemestrina	ns	ns	ns	ns	**<0.0001**	ns	1.0000	-	-	-
M. fascicularis	ns	ns	ns	ns	**<0.0001**	ns	ns	1.0000	-	-
N. larvatus	**<0.05**	**<0.01**	ns	ns	**<0.0001**	ns	ns	**<0.01**	1.0000	-
P. rubicunda	ns	ns	ns	ns	**<0.0001**	ns	ns	ns	**<0.05**	1.0000
H. lar	ns	ns	ns	ns	**<0.0001**	ns	ns	ns	**<0.05**	ns
P. abelii	**<0.0001**	**<0.0001**	**<0.01**	**<0.05**	**<0.0001**	**<0.0001**	**<0.0001**	**<0.0001**	ns	**<0.0001**
P. pygmaeus	**<0.0001**	**<0.0001**	**<0.01**	**<0.01**	**<0.0001**	**<0.0001**	**<0.0001**	**<0.0001**	ns	**<0.0001**
G.b. beringei	ns	ns	ns	ns	**<0.0001**	ns	ns	ns	ns	ns
G.g. gorilla	ns	ns	ns	ns	**<0.0001**	ns	ns	ns	ns	ns
G.b. graueri	ns	ns	ns	ns	**<0.0001**	ns	ns	ns	ns	ns
P. paniscus	ns	ns	ns	**<0.05**	**<0.0001**	**<0.05**	ns	ns	**<0.0001**	ns
P. troglodytes	ns	ns	ns	ns	**<0.0001**	ns	ns	ns	ns	ns
H. sapiens	**<0.0001**	**<0.0001**	**<0.0001**	**<0.0001**	ns	**<0.0001**	**<0.0001**	**<0.0001**	**<0.0001**	**<0.0001**

(Continued on next page)

Table 5.9 *Post-hoc* Tukey's HSD results on PC 2 comparing anthropoid genera following a MANOVA on MTPJ 3 shape variables (PC 1 - 5). PC 2 principally tracked MT head orientation. The cursorial patas monkey and modern humans overlap to the exclusion of all other groups. Bold = significance at $\alpha = 0.05$.

Species	*H. lar*	*P. abelii*	*P. pygmaeus*	*G.b. beringei*	*G.g. gorilla*	*G.b. graueri*	*P. paniscus*	*P. troglodytes*	*H. sapiens*
A. seniculus	-	-	-	-	-	-	-	-	-
A. fusciceps	-	-	-	-	-	-	-	-	-
C. apella	-	-	-	-	-	-	-	-	-
C. aethiops	-	-	-	-	-	-	-	-	-
E. patas	-	-	-	-	-	-	-	-	-
M. mulatta	-	-	-	-	-	-	-	-	-
M. nemestrina	-	-	-	-	-	-	-	-	-
M. fascicularis	-	-	-	-	-	-	-	-	-
P. ursinus	-	-	-	-	-	-	-	-	-
N. larvatus	-	-	-	-	-	-	-	-	-
P. rubicunda	-	-	-	-	-	-	-	-	-
H. lar	1.0000	-	-	-	-	-	-	-	-
P. abelii	**<0.0001**	1.0000	-	-	-	-	-	-	-
P. pygmaeus	**<0.0001**	ns	1.0000	-	-	-	-	-	-
G.b. beringei	ns	ns	**<0.05**	1.0000	-	-	-	-	-
G.g. gorilla	ns	**<0.0001**	**<0.0001**	ns	1.0000	-	-	-	-
G.b. graueri	ns	**<0.05**	**<0.01**	ns	ns	1.0000	-	-	-
P. paniscus	ns	**<0.0001**	**<0.0001**	**<0.01**	**<0.01**	**<0.0001**	1.0000	-	-
P. troglodytes	ns	**<0.0001**	**<0.0001**	ns	ns	ns	**<0.01**	1.0000	-
H. sapiens	**<0.0001**	**<0.0001**	**<0.0001**	**<0.0001**	**<0.0001**	**<0.0001**	**<0.0001**	**<0.0001**	1.0000

Table 5.9 *Post-hoc* Tukey's HSD results on PC 2 comparing anthropoid genera following a MANOVA on MTPJ 3 shape variables (PC 1 - 5). PC 2 principally tracked MT head orientation. The cursorial patas monkey and modern humans overlap to the exclusion of all other groups. Bold = significance at $\alpha = 0.05$.

Taxon	r-PLS	p	Covariance Explained (%)
Alouatta seniculus	0.789	ns	34.6
Ateles fusciceps	0.783	ns	50.5
Cebus apella	0.805	ns	50.4
Chlorocebus aethiops	0.785	ns	55.7
Erythrocebus patas	0.709	ns	40.0
Macaca fascicularis	0.86	ns	36.3
Macaca mulatta	0.764	ns	33.4
Macaca nemestrina	0.846	ns	47.0
Papio ursinus	0.827	ns	31.3
Nasalis larvatus	0.786	ns	42.6
Presbytis rubicunda	0.823	ns	58.8
Hylobates lar	0.869	**<0.05**	60.0
Pongo sp.	0.855	ns	45.5
G.b. beringei	0.861	ns	49.6
G.g. gorilla	0.861	**<0.001**	30.4
G. b. graueri	0.786	ns	37.4
Pan paniscus	0.732	ns	33.6
Pan troglodytes	0.686	ns	37.9
Homo sapiens	0.744	**<0.05**	48.6

Table 5.10 Within-species and subspecies 2-Block Partial Least Squares (2B-PLS) results for MTPJ 1. *Pongo* species were pooled due to small sample size in *P. abelii*. r-PLS results did not support functional hypotheses; most covariance regressions were non-significant (ns). Bold = significance at $\alpha = 0.05$.

Taxon	r-PLS	p	Covariance Explained (%)
NWM	0.802	ns	39.2
Chlorocebus aethiops	0.897	ns	42.7
Erythrocebus patas	0.854	ns	42.8
Macaca sp.	0.773	**<0.05**	51.8
Nasalis larvatus	0.844	ns	35.4
Presbytis rubicunda	0.806	ns	46.4
Hylobates lar	0.872	ns	42
Pongo sp.	0.71	ns	41.7
Gorilla sp.	0.656	ns	31.6
Pan sp.	0.802	**<0.001**	76.1
Home sapiens	0.754	**<0.05**	53.2

Table 5.11 Within-species 2-Block Partial Least Squares (2B-PLS) results for MTPJ 3. Subspecies were pooled in the MTPJ 3 dataset due to small sample sizes. r-PLS results did not support functional hypotheses; most covariance regressions were non-significant (ns). Bold = significance at $\alpha = 0.05$.

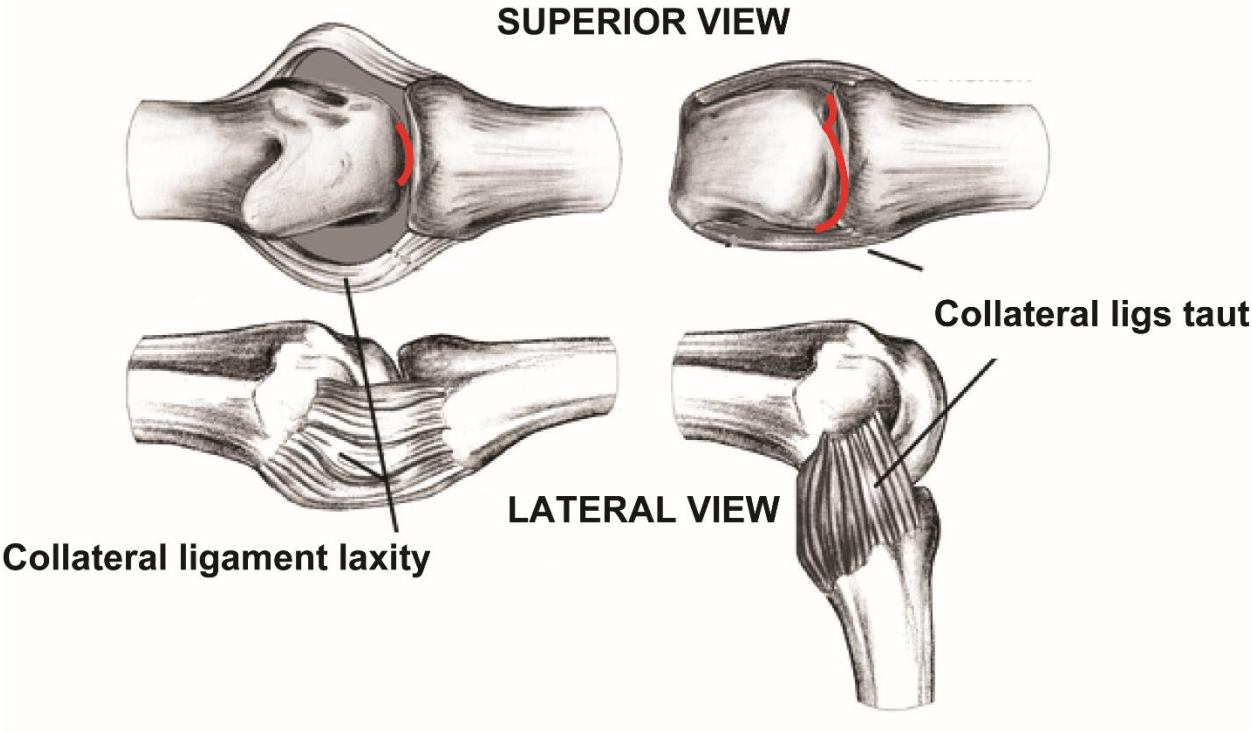

Figure 5.1: Joint range of motion and congruence in the human metacarpophalangeal joints. On the left, the extended posture is characterized by a low amount of joint contact (red arc) and lax collateral ligaments. On the right, when the joint is fully flexed, the collateral ligaments are taut and joint contact increases dramatically (red arcs). This is the closed-packed position. Modified from Watson and Weinzweig (1998).

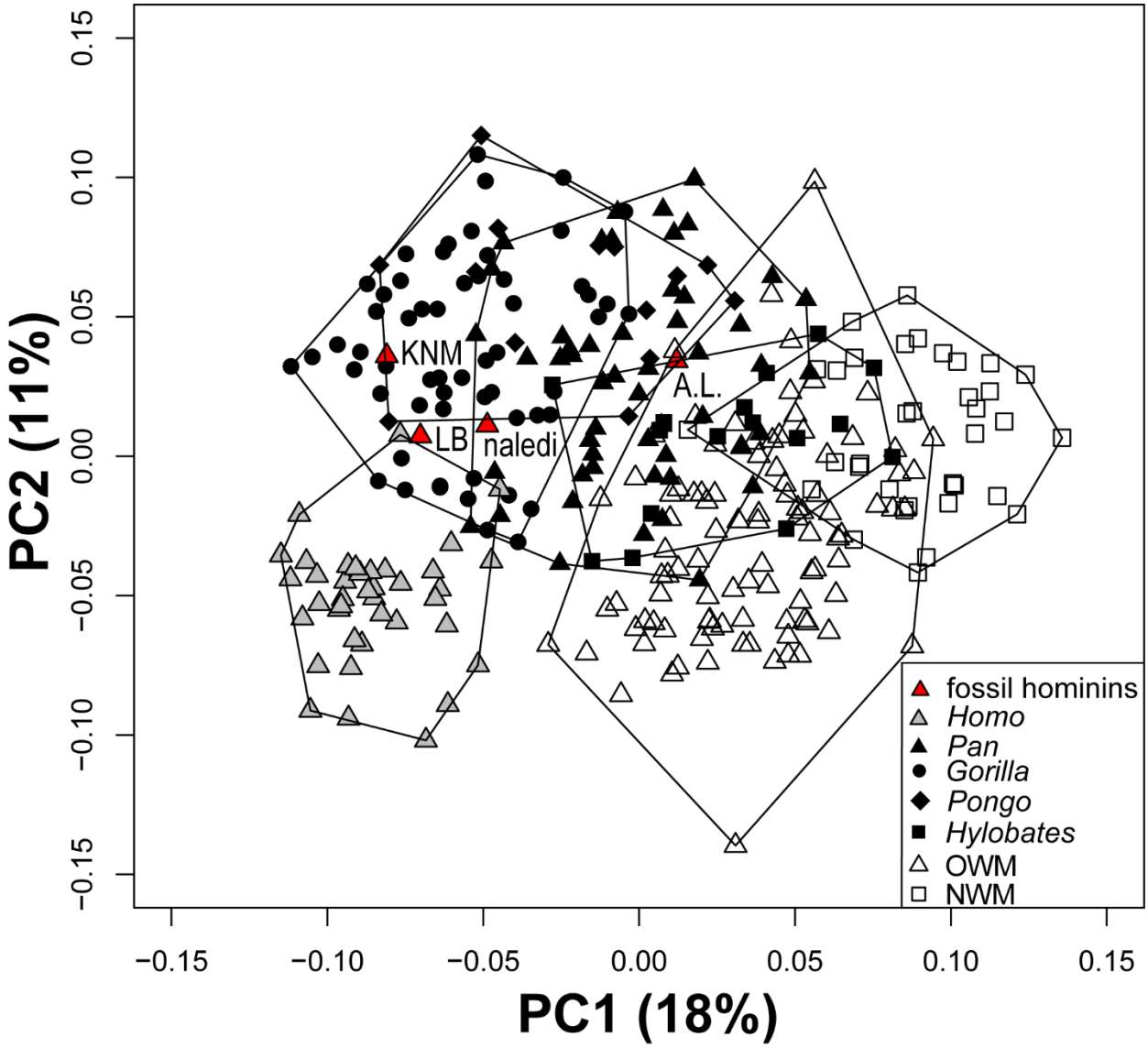

Figure 5.2: PCA Scatterplot of PC 1 vs PC 2 for the anthropoid hallucal ray. Minimum convex polygons are constructed for these groups to illustrate their ranges in the morphospace. Note modern human separation from other anthropoids.

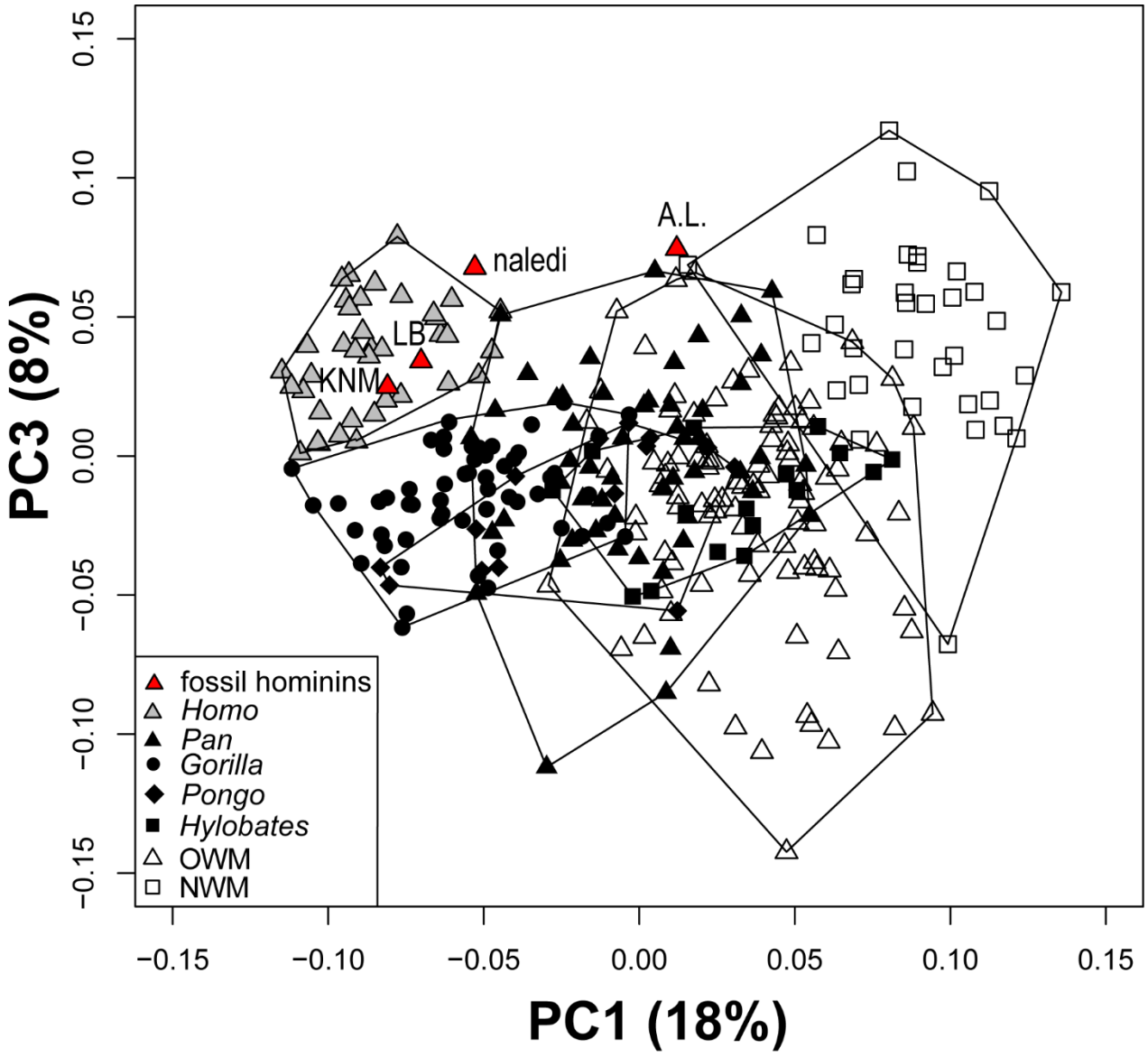

Figure 5.3: PCA Scatterplot of PC 1 vs PC 3 for the anthropoid hallucal ray. Minimum convex polygons are constructed for these groups to illustrate their ranges in the morphospace. Note modern human and hominin overlap on this morphospace, except for *Au. afarensis*, which is more ape-like on PC 1.

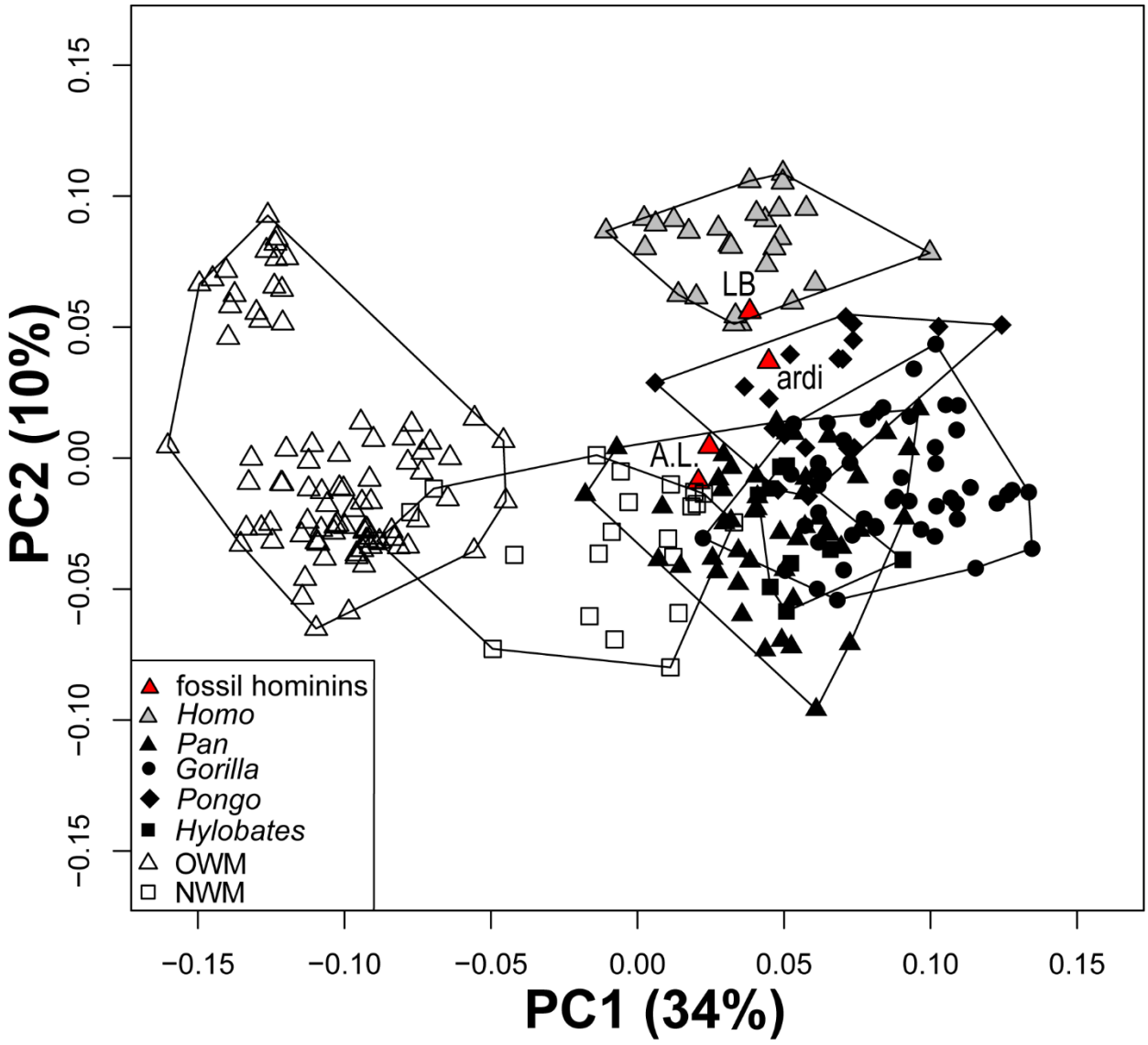

Figure 5.4: PCA Scatterplot of PC 1 vs PC 2 for the anthropoid MTPJ 3. Minimum convex polygons are constructed for these groups to illustrate their ranges in the morphospace. Note modern human separation from other anthropoids, but that they overlap with cercopithecoids (*E. patas*) on PC 2.

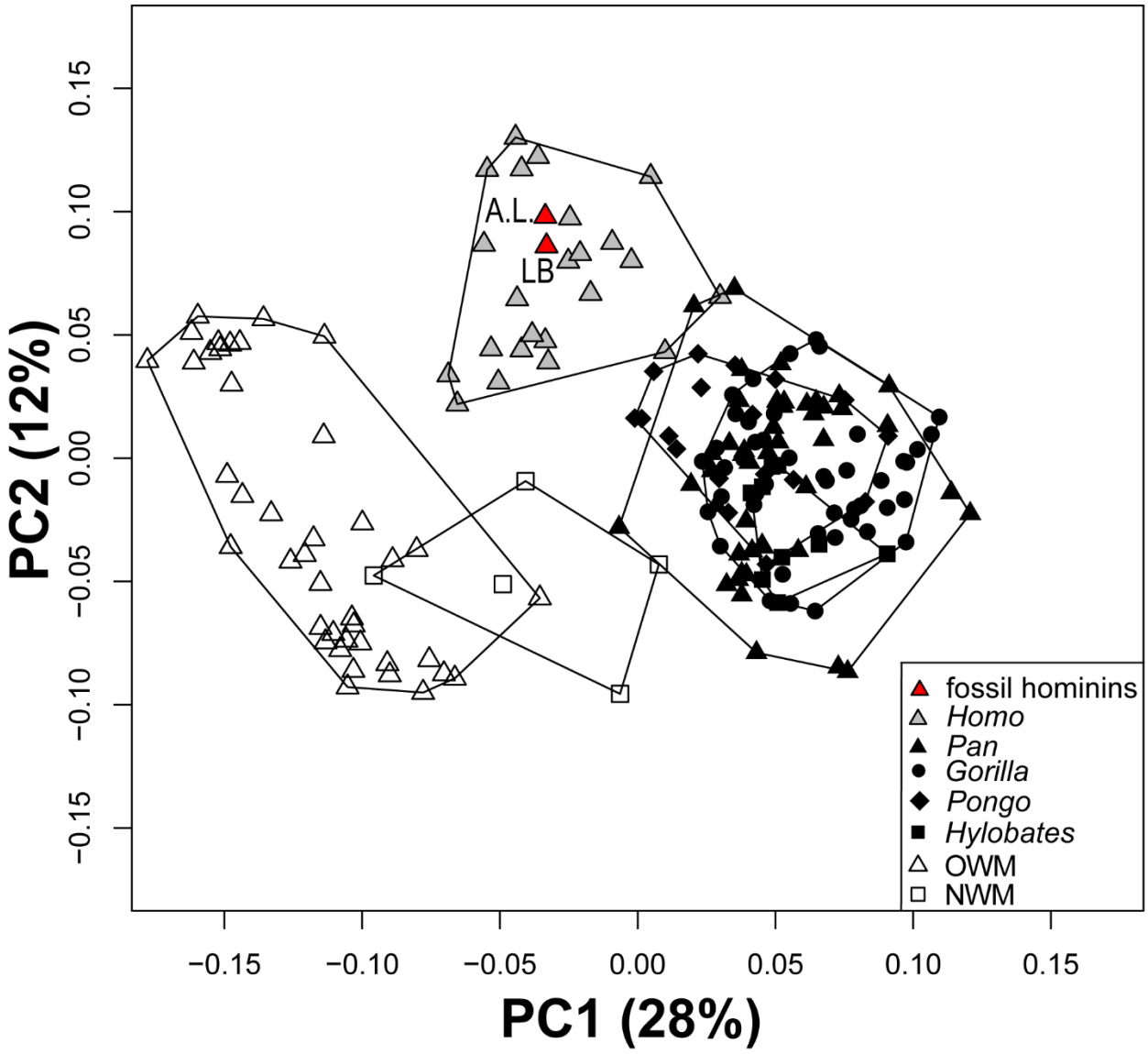

Figure 5.5: PCA Scatterplot of PC 1 vs PC 2 for the anthropoid MTPJ 5. Minimum convex polygons are constructed for these groups to illustrate their ranges in the morphospace. Note modern human separation from other anthropoids on PC 2.

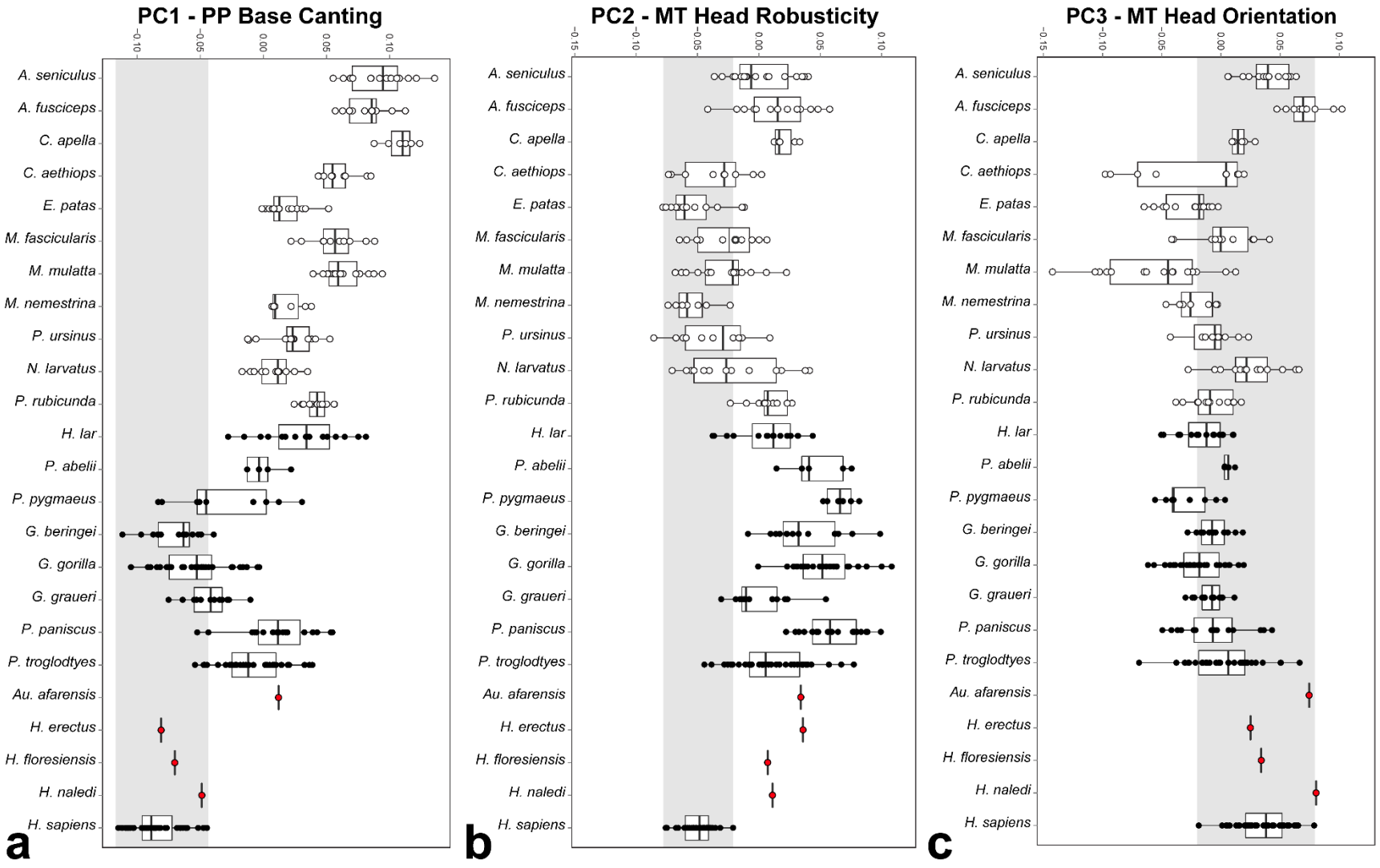

Figure 5.6: Cleveland box-and-whisker plots of PC 1 (a), PC 2 (b), and PC 3 (c) scores for the anthropoid MTPJ 1. Humans and hominins overlap with apes on PC 1, humans overlap with terrestrial monkeys on PC 2, and humans/hominins overlap with most groups on PC 3. Shaded bar: modern human range.

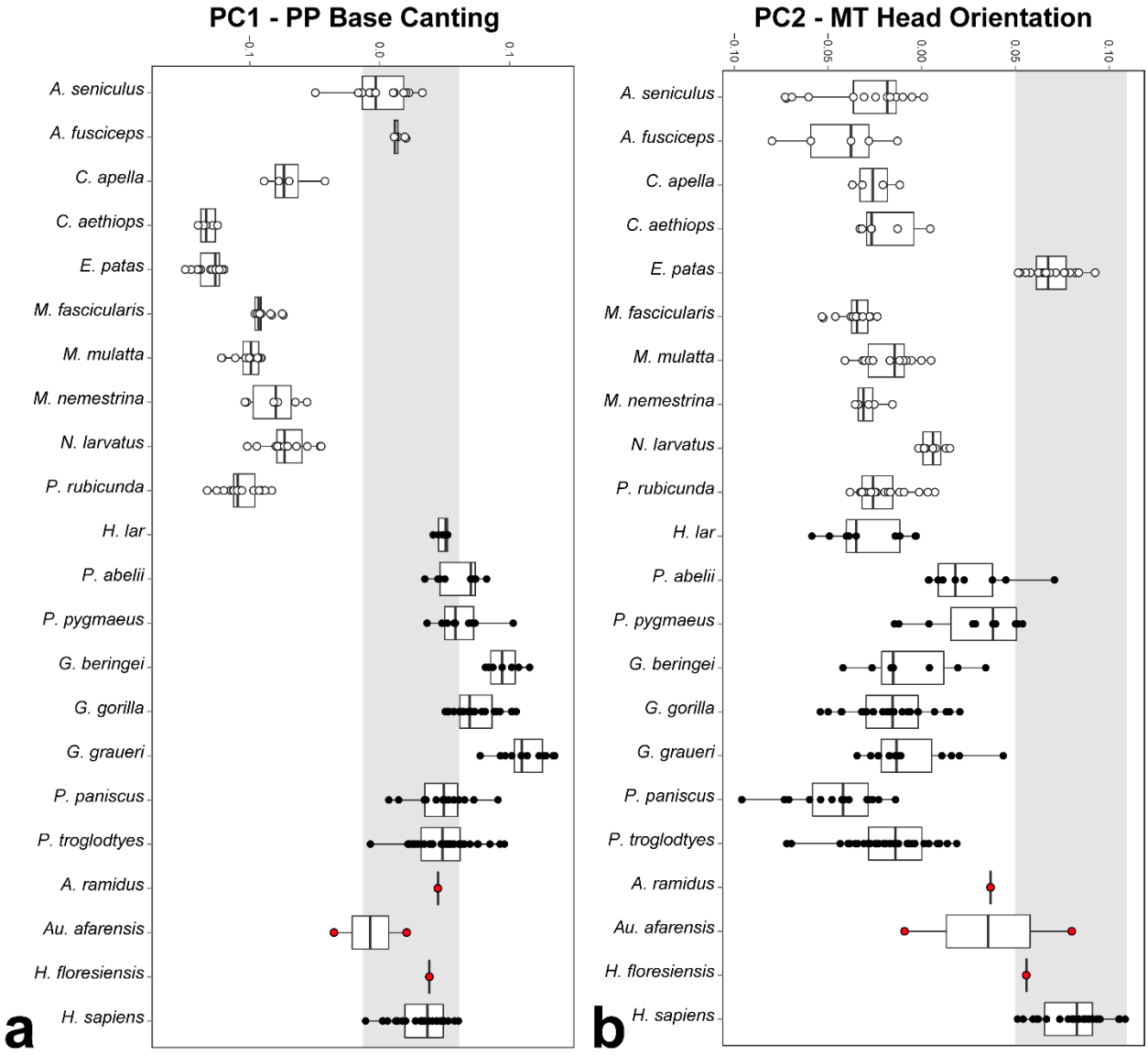

Figure 5.7: Cleveland box-and-whisker plots of PC 1 (a), and PC 2 (b) scores for the anthropoid MTPJ 3. Humans and hominins overlap with apes on PC 1, humans overlap considerably with the cursorial patas monkey on PC 2. Shaded bar: modern human range.

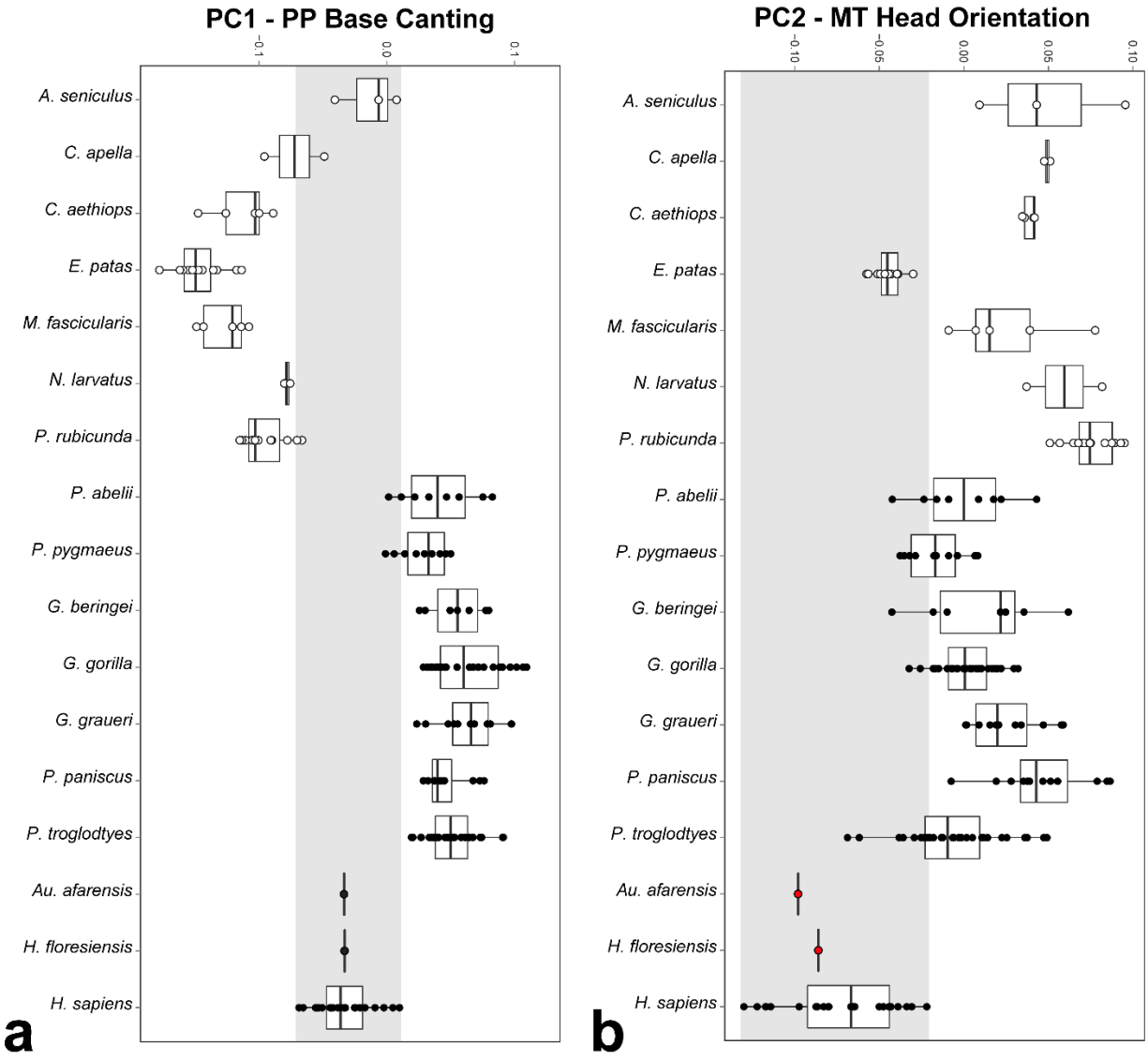

Figure 5.8: Cleveland box-and-whisker plots of PC 1 (a), and PC 2 (b) scores for the anthropoid MTPJ 5. Humans and NWMs are intermediate between apes and OWMs on PC 1, whereas humans overlap considerably with the cursorial patas monkey on PC 2. Shaded bar: modern human range.

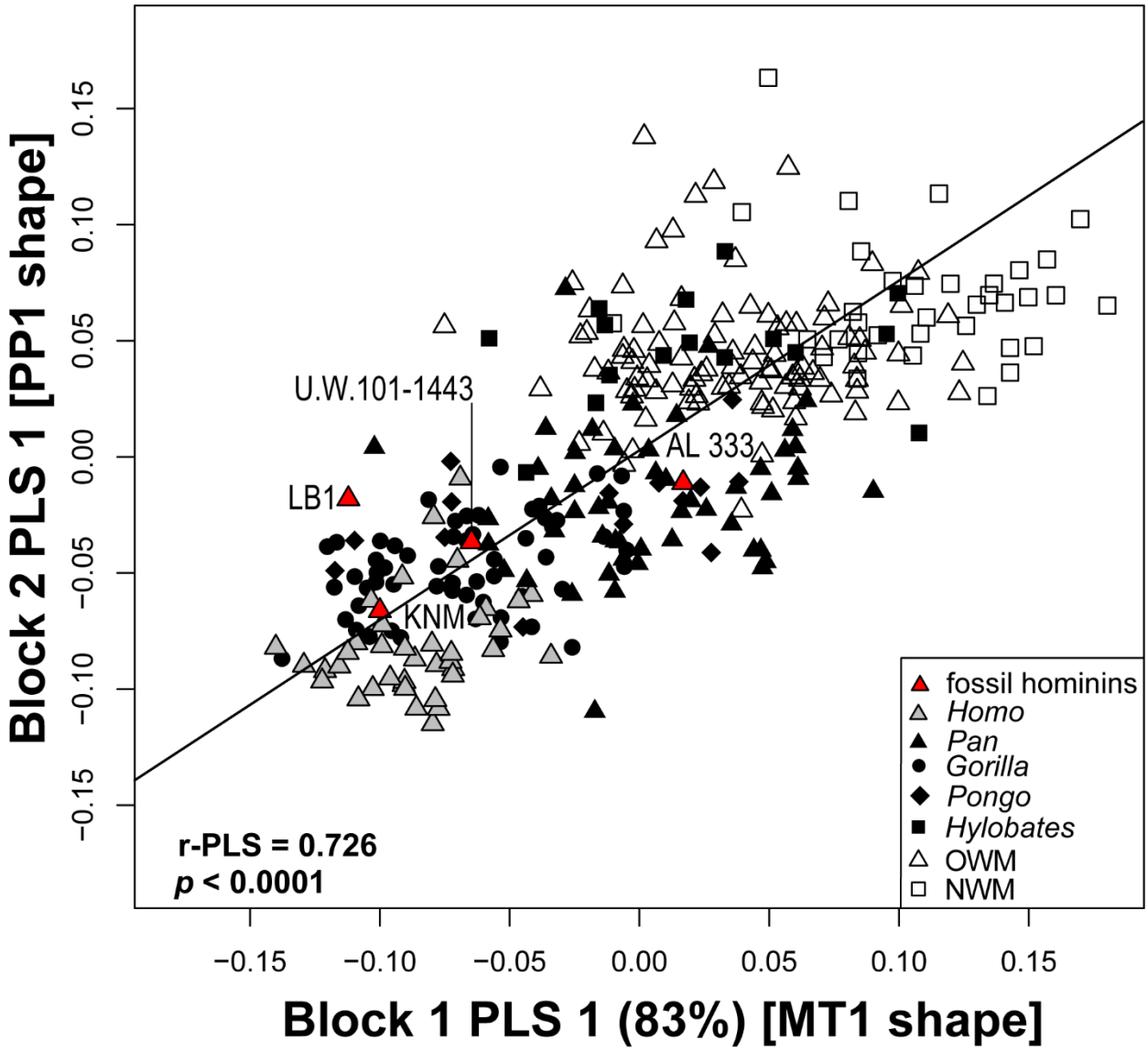

Figure 5.9: Scatter plot of the singular warps analysis scores for the anthropoid MTPJ 1. PLS axis 1 for blocks 1 and 2 together explain 83% of the total covariance between the metatarsal and phalangeal datasets. The solid black line represents the best-fit linear regression to the data.

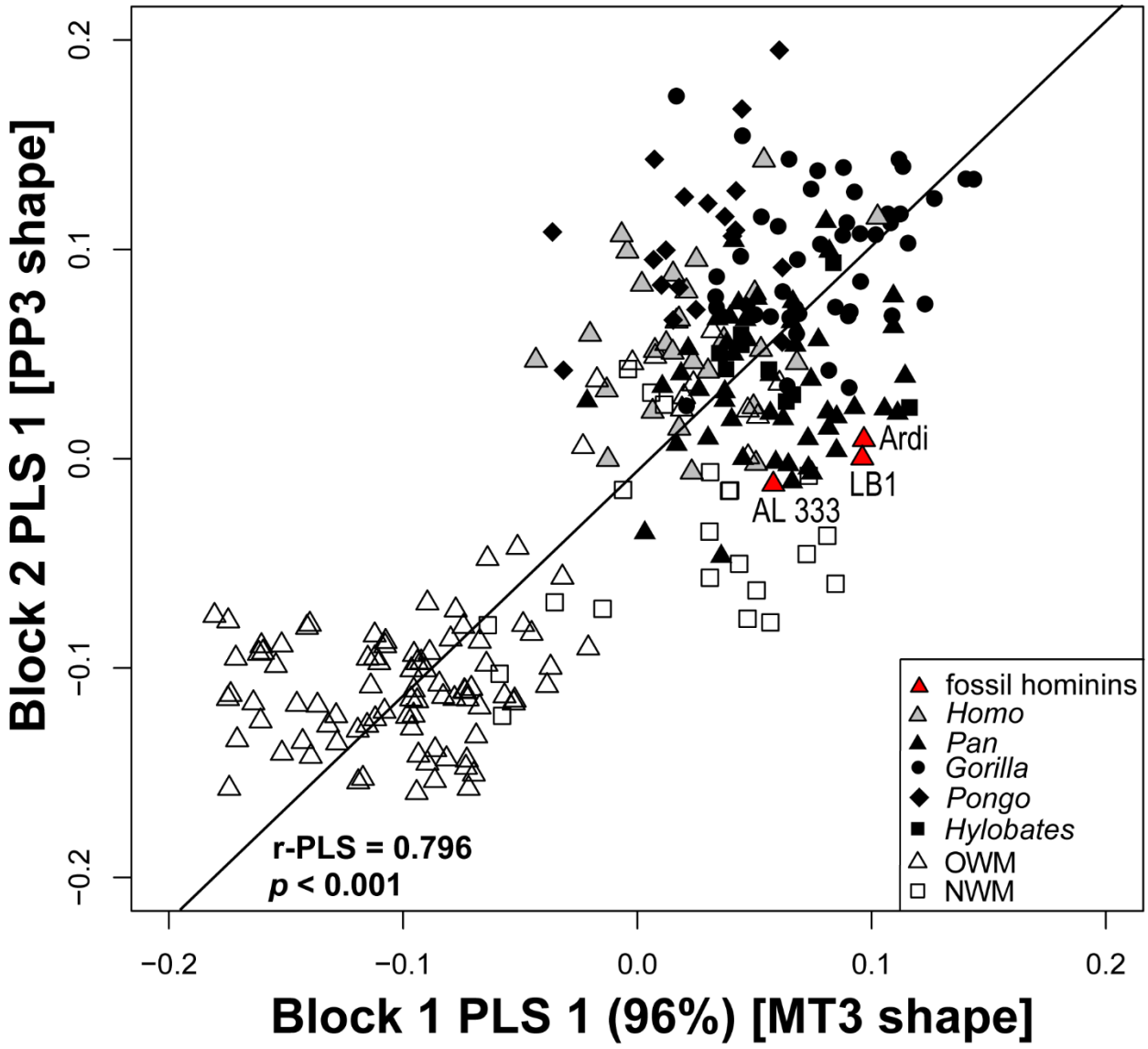

Figure 5.10: Scatter plot of the singular warps analysis scores for the anthropoid MTPJ 3. PLS axis 1 for blocks 1 and 2 together explain 96% of the total covariance between the metatarsal and phalangeal datasets. The solid black line represents the best-fit linear regression to the data.

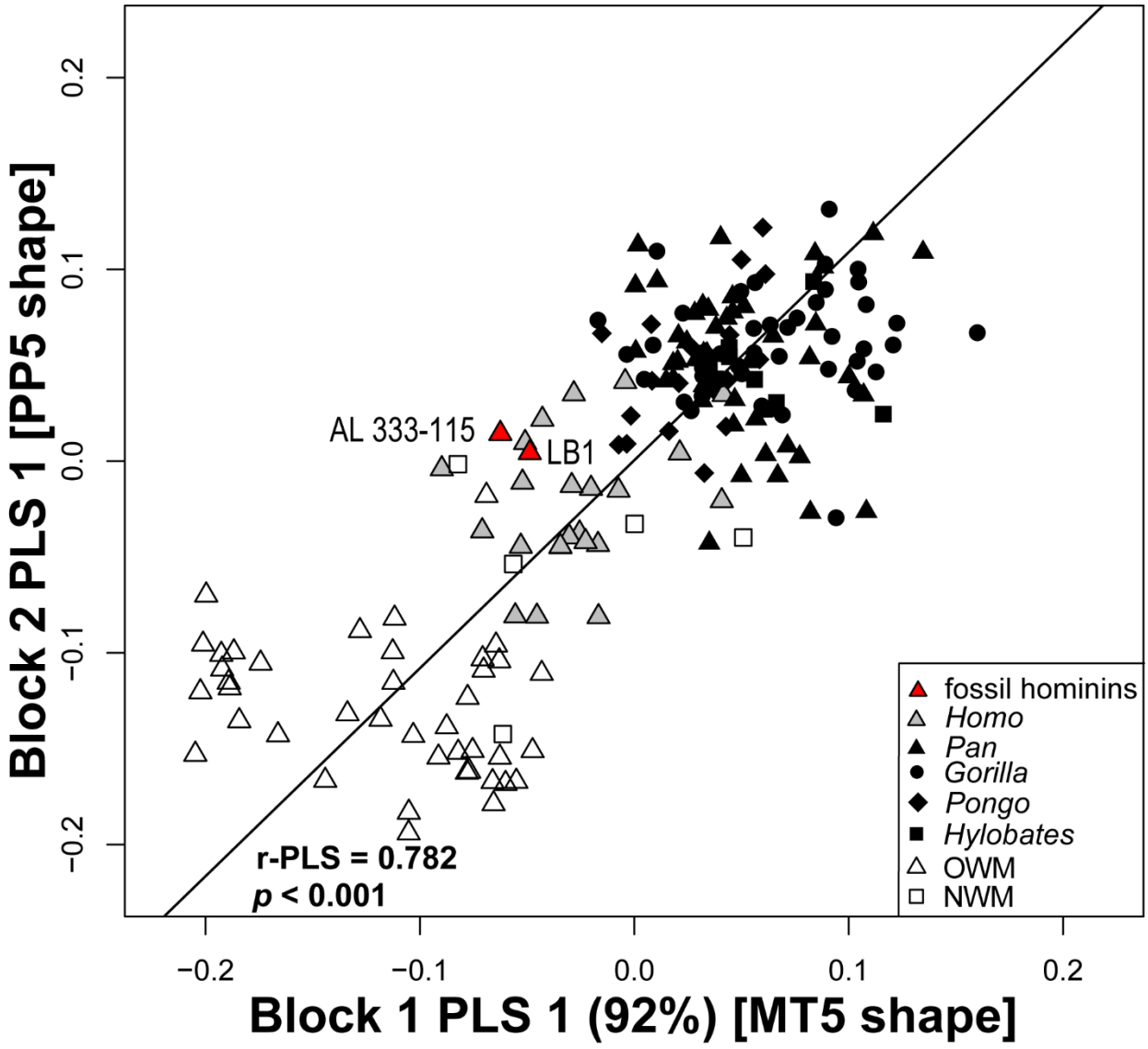

Figure 5.11: Scatter plot of the singular warps analysis scores for the anthropoid MTPJ 5. PLS axis 1 for blocks 1 and 2 together explain 92% of the total covariance between the metatarsal and phalangeal datasets. The solid black line represents the best-fit linear regression to the data.

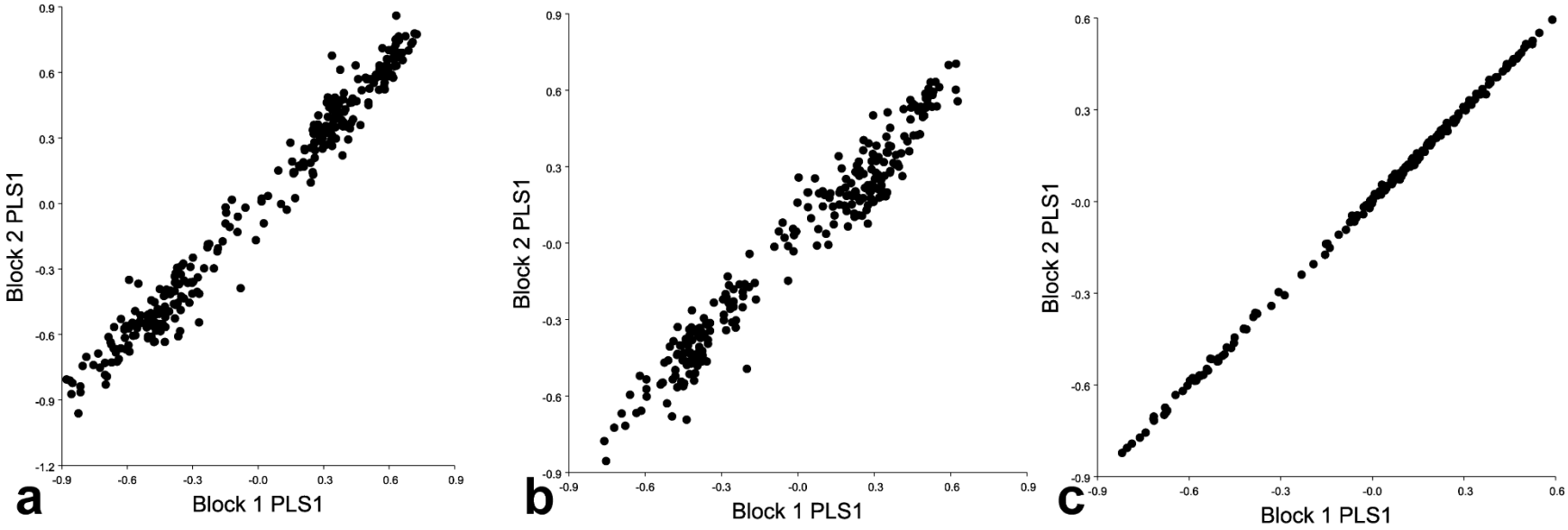

Figure 5.12: Scatter plot of the singular warps analysis scores for the anthropoid MTPJs using the Procrustes form matrix. a. MTPJ 1; PLS axis 1 for blocks 1 and 2 together explain 99.5% of the total covariance between the metatarsal and phalangeal datasets, r-PLS = 0.975. **b.** MTPJ 3; PLS axis 1 for blocks 1 and 2 together explain 99.6% of the total covariance between the metatarsal and phalangeal datasets, r-PLS = 0.988. **c.** MTPJ 5; PLS axis 1 for blocks 1 and 2 together explain 99.95% of the total covariance between the metatarsal and phalangeal datasets, r-PLS = 0.966. In all cases, the r-PLS and amount of covariance explained increases when using the Procrustes form matrix over the Procrustes shape matrix.

Chapter 6

Chimpanzee, human, and early hominin forefoot push off mechanics

Introduction

During the evolution of bipedalism the hominin foot underwent a number of dramatic changes that converted it from a prehensile grasping organ to a strong propulsive lever. Among the features affected by these changes, those of the forefoot region have received much attention in comparative morphology studies due to their role in the push off phase of bipedal walking (Susman, 1983; Latimer and Lovejoy, 1990b; Proctor et al., 2008; Griffin et al., 2010a; Proctor, 2010a, b, 2013; Fernández et al., 2015). The extant great ape forefoot is characterized by an abducent opposable hallux and metatarsal (MT) heads that are plantarly oriented in sagittal profile and dorsally narrow (Morton, 1922; Wood-Jones, 1944; Bojsen-Møller, 1979; Lewis, 1980; Susman, 1983). Additionally, the phalanges are long and curved, enabling them to resist the bending strains incurred during pedal grasping (Preuschoft, 1970). In contrast, the human forefoot is characterized by a permanently adducted hallux that is incapable of opposing the other digits, and more dorsally oriented and mediolaterally broad metatarsal head articular surfaces. The phalanges of modern humans are short and straight, and the proximal phalangeal bases demonstrate dorsal canting (Latimer and Lovejoy, 1990b; Duncan et al., 1994; Patel, 2008, 2009; Griffin and Richmond, 2010).

The interfaces of the metatarsal heads and proximal phalangeal bases, the ellipsoidal metatarsophalangeal joints (MTPJs), allow plantarflexion for pedal grasping and dorsiflexion during push off. The dorsally oriented MT heads in the human forefoot are thought to increase the dorsiflexion range of motion (ROM) at the MTPJs (Stern and Susman, 1983; Latimer and Lovejoy, 1989) by providing more dorsal articular surface area on which the proximal

phalangeal base can slide. In humans, dorsiflexion at the MTPJs causes tightening of the plantar aponeurosis, which is a thick band of ligamentous tissue that originates from the calcaneal tuberosity and inserts distally on the proximal phalangeal bases. Tightening of this structure acts as a "windlass mechanism" (Hicks, 1954) that raises the longitudinal arch, providing midfoot stability and facilitating propulsive force production at push off (Erdemir et al., 2004). The plantar aponeurosis is only weakly developed in great apes, and consequently these species are believed to lack a windlass mechanism (Bojsen-Møller, 1979; Susman, 1983). Additionally, the more plantarly oriented MT head in great apes is hypothesized to increase plantarflexion ROM for arboreal pedal grasping (Stern and Susman, 1983; Susman et al., 1984; Latimer and Lovejoy, 1990a; Fernández et al., 2015) at the expense of dorsiflexion ROM during push off on terrestrial substrates (Stern and Susman, 1983; Latimer and Lovejoy, 1989; Griffin et al., 2010b).

The mediolaterally expanded dorsal MT head in humans has been argued to enhance joint stability under increased loads during push off from highly dorsiflexed MTPJs (Susman et al., 1984; Susman and Brain, 1988; Susman and de Ruiter, 2004; Pontzer et al., 2010; Fernández et al., 2015). Dorsal mediolateral expansion of the MT heads also allows for close-packing of the MTPJs by tightening the collateral MTP ligaments when the joints are in dorsiflexed postures (MacConaill and Basmajian, 1969; Susman and Brain, 1988; Susman and de Ruiter, 2004). In the close-packed position the contact surface of the MT head and proximal phalangeal base articular surfaces is maximized, and tightening of collateral ligaments limits joint motion outside of the sagittal plane, thus increasing joint stability when maximum joint congruency is achieved (MacConaill and Basmajian, 1969; Susman et al., 1984). This same mechanism is hypothesized to close-pack the great ape MTPJs in plantarflexion for increased stability during pedal grasping.

These differences in human and great ape MTPJ functional morphology have been used in analyses of fossil hominin pedal remains to assess the degree to which early hominins were capable of pushing off in a manner similar to humans during bipedal locomotion. Typically, human-like morphology is interpreted as indicating a modern human-like push off, whereas ape-like features are taken to indicate less derived push off mechanics. For instance, the presence of dorsally oriented MT heads has been interpreted as indicative of human-like bipedalism in *Australopithecus afarensis* (Latimer and Lovejoy, 1990a), but others have argued that the relatively narrow dorsal breadth of the MT heads in this species suggests a push off that was different from that of modern humans (Susman and de Ruiter, 2004). Conflicting interpretations

of MT head morphology such as these can only be resolved by combining comprehensive shape analyses with quantitative foot motion data and by establishing functional links between joint surface shape and joint motion. Three-dimensional geometric morphometric (3DGM) methods allow for the quantification of shape differences in bony elements between individuals or among species. Recently, Fernández et al. (2015) demonstrated the power of 3DGM to distinguish MT head morphology among primate taxa that possess different locomotor repertoires. Expanding on this approach, here we relate the shape differences between species that were captured in that study to differences in joint function in chimpanzees and humans during terrestrial locomotion.

The extent to which the MTPJ motion of humans and other great apes differs during locomotion has not been comprehensively established. In the only study that quantified MTPJ motion *in vivo* in a non-human great ape, Griffin et al. (2010a) found significantly greater joint angles at push off in humans than in bonobos for the first two pedal rays. However, they were only able to analyze a small number of steps, and found some overlap between species in push off joint angles. This ambiguity suggests that African ape joint kinematics may be somewhat similar to that of humans during push off in terrestrial locomotion, undermining the form-function relationship assumed for the hominoid MTPJs. To investigate this relationship more thoroughly, a larger sample of great ape steps must be analyzed, and all five MTPJs should be assessed to determine if interspecies differences hold up across the pedal rays. These data can then be compared to matching morphological data to determine whether current form-function assumptions for the metatarsal heads are in fact valid.

Recent works have incorporated 3-dimensional (3D) shape analysis methods to robustly discern functional signals in skeletal elements (Almécija et al., 2013; Almécija et al., 2015; Green et al., 2015; Knigge et al., 2015), and the coupling of these data with accurate kinematic data will enable experimental testing of assumptions about MTPJ functional morphology. This design will facilitate the reconstruction of bipedal kinematics in extinct hominins from analyses of pedal fossils, thereby improving our understanding of the origins of bipedalism and human evolution. Pedal remains attributed to fossil hominins span a large temporal and geographic range, occupying much of Africa and Eurasia from 4.4 Ma – 35 ka. Nearly all of these taxa, including *Ardipithecus ramidus*, *Australopithecus afarensis*, *Homo erectus*, *Homo floresiensis*, and the assorted South African hominin material display a mosaic morphology of human and

ape-like features in the forefoot (e.g. Stern and Susman, 1983; Susman and Brain, 1988; Jungers et al., 2009; Lovejoy et al., 2009; Pontzer et al., 2010; Harcourt-Smith et al., 2015). Thus, a detailed understanding of how MTPJ function is related to joint anatomy is necessary to verify current hypotheses about hominin forefoot biomechanics and the evolution of bipedalism.

To this end, we collected 3D marker-based kinematic data for MTPJs 1-5 during bipedal and quadrupedal walking in chimpanzees (*Pan troglodytes*), and bipedal walking in humans (*Homo sapiens)*. We compared these data to landmark-based 3DGM data from the MT heads of all five pedal rays in these species to test the hypothesis that differences in human and chimpanzee MTPJ function during walking are reflected in morphological differences at their metatarsal heads. Following this hypothesis, we predicted that humans would use higher peak dorsiflexion angles than chimpanzees at all MTPJs, regardless of whether the latter walk bipedally or quadrupedally. To stabilize the MTPJs at higher dorsiflexion angles, we predicted that human MT heads would be more dorsally oriented and dorsally wider than the chimpanzee MT heads at all of the MTPJs. Additionally, we predicted that significant differences in peak dorsiflexion angles between MTPJs would reflect significant differences in metatarsal head morphology between rays within species.

Finally, we collected 3DGM data from fossil MT heads from rays 1-5 attributed to *A. afarensis* (Fig. 6.1). As previously discussed, different features of the *A. afarensis* MT heads have been used to argue either that this species walked with modern human-like kinematics (Latimer and Lovejoy, 1990a; Ward et al., 2011), or pushed off differently than humans during bipedal locomotion (Susman et al., 1984). To address this debate, we assess the morphological affinities of *A. afarensis* MT heads in comparison to those of humans and chimpanzees using 3DGM. Our findings are then placed in the context of the relationship between MT morphology and MTPJ function, and used to draw conclusions about bipedal gait kinematics in *A. afarensis*.

6.2 Materials and Methods

6.2.1 3D Kinematics

All experimental procedures involving human subjects were approved by Stony Brook University's Institutional Review Board, and all those involving chimpanzee subjects were approved by Stony Brook University's Institutional Animal Care and Use Committee.

Experiments were carried out in accordance with the approved guidelines and each human subject provided written and informed consent before participating in an experiment. We collected 3D kinematic data from five male humans (28±1 yrs, 68±6 kg) and two male chimpanzees (both 7-8 yrs, 35-50 kg over period of data collection) during locomotion on a flat 11 m long runway using a four camera high-speed (150 Hz) motion capture system (Xcitex Inc., Woburn, MA). Prior to data collection we applied 1 cm markers to the legs and feet of our subjects using non-toxic paint. To capture MTPJ motion we applied markers to skin over the head and base of each metatarsal, and to the skin over the proximal and distal ends of each proximal phalanx (Fig. 6.2). During locomotion experiments, all subjects were recorded while walking at self-selected speeds. Chimpanzee subjects were encouraged to walk bipedally and quadrupedally over the runway by an animal trainer who used a fruit or juice reward.

3D kinematic data were extracted from video recordings using ProAnalyst software (Xcitex, Inc.) and imported into MATLAB software (The Mathworks Inc., Natick, MA, USA) for further analysis. We analyzed 10 bipedal and five quadrupedal steps per chimpanzee subject, and five steps per human subject. The lower sample size for chimpanzee quadrupedal steps is due to our difficulty obtaining videos of steps where the view of the foot was not obstructed by the ipsilateral forelimb. Accurate marker tracking requires the use of zoomed-in camera views, which precluded the measurement of velocity of locomotion. Therefore, we measured velocity in separate trials using zoomed-out camera views, and calculated least-squares linear regression equations for the relationship between stance phase duration and dimensionless walking velocity (Winter, 2005) for each subject (Table 6.1). We then used these equations to estimate dimensionless velocity for each step selected for analysis. Average estimated dimensionless velocities for all steps were similar between species (0.46 ± 0.05 bipedal chimpanzees; 0.42 ± 0.04 quadrupedal chimpanzees; 0.45 ± 0.02 humans; Table 6.1). Raw coordinate data of kinematic markers were filtered using a fourth order, low pass Butterworth filter with a 5-7 Hz cutoff frequency as determined appropriate by residual analysis (O'Neill et al., 2015). MTPJ dorsiflexion was calculated by using the filtered coordinates for each marker to calculate the position of the metatarsal and proximal phalanx of each ray as segment vectors. Joint angles were calculated for each frame of stance phase using vector algebra.

We assumed that motion at the MTPJs occurs primarily in a vertical plane aligned with and perpendicular to the long axis of the digit, and thus the angles that we measured in this manner represent plantarflexion-dorsiflexion. From these angles, we calculated the maximum MTPJ joint dorsiflexion angle that occurred in the last 15% of stance prior to liftoff (Fig. 6.3). We used non-parametric Mann-Whitney U tests (Abdi, 2010) to test for differences in MTPJ angles between groups in the following comparisons: human steps *vs.* chimpanzee bipedal steps, human steps *vs*. chimpanzee quadrupedal steps, and chimpanzee bipedal *vs*. quadrupedal steps. We also used non-parametric Kruskal-Wallis tests (Sokal and Rohlf, 2011) to test for differences in MTPJ angles between rays within species. In cases of significant difference, we conducted *post hoc* tests to look for differences between ray pairs. For all Mann-Whitney U and *post-hoc* tests, a sequential Bonferroni correction was applied to the alpha value (Abdi, 2010). All statistical tests involving kinematic data were carried out using MATLAB software.

6.2.2 Speed estimation

Due to the density of markers that we used to capture foot kinematics we had to use zoomed-in camera views that precluded the measurement of velocity of progression for complete strides. Therefore, we measured velocity (v_d) in separate trials using zoomed-out camera views as the anteroposterior distance traveled by a marker placed on the pelvis (anterior superior iliac spine or posterior superior iliac spine) over the duration of a stride. We also measured hip height (L) at 50% of stance using a marker placed over the greater trochanter, and used these variables to calculate dimensionless velocity (v) following the equation used by O'Neill et al. (2015):

$$v = v_d/(g * L)^{1/2}$$

where g is the gravitational constant 9.81 ms^{-2}. We measured stance phase duration in each of these trials, and calculated least-squares linear regression equations for the relationship between natural logs of the inverse of stance duration and dimensionless velocity for each subject (Table 6.1). We then used these equations to estimate dimensionless velocity for each step selected for analysis.

6.2.3 3D Morphometrics

Shape differences in MT 1 – MT 5 were quantified within a comparative sample (n = 25) of *Pan troglodytes* and modern, minimally shod *Homo sapiens* from South Asia. Specimens

were sampled from the American Museum of Natural History (AMNH), the Smithsonian's National Museum of Natural History (USNM), the Cleveland Museum of Natural History (CMNH), and collections housed in the Anatomical Sciences Department at Stony Brook University (SBU). A.L. 333-115A-E surface landmark data were collected from high resolution, research quality casts without any reconstruction housed at the Institute of Human Origins (Arizona State University). The scans were provided by Dr. Caley Orr (Dept. of Cell and Developmental Biology, School of Medicine, University of Colorado – Denver) and Dr. William Kimbel (Institute of Human Origins, Arizona State University). Distal metatarsal morphology was explored using 3D digital polygon models reconstructed from medical computed tomography (CT) and 3D laser surface scans. Measurement error due to data acquisition method is known to be insignificant (Tocheri et al., 2011), so all imaging data were pooled. Scanning was conducted using a NextEngine 3D laser scanner (10,000 pts/inch^2 resolution per scan, 12 scans per bone) or a General Electric Lightspeed VCT Scanner at the Health Sciences Center, Stony Brook University (120 kV, 250 mA, 1mm slice thickness, 0.187 mm reconstruction increment, bone plus reconstruction). 3D models from laser scans were merged using ScanStudio HD PRO (NextEngine, Inc) and Geomagic Studio 2012 SR1 (3D Systems, Inc) software packages. 3D models from CT scans were constructed from DICOM data using Amira 5.3.3 software (Visage Imaging, Inc.). Additionally, any scanning artifacts or anomalies in polygonal meshes were corrected in Geomagic and MeshLab 1.3.2 (Visual Computing Lab—ISTI—CNR). All data were collected from right metatarsals whenever possible but some left metatarsals were mirrored in Geomagic when right elements were unavailable.

The 3D shapes of all five metatarsal heads were evaluated using a landmark-based approach. A 5x5 3D surface patch of nine user-defined landmarks (see Table 6.2) and 16 semi-landmarks was applied using *Landmark Editor* (Wiley et al., 2005) following the methods detailed in Fernández et al. (2015). This landmark set has been shown to be repeatable while also capturing the full articular surface morphology of the metatarsal head. The surface patch was bounded mediolaterally by the proximal termination of the distal epicondyles, dorsally at the proximal termination of the distal articular surface, and plantarly at the proximal termination of the plantar condyles. See previous work for specific anatomical locations of each landmark (Fernández et al., 2015). Because the hallux differs from the lateral metatarsals in its ontogenetic development and gene expression (Indjeian et al., 2016), it possesses a unique shape that

presents possible homology problems with the surface landmarks used in MT 2 – MT 5. Therefore, MT 1 morphometric data were analyzed separately from those of the lesser toes.

Semi-landmarks were slid using the minimized Procrustes distance criterion (Rohlf, 2010), but similar results were obtained using minimized bending energy algorithms (Bookstein, 1997). The slid coordinates were then subjected to a Generalized Procrustes Analysis (GPA) (Gower, 1975), and principal component analysis (PCA) was used to summarize and explore the observed variation in metatarsal head shape. Articular surface wireframes and polygonal mesh warps were constructed to visualize shape changes. Significant differences in PC scores between taxonomic groups were analyzed using multivariate analysis of variance (MANOVA); Tukey's HSD was used for pairwise *post hoc* between-species and between-ray comparisons. All PCs explaining at least 5% of the total shape variance were subjected to these analyses, but because the study sample completely overlapped in all PCs beyond the first two, only the results from PC 1 and PC 2 are presented. Box-and-whisker plots are shown to visualize the variation within and between species in specific MT head morphologies (Fig. 6.4). Semi-landmark sliding, GPA, PCA, and linear regression analyses were performed in the R package *Geomorph* (ver. 2.17) (Adams and Otárola-Castillo, 2013; Adams et al., 2015). All statistical tests and associated graphics were executed in R 3.2.2 base package (https://www.R-project.org). Wireframe construction and allometric regressions were performed in *MorphoJ* (ver. 1.06b) (Klingenberg, 2011).

6.3 Results

6.3.1 Chimpanzee and human MTPJ kinematics

We analyzed MTPJ motion in five steps per human subject (N = 25), ten bipedal steps per chimpanzee subject (N = 20), and five quadrupedal steps per chimpanzee subject (N=10). In both species MTPJ dorsiflexion for all joints peaked in the final 20% of stance phase, just prior to liftoff (Fig. 6.3). Humans exhibited significantly greater dorsiflexion angles at all five joints than chimpanzees did during both bipedal and quadrupedal locomotion (Table 6.3; Fig. 6.5; Mann-Whitney U [MWU] test, $P < 0.001$ all comparisons). The greatest disparity in joint angles occurred at MTPJ 1, where humans dorsiflexed their joints 36° more on average than chimpanzees. Moving laterally across MTPJs 2-5, both humans and chimpanzees exhibited a decrease in peak joint angles, although the gradient of this decline was steeper in chimpanzees.

Peak MTPJ angles were similar in chimpanzees during bipedal and quadrupedal walking, with the only significant difference between locomotor modes occurring at MTPJ 3, where chimpanzees used 5° more dorsiflexion during quadrupedalism on average (Table 6.3; Fig. 6.5; MWU test, $P = 0.001$).

For both humans and chimpanzees, peak dorsiflexion angles were significantly different among the MTPJs (Table 6.4; Kruskal-Wallis [KW] test, $P < 0.001$ for all tests). In the human steps, MTPJ peak dorsiflexion angles were statistically indistinguishable among the first four joints, but MTPJ 5 had significantly lower peak dorsiflexion angles than all other joints (*post hoc* KW test, $P < 0.001$ for all comparisons involving MTPJ 5). Among the chimpanzee bipedal and quadrupedal steps, MTPJ 1 peak dorsiflexion angle was statistically indistinguishable from those of MTPJs 4 and 5, but significantly lower than those of MTPJs 2 and 3 (*post hoc* KW test, $P < 0.001$ for all comparisons). In bipedalism, MTPJs 2 and 3 had significantly greater peak dorsiflexion angles than those of all other joints (*post hoc* KW test, $P < 0.005$ for all comparisons), but were statistically indistinguishable from one another. In quadrupedalism, MTPJ 2 had significantly greater angles than all other joints except MTPJ 3, and MTPJ 3 had significantly greater angles than MTPJs 1 and 5 (*post hoc* KW test, $P < 0.001$ for all comparisons).

6.3.2 3D Geometric Morphometrics

For all MTs, each of the first 5 PCs accounted for > 5% of the variance in the data. Because PC 1 and PC 2 captured MTPJ articular surface morphology that was hypothesized to be related to dorsiflexion at push off (Fernández et al., 2015), results for these two axes are reported in further detail. Morphometric data for MTs 2-5 were pooled in order to examine intraspecific MTPJ comparisons; pooling these data was possible because PC 1 and PC 2 capture the same shape differences for MT 2 – MT 5 in humans, chimpanzees, and other catarrhines (Fernández et al., 2015). MT 1 was analyzed separately due to homology constraints related to differences in ontogenetic development and gene expression of the hallux (Indjeian et al., 2016).

For MT 1, PC 1 completely separated humans and chimpanzees (*post hoc* Tukey's HSD, $P < 0.001$), whereas the groups overlapped on PC 2 (Fig. 6.6a). PC 1 (38% of variance) captured shape changes related to the overall dorsal versus plantar orientation of the MT head in sagittal profile as well as shape changes in plantar condylar morphology. Negative PC 1 scores, as

exhibited by human MT 1s, indicate more dorsally oriented MT heads with a broader, shallower plantar condyle. Positive PC 1 scores, as exhibited by chimpanzee MT 1s, characterize more plantarly oriented MT heads with a deeply projecting plantar condyle flanked by steep, angular facets for articulation with the hallucal sesamoid bones; humans have dorsally wide MT 1 heads, whereas chimpanzees have plantarly wide MT 1 heads. PC 2 (11% of variance) captured variance in the relative mediolateral breadth (robusticity) of the MT 1 head. High PC 2 scores indicate greater overall mediolateral robusticity of the MT head. There is no separation between species on this axis.

The pattern observed in MT 2 – MT 5 was similar. PC 1 (29% of variance) tracked two principal shape changes: epicondylar breadth and dorsal versus plantar orientation of the MT head relative to the epicondyles, which completely separated humans and chimpanzees (*post hoc* Tukey's HSD, $P < 0.001$) (Fig. 6.6b). PC 2 (12% of variance) captured overall mediolateral robusticity of the MT 2 – MT 5 head, with higher PC 2 scores indicating greater relative mediolateral width and serving to separate medial from lateral MTs within species (Table 6.4). In humans, MT 2 (*post hoc* Tukey's HSD, $P < 0.001$) was significantly more mediolaterally robust than MT 3 – MT 5, and MT 3 was significantly more robust than MT 4 – MT 5. The pattern found in chimpanzees was slightly different; MT 2 was indistinguishable from MT 3, but was significantly more robust than MT 4 – MT 5 (*post hoc* Tukey's HSD, $P < 0.001$; $P < 0.001$), MT 3 was indistinguishable from MT 4 but was significantly more robust than MT 5 (*post hoc* Tukey's HSD, $P < 0.001$), and MT 4 was indistinguishable from MT 5. Overall, MT 2 – MT 5 PC 2 scores and peak MTPJ dorsiflexion angles decrease from medial to lateral across the forefoot in both species.

The A.L. 333-115 MTs fell within the human and chimpanzee ranges of variation on both PC 1 and PC 2 (see Fig. 6.4). The hallucal element, A.L. 333-115A, just barely overlapped with the chimpanzee range on PC 1 and was well outside the range of modern human variation (Fig. 6.6), but it also fell outside the range of chimpanzees on PC 2. Although A.L. 333-115A exhibits marked dorsal doming, especially when viewed laterally (Fig. 6.1), it does so in a way unlike modern humans. The *A. afarensis* MT 1 head is expanded dorsally, but not mediolaterally widened as seen in *Homo*; rather, the dorsal MT head is narrow and rounded, similar to the chimpanzee condition. Thus, while A.L. 333-115A undoubtedly shows some human-like MT

head shape characteristics, shape analyses demonstrate that the overall MT 1 head shape of the *A. afarensis* is most similar to extant *Pan*. This is immediately contrasted in A.L. 333-115B (MT 2), which falls directly in the *Homo* MT 2 morphospace. It demonstrates both the dorsal expansion and widening of the MT head seen in modern humans, and this is confirmed by its overlap with humans on both PC 1 and PC 2 to the exclusion of chimpanzees. A.L. 333-115C (MT 3) falls intermediate between humans and chimpanzees on PC 1, but overlaps both species on PC 2. A.L. 333-115D (MT 4) is chimpanzee-like on both axes, and A.L. 333-155E (MT 5) is human-like on PC 1, but overlaps both species on PC 2. Overall, the *A. afarensis* forefoot is mosaic and unique in its morphology.

6.4 Discussion

We hypothesized that differences in human and chimpanzee MTPJ function during terrestrial locomotion would be reflected in morphological differences at the metatarsal heads. When viewed in parallel, the kinematic and morphometric data collected in this study strongly support this hypothesis and both of our predictions. In support of the first prediction, humans exhibit greater peak dorsiflexion angles than chimpanzees at the MTPJs whether the latter walk on two or four limbs, which is reflected in distal MT articular surface morphology. The interspecific difference in MTPJ motion is driven by proximal hind limb angular motion; humans extend their hips and knees, and plantarflex their ankles to a greater degree than chimpanzees during the second double-support phase of stance (Pontzer et al., 2014; O'Neill et al., 2015), resulting in feet that are positioned at a greater angle to the ground during push off. This drives the human MTPJs into higher passive dorsiflexion angles, which tautens the plantar aponeurosis and helps to convert ankle power into propulsive force (Erdemir et al., 2004). Chimpanzees possess a far less developed plantar aponeurosis than humans (Susman, 1983), so greater dorsiflexion of the MTPJs will not stabilize the midfoot and facilitate propulsion as in humans.

The interspecies differences in MTPJ kinematics revealed in this study can be related back to joint morphology: Compared to chimpanzees, humans possess metatarsal heads that are more dorsally oriented, allowing them to push off with more dorsiflexed MTPJs. The results of this study indicate that this feature is an especially good predictor of hominoid MTPJ function during push off in terrestrial locomotion. The similarity in chimpanzee MTPJ kinematics during bipedal and quadrupedal locomotion bolsters this notion. Chimpanzees used slightly greater

dorsiflexion angles at MTPJs 2-5 during quadrupedal locomotion, possibly as a result of more retracted hind limb postures that would increase the angle of the foot with the ground at push off (Pontzer et al., 2014). However, the magnitude of this difference between locomotor modes is small (2-5° on average) and only reaches significance for MTPJ 3. Thus, MT head morphology appears to be a good predictor of chimpanzee MTPJ kinematics across terrestrial locomotor modes.

Our results also strongly support our second prediction, that within species inter-ray differences in MTPJ dorsiflexion angles reflect differences in MT head morphology. Humans exhibit diminishing peak dorsiflexion angles from medial to lateral, which is consistent with the findings of previous studies (Griffin et al., 2010a; Pontzer et al., 2014). Chimpanzees, on the other hand, exhibit significantly lower peak dorsiflexion angles at MTPJ 1 than at MTPJ 2, but like humans exhibit diminishing peak dorsiflexion angles from MTPJ 2 to 5. The drop-off in dorsiflexion angle magnitude is steeper in chimpanzees, perhaps due to the oblique orientation of their feet relative to the direction of travel during terrestrial locomotion. In this position the hallux is directed anteromedially, and the lateral digits are directed anterolaterally. Push off occurs at the medial forefoot near MT heads 2 and 3 (Elftman and Manter, 1935; Wunderlich, 1999), so the MTPJs further from this location exhibit progressively lower peak dorsiflexion angles and contact pressures. As a result, the lateral MTPJs of chimpanzees require less structural reinforcement dorsally during push off.

The kinematic trend in MTPJs 2-5 in humans and chimpanzees is mirrored in the morphometric PC 2 scores, which reflect relative MT head robusticity (mediolateral breadth). The patterns of statistically significant differences between rays in MTPJ kinematics and MT head robusticity are similar, particularly for chimpanzees. Inter-ray differences in chimpanzee MT head robusticity mirror quadrupedal MTPJ kinematics exactly, and closely track differences in bipedal kinematics as well. The decline in MT head robusticity that runs laterally across the forefoot in humans and chimpanzees likely reflects both relative peak MTPJ dorsiflexion angle and load at push off. The magnitude of the decline between MT 2 and MT 3 is steeper for humans than for chimpanzees, likely due to differences in the position of the foot's push off axis during walking: In humans this axis is centered between MTPJs 1 and 2, whereas in chimpanzees it is located closer to MTPJs 2 and 3 (Bojsen-Møller, 1979).

The kinematic results of this study extend those of Griffin et al. (2010a) for bonobos, but unlike in that study we found no potential for overlap in peak MTPJ dorsiflexion angles between humans and chimpanzees. In particular the chimpanzees in the present study exhibited markedly lower peak dorsiflexion angles for the first MTPJ than those reported by Griffin et al. for bonobos. This discrepancy could reflect an actual interspecific difference, but it is more likely to be the product of methodological differences in kinematic data collection between studies. Griffin et al. were unable to place markers on their subjects, which can result in errors associated with estimating joint position from static video frames. In the present study, we applied markers to the feet and digits of our subjects to more rigorously quantify MTPJ position.

The morphometric results for A.L. 333-115 reveal a mixed human-chimpanzee morphological pattern for the MT heads of *A. afarensis*. Specifically, MT 1 and MT 4 are chimpanzee-like on PC 1, MT 2 and MT 5 are human-like, and MT 3 falls intermediate between the human and chimpanzee clusters. The morphology pushing some of the A.L. 333 MTs into the chimpanzee distribution is the narrow, chimpanzee-like epicondylar breadth found on some of the *A. afarensis* MT heads. This morphology is correlated with dorsal MT head gracility and suggests that some australopithecine MTPJs would not have been as stable as those of modern humans during moments of high dorsiflexion, such as those occurring during bipedal push off. Although hallux position in *A. afarensis* is debated (Latimer and Lovejoy, 1990b; Doran, 1993), several recent quantitative studies of the first tarsometatarsal joint (Stern, 2000; Proctor et al., 2008; Proctor, 2010a) indicate that *A. afarensis* retained a somewhat abducted hallux. If this were the case, then it follows that this species would push off from an axis centered between MTPJs 2 and 3, as in chimpanzees. This would explain the more human-like morphology of the MT 2 and 3 heads, and the more chimpanzee-like morphology of the MT 1 head in this species. The discrepant signals of the MT 4 and 5 heads for *A. afarensis* are more difficult to interpret. However, lower peak dorsiflexion occurs at MTPJs 4 and 5 in both humans and chimpanzees compared to MTPJ 2 and 3 during push off, and thus the morphology at these joints may be of less importance to fossil locomotor behavior reconstructions.

In sum, these results suggest that the forefoot kinematics of *A. afarensis* during push off in bipedal walking were likely to have been unique, somewhat intermediate between modern humans and chimpanzees. *A. afarensis* probably pushed off from an axis located near the MT 2

head, and lacked the joint stability to dorsiflex its first MTPJ as much as humans during at the end of stance. It is currently unclear if *A. afarensis* possessed a human-like plantar aponeurosis, but if it did it probably did not utilize it in propulsive force production and midfoot stabilization as effectively as humans. Additionally, these results accord with those suggesting a somewhat divergent hallux in this species (Berillon, 1999; Stern 2000; Proctor et al., 2008; Proctor, 2010a), as this would have influenced the forefoot push off axis in the manner suggested by the results of this study. These factors may have resulted in a less efficient form of bipedal locomotion in *A. afarensis* as compared to that of modern humans.

Others, however, have interpreted *A. afarensis* MT head morphology as indicating that this species did in fact use human-like push off kinematics. In particular, Latimer and Lovejoy (1990) and Ward et al. (2011) have argued that the MT heads of this species resemble those of humans in being 'domed' dorsally, which would facilitate human-like dorsiflexion angles at push off. However, these inferences were based on qualitative descriptions of joint morphology, whereas the present study used quantitative 3D shape analyses to diagnose a more intermediate morphological affinity of the *A. afarensis* MT heads. In support of our results, Duncan et al. (1994) also found that the MTPJ morphology of *A. afarensis* fell between that of humans and chimpanzees based on a multivariate discriminant analysis. Thus, qualitative interpretation of MT head morphology may not be a reliable mode for reconstructing MTPJ function from fossil hominin material.

One caveat that must be acknowledged is the condition of the MT heads in the A.L. 333-115 fossils. These fossils demonstrate some weathering, but most of the important morphological features are well preserved (Latimer et al., 1982). Damage to the metatarsal heads is reported in the original descriptions for the plantar aspects of the MT heads, where cancellous bone has been exposed in the plantar condyles of A.L. 333-115B, D and E. Because shape changes associated with plantar condylar morphology explained a comparatively small amount of shape variance (< 5%) by PCs not presented here, we believe that the damage to most of these fossils does not significantly impact our results. A.L. 333-115C (the MT 3) is one major exception because a small part of the dorsal articular surface of the MT head has broken off such that the articular surface does not project above the dorsum of the diaphysis as it does in A.L. 333-115B, the MT 2 (Fig. 6.1). This damage has a probable influence on the PC 1 score that may shift the fossil

towards the chimpanzee PC 1 distribution. If complete, this fossil might actually fall within the human distribution, making it more like the A.L. 333-115B MT 2 specimen. In this case the overall morphology of the *A. afarensis* foot would still be mosaic about the pre- and postaxial pedal rays, which would not diminish our suggestion that *A. afarensis* pushed off from a forefoot axis situated between MT heads 2 and 3.

With regard to the broader significance of this study, no previous investigation of hominoid functional morphology has provided both detailed 3D morphometric and kinematic data to rigorously test postcranial joint form-function relationships. In this study we present marker-based 3D kinematics collected from human and chimpanzee subjects *in vivo* along with modern shape analysis techniques to illustrate the strong relationship between MTPJ articular surface morphology and joint function during terrestrial locomotion. Our results provide a case in which 3DGM shape variables can be used to discern functional aspects of postcranial anatomy, and therefore may be useful in gait biomechanics from fossil material. Some have recommended caution when using 3DGM to assess form-function relationships due to the many factors that influence bone shape in addition to mechanical function (e.g., phylogeny, pathology, and ontogeny) (McNulty and Vineyard, 2015). However, this study provides an example of how clearly defined hypotheses and careful experimental design can be implemented to verify functional signals in 3DGM analyses. Previous work has shown that phylogenetic signal was not a significant determinant of MT head shape, at least in the hallux (Fernández et al., 2015), which provides further support to the notion that the MTPJ morphological signals quantified in this study are related to biomechanical function. Studies that integrate experimental approaches and morphological analysis are rare, yet they are critical to establishing true form-function relationships that can be used in the interpretation of skeletal material, and will ultimately provide researchers with the best tools for understanding the evolution of bipedalism.

6.5 References

Abdi, H., 2010. Holm's sequential Bonferroni procedure in: Salkind, N. (Ed.), Encyclopedia of research design SAGE Publications, Inc. , Thousand Oaks.

Adams, D.C., Collyer, M.L., Otárola-Castillo, E., Sherratt, E., 2015. Geomorph: software for geometric morphometric analyses. R package version 2.1.2.

Adams, D.C., Otárola-Castillo, E., 2013. Geomorph: an R package for the collection and analysis of geometric morphometric shape data. Meth. Ecol. Evol. 4, 393-399.

Almécija, S., Orr, C.M., Tocheri, M.W., Patel, B.A., Jungers, W.L., 2015. Exploring phylogenetic and functional signals in complex morphologies: the hamate of extant anthropoids as a test-case study. Anat. Rec. 298, 212-229.

Almécija, S., Tallman, M., Alba, D.M., Pina, M., Moyà-Solà, S., Jungers, W.L., 2013. The femur of *Orrorin tugenensis* exhibits morphometric affinities with both Miocene apes and later hominins. Nat. Commun. 4, 2888.

Berillon, G. Geometric pattern of the hominoid hallucal tarsometatarsal complex. Quantifying the degree of hallux abduction in early hominids. *C. R. Acad. Sci. Paris Séria IIa* **328**, 627-633, (1999).

Bojsen-Møller, F., 1979. Calcaneocuboid joint and stability of the longitudinal arch of the foot at high and low gear push off. J. Anat. 129, 165-176.

Bookstein, F.L., 1997. Morphometric tools for landmark data: geometry and biology. Cambridge University Press, Cambridge.

Caravaggi, P., Pataky, T., Goulermas, J. Y., Savage, R. & Crompton, R. A dynamic model of the windlass mechanism of the foot: evidence for early stance phase preloading of the plantar aponeurosis. *J. Exp. Biol.* 212, 2491-2499, (2009).

Doran, D.M., 1993. Comparative locomotor behavior of chimpanzees and bonobos: the influence of morphology on locomotion. Am. J. Phys. Anthropol. 91, 83-98.

Duncan, A.S., Kappelman, J., Shapiro, L.J., 1994. Metatarsophalangeal joint function and positional behavior in *Australopithecus afarensis*. Am. J. Phys. Anthropol. 93, 67-81.

Elftman, H., Manter, J., 1935. The evolution of the human foot, with especial reference to the joints. J. Anat. 70, 56-67.

Erdemir, A., Hamel, A.J., Fauth, A.R., Piazza, S.J., Sharkey, N.A., 2004. Dynamic loading of the plantar aponeurosis in walking. J. Bone Joint Surg. 86, 546-552.

Fernández, P.J., Almécija, S., Patel, B.A., Orr, C.M., Tocheri, M.W., Jungers, W.L., 2015. Functional aspects of metatarsal head shape in humans, apes, and Old World monkeys. J. Hum. Evol. 86, 136-146.

Gower, J.C., 1975. Generalized procrustes analysis. Psychometrika 40, 33-51.

Green, D.J., Serrins, J.D., Seitelman, B., Martiny, A.R., Gunz, P., 2015. Geometric Morphometrics of Hominoid Infraspinous Fossa Shape. Anat. Rec. 298, 180-194.

Griffin, N.L., D'Août, K., Richmond, B., Gordon, A., Aerts, P., 2010a. Comparative in vivo forefoot kinematics of *Homo sapiens* and *Pan paniscus*. J. Hum. Evol. 59, 608-619.

Griffin, N.L., D'Août, K., Ryan, T.M., Richmond, B.G., Ketcham, R.A., Postnov, A., 2010b. Comparative forefoot trabecular bone architecture in extant hominids. J. Hum. Evol. 59, 202-213.

Griffin, N.L., Richmond, B.G., 2010. Joint orientation and function in great ape and human proximal pedal phalanges. Am. J. Phys. Anthropol. 141, 116-123.

Harcourt-Smith, W.E.H., Throckmorton, Z., Congdon, K.A., Zipfel, B., Deane, A.S., Drapeau, M.S.M., Churchill, S.E., Berger, L.R., DeSilva, J.M., 2015. The foot of *Homo naledi*. Nat. Commun. 6.

Hicks, J.H., 1954. The mechanics of the foot: II. the plantar aponeurosis and the arch. J. Anat. 88, 25-30.21.

Indjeian, Vahan B., Kingman, Garrett A., Jones, Felicity C., Guenther, Catherine A., Grimwood, J., Schmutz, J., Myers, Richard M., Kingsley, David M., 2016. Evolving new skeletal traits by cis-regulatory changes in bone morphogenetic proteins. Cell 164, 45-56.

Jungers, W.L., Harcourt-Smith, W.E.H., Wunderlich, R.E., Tocheri, M.W., Larson, S.G., Sutikna, T., Due, R.A., Morwood, M.J., 2009. The foot of *Homo floresiensis*. Nature 459, 81-84.

Klingenberg, C.P., 2011. MorphoJ: an integrated software package for geometric morphometrics. Mol. Ecol. Resour. 11, 353-357.

Knigge, R.P., Tocheri, M.W., Orr, C.M., McNulty, K.P., 2015. Three-dimensional geometric morphometric analysis of talar morphology in extant gorilla taxa from highland and lowland habitats. Anat. Rec. 298, 277-290.

Latimer, B., Lovejoy, C.O., 1989. The calcaneus of *Australopithecus afarensis* and its implications for the evolution of bipedality. Am. J. Phys. Anthropol. 78, 369-386.

Latimer, B., Lovejoy, C.O., 1990a. Metatarsophalangeal joints of *Australopithecus afarensis*. Am. J. Phys. Anthropol. 83, 13-23.

Latimer, B.M., Lovejoy, C.O., 1990b. Hallucal tarsometatarsal joint in *Australopithecus afarensis*. Am. J. Phys. Anthropol. 82, 125-133.

Lewis, O.J., 1980. The joints of the evolving foot. Part III. The fossil evidence. J. Anat. 131, 275-298.

Lovejoy, C.O., Latimer, B., Suwa, G., Asfaw, B., White, T.D., 2009. Combining prehension and propulsion: the foot of *Ardipithecus ramidus*. Science 326, 72, 72e71-72e78.

MacConaill, M.A., Basmajian, J.V., 1969. Muscles and movements. Williams & Williams Baltimore.

McNulty, K. P. & Vinyard, C. J. Morphometry, geometry, function, and the future. *Anat. Rec.* **298**, 328-333, (2015).

Morton, D.J., 1922. Evolution of the human foot. Am. J. Phys. Anthropol. 5, 305-336.

O'Neill, M.C., Lee, L.-F., Demes, B., Thompson, N.E., Larson, S.G., Stern Jr, J.T., Umberger, B.R., 2015. Three-dimensional kinematics of the pelvis and hind limbs in chimpanzee (*Pan troglodytes*) and human bipedal walking. J. Hum. Evol. 86, 32-42.

Patel, B.A., 2008. Functional morphology and biomechanics of digitigrade hand postures in cercopithecoid primates. Stony Brook University.

Patel, B.A., 2009. Not so fast: speed effects on forelimb kinematics in cercopithecine monkeys and implications for digitigrade postures in primates. Am. J. Phys. Anthropol. 140, 92-112.

Pontzer, H., Raichlen, D.A., Rodman, P.S., 2014. Bipedal and quadrupedal locomotion in chimpanzees. J. Hum. Evol. 66, 64-82.

Pontzer, H., Rolian, C., Rightmire, G.P., Jashashvili, T., Ponce de León, M.S., Lordkipanidze, D., Zollikofer, C.P.E., 2010. Locomotor anatomy and biomechanics of the Dmanisi hominins. J. Hum. Evol. 58, 492-504.

Preuschoft, H., 1970. Functional anatomy of the lower extremity, in: Bourne, G.H. (Ed.), The chimpanzee, vol. 3. Karger, Basel, pp. 221-294.

Proctor, D.J., 2010a. Brief communication: shape analysis of the MT 1 proximal articular surface in fossil hominins and shod and unshod *Homo*. Am. J. Phys. Anthropol. 143, 631-637.

Proctor, D.J., 2010b. Three-dimensional morphometrics of the proximal metatarsal articular surfaces of *Gorilla, Pan, Hylobates,* and shod and unshod humans. University of Iowa.

Proctor, D.J., 2013. Proximal metatarsal articular surface shape and the evolution of a rigid lateral foot in hominins. J. Hum. Evol. 65, 761-769.

Proctor, D.J., Broadfield, D., Proctor, K., 2008. Quantitative three-dimensional shape analysis of the proximal hallucial metatarsal articular surface in *Homo, Pan, Gorilla,* and *Hylobates*. Am. J. Phys. Anthropol. 135, 216-224.

Rohlf, F.J., 2010. tspRelw: relative warps analysis. Version 1.49. Department of Ecology and Evolution, University of New York at Stony Brook, Stony Brook.

Sokal, R.R., Rohlf, F.J., 2011. Biometry: 4th edition. W.H. Freeman, New York.

Stern, J.T., 2000. Climbing to the top: a personal memoir of *Australopithecus afarensis*. Evol. Anthropol. 9, 111-148.

Stern, J.T., Susman, R.L., 1983. The locomotor anatomy of *Australopithecus afarensis*. Am. J. Phys. Anthropol. 60, 279-317.

Susman, R.L., 1983. Evolution of the human foot: evidence from Plio-Pleistocene hominids. Foot Ankle 3, 365-376.

Susman, R.L., Brain, T.M., 1988. New first metatarsal (SKX 5017) from Swartkrans and the gait of *Paranthropus robustus*. Am. J. Phys. Anthropol. 77, 7-15.

Susman, R.L., de Ruiter, D.J., 2004. New hominin first metatarsal (SK 1813) from Swartkrans. J. Hum. Evol. 47, 171-181.

Susman, R.L., Stern, J.J.T., Jungers, W.L., 1984. Arboreality and bipedality in the Hadar hominids. Folia Primatol. 43, 113-156.

Tocheri, M.W., Solhan, C.R., Orr, C.M., Femiani, J., Frohlich, B., Groves, C.P., Harcourt-Smith, W.E., Richmond, B.G., Shoelson, B., Jungers, W.L., 2011. Ecological divergence and medial cuneiform morphology in gorillas. J. Hum. Evol. 60, 171-184.

Ward, C.V., Kimbel, W.H., Johanson, D.C., 2011. Complete fourth metatarsal and arches in the foot of *Australopithecus afarensis*. Science 331, 750-753.

Wiley, D. F. *et al.* Evolutionary morphing *IEEE Visualization Conference, Minneapolis, MN*, 431-438, (2005).

Winter, D., 2005. Biomechanics and motor control of human movement. 3rd edition. John Wiley and Sons, Inc. , Hoboken.

Wood-Jones, F., 1944. Structure and function as seen in the foot. Bailliere and Co. , London.

Wunderlich, R.E., 1999. Pedal form and plantar pressure distribution in anthropoid primates. . Stony Brook University.

Subject	Equation	SEE*	R^2	t_s (s)	Estimated v
Chimpanzee Biped					
A	$\ln(v) = 0.76*\ln(t_s^{-1}) - 1.25$	0.034	0.78	0.6 ± 0.06	0.42 ± 0.03
B	$\ln(v) = 0.79*\ln(t_s^{-1}) - 1.17$	0.03	0.72	0.58 ± 0.06	0.48 ± 0.02
Average				*0.58 ± 0.05*	*0.46 ± 0.05*
Chimpanzee Quadruped					
A	$\ln(v) = 1.41*\ln(t_s^{-1}) - 1.39$	0.11	0.73	0.68 ± 0.02	0.43 ± 0.02
B	$\ln(v) = 1.37*\ln(t_s^{-1}) - 1.34$	0.071	0.91	0.73 ± 0.08	0.41 ± 0.05
Average				*0.71 ± 0.06*	*0.42 ± 0.04*
Human					
A	$\ln(v) = 1.54*\ln(t_s^{-1}) - 1.59$	0.033	0.98	0.59 ± 0.01	0.46 ± 0.01
B	$\ln(v) = 2.07*\ln(t_s^{-1}) - 1.73$	0.039	0.95	0.65 ± 0.01	0.43 ± 0.01
C	$\ln(v) = 1.63*\ln(t_s^{-1}) - 1.42$	0.027	0.98	0.69 ± 0.02	0.44 ± 0.02
D	$\ln(v) = 1.47*\ln(t_s^{-1}) - 1.36$	0.046	0.96	0.66 ± 0.01	0.47 ± 0.01
E	$\ln(v) = 1.85*\ln(t_s^{-1}) - 1.47$	0.053	0.96	0.68 ± 0.01	0.47 ± 0.01
Average				*0.66 ± 0.04*	*0.45 ± 0.02*

Table 6.1. Least-squares linear regression equations describing the relationship between dimensionless velocity (v) and stance phase duration (t_s) for each subject, and average t_s measured and v estimated from all steps analyzed for each subject. See preceding text for description of equation. *Standard error of estimate.

Landmark Number	Type	Landmark Description
1	Type II	most medially protruding point on medial epicondyle
2	Type III	midpoint between point 1 and 3, medial ridge separating distal articular surface from MT diaphysis
3	Type II	most plantarly projecting point on medial plantar condyle
4	Type II	dorsal most point on dorsal surface of MT articular surface
5	Type II	most distally projecting point on MT head
6	Type III	most plantarly projecting point on intercondylar ridge
7	Type II	most laterally protruding point on lateral epicondyle
8	Type III	midpoint between point 7 and 9, lateral ridge separating distal articular surface from MT diaphysis
9	Type II	most plantarly projecting point on lateral plantar condyle

Table 6.2. List of landmarks on each metatarsal head. Semilandmark locations are calculated using minimized Procrustes distance between reference landmarks. Refer to Figure 2 Fernández et al. (2015) for semilandmark location placement on the distal MT articular surface.

MTPJ	Human (N=25)	Chimp Biped (N=20)	Chimp Quadruped (N=10)
1	48±12°*	12 ± 7°	12 ± 4°
2	48±4°*	30 ± 6°	33 ± 5°
3	47±4°*	23 ± 5°§	28 ± 3°
4	41±7°*	14 ± 4°	17 ± 3°
5	21±6°*	11 ± 3°	13 ± 6°

Table 6.3. Average ± SD peak metatarsophalangeal joint (MTPJ) dorsiflexion angles during push off in humans and chimpanzees. *Significant difference between human and chimpanzee (bipedal *and* quadrupedal) angles ($p < 0.001$). §Significant difference between chimpanzee bipedal and chimpanzee quadrupedal angles ($p < 0.003$).

Pedal Rays Compared	Human		Chimpanzee Biped		Chimpanzee Quadruped	
	MTPJ Angles*	MT Head PC 2§	MTPJ Angles*	MT Head PC 2§	MTPJ Angles*	MT Head PC 2§
1 vs. 2	n.s.	--	2 > 1 ($P < 0.001$)	--	2 > 1 ($P < 0.001$)	--
1 vs. 3	n.s	--	3 > 1 ($P < 0.001$)	--	3 > 1 ($P < 0.001$)	--
1 vs. 4	n.s.	--	n.s.	--	n.s.	--
1 vs. 5	1 > 5 ($P < 0.001$)	--	n.s.	--	n.s.	--
2 vs. 3	n.s.	2 > 3 ($P < 0.001$)	n.s.	n.s.	n.s.	n.s.
2 vs. 4	n.s.	2 > 4 ($P < 0.001$)	2 > 4 ($P < 0.001$)	2 > 4 ($P < 0.001$)	2 > 4 ($P = 0.006$)	2 > 4 ($P < 0.001$)
2 vs. 5	2 > 5 ($P < 0.001$)	2 > 5 ($P < 0.001$)	2 > 5 ($P < 0.001$)	2 > 5 ($P < 0.001$)	2 > 5 ($P < 0.001$)	2 > 5 ($P < 0.001$)
3 vs. 4	n.s.	3 > 4 ($P < 0.001$)	3 > 4 ($P = 0.002$)	n.s.	n.s.	n.s.
3 vs. 5	3 > 5 ($P < 0.001$)	3 > 5 ($P < 0.001$)	3 > 5 ($P < 0.001$)	3 > 5 ($P < 0.001$)	3 > 5 ($P < 0.001$)	3 > 5 ($P < 0.001$)
4 vs. 5	4 > 5 ($P < 0.001$)	n.s.	n.s.	n.s.	n.s.	n.s.

Table 6.4. *Post hoc* pairwise comparisons of peak metatarsophalangeal joint (MTPJ) angles and metatarsal (MT) head PC 2 scores between pedal rays in humans and chimpanzees. *Significant difference between peak dorsiflexion angles of MTPJs based on Kruskal-Wallis *post hoc* tests with a sequential Bonferroni correction. §Significant difference in MT head PC 2 scores based on Tukey's HSD *post hoc* tests. No comparisons involving the head of MT 1 were performed, because non-homologous landmarks were used to capture the shape of this element that were not used for heads of MTs 2-5.

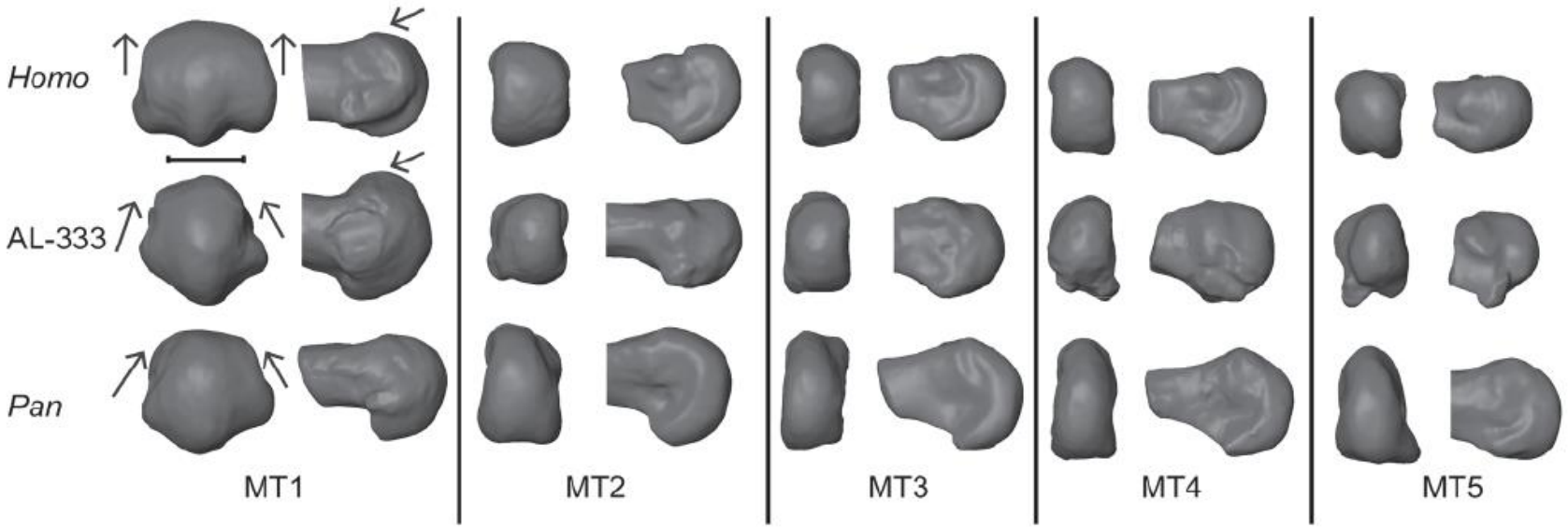

Figure 6.1: Comparative morphology of *Homo, Pan,* and *A. afarensis* metatarsals (MT 1 – MT 5). Note that *Homo* is characterized by dorsal overlap of the distal articular surface onto the MT shaft and by wide flattening of the dorsal articular surface (arrows). AL-333-115 demonstrates *Homo*-like dorsal overlap but lacks mediolateral widening at the MT 1, similar to the condition seen in *Pan*. Left column: distal view. Right column: medial view. Bar: 1 cm.

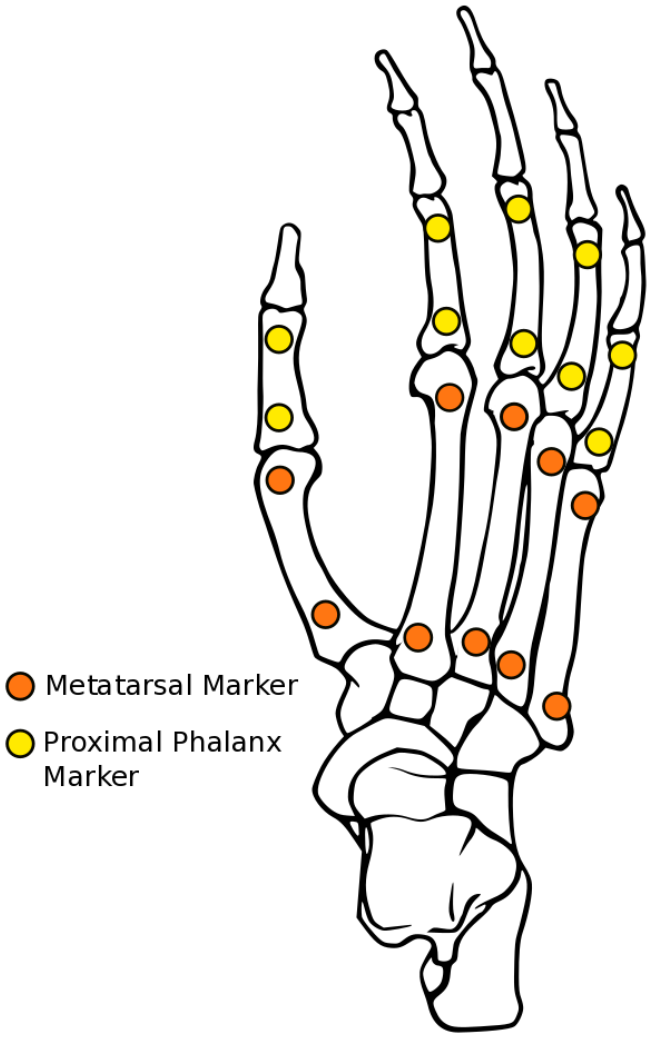

Figure 6.2. Locations for kinematic markers used to measure metatarsophalangeal joint dorsiflexion in all subjects.

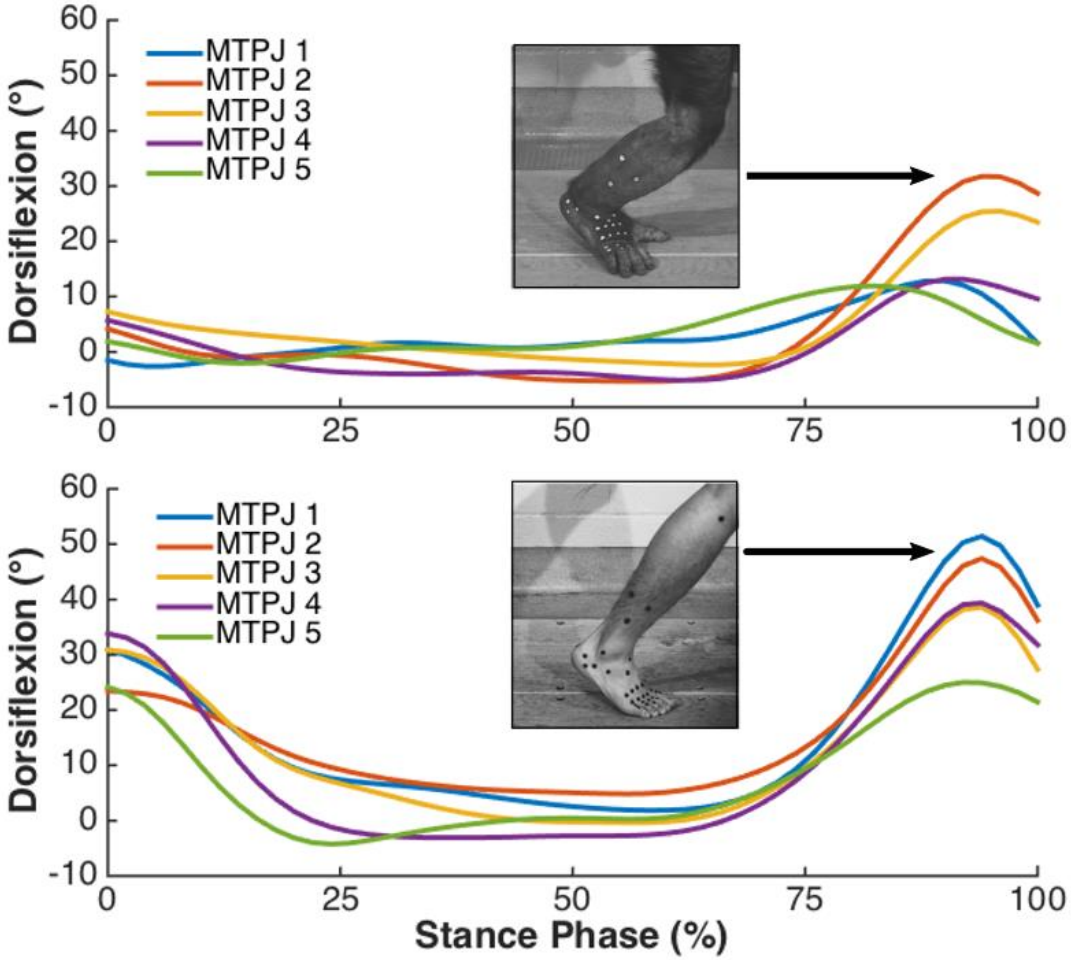

Figure 6.3. Examples of metatarsophalangeal joint motion during stance phase of bipedal steps from a chimpanzee (above) and a human (below). The peak dorsiflexion angles at the end of stance were used in statistical analyses.

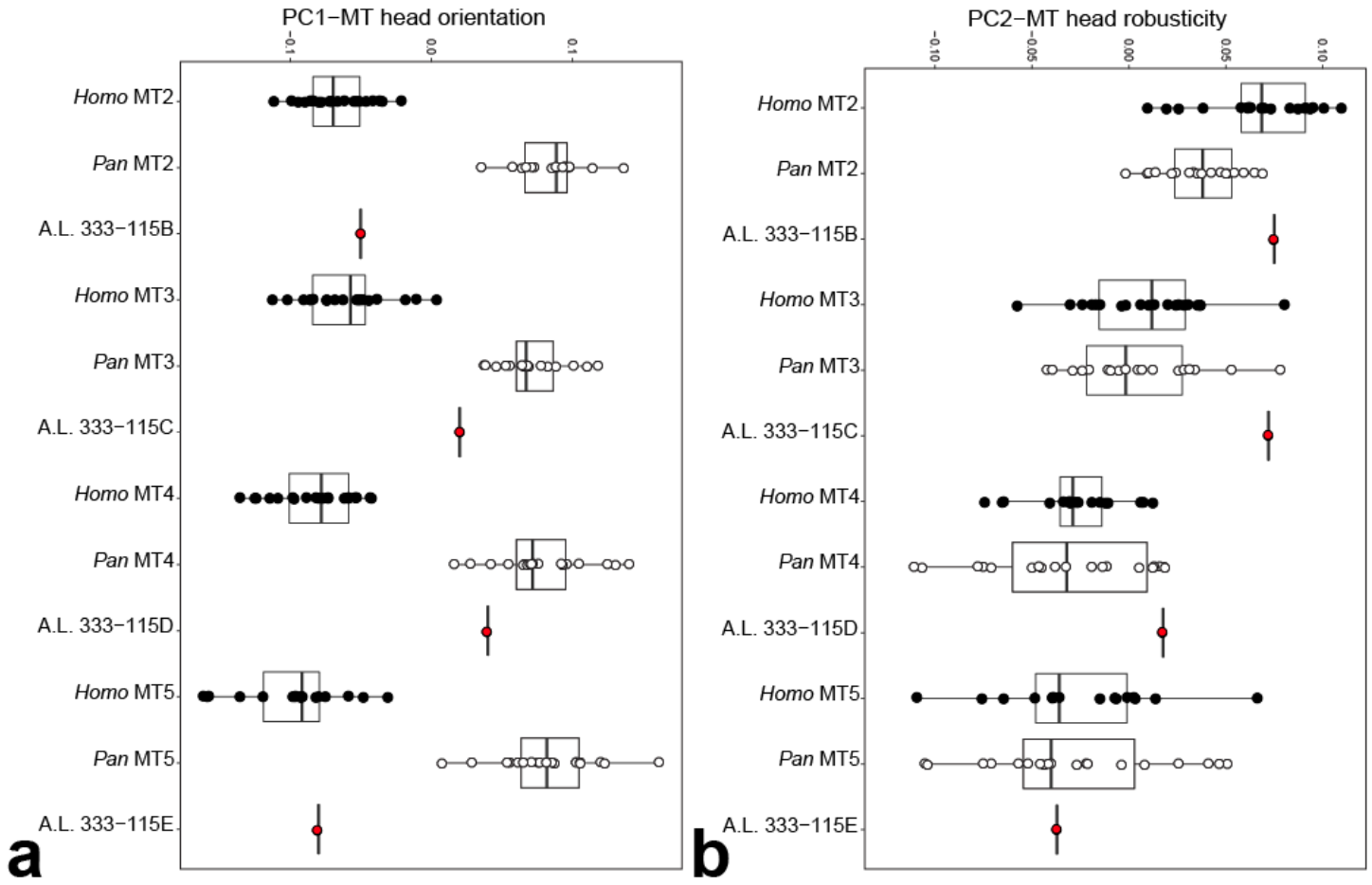

Figure 6.4. Cleveland box-and-whisker plots of PC 1 (a) and PC 2 (b) scores for MT 2 – MT 5 in humans, chimpanzees, and *Au, afarensis*. PC 1 tracked overall dorsoplantar MT head orientation and PC 2 tracked overall MT head robusticity. For AL-333-115, the MT 2 is human-like on PC 1 and PC 2, the MT 3 is intermediate on PC 1 and within the chimpanzee and human range on PC 2, the MT 4 is human-like on PC 1 and PC 2, and the MT 5 is human-like on PC 1 while overlapping both species on PC 2. Vertical bars: median. Rectangles: interquartile range. Horizontal bars: range.

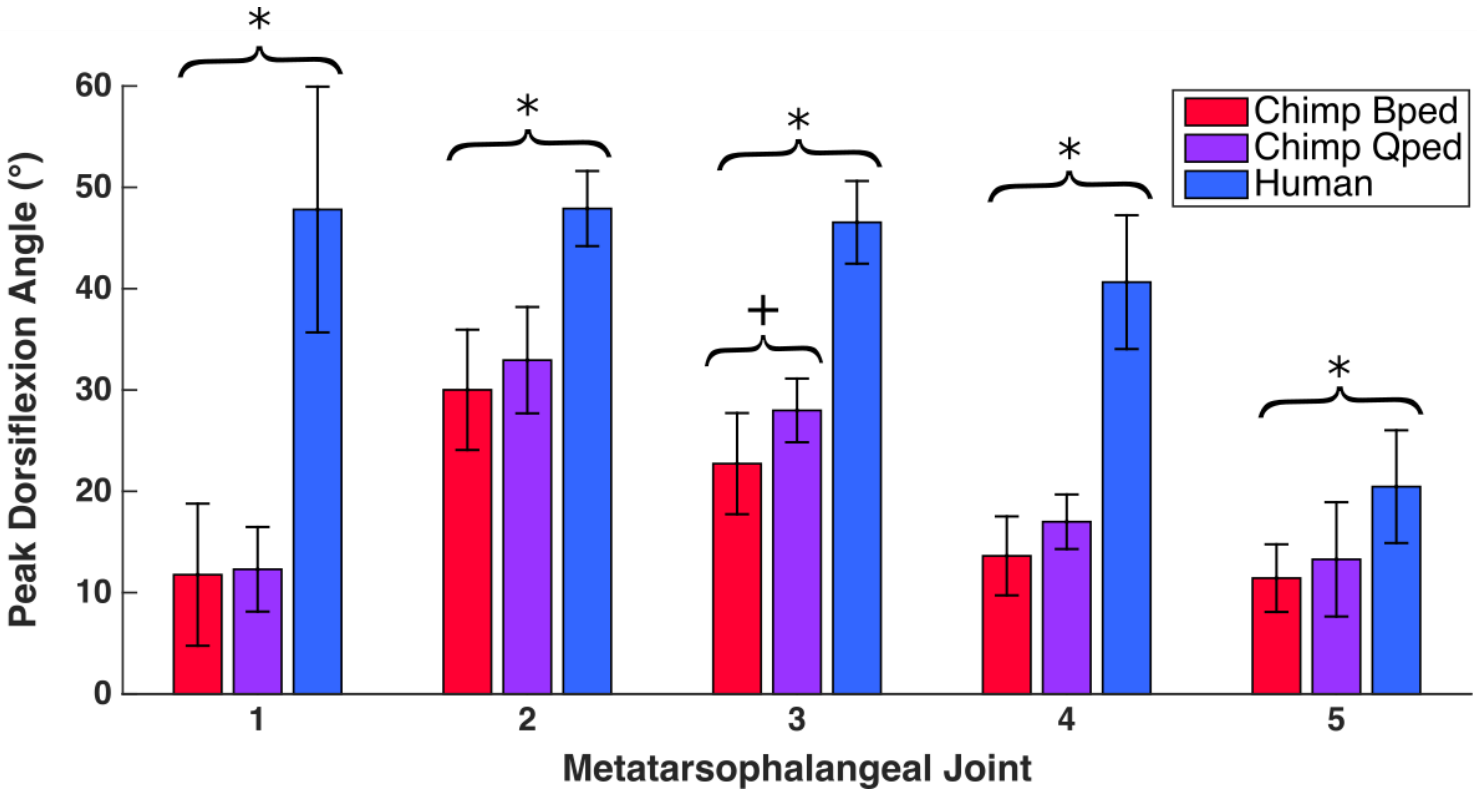

Figure 6.5. Average peak metatarsophalangeal joint dorsiflexion angles during push off in humans and chimpanzees. Plus/minus one standard deviation is indicated by error bars. *Human angles are significantly different from both bipedal and quadrupedal chimpanzee angles (Mann-Whitney U test, $P < 0.001$). $^{+}$Chimpanzee bipedal and quadrupedal angles are significantly different from one another (Mann-Whitney U test, $P = 0.001$).

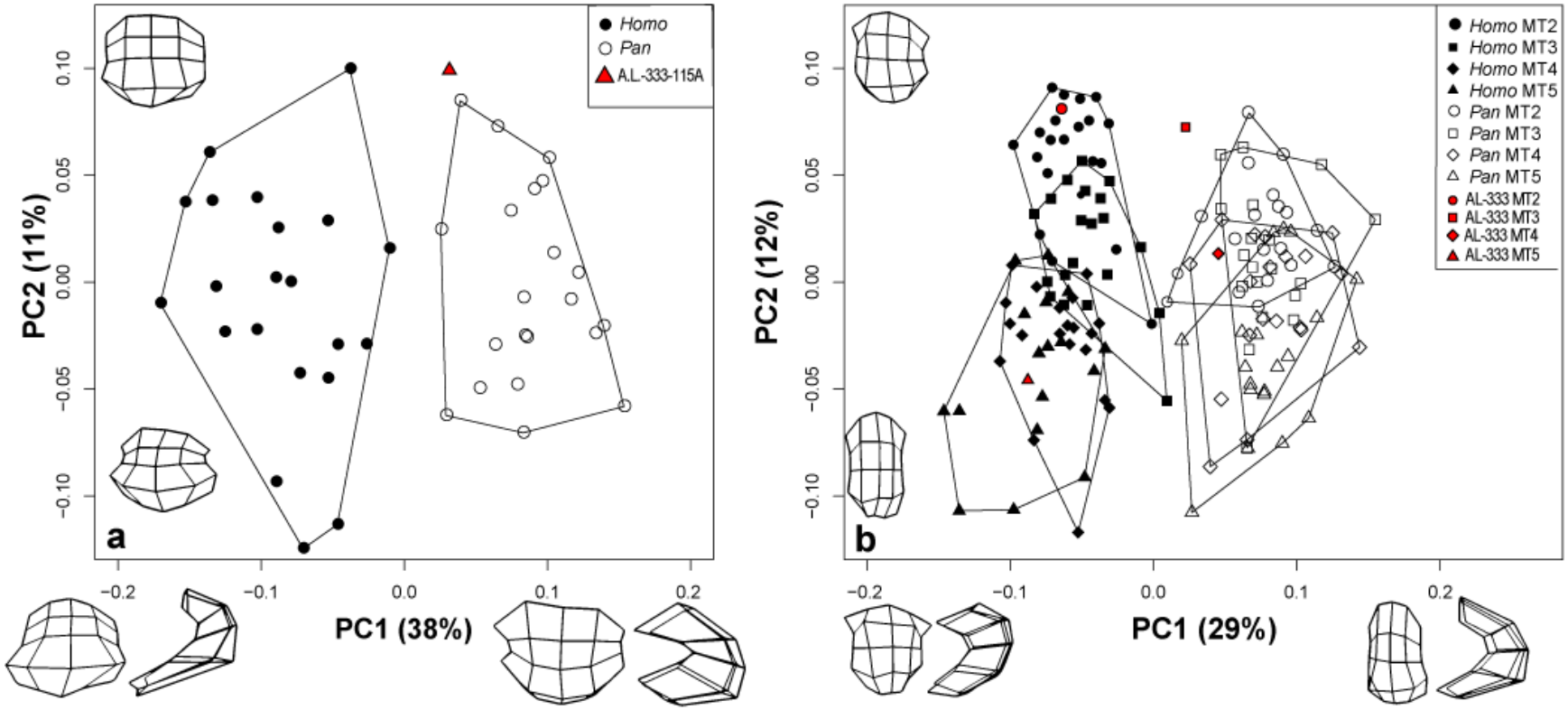

Figure 6.6: PCA scatterplot of PC 1 vs. PC 2 for MT 1 (a) and MT 2 – MT 5 (b). PC 1 tracks orientation of the MT head, PC 1 tracks dorso-plantar orientation of the MT head whereas PC 2 tracks mediolateral MT head breadth. More negative PC 1 scores are more dorsally oriented, whereas more positive PC 1 scores are more plantarly oriented. PC 2 captures overall MT head robusticity, with considerable overlap between species. Wireframes represent articular shape differences of observed extremes for MT 1 (PC 1: -0.19–0.16; PC 2: -0.10–0.12) and MT 2 – MT 5 (0.12–0.15; PC 2: -0.08–0.12).

Chapter 7

Conclusions

7.1 Summary

The overarching aim of this dissertation was to characterize the functional morphology of the anthropoid forefoot in order to test long-standing hypotheses about forefoot function and its relationship to the origins of bipedalism. Specifically, I wanted to test the validity of several functional hypotheses involving the two bony elements that constitute the proximal forefoot joints—the metatarsal head and the proximal pedal phalangeal (PP) base. Although much has been said regarding the morphological properties of the metatarsal (MT) head (Latimer et al., 1982; Stern and Susman, 1983; Susman, 1983; Susman and Brain, 1988; Susman and de Ruiter, 2004; Lovejoy et al., 2009; DeSilva et al., 2012; Harcourt-Smith et al., 2015) and the phalangeal base (Latimer and Lovejoy, 1990a; Duncan et al., 1994; Griffin and Richmond, 2010), the complex articular surface shapes of the MT head and PP base had not been quantified prior to this investigation. After the forefoot joint shapes were quantified using 3-dimensional geometric morphometrics (3DGM), functional hypotheses of anthropoid forefoot form were investigated using comparative methods and collaboration with experimental research in order to determine the functional role of the forefoot joints in bipedalism. I accrued a large dataset of shape variables for every MT and select phalanges (PP 1, 3, 5) in a wide group of anthropoids and fossil hominins in order to infer the forefoot morphology of the stem hominin, and to explore patterns of forefoot evolution that had occurred throughout the anthropoid clade more widely. Secondly, I investigated the relationship between forefoot joint form and function directly by collaborating with Dr. Brigitte Demes and Dr. Nicholas Holowka (Harvard University) to verify that functional hypotheses about forefoot morphology held true for extant humans and apes. My results revealed several broad patterns in anthropoid forefoot evolution. First, it seems the lateral forefoot began to evolve first, with the hallux retaining a primitive form until relatively late in evolution. A similar pattern was found in the pedal phalanges, which looked more primitive than the metatarsals overall. Within phalanges, generally hominins looked more human-like on PP 5

and less so on PP 3 and PP 1, which corroborates the pattern seen in the metatarsals. This staggered timing of forefoot evolution perhaps reflects the importance of arboreal locomotion persisting well into the hominin lineage, due to the functional role the hallux plays in pedal grasping. Evidence of convergent evolution between highly terrestrial cercopithecoids (*Erythrocebus patas*) and hominins was found. Patas monkeys have undergone a suite of adaptations in the lower limb related to their cursorial lifestyle (Meldrum, 1991; Strasser, 1992; Gebo and Sargis, 1994; Polk, 2004), and my findings add to the list of skeletal changes in this taxon. Patterns of forefoot joint covariance seem to be related to the amount of stereotypical positional behavior employed by a given taxonomic group. Finally, correlations with kinematic data in human and chimpanzee forefoot joints suggest that morphological aspects of the forefoot joint are strongly correlated with forefoot dorsiflexion range of motion in these two species. The results from each of these chapters are summarized in more detail below.

7.1.1 Evolution of the anthropoid hallux

Shape analyses on the extant anthropoid and fossil hominin hallux provided mixed support for my hypotheses and predictions. While shape analyses did capture hallucal characters of functional interest (e.g., dorsal orientation of the articular surface, dorsal robusticity of the articular surface), my hypothesis of human convergence with terrestrial taxa (e.g., terrestrial mountain gorillas) was rejected based on the multi OU modeling analyses. OU modeling did however reveal three distinct adaptive optima, which does correspond to the general layout of the MT 1 tangent space. Moreover, significant overlap between humans and the highly terrestrial mountain gorilla (Doran, 1996; Doran, 1997; Doran and McNeilage, 1998) on PC 1 to the exclusion of all other groups suggests that signals of terrestriality are distinguishable in the MT 1 head from signals of bipedalism. PC 1 tracked mediolaterally robusticity of the metatarsal head, and this measure included a flat and dorsally robust hallucal head morphology, which is very human-like. Perhaps because of increased terrestriality and large body size, mountain gorillas have had to adapt a significantly different hallucal head morphology for more stability during terrestrial quadrupedalism. Grauer's gorillas were also found to be distinct from mountain or eastern gorillas, but this may be due to genetic drift and in-breeding present in their very small population (Yamagiwa et al., 1993; Tocheri et al., 2016), leading to unusual phenotypes in this subspecies. The shape analysis results on the Swartkrans and Hadar fossil material provides

further evidence that these hominins still lacked all of the lower limb synapomorphies present in modern humans, suggesting that they practiced bipedalism in a different manner than modern humans, perhaps adopting the facultative bent-knee, bent-hip gait that others have suggested (Stern and Susman, 1983; Susman et al., 1984). My findings lend support to arguments laid out recently by Harcourt-Smith et al. (2015) that the foot of *H. naledi* is essentially modern and its MT head shape certainly supports a modern human-like windlass push off mechanism. Although the Rising Star material has yet to be dated, it is suspected to be relatively young (Williams, pers. comm.) and other parts of the *H. naledi* postcrania look more primitive like the thorax and femoral neck (Berger et al., 2015). Thus, it is unclear as to how the foot of *H. naledi* impacts the evolution of the modern human forefoot. Regardless, it does provide a clear example of a hominin in South Africa with pedal bones essentially indistinguishable from modern humans. Collectively, hallucal head evolution within hominins splays diversely into a multitude of configurations. No consensus pattern towards a modern human-like hallucal head emerges in the fossil record until *H. naledi*, an undated specimen. Regardless, these findings suggest that the emergence of a human-like MT 1 emerges relatively late in hominin evolution. Only once hominins fully committed to obligate terrestrial bipedalism with a fully adducted hallux did the MT 1 head begin to reshape into a modern-like form.

7.1.2 Evolution of the anthropoid lesser metatarsals

Shape analyses of the anthropoid non-hallucal forefoot provided strong support for my hypotheses and predictions. Eigenanalyses captured the functional characters of the metatarsal head (e.g., head orientation and robusticity), and yielded many intriguing results throughout the metatarsals. Unlike what was observed in the hallucal data alone, analyses of all the metatarsals allowed for a more complete picture of forefoot evolution. OU modeling supported my hypothesis that humans would show convergence in the forefoot with highly terrestrial taxa. The OU modeling analysis found evidence for a convergent regime between hominins and *Erythrocebus patas*—the patas monkey, in the MT 2 and MT 3 shape data. Patas monkeys are the most digitigrade (Meldrum, 1991; Gebo and Sargis, 1994; Nowak et al., 2010) and cursorial (*sensu* Patel, 2009) of the primates, with many morphological differences separating them from closely related cercopithecines (e.g., vervet monkeys) including relatively longer hind limbs (Strasser, 1992; Polk, 2004), forelimbs (Polk, 2004), and an elongated tarsus (Strasser, 1992).

These morphological differences likely contribute to the higher locomotor speeds observed in patas monkeys compared to other cercopithecines (Polk, 2004; Arsuaga and Martinez, 2006; Patel, 2009), and may possibly lower cost of locomotion compared to baboons (Polk, 2004). My shape analyses provide additional morphological support for the cursorial nature of patas monkeys—they displayed unique MT head morphology, especially in MT 2 and MT 3. This finding lends support to kinematic observations that estimate the central axis of the cercopithecine foot passing through digit III, with the hallux contributing little to forefoot dorsiflexion on terrestrial substrates (Meldrum, 1991). Patas monkeys consistently had extreme PC 1 values, owing to markedly wide, robust MT heads, as well as high PC 2 values, which denote a dorsally oriented MT head. Additionally, the wide patas MT heads are often terminated proximodorsally by a wide, transverse ridge of bone similar to what is seen in the weight-bearing metacarpals (MC 3, 4) of knuckle-walkers (Susman, 1979). It is likely that the overall morphology of the patas monkey distal metatarsus allows for improved forefoot joint stability during the habitually dorsiflexed foot postures of this highly cursorial primate. Convergent regimes were not found between hominins and other terrestrial primates in MT 4 or MT 5, and this is probably due to the reduced functional importance of these forefoot joints in generating propulsive forces at the end of stance phase in primates generally; kinematic data in humans and chimpanzees supports this notion (Griffin et al., 2010a; Holowka and Fernández, 2016). Convergent regimes were also not found between hominins and other highly terrestrial anthropoids such as baboons (*Papio* sp.) or mountain gorillas (*G. b. beringei*), however, aspects of MT head shape in these more terrestrial taxa did show some similarities to humans. For instance, *Papio* likewise demonstrated the extremely high PC 1 scores observed in *E. patas*, suggesting a similar mechanism of forefoot joint stability is present in this terrestrial species. However, baboons do not demonstrate the marked dorsal orientation of the MT head seen in hominins and the cursorial patas monkey. Overall, it appears that the strength of the functional signal is concentrated more in the medial forefoot (MTs 1 – 3), with a diminished signal present in MT 4 and 5. This is supported by the convergent regimes found in MT 2 and 3 but not 4 and 5, the significant allometric signal and phylogenetic structure to the morphospace in MT 5, and by quantitative 3D kinematic data in humans and chimpanzees. Kinematic data have demonstrated greatly diminished dorsiflexion excursions across the forefoot, with higher dorsiflexion angles observed medially and lower dorsiflexion angles observed laterally, with especially insignificant

amounts of dorsiflexion occurring at MT 5, even in humans (Holowka and Fernández, 2016). Critically, unlike what was generally seen in the hallucal data, hominin MT 2 – 5 head shape looked very similar to that of extant modern humans, which corroborates prior work that suggests initial evolutionary change first acted upon the lateral column of the foot (Proctor, 2013) before proceeding more medially. In all cases, hominins were discriminated from all other non-human groups due to high PC 2 scores, which tracked dorsal head orientation. Even in those fossil specimens that appeared mosaic in MT head shape like *Paranthropus* and StW 89, these fossils demonstrated human-like PC 2 scores and thus were likely to have come from a biped based on their MT head orientation alone, although they likely lacked modern proficiency in striding bipedalism.

7.1.3 Evolution of the anthropoid proximal pedal phalanges

Overall, I found mixed support for my hypotheses and predictions in the pedal phalangeal data. Unlike what I found in the metatarsals, the grand majority of the shape variation in the phalangeal base shape data was well captured on just the first two principal components; typically over half of total variance in phalangeal shape was explained entirely by PC 1 and PC 2. Although shape analyses did capture functional signals in the phalangeal base, including the dorsal orientation of the base (i.e., dorsal canting), it was often not the discriminating factor between humans and other hominoids. Instead, the morphology most indicative of a human-like phalangeal base appeared to be a pronounced dorsal rim of bone buttressing the perimeter of a deeply convex base. This morphology is noted in the description of the Hadar material by Latimer et al. (1982), but here it has been quantified in a reliable manner. Interestingly, there is no single character of the phalangeal base that is entirely 'human-like', but a combination of several characters that yield an overall modern-human looking form. While humans and apes often demonstrate varying degrees of dorsal canting, humans also have the pronounced, dorsally buttressed rim that has been hypothesized to limit extreme dorsiflexion during terrestrial bipedalism (Latimer and Lovejoy, 1990). Regardless of whether or not this hypothesized function is accurate, this feature does seem to better characterize a human-like phalangeal base than dorsal canting, when only looking at the phalangeal base morphology. Thus, this metric may be more useful than the dorsal canting angle, especially in fragmentary fossil specimens. The multivariate shape data on the anthropoid phalangeal base describe more completely this half of the metatarsophalangeal joins (MTPJs) than has so far been accomplished. The data

suggest that dorsal canting may not be as reflective of function as previously thought (Latimer and Lovejoy, 1990; Duncan et al., 1994; Griffin and Richmond, 2010; Rein and McCarty, 2012). The comparative sample and fossil data suggest that not only the orientation of the phalangeal base but also several shape changes in the phalangeal base all contribute to a modern human-like morphology. This suite of features significantly distinguished humans from all other anthropoids sampled, but most hominins did not fully resemble a modern human phalangeal base shape. One possible explanation for this finding is the dual role that the pedal phalanges play in terrestrial locomotion and pedal grasping; thus my findings lend support to the hypothesis that arboreality played a major role in the positional behavior of early hominins.

7.1.4 Forefoot joint covariation in anthropoids

Forefoot covariance results for pedal rays I, III, and V are indicative of a high association between metatarsal head shape and phalangeal base shape in anthropoids. The metrics I used explored the association between a specific set of functionally interpretably morphologies at the forefoot joints by comparing the covariance coefficient (r-PLS) between the major PLS axes in each shape data block directly. Results suggest that the level of covariance in great apes is greater than that seen in hylobatids and cercopithecoids, and I suspect this has to do with the variation of positional behavior seen in monkeys, possible covariance mis-matches in shape due to the diminutive nature of the NWM hallux, and the odd association of hylobatid pedal morphology with that of NWMs (Lewis, 1972). Multivariate statistics and 3D shape data have provided some insight into appositional joint surface morphology in the lower limb (Harcourt-Smith et al., 2008; Turley and Frost, 2014), and my results expand this body of research to the anthropoid forefoot. While this method may have some application for fossil specimen assessment, this usefulness is somewhat marred by the finding that the covariance between block PLS axes rises dramatically when a size proxy (log centroid size) is factored into the cross-covariance matrix (Harcourt-Smith et al., 2008; Chapter 5). The reason for this discrepancy may be due to scaling issues inherent to generalized Procrustes analysis, and so caution should be used when interpreting covariance results as "joint congruence". Other applications may be better approximations of congruence (Peeters et al., 2013; Halilaj et al., 2014), but these methods have some drawbacks as well. Despite the claim that shape covariance can serve as a strong proxy for joint congruence (Harcourt-Smith et al., 2008; Turley and Frost, 2014), it is not an especially useful measure of congruence because the PLS axes, due to the strong correlation (as

shown by r-PLS scores), are not as readily interpretable as the shape space of a principal components analysis. Therefore, even if the shape covariance data were to equate closely with joint congruence, the covariance data does not allow one to extrapolate in a more detailed manner on the nature of the congruence analysis.

7.1.5 Functional morphology and kinematics of the forefoot joints

Based on morphometric results from the earlier chapters, I hypothesized that differences in human and chimpanzee forefoot function during terrestrial locomotion would be reflected in morphological differences at the metatarsal heads. Predictions from this hypothesis included that humans would exhibit greater dorsiflexion range of motion (ROM) across the forefoot joints, and that this would be reflected by a dorsal orientation and robusticity present at the forefoot joints. When viewed in parallel, the kinematic and morphometric data collected in my final chapter strongly support my hypotheses and predictions. In support of my predictions, humans exhibited greater peak dorsiflexion angles than chimpanzees at the MTPJs, which is reflected in distal MT articular surface morphology. The interspecies difference in MTPJ motion is driven by proximal hind limb angular motion; humans extend their hips and knees, and plantarflex their ankles to a greater degree than chimpanzees during the second double-support phase of stance (O'Neill et al., 2015), resulting in feet that are positioned at a greater angle to the ground during push off. This drives the human MTPJs into higher passive dorsiflexion angles, which tautens the plantar aponeurosis and helps to convert ankle power into propulsive force (Erdemir et al., 2004). Chimpanzees possess a far less developed plantar aponeurosis than humans (Susman, 1983), so greater dorsiflexion of the MTPJs will not stabilize the midfoot and facilitate propulsion as in humans. These interspecies differences can be related back to joint morphology: compared to chimpanzees, humans possess metatarsal heads that are more dorsally oriented, allowing them to push off with more dorsiflexed MTPJs. The results of this study indicate that this feature is an especially good predictor of hominoid MTPJ function during locomotion. Taken together with the morphometric findings in fossil hominins, it is probable that the forefoot kinematics of *A. afarensis* during push off in bipedal walking were likely to have been unique, somewhat intermediate between modern humans and chimpanzees. *A. afarensis* probably pushed off from an axis located near the MT 2 head, and lacked the joint stability to dorsiflex its MTPJs as much as humans during push off. There is no way of knowing if *A. afarensis* possessed a human-like

plantar aponeurosis, but if it did, it probably did not utilize it in propulsive force production and midfoot stabilization as effectively as humans. Additionally, these results accord with those suggesting a somewhat divergent hallux in this species (Berillon, 1999; Stern, 2000; Proctor et al., 2008; Proctor, 2010), as this would have influenced the forefoot push off axis. These factors may have resulted in a less efficient form of bipedal locomotion in *A. afarensis* as compared to that of modern humans.

7.1.6 Overall implications for fossil hominins

The findings of my dissertation have direct bearing on the interpretation of the locomotor behavior of fossil hominins. Taken together, my results suggest that the lateral aspect of the forefoot evolved into a modern-like form before the more medial foot. This finding corroborates earlier findings of the bony hominoid midfoot (Proctor, 2013). The ancestral state reconstruction (ASR) of the hominin last common ancestor (LCA) is most informed in the hallucal data because of the greater number of fossils (n = 10) sampled, which better calibrates the squared-change parsimony reconstruction algorithm. My results reconstructed the LCA as possessing an extant ape-like hallucal head, most similar to *Pan troglodytes* and *Pongo abelii*. This reconstruction is logical given the phylogenetic position of the LCA, as well as the possible arboreal nature of the LCA (Stern, 1975; Hunt, 1996; Kivell and Schmitt, 2009; but see Richmond et al., 2001 for an opposing view). Regardless of the predominant locomotor mode practiced by the LCA, it likely incorporated significant amounts of arboreality in its positional behavior. *Ardipithecus ramidus* was found to have hallucal morphology similar to the LCA (i.e., ape-like), and although the *Ardipithecus* hallux has been said to look most like a chimpanzee (Lovejoy et al., 2009a), shape analyses resolved its hallucal head as most similar to *Gorilla beringei*. This finding lends support to the notion that *Ardipithecus* was more adept for terrestrial locomotion than extant chimpanzees based on evidence from other postcranial elements (Lovejoy et al., 2009a). Given this finding, it is tempting to conclude that the LCA was terrestrial and if this was true, the most parsimonious reconstruction is that the LCA a knuckle-walker, but this has not been supported morphologically in *Ardipithecus* wrist and hand (Lovejoy et al., 2009b), or in the carpus/manus of any other hominin. Finally, the phalanges of *Ardipithecus* were found to possess a morphology intermediate between apes and cercopithecoids, which supports the original arguments made about Ardipithecus as proficient above-branch arboreal quadruped (Lovejoy et

al., 2009a; b). That said however, I find this unlikely first based on the fact that this finding was only seen in a few pedal phalanges and not in the metatarsal anatomy, and second based on the body size reconstructions for *Ardipithecus* (> 50 kg; White et al., 2009).

Within *Australopithecus, Au. afarensis and Au. africanus* both have undergone much hallucal head shape change, although in different directions. Regardless, both species retain a hallucal head form much more similar to extant apes than modern humans or early *Homo*. *Au. afarensis*, for which a complete forefoot is available (Latimer et al., 1982), demonstrates strong mosaicism compared to extant hominoids and within its own forefoot. The hallucal MT and phalanx both look more chimpanzee-like compared to the morphology observed in its lesser toes. Many of the *Au. afarensis* forefoot joints look very human-like, but others retain a primitive morphology. Results indicate that *Au afarensis* probably pushed-off the forefoot in a way intermediate to that of modern humans and chimpanzees, perhaps with an axis located closer to the MT 2 head. *Au. africanus* retains a morphology most similar to *Ardipithecus*, although I caution that the *Au. africanus* position in the morphospace is contentious because of the dubious taxonomic affiliations of the StW 562 and StW 595 halluces (Clarke, 2008; DeSilva et al., 2012). If these two fossils are placed into two different groups, then *Au. afarensis* and *Au. africanus* would fall much more closely together in the morphospace and another, yet unnamed taxon would occupy a space near *Ar. ramidus*. Because of the poor pedal fossil record available for *Au. africanus*, and the lack of MT heads preserved in *Au. sediba* (Berger et al., 2010), the picture of early hominin hallucal head shape evolution in South Africa ultimately remains unclear. However, the difference between these two fossils in shape space is greater than the range of variation seen in a single species of *Pan* or *Gorilla*, which lends support for these two fossils representing different species. This is especially true because African apes already show considerable variation in the large sample sizes (n > 30) I collected for my analyses, which exceeds the range of variation observed in modern humans, and thus may exceed the range of variation possible in *Australopithecus*. However, StW 562 and StW 595 both fall within the genus-wide range of variation observed in African apes, and so could conservatively at least belong to the same genus, assuming these ancestral lineages possessed ranges of morphological variation comparable to those of extant hominoids.

Results of the StW 89 shape analysis are truly strange, and this is not surprising based on its peculiar MT head morphology. Although not associated with any craniodental material, the

general consensus in the literature is that StW 89 belongs to *Au. africanus* (DeSilva et al., 2012) based on other material excavated from Sterkfontein Member 4. While the StW 89 metatarsal has a very dorsally oriented MT head, the MT head is also very mediolaterally gracile and rounded, and this combination typifies terrestrial cercopithecines. Shape analysis confirmed this intuition, and showed that StW 89 bears greatest resemblance to patas monkeys overall. This similarity was driven by PC 1 scores that fell outside the range of hominoid shape variation. Some researchers have expressed doubt as to whether StW 89 belongs to a hominin or not (Wallace, pers. comm.), and my results tentatively support this conjecture. Important to note, however, is that many putative hominins do tend to fall at the extreme edge of modern human variation on PC 1 (e.g., A.L. 333-72, KNM-ER 64062, U.W. 101-269) and the overall shape of the nearly intact MT 2 does not tend to particularly resemble that of extant *Erythrocebus* (pers. obs.). Based solely on quantitative analysis of its MT head morphology however, it is ultimately unclear what is represented by the StW 89 metatarsal. What can be said definitely about this MT 2 is that its head shows morphologies consistent with other highly terrestrial taxa. Hallucal remains from *P. robustus* most resemble *H. erectus* and *H.* sapiens on PC 2, but are far more monkey-like on PC 1, resulting in a unique hallucal morphology unlike any extant anthropoid. In fact, this combination results in a hallucal form similar to the StW 89 condition but in the hallux instead of MT 2. Such a configuration presumably facilitated increased dorsiflexion ROM at the MTPJs, but perhaps not with the added stability granted by a wide, robust head seen in modern humans and some other hominin fossils. The overall pattern seen in the *P. robustus* MT 1 is not unlike what has been observed in other derived *P. robustus* postcranial elements (Susman, 1988), providing further evidence that *Paranthropus* was more human-like in its postcranial morphology than previously thought, in contrast to other aspects of its forefoot morphology (Proctor, 2008; Proctor, 2010a; Proctor, 2010b).

Results from fossils that represent genus *Homo* also offer mixed results. The MT 1 of *H. floresiensis*, although undoubtedly derived, still differs from what is seen in modern humans and other extinct *Homo*. It is remarkably short, even when compared to pygmy humans and the foot to lower limb proportions are more similar to chimpanzees than modern humans (Jungers et al., 2009). The LB1 hallux deviates significantly on PC 1 from other early *Homo*, supporting the notion that *H. floresiensis* did not adopt a modern human-like gait (Jungers et al., 2009). The lesser metatarsals from LB 1 all fell within the human cloud, however. The morphology of the

unpublished hallucal phalanges (see Chapter 4) from Liang Bua both fall near the centroid of the minimum convex polygon of great apes. These results provide further evidence that the foot of *H. floresiensis*, especially the hallucal ray, was primitive in many aspects (Jungers et al., 2009). LB 1 phalangeal base shape was found to look more ape-like than human-like, providing further evidence that primitive characters of the pedal phalanges (e.g., base shape, curvature) seem to persist for very long into human evolution. In fact, the hallucal pedal phalanx of *Homo naledi* also looked unlike that of modern humans. This corroborates the ape-like phalangeal curvature found in this specimen, in a foot that otherwise looks essentially modern (Harcourt-Smith et al., 2015), and this includes the shape analysis of all *H. naledi* metatarsals complete enough for analysis in this dissertation (e.g., MT 1, 2, 4). Note that many other *H. naledi* pedal phalanges exist, including non-hallucal phalanges, and it is my hope to add these to the data set in future work as they become available. I suspect that they will follow the pattern observed in other extinct *Homo*, however. Similar to the hobbits and *H. naledi*, KNM-ER 64062 (*Homo.* sp.) most closely resembled modern humans in the lesser metatarsals, all of which looked human-like. In this taxon, the hallux did not look exactly human-like due to its ape-like plantar morphology, which may reflect differences in hallucal sesamoid morphology (Le Minor, 1989). Chimpanzee hallucal sesamoid bones are relatively smaller than those in modern humans (Le Minor 1989; pers. obs), which probably results in reduced mechanical advantage in the moment arm of the tendons of mm. flexor hallucis brevis, which are thought to play an important role in lift-off hallucal dorsiflexion (Aiello and Dean, 1990; Aper et al., 1996). Further, KNM-ER 64062's ape-like plantar morphology may reduce the ability of the hallucal sesamoids to protect the tendon of mm. flexor hallucis longus from impact during terrestrial bipedalism (Richardson, 1999). A geologically younger specimen attributed to *Homo* cf. *erectus* (Leakey et al., 1970; Solan and Day, 1992; Deino and McBrearty, 2002; Fisher and McBrearty, 2002), KNM BK- 63, displays the same morphological pattern as KNM-ER 64062, but to a more extreme extent. The MT head is very strongly dorsally oriented but rounded and relatively narrow, and the plantar surface is cut by deeply sharp facets for the hallucal sesamoids. The overall functional significance of these hallucal head characters is unclear, given that the rest of the *H. erectus* postcrania look very modern, though the most complete material available for this taxon is lacking forefoot material (Brown et al., 1985). In sum, the most salient pattern in hominin forefoot evolution appears to be that the lateral forefoot began evolving towards a human-like joint shape early on, and that

changes in the hallucal phalanx occurred after these initial lateral forefoot changes. This finding mirrors that of midfoot analyses that examined the metatarsal bases, and it is encouraging that shape analyses of both the proximal and distal metatarsal articular surfaces are in agreement (Proctor, 2013). The second major trend is that pedal phalangeal base morphology tends to be more primitive than that of the metatarsals. Such a finding supports earlier hypotheses about foot evolution suggesting that more proximal pedal joint elements (e.g., talocrural, midtarsal) began evolving towards a more human-like form before more distal joint elements (Harcourt-Smith and Aiello, 2004). Taken together, both of these findings suggest that adaptations for pedal grasping and therefore continued use of arboreal substrates persisted well into human evolution— at least through *Australopithecus*, conservatively. Although it is not possible to discern the relative position of the hallux from hallucal head morphology alone, shape analysis results from both *Au. afarensis* and *Au. africanus* hallux support the notion that this genus was typified by at least a partially abducted hallux, as some other researchers have suspected (Berillon, 1999; Stern, 2000; Proctor et al., 2008; Proctor, 2010a).

7.2 Future Directions

During the course of completing my dissertation, new questions about foot functional morphology became evident, and it is my hope to pursue these in future studies. Before detailing these however, the immediate future application of my dissertation work is to include those fossils I was yet unable to access in order to bring my shape analyses to bear on these important specimens. Of the material so far not included, the Burtele hominin (Haile-Selassie et al., 2012) and the hallucal material from Dmanisi (Lordkipanidze et al., 2007) are the most critical omissions needed to answer questions about early hominin and early *Homo* evolution, respectively. It is my hope that with the finalization of my forthcoming forefoot manuscripts, that the arbiters of these crucial fossils will be persuaded to collaborate on future projects. The addition of fossils groups represented by a mostly intact forefoot (e.g., *H. floresiensis*, KNM-ER 64062, *H. neanderthalensis*) would help bolster the hominin interpretations concluded in Chapter 6, and will be pursued very soon. I suspect that those fossils, which are all from genus *Homo*, would look quite similar to modern humans compared to *Au. afarensis*. Because all of these fossil taxa represent relatively late hominin evolution, they are not critical to the interpretations reached in Chapter 6, which is more focused on understanding the earlier adoption of the bipedal

gait in hominin evolution. Other specimens will be included in future work but are somewhat less critical to the main interpretations of this dissertation; these include more material from Liang Bua (the LB6 pedal phalanges), as well as more pedal phalanges from *Homo naledi*, which I hope to analyze as part of an ongoing collaboration with Dr. William Harcourt-Smith (American Museum of Natural History). Beyond expanding the fossil sample sizes of my datasets, I hope to investigate other MTPJ morphological properties thought to influence function, including MT torsion. The most recent comprehensive study of MT torsion (Drapeau and Harmon, 2013) was a good first step but contains some methodological shortcomings, which plan to be improved by a forthcoming quantification method of MT torsion that is being developed by Dr. Tea Jashiashvili (University of Witswatersrand) and Dr. Biren Patel (University of Southern California). I plan to collaborate with both Drs. Jashiashvili and Patel on a study that will better quantify MT torsion, and its relationship to taxonomic groups for which there exists an observed gradient in positional behavior (i.e., more arboreal and more terrestrial species within a given genus). I am also planning on developing a model of pedal element function based on finite element analysis in collaboration with Dr. Harcourt-Smith, the details of which will be fleshed out in forthcoming months. In addition to investigating the relationship between kinematic variables and morphology at the forefoot, I hope to pursue a similar project that examines kinetic variables and robusticity, as it is thought that dorsal MT head robusticity exists to better cope with the increased plantar pressures borne by the forefoot during bipedalism. The data for this project have already been collected by collaborators Dr. Nicholas Holowka and Dr. Kevin Hatala (The George Washington University), and I hypothesize that a pattern similar to what was seen in the kinematic data will be observed, based on prior work (Wunderlich, 1999; Vereecke et al., 2003). Another project I am currently pursuing is investigating alternate ways to capture shape variables of the forefoot joints. Although the 3DGM approach has many advantages, it is not without some shortcomings, which include a very laborious data collection process and some scaling issues related to size-correlated shape change that cannot be controlled for in a generalized Procrustes analysis. I plan to perform an elliptical Fourier analysis (EFA) on shape outline data of the MT heads in distal view, and although this is a much more simple quantification than the one performed for this dissertation, I suspect it may yield some interesting results based on pilot data collected recently. I have completed EFA data collection for my entire hallucal sample and will be analyzing these in the coming months. Once collected, I will perform

a block analysis of shape data versus EFA outline data, which will provide a measure of covariance between the two data collection measures. This will allow me to see to what degree these two methods are measuring the same functional morphologies of the forefoot joints. If the covariance is high, then EFA methods might be more suitable going forward because the data collection required for this method is greatly reduced compared to that of 3DGM.

Finally, I hope to expand greatly on my initial attempts to investigate forefoot joint congruence. This was attempted morphometrically (using appositional shape covariance as a congruence proxy *sensu* Harcourt-Smith et al., 2008) in this dissertation but in performing these analyses, I now believe that this question is best answered by experimental methods, which I hope will be my main pursuit going forward in the study of human evolution. Because relative levels of joint congruence in the foot are of keen interest to hypotheses of pedal functional morphology and evolution (Susman, 1983; Lovejoy et al., 2009), what is needed is an approach that will allow for a more detailed view into joint contact during locomotion. Other novel morphometric attempts to quantify joint congruence have included ratios of curvatures and dimensions between appositional surfaces (Peeters et al., 2013) and a polar coordinate approach using a modified Bhattacharyaa distance criterion (Halilaj et al., 2014) .Ultimately, all morphometric approaches are sensitive to assumptions about the proper reference frame of the elements in question, which is not trivial in a comparative morphology study because of interspecific differences in habitual foot posture, substrate use, and soft tissue structures. In order to best examine forefoot joint congruence, cineradiographic and computed tomography (CT) data are needed to visualize joint motion and morphology together. New experimental techniques developed recently such as X-Ray Reconstruction of Moving Morphology (XROMM) would allow for pinpointing that moment in the gait cycle where maximum joint congruency is achieved between the distal metatarsus and the phalangeal base, and it is predicted that this would occur at around the end of stance phase during lift-off in humans. Since it is already known that maximum plantar pressure under the MTPJs is achieved at this time (Vereecke et al., 2003; Griffin et al., 2010a), such a study could potentially tie maximum plantar pressure and maximum dorsiflexion angle excursions to maximum achieved joint congruency in the MTPJs—a finding that would provide robust support for the hypothesis that maximal joint congruence (i.e., the closed-packed position; MacConaill and Basmajian, 1969) is a critical component of joint stability in the hominin forefoot, as some researchers have suggested (Susman, 1983;

Susman and Brain, 1988; Susman and de Ruiter, 2004). It is my suspicion that this relationship (i.e., joint congruence and stability) may not be as tight as previous researchers have thought. In order to test this, it is my hope to pursue an experimental design that can help answer questions about joint function and stability in the forefoot, and how this can be applied generally to other synovial joints. This will be a large project that will investigate not only the forefoot joints but also other pedal joints whose motions and joint contact patterns are very complex and not fully understood (e.g., the subtalar joint; Lewis, 1980) but nevertheless have been assumed to be fully known in studies of hominin pedal functional morphology (Prang, 2016). Results from this experimental work will not only have wide implications for hominin pedal evolution, but may also provide important experimental data for clinical researchers interested in joint contact and prosthesis design. I end this dissertation by asserting that studies of comparative morphology are useful for advancing our understand of human evolution, but it is only the union of both morphometric studies and experimental studies together that can truly characterize what all physical anthropologist seek to infer—behavior from bone.

References

Abdi, H., 2010. Holm's sequential Bonferroni procedure in: Salkind, N. (Ed.), Encyclopedia of research design SAGE Publications, Inc. , Thousand Oaks.

Adams, D.C., 2014. A generalized K statistic for estimating phylogenetic signal from shape and other high-dimensional multivariate data. Sys. Biol. 63, 685-697.

Adams, D.C., 2016. Evaluating modularity in morphometric data: challenges with the RV coefficient and a new test measure. Meth. Ecol. Evol., n/a-n/a.

Adams, D.C., Otárola-Castillo, E., 2013. Geomorph: an R package for the collection and analysis of geometric morphometric shape data. Meth. Ecol. Evol. 4, 393-399.

Adams, D.C., Collyer, M.L., Otárola-Castillo, E., Sherratt, E., 2015. Geomorph: software for geometric morphometric analyses. R package version 2.1.2.

Aiello, L., Dean, C., 1990. An introduction to human evolutionary anatomy. Academic Press, London.

Alba, D.M., Moyà-Solà, S., Köhler, M., 2003. Morphological affinities of the Australopithecus afarensis hand on the basis of manual proportions and relative thumb length. J. Hum. Evol. 44, 225-254.

Alba, D.M., Almécija, S., Moyà-Solà, S., 2010. Locomotor inferences in Pierolapithecus and Hispanopithecus: Reply to. J. Hum. Evol. 59, 143-149.

Alexander, R.M., Jayes, A.S., 1983. A dynamic similarity hypothesis for the gaits of quadrupedal mammals. Journal of Zoology 201, 135-152.

Almécija, S., Alba, D.M., Moyà-Solà, S., Köhler, M., 2007. Orang-like manual adaptations in the fossil hominoid Hispanopithecus laietanus: first steps towards great ape suspensory behaviours. Proc. Royal Soc. B. 274, 2375-2384.

Almécija, S., Alba, D.M., Moyà-Solà, S., 2009. Pierolapithecus and the functional morphology of Miocene ape hand phalanges: paleobiological and evolutionary implications. J. Hum. Evol. 57, 284-297.

Almécija, S., Moyà-Solà, S., Alba, D.M., 2010. Early origin for human-like precision grasping: a comparative study of pollical distal phalanges in fossil hominins. PLoS ONE 5, e11727.

Almécija, S., Tallman, M., Alba, D.M., Pina, M., Moyà-Solà, S., Jungers, W.L., 2013. The femur of Orrorin tugenensis exhibits morphometric affinities with both Miocene apes and later hominins. Nat. Commun. 4, 2888.

Almécija, S., Orr, C.M., Tocheri, M.W., Patel, B.A., Jungers, W.L., 2015a. Exploring phylogenetic and functional signals in complex morphologies: yhe hamate of extant anthropoids as a test-case study. Anat. Rec. 298, 212-229.

Almécija, S., Smaers, J.B., Jungers, W.L., 2015b The evolution of human and ape hand proportions. Nat. Commun. 6.

Aper, R.L., Saltzman, C.L., Brown, T.D., 1996. The effect of hallux sesamoid excision on the flexor hallucis longus moment arm. Clinical Orthopaedics and Related Research 325, 209-217.

Arnold, C., Matthews, L.J., Nunn, C.L., 2010. The 10kTrees website: a new online resource for primate phylogeny. Evol. Anthropol. 19, 114-118.

Arsuaga, J., Martinez, M., 2006. The chosen species: the long march of human evolution. Blackwell Publishing, Ltd. , Malden

Bates, K.T., Collins, D., Savage, R., McClymont, J., Webster, E., Pataky, T.C., D'Aout, K., Sellers, W.I., Bennett, M.R., Crompton, R.H., 2013. The evolution of compliance in the human lateral mid-foot. Proc. Royal Soc. B. 280, 20131818.

Begun, D.R., Teaford, M.F., Walker, A., 1994. Comparative and functional anatomy of Proconsul phalanges from the Kaswanga Primate Site, Rusinga Island, Kenya. J. Hum. Evol. 26, 89-165.

Berger, L.R., de Ruiter, D.J., Churchill, S.E., Schmid, P., Carlson, K.J., Dirks, P.H.G.M., Kibii, J.M., 2010. Australopithecus sediba: a new species of Homo-like australopith from South Africa. Science 328, 195-204.

Berger, L.R., Hawks, J., de Ruiter, D.J., Churchill, S.E., Schmid, P., Delezene, L.K., Kivell, T.L., Garvin, H.M., Williams, S.A., DeSilva, J.M., Skinner, M.M., Musiba, C.M., Cameron, N., Holliday, T.W., Harcourt-Smith, W., Ackermann, R.R., Bastir, M., Bogin, B., Bolter, D., Brophy, J., Cofran, Z.D., Congdon, K.A., Deane, A.S., Dembo, M., Drapeau, M., Elliott, M.C., Feuerriegel, E.M., Garcia-Martinez, D., Green, D.J., Gurtov, A., Irish, J.D., Kruger, A., Laird, M.F., Marchi, D., Meyer, M.R., Nalla, S., Negash, E.W., Orr, C.M., Radovcic, D., Schroeder, L., Scott, J.E., Throckmorton, Z., Tocheri, M.W., VanSickle, C., Walker, C.S., Wei, P., Zipfel, B., 2015. Homo naledi, a new species of the genus Homo from the Dinaledi Chamber, South Africa. eLife 4.

Bergeson, D., 1998. Patterns of suspensory feeding in *Alouatta palliata*, *Ateles geoffroyi*, and *Cebus capucinus*, in: Strasser, E., Fleagle, J.G., Rosenberger, A.L., McHenry, H. (Eds.), Primate locomotion. Plenum Press, New York, pp. 45-60.

Berillon, G., 1999. Geometric pattern of the hominoid hallucal tarsometatarsal complex. Quantifying the degree of hallux abduction in early hominids. C. R. Acad. Sci. Paris Séria IIa 328, 627-633.

Bloch, J.I., Boyer, D.M., 2002. Grasping primate origins. Science 298, 1606-1610.

Blomberg, S.P., Garland, T., Ives, A.R., Crespi, B., 2003. Testing for phylogenetic singnal in comparative data: behavioral traits are more labile. Evolution 57, 717-745.

Bojsen-Møller, F., 1979. Calcaneocuboid joint and stability of the longitudinal arch of the foot at high and low gear push off. J. Anat. 129, 165-176.

Bookstein, F.L., 1997. Morphometric tools for landmark data: geometry and biology. Cambridge University Press, Cambridge.

Bookstein, F.L., Gunz, P., Mitterœcker, P., Prossinger, H., Schæfer, K., Seidler, H., 2003. Cranial integration in Homo: singular warps analysis of the midsagittal plane in ontogeny and evolution. J. Hum. Evol. 44, 167-187.

Boonratana, R., 2000. Ranging behavior of proboscis monkeys (*Nasalis larvatus*) in the Lower Kinabatangan, Northern Borneo. International Journal of Primatology 21, 497-518.

Brown, F., Harris, J., Leakey, R., Walker, A., 1985. Early *Homo erectus* skeleton from west Lake Turkana, Kenya. Nature 316, 788-792.

Brown, P., Sutikna, T., Morwood, M.J., Soejono, R.P., Jatmiko, Wayhu Saptomo, E., Awe Due, R., 2004. A new small-bodied hominin from the Late Pleistocene of Flores, Indonesia. Nature 431, 1055-1061.

Bush, M.E., Lovejoy, C.O., Johanson, D.C., Coppens, Y., 1982. Hominid carpal, metacarpal, and phalangeal bones recovered from the Hadar formation: 1974–1977 collections. Am. J. Phys. Anthropol. 57, 651-677.

Cant, J.G.H., 1987. Positional behavior of female bornean orangutans (*Pongo pygmaeus*). Am. J. Primatol. 12, 71-90.

Cant, J.G.H., 1988. Positional behavior of long-tailed Macaques (*Macaca fascicularis*) in Northern Sumatra. Am. J. Phys. Anthropol. 76, 29-37.

Cant, J.G.H., Youlatos, D., Rose, M.D., 2001. Locomotor behavior of *Lagothrix lagothricha* and *Ateles belzebuth* in Yasuni National Park, Ecuador: general patterns and nonsuspensory modes. J. Hum. Evol. 41, 141-166.

Caravaggi, P., Pataky, T., Goulermas, J.Y., Savage, R., Crompton, R., 2009. A dynamic model of the windlass mechanism of the foot: evidence for early stance phase preloading of the plantar aponeurosis. J. Exp. Biol. 212, 2491-2499.

Clarke, R., 1988. A new Australopithecus cranium from Sterkfontain and its bearing on the ancestry of Paranthropus in: Grine, F.E. (Ed.), Evolutionary history of the "robust" australopithecines Transaction Publishers, New Brunswick pp. 285-292.

Clarke, R., 2008. Latest information on Sterkfontein's *Australopithecus* skeleton and a new look at *Australopithecus*. South African Journal of Science 104, 443-449.

Clarke, R., Tobias, P., 1995. Sterkfontein member 2 foot bones of the oldest South African hominid. Science 269, 521-524.

Congdon, K.A., Ward, C.V., Kimbel, W.H., 2011. The first complete fourth metatarsal of Australopithecus afarensis from Hadar. Ethiopia. Am. J. Phys. Anthropol. 144, 111.

Day, M., Napier, J., 1964. Hominid fossils from Bed I, Olduvai Gorge, Tanganyika: fossil foot bones. Nature 201, 969-970.

Deane, A.S., Begun, D.R., 2008. Broken fingers: retesting locomotor hypotheses for fossil hominoids using fragmentary proximal phalanges and high-resolution polynomial curve fitting (HR-PCF). J. Hum. Evol. 55, 691-701.

Deino, A.L., McBrearty, S., 2002. $^{40}Ar/^{39}Ar$ dating of the Kapthurin Formation, Baringo, Kenya. J. Hum. Evol. 42, 185-210.

Deloison, Y., 2003. Anatomie des os fossils de pieds des hominids d'Afrique du suddates entre 2,4 et 3,5 millions d'annés. Interprétation quant à leur mode de locomotion. Biométrie Hum. Anthropol. 21, 189-230.

DeSilva, J.M., 2008. Vertical climbing adaptations in the anthropoid ankle and midfoot: implications for locomotion in Miocene catarrhines and Plio-Pleistocene hominins. University of Michigan.

DeSilva, J.M., 2009. Functional morphology of the ankle and the likelihood of climbing in early hominins. Proc. Nat. Acad. Sci. 106, 6567-6572.

DeSilva, J.M., 2010. Revisiting the "midtarsal break". Am. J. Phys. Anthropol. 141, 245-258.

DeSilva, J.M., Gill, S.V., 2013. Brief communication: a midtarsal (midfoot) break in the human foot. Am. J. Phys. Anthropol. 151, 495-499.

DeSilva, J.M., Proctor, D.J., Zipfel, B., 2012. A complete second metatarsal (StW 89) from Sterkfontein Member 4, South Africa. J. Hum. Evol. 63, 487-496.

Diawol, V.P., Giri, F., Collins, P.A., 2015. Shape and size variations of Aegla uruguayana (Anomura, Aeglidae) under laboratory conditions: a geometric morphometric approach to the growth. Iheringia. Série Zoologia 105, 76-83.

Dingwall, H.L., Tocheri, M.W., Awe, R.D., Sutikna, T., Saptomo, E.W., Jatmiko, Wasisto, S., Jungers, W.L., 2014. Comparative morphology of the proximal hallucal phalanges of Homo floresiensis, Am. J. Phys. Anthropol. WILEY-BLACKWELL 111 RIVER ST, HOBOKEN 07030-5774, NJ USA, pp. 106-106.

Doran, D.M., 1992. The ontogeny of chimpanzee and pygmy chimpanzee locomotor behavior: a case study of paedomorphism and its behavioral correlates. J. Hum. Evol. 23, 139-157.

Doran, D.M., 1993a. Comparative locomotor behavior of chimpanzees and bonobos: the influence of morphology on locomotion. Am. J. Phys. Anthropol. 91, 83-98.

Doran, D.M., 1993b. Sex differences in adult chimpanzee positional behavior: the influence of body size on locomotion and posture. Am. J. Phys. Anthropol. 91, 99-115.

Doran, D.M., 1996. Comparative positional behavior of the African apes, in: McGrew, W.C., Marchant, L.F., Nishida, T. (Eds.), Great ape societies University Press, Cambridge, pp. 213-224.

Doran, D.M., 1997. Ontogeny of locomotion in mountain gorillas and chimpanzees. J. Hum. Evol. 32, 323-344.

Doran, D.M., McNeilage, A., 1998. Gorilla ecology and behavior. Evol. Anthropol. 6, 120-131.

Drapeau, M.S.M., Harmon, E.H., 2013. Metatarsal torsion in monkeys, apes, humans and australopiths. J. Hum. Evol. 64, 93-108.

Dryden, I.L., Mardia, K.V., 1998. Statistical shape analysis. J. Wiley Chichester.

Dunbar, R.I.M., Dunbar, E.P., 1974. Ecological relations and niche separation between sympatric terrestrial primates in Ethiopia. Folia Primatol. 21, 36-60.

Duncan, A.S., Kappelman, J., Shapiro, L.J., 1994. Metatarsophalangeal joint function and positional behavior in Australopithecus afarensis. Am. J. Phys. Anthropol. 93, 67-81.

Dunn, R.H., Tocheri, M.W., Orr, C.M., Jungers, W.L., 2014. Ecological divergence and talar morphology in gorillas. Am. J. Phys. Anthropol. 153, 526-541.

Elftman, H., Manter, J., 1935a. Chimpanzee and human feet in bipedal walking. Am. J. Phys. Anthropol. 20, 69-79.

Elftman, H., Manter, J., 1935b. The evolution of the human foot, with especial reference to the joints. J. Anat. 70, 56-67.

Erdemir, A., Hamel, A.J., Fauth, A.R., Piazza, S.J., Sharkey, N.A., 2004. Dynamic loading of the plantar aponeurosis in walking. J. Bone Joint Surg. 86, 546-552.

Fernández, P.J., Almécija, S., Patel, B.A., Orr, C.M., Tocheri, M.W., Jungers, W.L., 2015. Functional aspects of metatarsal head shape in humans, apes, and Old World monkeys. J. Hum. Evol. 86, 136-146.

Fisher, R., McBrearty, S., 2002. The comparative morphology of hominin postcranial remains from the Kaputhrian formation, Baringo district, Kenya. Am. J. Phys. Anthropol. 34, 70.

Fleagle, J.G., 1978. Locomotion, posture and habitat utilization of two sympatric Malaysian leaf-monkeys (Presbytis obscura and Presbytis melalophos), in: Montgomery, G. (Ed.), Ecology of arboreal folivores. Smithsonian Press, Washington, D.C., pp. 243-251.

Fleagle, J.G., 1980. Locomotion and posture, in: Chivers, D. (Ed.), Malayan forest primates: ten years' study in tropical rain forest. Plenum Press, pp. 191-207.

Fleagle, J.G., 2013. Primate adaptation and evolution. Academic Press, San Diego.

Fleagle, J.G., Mittermeier, R.A., 1980. Locomotor behavior, body size, and comparative ecology of seven Surinam monkeys. Am. J. Phys. Anthropol. 52, 301-314.

Galdikas, B.M.F., Orangutan diet, range, and activity at Tanjung Puting, Central Borneo. International Journal of Primatology 9, 1-35.

Gebo, D.L., 1992. Locomotor and postural behavior in Alouatta palliata and Cebus capucinus. Am. J. Primatol. 26, 277-290.

Gebo, D.L., 1993. Postcranial adaptation in nonhuman primates. Northern Illinois University Press, DeKalb.

Gebo, D.L., 2014. Primate comparative anatomy. Johns Hopkins University Press, Baltimore.

Gebo, D.L., Sargis, E.J., 1994. Terrestrial adaptations in the postcranial skeletons of guenons. Am. J. Phys. Anthropol. 93, 341-371.

Gittins, S.P., 1983. Use of the forest canopy by the agile gibbon. Folia Primatol. 40, 134-144.

Gomberg, D.N., 1985. Functional differences of three ligaments of the transverse tarsal joint in hominoids. J. Hum. Evol. 14, 553-562.

Gosselin-Ildari, A.D., 2013. The evolution of the human foot, with special reference to the joints. Stony Brook University.

Gower, J.C., 1975. Generalized procrustes analysis. Psychometrika 40, 33-51.

Grabowski, M.W., Polk, J.D., Roseman, C.C., 2011. Divergent patterns of integration and reduced constraint in the human hip and the origins of bipedalism. Evolution 65, 1336-1356.

Green, D.J., Alemseged, Z., 2012. Australopithecus afarensis scapular ontogeny, function, and the role of climbing in human evolution. Science 338, 514-517.

Green, D.J., Serrins, J.D., Seitelman, B., Martiny, A.R., Gunz, P., 2015. Geometric Morphometrics of Hominoid Infraspinous Fossa Shape. Anat. Rec. 298, 180-194.

Griffin, N.L., Richmond, B.G., 2010. Joint orientation and function in great ape and human proximal pedal phalanges. Am. J. Phys. Anthropol. 141, 116-123.

Griffin, N.L., D'Août, K., Richmond, B., Gordon, A., Aerts, P., 2010a. Comparative in vivo forefoot kinematics of Homo sapiens and Pan paniscus. J. Hum. Evol. 59, 608-619.

Griffin, N.L., D'Août, K., Ryan, T.M., Richmond, B.G., Ketcham, R.A., Postnov, A., 2010b. Comparative forefoot trabecular bone architecture in extant hominids. J. Hum. Evol. 59, 202-213.

Grine, F.E., 1988. New craniodental fossils of Paranthropus from the Swartkrans Formation and their significance in "robust" australopithecine evolution, in: Grine, F.E. (Ed.), Evolutionary history of the "robust" australopithecines Transaction Publishers, New Brunswick, pp. 223-243.

Haile-Selassie, Y., 2001. Late Miocene hominids from the Middle Awash, Ethiopia. Nature 412, 178-181.

Haile-Selassie, Y., Saylor, B.Z., Deino, A., Levin, N.E., Alene, M., Latimer, B.M., 2012. A new hominin foot from Ethiopia shows multiple Pliocene bipedal adaptations. Nature 483, 565-569.

Haile-Selassie, Y., Gibert, L., Melillo, S.M., Ryan, T.M., Alene, M., Deino, A., Levin, N.E., Scott, G., Saylor, B.Z., 2015. New species from Ethiopia further expands Middle Pliocene hominin diversity. Nature 521, 483-488.

Halilaj, E., Laidlaw, D.H., Moore, D.C., Crisco, J.J., 2014. Polar histograms of curvature for quantifying skeletal joint shape and congruence. Journal of Biomechanical Engineering 136, 094503-094503.

Hammond, A.S., 2014. In vivo baseline measurements of hip joint range of motion in suspensory and nonsuspensory anthropoids. Am. J. Phys. Anthropol. 153, 417-434.

Hammond, A.S., Ning, J., Ward, C.V., Ravosa, M.J., 2010. Mammalian limb loading and chondral modeling during ontogeny. The Anatomical Record: Advances in Integrative Anatomy and Evolutionary Biology 293, 658-670.

Hamrick, M.W., 1996. Articular size and curvature as determinants of carpal joint mobility and stability in strepsirhine primates. J. Morphol. 230, 113-127.

Hamrick, M.W., 1999. A chondral modeling theory revisited. Journal of Theoretical Biology 201, 201-208.

Harcourt-Smith, W.E.H., 2002. Form and function in the hominoid tarsal skeleton. University College London.

Harcourt-Smith, W.E.H., Aiello, L.C., 2004. Fossils, feet and the evolution of human bipedal locomotion. J. Anat. 204, 403-416.

Harcourt-Smith, W.E.H., Tallman, M., Frost, S.R., Wiley, D.F., Rohlf, F.J., Delson, E., 2008. Analysis of selected hominoid joint surfaces using laser scanning and geometric morphometrics: a preliminary report, in: Sargis, E.J., Dagosto, M. (Eds.), Mammalian Evolutionary Morphology: A Tribute to Frederick S. Szalay. Springer Netherlands, Dordrecht, pp. 373-383.

Harcourt-Smith, W.E.H., Throckmorton, Z., Congdon, K.A., Zipfel, B., Deane, A.S., Drapeau, M.S.M., Churchill, S.E., Berger, L.R., DeSilva, J.M., 2015. The foot of Homo naledi. Nat. Commun. 6.

Häusler, M., 2002. New insights into the locomotion of *Australopithecus africanus* based on the pelvis. Evol. Anthropol. 11, 53-57.

Häusler, M., Berger, L., 2001. Stw 441/465: a new fragmentary ilium of a small-bodied *Australopithecus africanus* from Sterkfontein, South Africa. J. Hum. Evol. 40, 411-417.

Heiple, K.G., Lovejoy, C.O., 1971. The distal femoral anatomy of *Australopithecus*. Am. J. Phys. Anthropol. 35, 75-84.

Hicks, J.H., 1954. The mechanics of the foot: II. the plantar aponeurosis and the arch. J. Anat. 88, 25-30.21.

Hlaváček, M., Vokoun, D., 1998. The influence of articular surface incongruity on lubrication and contact pressure distribution of loaded synovial joints. Proceedings of the Institution of Mechanical Engineers, Part H: Journal of Engineering in Medicine 212, 11-22.

Holowka, N.B., Fernández, P.J., 2016. Functional morphology of the metatarsophalangeal joints in chimpanzees and humans: a kinematic and morphometric approach. Am. J. Phys. Anthropol. 159, 176.

Holowka, N.B., O'Neill, M.C., Demes, B., 2014. Three-dimensional foot kinematics of chimpanzees and humans during bipedal location. Am. J. Phys. Anthropol. 153, 144.

Hunt, K., 1996. The postural feeding hypothesis: an ecological model for the origin of bipedalism. South African Journal of Science 9, 77-90.

Indjeian, Vahan B., Kingman, Garrett A., Jones, Felicity C., Guenther, Catherine A., Grimwood, J., Schmutz, J., Myers, Richard M., Kingsley, David M., 2016. Evolving new skeletal traits by cis-regulatory changes in bone morphogenetic proteins. Cell 164, 45-56.

Ingram, T., Mahler, D.L., 2013. SURFACE: detecting convergent evolution from comparative data by fitting Ornstein-Uhlenbeck models with stepwise Akaike Information Criterion. Meth. Ecol. Evol. 4, 416-425.

Iwata, H., Ukai, Y., 2002. SHAPE: a computer program package for quantitative evaluation of biological shapes based on elliptic Fourier descriptors. J. Hered. 93, 384-385.

Johanson, D.C., Lovejoy, C.O., Kimbel, W.H., White, T.D., Ward, S.C., Bush, M.E., Latimer, B.M., Coppens, Y., 1982. Morphology of the Pliocene partial hominid skeleton (A.L. 288-1) from the Hadar formation, Ethiopia. Am. J. Phys. Anthropol. 57, 403-451.

Jungers, W.L., Godfrey, L.R., Simons, E.L., Chatrath, P.S., 1997. Phalangeal curvature and positional behavior in extinct sloth lemurs (Primates, Palaeopropithecidae). Proc. Nat. Acad. Sci. 94, 11998-12001.

Jungers, W.L., Burr, D.B., Cole, M.S., 1998. Body size and scaling of long bone geometry, bone strength, and positional behavior in cercopithecoid primates, in: Strasser, E., Fleagle, J.G., Rosenberger, A.L. (Eds.), Primate locomotion: recent advances. Springer, New York.

Jungers, W.L., Harcourt-Smith, W.E.H., Wunderlich, R.E., Tocheri, M.W., Larson, S.G., Sutikna, T., Due, R.A., Morwood, M.J., 2009. The foot of Homo floresiensis. Nature 459, 81-84.

Jungers, W.L., Grine, F.E., Leakey, M.G., Leakey, L., Brown, F., Yang, D., Tocheri, M.W., 2015. New hominin fossils from Ileret (Kolom Odiet), Kenya. Am. J. Phys. Anthropol. 156, 181.

Kelkar, R., Wang, V.M., Flatow, E.L., Newton, P.M., Ateshian, G.A., Bigliani, L.U., Pawluk, R.J., Mow, V.C., 2001. Glenohumeral mechanics: A study of articular geometry, contact, and kinematics. Journal of Shoulder and Elbow Surgery 10, 73-84.

Kidd, R.S., O'Higgins, P., Oxnard, C.E., 1996. The OH8 foot: a reappraisal of the functional morphology of the hindfoot utilizing a multivariate analysis. J. Hum. Evol. 31, 269-291.

Kimbel, W.H., Delezene, L.K., 2009. "Lucy" redux: A review of research on Australopithecus afarensis. Am. J. Phys. Anthropol. 140, 2-48.

Kivell, T.L., Skinner, M.M., Lazenby, R., Hublin, J.-J., 2011. Methodological considerations for analyzing trabecular architecture: an example from the primate hand. J. Anat. 218, 209-225.

Klingenberg, C.P., 2011. MorphoJ: an integrated software package for geometric morphometrics. Mol. Ecol. Resour. 11, 353-357.

Klingenberg, C.P., Gidaszewski, N.A., 2010. Testing and quantifying phylogenetic signals and homoplasy in morphometric data. Sys. Biol. 59, 245-261.

Knigge, R.P., Tocheri, M.W., Orr, C.M., McNulty, K.P., 2015. Three-dimensional geometric morphometric analysis of talar morphology in extant gorilla taxa from highland and lowland habitats. Anat. Rec. 298, 277-290.

Kuman, K., Clarke, R.J., 2000. Stratigraphy, artefact industries and hominid associations for Sterkfontein, Member 5. J. Hum. Evol. 38, 827-847.

Laroche, D., Pozzo, T., Ornetti, P., Tavernier, C., Maillefert, J.F., 2006. Effects of loss of metatarsophalangeal joint mobility on gait in rheumatoid arthritis patients. Rheumatology 45, 435-440.

Larson, S.G., 2007. Evolutionary transformation of the hominin shoulder. Evol. Anthropol. 16, 172-187.

Larson, S.G., 2009. Evolution of the hominin shoulder: early Homo, in: Grine, F.E., Fleagle, J.G., Leakey, R.E. (Eds.), The first humans – origin and early evolution of the genus Homo: contributions from the third Stony Brook Human Evolution Symposium and Workshop October 3 – October 7, 2006. Springer Netherlands, Dordrecht, pp. 65-75.

Latimer, B.M., 1991. Locomotor adaptations in *Australopithecus afarensis:* the issue of arboreality, in: Coppens, Y., Senut, B. (Eds.), Origine(s) de la bipédie chez les hominidés. SNRS, Paris.

Latimer, B., Lovejoy, C.O., 1989. The calcaneus of *Australopithecus afarensis* and its implications for the evolution of bipedality. Am. J. Phys. Anthropol. 78, 369-386.

Latimer, B., Lovejoy, C.O., 1990a. Metatarsophalangeal joints of Australopithecus afarensis. Am. J. Phys. Anthropol. 83, 13-23.

Latimer, B.M., Lovejoy, C.O., 1990b. Hallucal tarsometatarsal joint in Australopithecus afarensis. Am. J. Phys. Anthropol. 82, 125-133.

Latimer, B.M., Lovejoy, C.O., Johanson, D.C., Coppens, Y., 1982. Hominid tarsal, metatarsal, and phalangeal bones recovered from the Hadar formation: 1974–1977 collections. Am. J. Phys. Anthropol. 57, 701-719.

Leakey, M., Tobias, P.V., Martyn, J.E., Leakey, R.E.F., 1970. An Acheulean industry with prepared core technique and the discovery of a contemporary hominid mandible at Lake Baringo, Kenya. Prec. Prehist. Soc. 35, 48-76.

Lewis, O.J., 1972. The evolution of the hallucial tarsometatarsal joint in the anthropoidea. Am. J. Phys. Anthropol. 37, 13-33.

Lewis, O.J., 1980. The joints of the evolving foot. Part III. The fossil evidence. J. Anat. 131, 275-298.

Lewis, O.J., 1989. Functional morphology of the evolving hand and foot. Oxford University Press, Oxford.

Lordkipanidze, D., Jashashvili, T., Vekua, A., de Leon, M.S.P., Zollikofer, C.P.E., Rightmire, G.P., Pontzer, H., Ferring, R., Oms, O., Tappen, M., Bukhsianidze, M., Agusti, J., Kahlke, R., Kiladze, G., Martinez-Navarro, B., Mouskhelishvili, A., Nioradze, M., Rook, L., 2007. Postcranial evidence from early Homo from Dmanisi, Georgia. Nature 449, 305-310.

Lovejoy, C.O., 2005. The natural history of human gait and posture: part 1. spine and pelvis. Gait & Posture 21, 95-112.

Lovejoy, C.O., Simpson, S.W., White, T.D., Asfaw, B., Suwa, G., 2009. Careful climbing in the Miocene: the forelimbs of *Ardipithecus ramidus* and humans are primitive. Science 326, 70-70e78.

Lovejoy, C.O., Latimer, B., Suwa, G., Asfaw, B., White, T.D., 2009. Combining prehension and propulsion: the foot of Ardipithecus ramidus. Science 326, 72, 72e71-72e78.

MacConaill, M.A., Basmajian, J.V., 1969. Muscles and movements. Williams & Williams Baltimore.

MacLatchy, L.M., 1996. Another look at the australopithecine hip. J. Hum. Evol. 31, 455-476.

MacLatchy, L.M., Bossert, W.H., 1996. An analysis of the articular surface distribution of the femoral head and acetabulum in anthropoids, with implications for hip function in Miocene hominoids. J. Hum. Evol. 31, 425-453.

Marzke, M.W., 1983. Joint functions and grips of the Australopithecus afarensis hand, with special reference to the region of the capitate. J. Hum. Evol. 12, 197-211.

McHenry, H., 1975. Biomechanical interpretation of the early hominid hip. J. Hum. Evol. 4, 343-355.

McNulty, K.P., 2009. Computing singular warps from Procrustes aligned coordinates. J. Hum. Evol. 57, 191-194.

McNulty, K.P., Vinyard, C.J., 2015. Morphometry, geometry, function, and the future. Anat. Rec. 298, 328-333.

McNulty, K.P., Begun, D.R., Kelley, J., Manthi, F.K., Mbua, E.N., 2015. A systematic revision of Proconsul with the description of a new genus of early Miocene hominoid. J. Hum. Evol. 84, 42-61.

Meldrum, D.J., 1991. Kinematics of the cercopithecine foot on arboreal and terrestrial substrates with implications for the interpretation of hominid terrestrial adaptations. Am. J. Phys. Anthropol. 84, 273-289.

Meldrum, D.J., 2007. Letter to the editor:Hyper bipeds—or—from biped to strider. Am. J. Phys. Anthropol. 134, 292-294.

Midlo, C., 1934. Form of hand and foot in primates. Am. J. Phys. Anthropol. 19, 337-389.

Mitchell, P.J., Sarmiento, E.E., Meldrum, D.J., 2012. The AL 333-160 fourth metatarsal from Hadar compared to that of humans, great apes, baboons and proboscis monkeys: non-conclusive evidence for pedal arches or obligate bipedality in Hadar hominins. Homo 63, 336-367.

Mitteroecker, P., Gunz, P., 2009. Advances in geometric morphometrics. Evolutionary Biology 36, 235-247.

Morton, D.J., 1922. Evolution of the human foot. Am. J. Phys. Anthropol. 5, 305-336.

Morton, D.J., 1924. Evolution of the human foot II. Am. J. Phys. Anthropol. 7, 1-52.

Nakagawa, N., 1989. Activity budget and diet of patas monkeys in Kala Maloue National Park, Cameroon: a preliminary report. Primates 30, 27-34.

Nowak, M.G., Carlson, K.J., Patel, B.A., 2010. Apparent density of the primate calcaneo-cuboid joint and its association with locomotor mode, foot posture, and the "midtarsal break". Am. J. Phys. Anthropol. 142, 180-193.

O'Neill, M.C., Lee, L.-F., Demes, B., Thompson, N.E., Larson, S.G., Stern Jr, J.T., Umberger, B.R., 2015. Three-dimensional kinematics of the pelvis and hind limbs in chimpanzee (Pan troglodytes) and human bipedal walking. J. Hum. Evol. 86, 32-42.

Orr, C.M., 2005. Knuckle-walking anteater: a convergence test of adaptation for purported knuckle-walking features of african Hominidae. Am. J. Phys. Anthropol. 128, 639-658.

Palastanga, N., Field, D., Soames, R., 2002. Anatomy and human movement. Butterworth-Heinemann, Oxford.

Patel, B.A., 2008. Functional morphology and biomechanics of digitigrade hand postures in cercopithecoid primates. Stony Brook University.

Patel, B.A., 2009. Not so fast: speed effects on forelimb kinematics in cercopithecine monkeys and implications for digitigrade postures in primates. Am. J. Phys. Anthropol. 140, 92-112.

Patel, B.A., 2010. Functional morphology of cercopithecoid primate metacarpals. J. Hum. Evol. 58, 320-337.

Patel, B., Polk, J., 2010. Distal forelimb kinematics in Erythrocebus patas and Papio anubis during walking and galloping. International Journal of Primatology 31, 191-207.

Peeters, K., Schreuer, J., Burg, F., Behets, C., Van Bouwel, S., Dereymaeker, G., Sloten, J.V., Jonkers, I., 2013. Alterated talar and navicular bone morphology is associated with pes planus deformity: a CT-scan study. Journal of Orthopaedic Research 31, 282-287.

Pickering, R., Kramers, J.D., 2010. Re-appraisal of the stratigraphy and determination of new U-Pb dates for the Sterkfontein hominin site, South Africa. J. Hum. Evol. 59, 70-86.

Pickering, T.R., Clarke, R.J., Moggi-Cecchi, J., 2004. Role of carnivores in the accumulation of the Sterkfontein Member 4 hominid assemblage: a taphonomic reassessment of the complete hominid fossil sample (1936–1999). Am. J. Phys. Anthropol. 125, 1-15.

Polk, J.D., 2004. Influences of limb proportions and body size on locomotor kinematics in terrestrial primates and fossil hominins. J. Hum. Evol. 47, 237-252.

Pontzer, H., Rolian, C., Rightmire, G.P., Jashashvili, T., Ponce de León, M.S., Lordkipanidze, D., Zollikofer, C.P.E., 2010. Locomotor anatomy and biomechanics of the Dmanisi hominins. J. Hum. Evol. 58, 492-504.

Prang, T.C., 2016. The subtalar joint complex of *Australopithecus sediba*. J. Hum. Evol. 90, 105-119.

Preuschoft, H., 1970. Functional anatomy of the lower extremity, in: Bourne, G.H. (Ed.), The chimpanzee, vol. 3. Karger, Basel, pp. 221-294.

Proctor, D.J., 2010. Three-dimensional morphometrics of the proximal metatarsal articular surfaces of Gorilla, Pan, Hylobates, and shod and unshod humans. University of Iowa.

Proctor, D.J., 2010a. Brief communication: shape analysis of the MT 1 proximal articular surface in fossil hominins and shod and unshod *Homo*. Am. J. Phys. Anthropol. 143, 631-637.

Proctor, D.J., 2010b. Three-dimensional morphometrics of the proximal metatarsal articular surfaces of *Gorilla, Pan, Hylobates*, and shod and unshod humans. University of Iowa.

Proctor, D.J., 2013. Proximal metatarsal articular surface shape and the evolution of a rigid lateral foot in hominins. J. Hum. Evol. 65, 761-769.

Proctor, D.J., Broadfield, D., Proctor, K., 2008. Quantitative three-dimensional shape analysis of the proximal hallucial metatarsal articular surface in Homo, Pan, Gorilla, and Hylobates. Am. J. Phys. Anthropol. 135, 216-224.

Rein, T.R., 2011. The correspondence between proximal phalanx morphology and locomotion: implications for inferring the locomotor behavior of fossil catarrhines. Am. J. Phys. Anthropol. 146, 435-445.

Rein, T., Harrison, T., 2007. Quantifying the angle of orientation of the metatarsophalangeal joint surface of proximal phalanges in extant primates. Am. J. Phys. Anthropol. 132, 197-197.

Rein, T.R., McCarty, L.A., 2012. Metacarpophalangeal joint orientation in anthropoid manual phalanges. The Anatomical Record: Advances in Integrative Anatomy and Evolutionary Biology 295, 2057-2068.

Revell, L.J., 2012. phytools: an R package for phylogenetic comparative biology (and other things). Methods Ecol. Evol. 3, 217-223.

Richardson, G.E., 1999. Hallucal sesamoid pain: causes and surgical treatment. Journal of the American Academy of Orthopaedic Surgeons 7, 270-278.

Richmond, B.G., Begun, D.R., Strait, D.S., 2001. Origin of human bipedalism: the knuckle-walking hypothesis revisited. Am. J. Phys. Anthropol. 116, 70-105.

Rijksen, H.D., 1978. A field study on Sumatran orang utans (Pongo pygmaeus abelii Lesson 1827) : ecology, behaviour and conservation. Veenman, Wageningen.

Roberts, N., 1989. The Holocene--an environment history Basil Blackwell Inc. , Oxford.

Rodman, P.S., 1979. Skeletal differentiation of Macaca fascicularis and Macaca nemestrina in relation to arboreal and terrestrial quadrupedalism. Am. J. Phys. Anthropol. 51, 51-62.

Rohlf, F.J., 2002. Geometric morphometrics and phylogeny, in: MacLeod, N., Forey, P.L. (Eds.), Morphology, shape, and phylogeny. Taylor & Francis, London, pp. 175-193.

Rohlf, F.J., 2010. tspRelw: relative warps analysis. Version 1.49. Department of Ecology and Evolution, University of New York at Stony Brook, Stony Brook.

Rohlf, F.J., Corti, M., 2000. Use of two-block partial least-squares to study covariation in shape. Sys. Biol. 49, 740-753.

Rose, M., 1979. Positional behavior of natural populations: some quantitative results of a field study of *Colobus guereza* and *Cercopithecus atheiops*, in: Morbeck, M.E., Preuschoft, H., Gomberg, N. (Eds.), Environment, behavior, and morphology: dynamic interactions in primates. Gustav Fischer, New York.

Sarmiento, E.E., 1983. The significance of the heel process in anthropoids. International Journal of Primatology 4, 127-152.

Sarmiento, E.E., 1994. Terrestrial traits in the hands and feet of gorillas. Am. Mus. Novit. 3091, 1-56.

Sarrafian, S.K., 1987. Functional characteristics of the foot and plantar aponeurosis under tibiotalar loading. Foot Ankle 8, 4-18.

Sati, J., Alfred, J., 2002. Locomotion and posture in Hoolock gibbon. Ann. For 10, 298-306.

Schmitt, D., Larson, S.G., 1995. Heel contact as a function of substrate type and speed in primates. Am. J. Phys. Anthropol. 96, 39-50.

Schwartz, J., Tattersall, I., 2005. The human fossil record craniodental morphology of genus Homo (Africa and Asia). Wiley-Liss.

Sealy, J., Pfeiffer, S., 2000. Diet, body size, and landscape use among Holocene people in the Southern Cape, South Africa. Curr. Anthropol. 41, 642-655.

Seiffert, E.R., Perry, J.M.G., Simons, E.L., Boyer, D.M., 2009. Convergent evolution of anthropoid-like adaptations in Eocene adapiform primates. Nature 461, 1118-1121.

Senut, B., Pickford, M., Gommery, D., Mein, P., Cheboi, K., Coppens, Y., 2001. First hominid from the Miocene (Lukeino Formation, Kenya). C. R. Acad. Sci. Paris Séria IIa 332, 137-144.

Smaers, J.B., Mongle, C.S., Kandler, A., 2016. A multiple variance Brownian motion framework for estimating variable rates and inferring ancestral states. Biological Journal of the Linnean Society 118, 78-94.

Sokal, R.R., Rohlf, F.J., 2011. Biometry: 4th edition. W.H. Freeman, New York.

Solan, M., Day, M.H., 1992. The Baringo (Kapthurin) ulna. J. Hum. Evol. 22, 307-313.

Stern, J., 1975. Before bipedality. Yearbook of Physical Anthropology 19, 59-68.

Stern, J.T., 2000. Climbing to the top: a personal memoir of *Australopithecus afarensis*. Evol. Anthropol. 9, 111-148.

Stern, J.T., Susman, R.L., 1983. The locomotor anatomy of *Australopithecus afarensis*. Am. J. Phys. Anthropol. 60, 279-317.

Stern, J. T., Susman, R.L., 1991. "Total morphological pattern" versus the "magic trait": conflicting approaches to the study of early hominid bipedalism." In: Coppens, Y., Senut,

B., (Eds.), Origine (s) de la bipédie chez les Hominidés. Cahiers de Paleoanthropologie, CNRS, Paris 99-112.

Stern, J.T., Jungers, W.L., Susman, R.L., 1995. Quantifying phalangeal curvature: An empirical comparison of alternative methods. Am. J. Phys. Anthropol. 97, 1-10.

Stock, J., Pfeiffer, S., 2001. Linking structural variability in long bone diaphyses to habitual behaviors: Foragers from the southern African Later Stone Age and the Andaman Islands. Am. J. Phys. Anthropol. 115, 337-348.

Strait, D.S., Grine, F.E., 2004. Inferring hominoid and early hominid phylogeny using craniodental characters: the role of fossil taxa. J. Hum. Evol. 47, 399-452.

Strasser, E., 1992. Hindlimb proportions, allometry, and biomechanics in old world monkeys (Primates, Cercopithecidae). Am. J. Phys. Anthropol. 87, 187-213.

Strasser, E., 1994. Relative development of the hallux and pedal digit formulae in Cercopithecidae. J. Hum. Evol. 26, 413-440.

Susman, R.L., 1979. Comparative and functional morphology of hominoid fingers. Am. J. Phys. Anthropol. 50, 215-236.

Susman, R.L., 1983. Evolution of the human foot: evidence from Plio-Pleistocene hominids. Foot Ankle 3, 365-376.

Susman, R.L, 1988. Hand of *Paranthropus robustus* from Member 1, Swartkrans: fossil evidence for tool behavior. Science 240, 781-784.

Susman, R.L., 1989. New hominid fossils from the Swartkrans formation (1979–1986 excavations): postcranial specimens. Am. J. Phys. Anthropol. 79, 451-474.

Susman, R.L., 1998. Hand function and tool behavior in early hominids. J. Hum. Evol. 35, 23-46.

Susman, R.L., Brain, T.M., 1988. New first metatarsal (SKX 5017) from Swartkrans and the gait of Paranthropus robustus. Am. J. Phys. Anthropol. 77, 7-15.

Susman, R.L., de Ruiter, D.J., 2004. New hominin first metatarsal (SK 1813) from Swartkrans. J. Hum. Evol. 47, 171-181.

Susman, R.L., Stern, J.J.T., Jungers, W.L., 1984. Arboreality and bipedality in the Hadar hominids. Folia Primatol. 43, 113-156.

Susman, R.L., de Ruiter, D., Brain, C.K., 2001. Recently identified postcranial remains of *Paranthropus* and early *Homo* from Swartkrans Cave, South Africa. J. Hum. Evol. 41, 607-629.

Thorpe, S.K.S., Crompton, R.H., 2005. Locomotor ecology of wild orangutans (*Pongo pygmaeus abelii*) in the Gunung Leuser Ecosystem, Sumatra, Indonesia: a multivariate analysis using log-linear modelling. Am. J. Phys. Anthropol. 127, 58-78.

Tocheri, M.W., Orr, C.M., Larson, S.G., Sutikna, T., Jatmiko, Saptomo, E.W., Due, R.A., Djubiantono, T., Morwood, M.J., Jungers, W.L., 2007. The primitive wrist of Homo floresiensis and its implications for hominin evolution. Science 317, 1743-1745.

Tocheri, M.W., Solhan, C.R., Orr, C.M., Femiani, J., Frohlich, B., Groves, C.P., Harcourt-Smith, W.E., Richmond, B.G., Shoelson, B., Jungers, W.L., 2011. Ecological divergence and medial cuneiform morphology in gorillas. J. Hum. Evol. 60, 171-184.

Tocheri, M.W., Dommain, R., McFarlin, S.C., Burnett, S.E., Troy Case, D., Orr, C.M., Roach, N.T., Villmoare, B., Eriksen, A.B., Kalthoff, D.C., Senck, S., Assefa, Z., Groves, C.P., Jungers, W.L., 2016. The evolutionary origin and population history of the grauer gorilla. Am. J. Phys. Anthropol. 159, 4-18.

Trinkaus, E., 1983. Functional aspects of Neandertal pedal remains. Foot Ankle 3, 377-390.

Turley, K., Frost, S.R., 2014. The appositional articular morphology of the talo-crural joint: the influence of substrate use on joint shape. Anat. Rec. 297, 618-629.

Tuttle, R.H., 1967. Knuckle-walking and the evolution of hominoid hands. Am. J. Phys. Anthropol. 26, 171-206.

Tuttle, R.H., 1970. Postural, propulsive, and prehensile capabilites in the cheiridia of chimpanzees, and other great apes, in: Bourne, G.H. (Ed.), The chimpanzee. Karger, Basel, pp. 167-263.

Tuttle, R.H., 1981. Evolution of hominid bipedalism and prehensile capabilities. Philos. T. Roy. Soc. B. 292, 89-94.

Vereecke, E., D'Août, K., De Clercq, D., Van Elsacker, L., Aerts, P., 2003. Dynamic plantar pressure distribution during terrestrial locomotion of bonobos (Pan paniscus). Am. J. Phys. Anthropol. 120, 373-383.

Waide, D.V., Lawlor, G.J., McCormack, B.A.O., Carr, A.J., 2000. The relationship between surface topography and contact in the elbow joint: development of a two-dimensional

geometrical model in the coronal plane. Proceedings of the Institution of Mechanical Engineers, Part H: Journal of Engineering in Medicine 214, 413-423.

Ward, C.V., 2002. Interpreting the posture and locomotion of Australopithecus afarensis: where do we stand? Am. J. Phys. Anthropol. 119, 185-215.

Ward, C.V., Latimer, B., 2005. Human evolution and the development of spondylolysis. Spine 30, 1808-1814.

Ward, C.V., Kimbel, W.H., Johanson, D.C., 2011. Complete fourth metatarsal and arches in the foot of Australopithecus afarensis. Science 331, 750-753.

Ward, C.V., Kimbel, W.H., Harmon, E.H., Johanson, D.C., 2012. New postcranial fossils of Australopithecus afarensis from Hadar, Ethiopia (1990–2007). J. Hum. Evol. 63, 1-51.

Watson, H., Weinzweig, J., 1998. Stiff joints, in: Green, D. (Ed.), Operative hand surgery. Churchill Livingstone New York, pp. 552-562.

Weidenreich, F., 1923. Evolution of the human foot. Am. J. Phys. Anthropol. 6, 1-10.

White, T.D., Black, M.T., Folkens, P.A., 2011. Human osteology. Academic press.

White, T.D., Suwa, G., Asfaw, B., 1994. Australopithecus ramidus, a new species of early hominid from Aramis, Ethiopia Nature 371, 306-312.

White, T.D., Asfaw, B., Beyene, Y., Haile-Selassie, Y., Lovejoy, C.O., Suwa, G., Wolde Gabriel, G., 2009. Ardipithecus ramidus and the paleobiology of early hominids. Science 326, 64-86.

Wiley, D.F., Amenta, N., Alcantara, D.A., Ghosh, D., Kil, Y.J., Delson, E., Harcourt-Smith, W.E.H., Rohlf, F.J., John, K.S., Hamann, B., 2005. Evolutionary morphing IEEE Visualization Conference, Minneapolis, MN, 431-438.

Williams, S.A., Ostrofsky, K.R., Frater, N., Churchill, S.E., Schmid, P., Berger, L.R., 2013. The vertebral column of Australopithecus sediba. Science 340.

Winter, D.A., 2005. Biomechanics and motor control of human movement. 3rd edition. John Wiley and Sons, Inc. , Hoboken.

Wood-Jones, F., 1944. Structure and function as seen in the foot. Bailliere and Co. , London.

Wunderlich, R.E., 1999. Pedal form and plantar pressure distribution in anthropoid primates. . Stony Brook University.

Yamagiwa, J., Mwanza, N., Spangenberg, A., Maruhashi, T., Yumoto, T., Fischer, A., Steinhauer-Burkart, B., 1993. A census of the eastern lowland gorillas *Gorilla gorilla graueri* in Kahuzi-Biega national park with reference to mountain gorillas *G. g. beringei* in the Virunga region, Zaire. Biol Conserv 64, 83-89.

Young, N.M., Wagner, G.P., Hallgrímsson, B., 2010. Development and the evolvability of human limbs. Proc. Nat. Acad. Sci. 107, 3400-3405.

Zipfel, B., Kidd, R., 2006. Hominin first metatarsals (SKX 5017 and SK 1813) from Swartkrans: a morphometric analysis. Homo 57, 117-131.

Zipfel, B., DeSilva, J.M., Kidd, R.S., 2009. Earliest complete hominin fifth metatarsal—Implications for the evolution of the lateral column of the foot. Am. J. Phys. Anthropol. 140, 532-545.

Zipfel, B., DeSilva, J.M., Kidd, R.S., Carlson, K.J., Churchill, S.E., Berger, L.R., 2011. The foot and ankle of *Australopithecus sediba*. Science 333, 1417-1420.